ornl

ORNL/Sub/84-00214/1

OAK RIDGE
NATIONAL
LABORATORY

MARTIN MARIETTA

Synthesis of High Purity Sinterable Silicon Carbide Powder

W. D. Boecker
B. L. Mehosky
R. S. C. Rogers
R. S. Storm
V. Venkateswaran

CERAMIC TECHNOLOGY FOR ADVANCED HEAT ENGINES

Prepared by
The Carborundum Company
Structural Ceramics Division
Niagara Falls, New York

OPERATED BY
MARTIN MARIETTA ENERGY SYSTEMS, INC.
FOR THE UNITED STATES
DEPARTMENT OF ENERGY

Report Number: ORNL/Sub/84-00214/1
Accession Number: 2624
Title: Synthesis of High Purity Sinterable
Silicon Carbide Powder
Personal Author: Boecker, W.D.; Mehosky, B.L.;
Rogers, R.S.C.; et al.
Contract Number: DE-AC05-84-OR21400
Corporate Author or Publisher: Carborundum Company, Structural
Ceramics Division, Niagara Falls, NY
1
Publication Date: Nov 01, 1989
Pages: 00305
Descriptors, Keywords: Synthesis Powder Sinterable Silicon
Carbide SiC Plasma Hydrogen Argon
Production Test Facility Purity
Volume Material

ORNL/Sub/84-00214/1

SYNTHESIS OF HIGH PURITY SINTERABLE SILICON CARBIDE POWDER

W. D. Boecker
B. L. Mehosky
R. S. C. Rogers
R. S. Storm
V. Venkateswaran

Date Published: November 1989

FINAL REPORT

Prepared by
The Carborundum Company
Structural Ceramics Division
Niagara Falls, New York
Subcontract No. 86X-00214C

Prepared for the
Assistant Secretary for Conservation and Renewable Energy
Office of Transportation Systems
Advanced Materials Development Program

for
OAK RIDGE NATIONAL LABORATORY
Oak Ridge, Tennessee 37831
operated by
MARTIN MARIETTA ENERGY SYSTEMS, INC.
for the
U.S. DEPARTMENT OF ENERGY
under Contract No. DE-AC05-84OR21400

TABLE OF CONTENTS

ABSTRACT

High purity, submicron silicon carbide powders were produced via gas phase synthesis using a hydrogen/argon plasma. Two test facilities were constructed, a bench-scale unit and a larger pilot scale reactor. Three candidate silicon sources were evaluated: silicon tetrachloride ($SiCl_4$), dimethyldichlorosilane ($(CH_3)_2SiCl_2$) and methyltrichlorosilane (CH_3SiCl_3). Product powders were evaluated on the basis of pressureless sinterability, surface area, agglomeration, particle size distribution, phase distribution and chemistry. Three commercial powders, Starck A10, Starck B10, and Carborundum submicron alpha silicon carbide, were also evaluated for comparison to the product powders.

Powders were reproducibly synthesized at a rate of one pound per hour for standard run times of five hours. Product powders exhibited chemical and physical properties equal to or exceeding the commercial powders evaluated. In limited attempts to pressureless sinter the product powders, densities of 91% of theoretical were obtained with as-produced powder. Post-processing permitted densities in excess of 97% of theoretical. X-ray diffraction of the product indicates that the product powders are primarily beta poly-types, with traces of alpha present.

Increased production rates to a target level of seven pounds per hour were not possible due to current transients produced by the pilot scale power supply. Extensive unsuccessful efforts to reduce or eliminate the transients are described. Low recovered product yields resulted from a failure of a product collection filter that was not discovered until the completion of the project.

---

* Research sponsored by the U.S. Department of Energy, Assistant Secretary for Conservation and Renewable Energy, Office of Transportation Systems, as part of the Ceramic Technology for Advanced Heat Engines Project of the Advanced Materials Development Program, under contract DE-AC05-840R21400 with Martin Marietta Energy Systems, Inc.

OBJECTIVE/SCOPE

The objective of this program was to develop a volume scalable process to produce high-purity, high-surface area, sinterable silicon carbide powder. Specifically, the project activities were targeted to develop a process to produce sub-micron, pressureless-sinterable silicon carbide powders with enhanced purity properties via gas phase synthesis using an argon/hydrogen plasma and appropriate silicon and carbon feedstocks. Initially, a small system was to be constructed to produce powder at a rate of 50 to 100 grams per hour, followed by a scale-up to 250 to 1000 grams per hour after operating conditions had been identified.

The project activities were divided into two phases, in keeping with the two projected production rates. Phase I activities included the following elements:

- Construction of a bench-scale plasma-reactor system.
- Verify the technical feasibility of gas phase synthesis route.
- Identify the best silicon feedstock on the basis of performance and cost.
- Optimize the production process at bench scale.
- Characterize the product powders and compare their properties with commercially available alternatives.
- Develop a theoretical model to assist in understanding the synthesis process, optimization of the operating conditions and scale-up.

Phase II activities included:

- Construction of a larger plasma reactor system.
- Operation of the larger system to confirm operating conditions and for the production of material for evaluation.
- Economic analysis and flowsheet development.

PROJECT ACTIVITIES

BACKGROUND - GAS PHASE SYNTHESIS ROUTE

Prior to commencing this project, five candidate processes for the production of ultrapure silicon carbide powders were evaluated. The candidate processes included Acheson Furnace synthesis followed by post-processing, rotary-kiln synthesis followed by post-processing, sol-gel synthesis, polymer pyrolysis, and gas phase synthesis. These processes were evaluated on the basis of a number of factors, including raw material requirements (costs, availability, purity), reaction chemistry, product yield, product properties (particle size, size distribution, surface area, purity, etc.) and potential process design factors (cost, control, pollution). Some of these factors are summarized in Table I.

The gas phase route was chosen as the process most likely to produce silicon carbide powders with the desired physical properties and still exhibit the ability to be scaled to a commercial production rate. Proprietary activities prior to this project conducted for the Carborundum company confirmed the feasibility of producing silicon carbide powders in a plasma reactor. The approach taken demonstrated the reaction of silicon tetrachloride ($SiCl_4$) with methane (CH_4) as the carbon source and hydrogen gas as a chlorine scavenger in an argon plasma. General operating conditions for synthesis of beta silicon carbide powders were determined. Particle surface areas between 25 and 124 m^2/g were obtained, with acceptable chemical purity levels. These activities were used as a starting point for the Phase I activities.

APPLICATION OF DC PLASMA TO SILICON CARBIDE POWDER SYNTHESIS

High enthalpy plasma represent an efficient method of elevating gas phase reactants rapidly and uniformly to desired reaction temperatures. Thermochemical equilibrium is typically achieved within milliseconds. This is followed by nucleation and product coalescence into fine powders. Since silicon carbide has no liquid phase, the condensation of products and growth of liquid droplets prior to freezing does not occur in this system. Thus, particle size is totally dependent on the gas/solid interactions as the reactor gas temperature falls. In theory, powders of high purity with tightly controlled particle size distribution may be produced in a plasma.

PROJECT WORK PLAN

As described above, the overall project was divided into two Phases and a number of discrete tasks. Each task is discussed individually, below.

TABLE I

PRELIMINARY COMPARISON OF ALTERNATE PROCESSES
FOR MANUFACTURE OF ULTRAFINE, ULTRAPURE β SILICON CARBIDE POWDER

I. Process Requirements	Acheson Furnace and Selected Processing[a]	Sol-Gel	Polymer Pyrolysis	Gas Phase Reactions
1. Raw Materials				
a. Carbon	• Petrol coke	• Organic carbon compounds (e.g., pitch)	• Organosilicon compounds (i.e., carbon and silicon)	• Methane and organic compounds
b. Silicon	• Silica sand - high grade	• Colloidal silica • Organosilicon compounds		• Silicon tetrachloride • Organosilicon compounds
c. Other	----------	----------	• Sodium • Potassium	• Hydrogen • Argon
2. Energy	Electric	Electric (ovens, kilns and furnaces)	Electric	Electric
II. Process Control (for Ultrafine, Ultrapure & SiC)	Poor	Fair	Fair	Good
III. Produce Quality				
• Particle size as BET surface area, m^2/gm	10-12	NA	NA	10-125
• Purity	Fair	Good	Good	Best
• Particle Size Distribution Control	Poor	Fair	Fair	Best

[a]Includes rotary kiln process

TABLE I (continued)

PRELIMINARY COMPARISON OF ALTERNATE PROCESSES
FOR MANUFACTURE OF ULTRAFINE, ULTRAPURE β SILICON CARBIDE POWDER

IV. Cost Elements ($/lb. SiC)	Acheson Furnace and Selected Processing[a]	Sol-Gel		Polymer Pyrolysis	Gas Phase Reactions
1. Raw Materials		A1	B1		
Carbon	0.02	0.03	-----	----------	0.11
Silicon	0.02	1.00	-----	----------	3.20
Organosilicon compounds	------	-----	5-10	5.00-10.00	-----
Sodium/Potassium	------	------	2.50	2.50	-----
Other**	0.01	0.10	0.10	0.10	5.70*
Total	0.05	1.13	7.60-12.60	7.60-12.60	9.01
2. Electric Energy	0.10$^{\Delta}$	0.05	0.05	0.05	1.00

** Includes solvent losses and other process materials.

* Electric are gases, and NaOH or $Ca(OH)_2$. These cost can be reduced significantly by gas recycle.

Δ Excludes energy for grinding and size separation.

I. Pitch plus colloidal silica based process.

II. Gels derived from organosilicon compounds.

Phase I

Task I - Design, Construct and Test Laboratory Scale System

The focus of this activity was to design, construct, commission, and test a bench-scale plasma facility capable of producing 50 to 100 grams of silicon carbide powder. The initial design was based on the work described briefly above, and centered on a DC argon plasma torch. After discussions with plasma torch vendors and evaluating the economics of argon operation, an effort was made to minimize the argon consumption process and increase the relative consumption of hydrogen. Since hydrogen was cheaper than argon as a plasma gas, and increased hydrogen assisted in scavenging the excess chlorides in the process, the facility was designed to run a hydrogen-rich plasma.

The torch used is a modification of a Norton (formerly Plasma Materials, Inc.) AA-60 gas heater. The unit is designed for operation on argon and various gas mixtures. A cross-sectional view of the torch is included as Figure I.

The standard torch configuration was modified to incorporate modular anode assemblies ("Secondary Anode Body", part 3 <two depicted> in Figure I) that are designed for powder or gas feed to the plasma via six injection ports in each anode assembly. Power for the torch is supplied by an arc welding power supply specially modified to Norton's specifications. The unit can be changed to change maximum current and voltage limits. The unit is nominally rated at 1500 amps at 80 volts, or in different configurations at 750 amps/160 volts or 375 amps/320 volts. In operation, the maximum arc voltage cannot exceed 60% of the rated open circuit voltage, so the nominal 120 kilowatt limit of the power supply is, in practice, derated to 72 kilowatt maximum operating power.

The torch/power supply is, in essence, a sophisticated TIG welder. Stable operation of the system depends on the electrical characteristics of the power supply, associated control and transmission wiring, and the torch itself. The electrical characteristics of the torch are further affected by the composition of the plasma gas fed to the torch and the ionization potential of the gas mixture, as well as the gas flow rates. Various gases have characteristic stable arc lengths, which vary due to their differing ionization energies. Thus, argon will have a substantially longer standing arc than either nitrogen or hydrogen. Introduction of hydrogen gas to a stable argon arc will have a tendency to shorten the arc if varying electrode gaps are available.

A second, less understood interaction is the tendency for a high gas flow rate to stretch out an arc longer than its stable arc length. A very high gas flow rate will "push" the arc outside the torch body, and the arc will bend

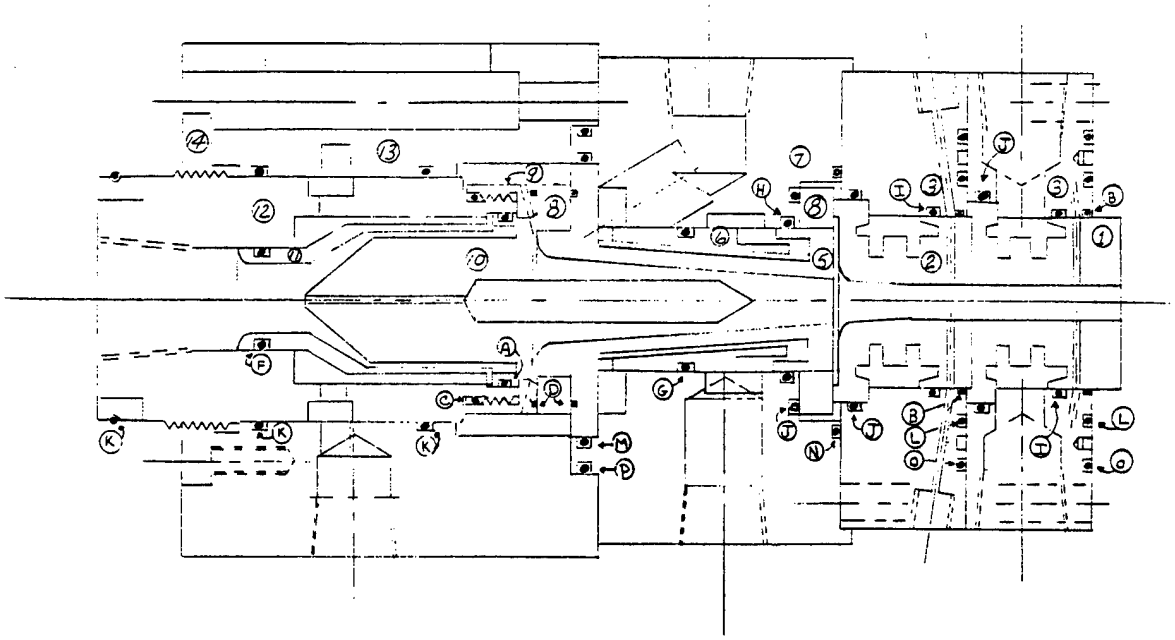

PLASMA MATERIALS INC.

MODEL AA60 PLASMA TORCH

FIGURE 1

1. Downstream Secondary Anode (60A2PE)	O-RINGS
2. Upstream Secondary Anode (60A1GP)	(Total Number Used)
3. Secondary Anode Body (60A13)	A. -028
5. Primary Anode (180A3)	B. -029 (2)
6. P.A. Water Separator (180A4)	C. -030
7. Primary Anode Body (60B11)	D. -031 (2)
8. Ceramic Insulator (150A5)	E. -115
9. Gas Injector (150A6)	F. -116
10. Cathode (60A7)	G. -122
11. Cathode Water Separator (150A8)	H. -124
12. Cathode Holder (150A9)	I. -128 (2)
13. Plastic Rear Body (60B12)	J. -132 (3)
14. Cathode Retainer (150A15)	K. -138 (3)
15. Cathode Safety Shield (not shown)	L. -136 (2)
	M. -142
	N. -144
	O. -148 (2)
	P. -150

back on to the anode. Such operation is characterized by abnormally high operating voltages (due to the longer arc path) and severe wear on the anode. Conversely, low flow rates will allow the arc to recede into the torch. A very short arc results, with resulting low voltage and very high current. The high current can then localize at a single point on the anode and significant metal migration can quickly result. The molten metal from the anode typically will move downstream under the influence of the plasma gas flow and solidify past the area of the plasma arc. The metal will eventually plug the torch exhaust port and cause the plasma to extinguish. A second, more catastrophic result is also possible. If sufficient metal is removed from the anode to reach the cooling water passage below, cooling water will be pumped into the electrically active portion of the torch. The resulting short circuit can potentially breach the torch body and permit reactant gases into the local area.

The plasma torch is connected by a flanged coupling to the reactor tube. The reactor is a 72-inch length of 16 BWG copper tubing (1.782-inch internal diameter, 0.109-inch thick walls). The tube is fitted with 66 surface thermocouples (Type K) welded to the external surface of the tube. The exterior surface of the reactor tube is helically wrapped with 60 feet of 5/8-inch OD soft copper tubing for the circulation of cooling water. The first 12 inches of the cooling coils were coated with Thermon heat conduction cement to improve heat dissipation at the reactor inlet. Spent once-through cooling water from the torch cooling water chiller is used to cool the reactor walls. The thermocouples are monitored by a Westronic DDR-10 multipoint recorder mounted in the system control console. Should any surface thermocouple exceed its individually programmed high-temperature setpoint, the recorder goes into alarm mode and shuts down the system. A West 801 high-temperature alarm unit backs up the recorder and monitors the hottest point in the reactor. If either the recorder or the West 801 alarms, the system automatically shuts down.

The torch and reactor assembly was oriented vertically, with the torch outlet pointed down, to minimize any powder fouling of any of the torch's electrical elements. The Dust Hopper (B 500) bolts to the bottom flange of the reactor/aftercooler. The unit has a conical bottom which funnels into a high temperature ball valve. Solids which salt out of the product gas stream can be removed from the system at this point. All remaining material exits the Dust Hopper via Stream 14 and flows to the Venturi scrubber (J 600) and tail gas scrubber (T 700).

The torch and power supply are supported by four additional subsystems. These include gas metering and induction, silicon supply and vaporizer, control systems and closed-loop cooling water system, and effluent cleanup. A Piping and Instrumentation Drawing is attached as Figure II.

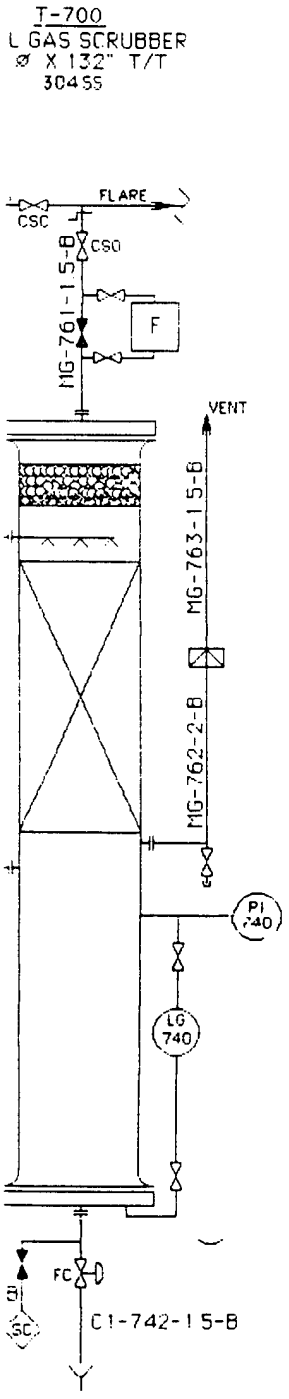

FIGURE II

PIPING KEY

__ Process Fluid
:
: __ Line Number
: :
: : __ Line Size
: : :
: : : __ Line Class
: : : :
AR-101-0.75-X

FLUIDS

AR Argon
H2 Hydrogen
CH Methane
W1 Once Through Cooling Water
CW Closed Loop Cooling Water
SI Silicon Tetrachloride
MG Mixed Gases

MATERIALS

A 316 ss
B 304 ss
C Monel 400
D Copper
E 316 ss Flexible Hose, Teflon Lined (2000 psi rating)
F Neoprene Hydraulic Hose, Nylon Reinforced (3000 psi rating)

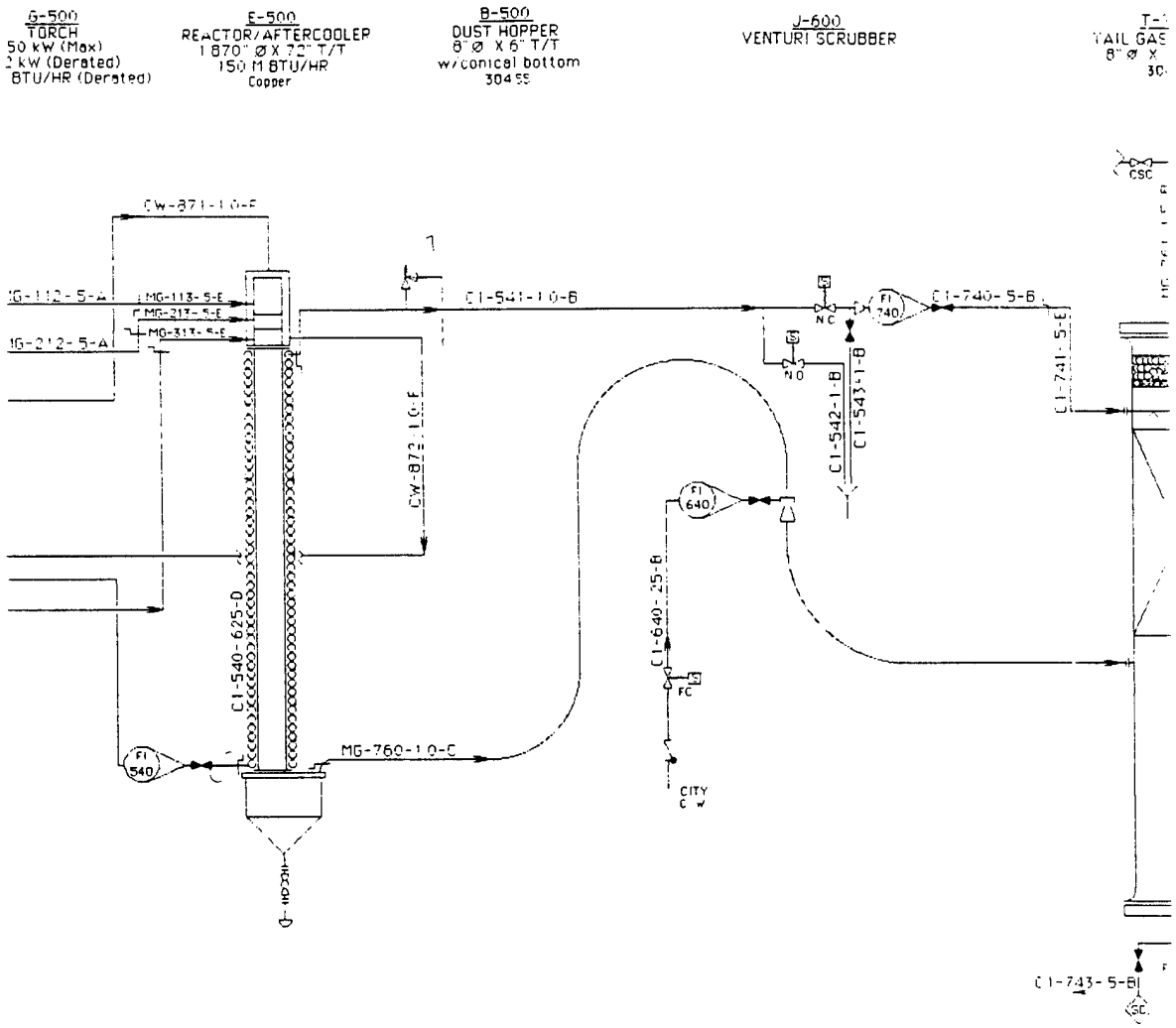

FIGURE II (CONT.)

H-300
GAS PREHEATER
416 Watts
304 SS

J-300
VAPORIZER
208 Watts
Monel 400

E-800
TORCH C W CHILLER
68.0 M BTU/HR

P-800
CLOSED LOOP C W
CIRC PUMP
6 GPM , 100 Psig

S-800
CLOSED LOOP C W
RESERVOIR
12 GAL

G-100
P M T CONTROL
CONSOLE

G-500
TORCH
50 kW (M
12 kW (Der
4 M BTU/HR

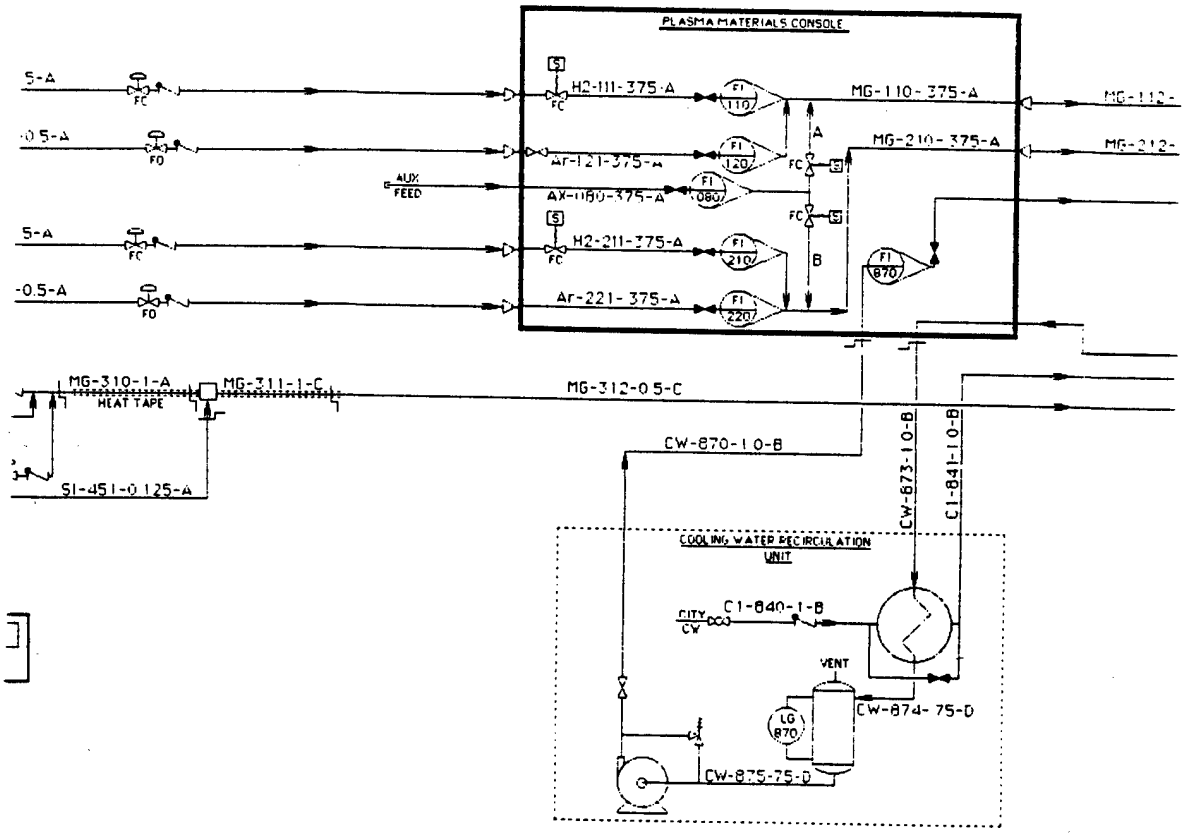

FIGURE II (CONT.)

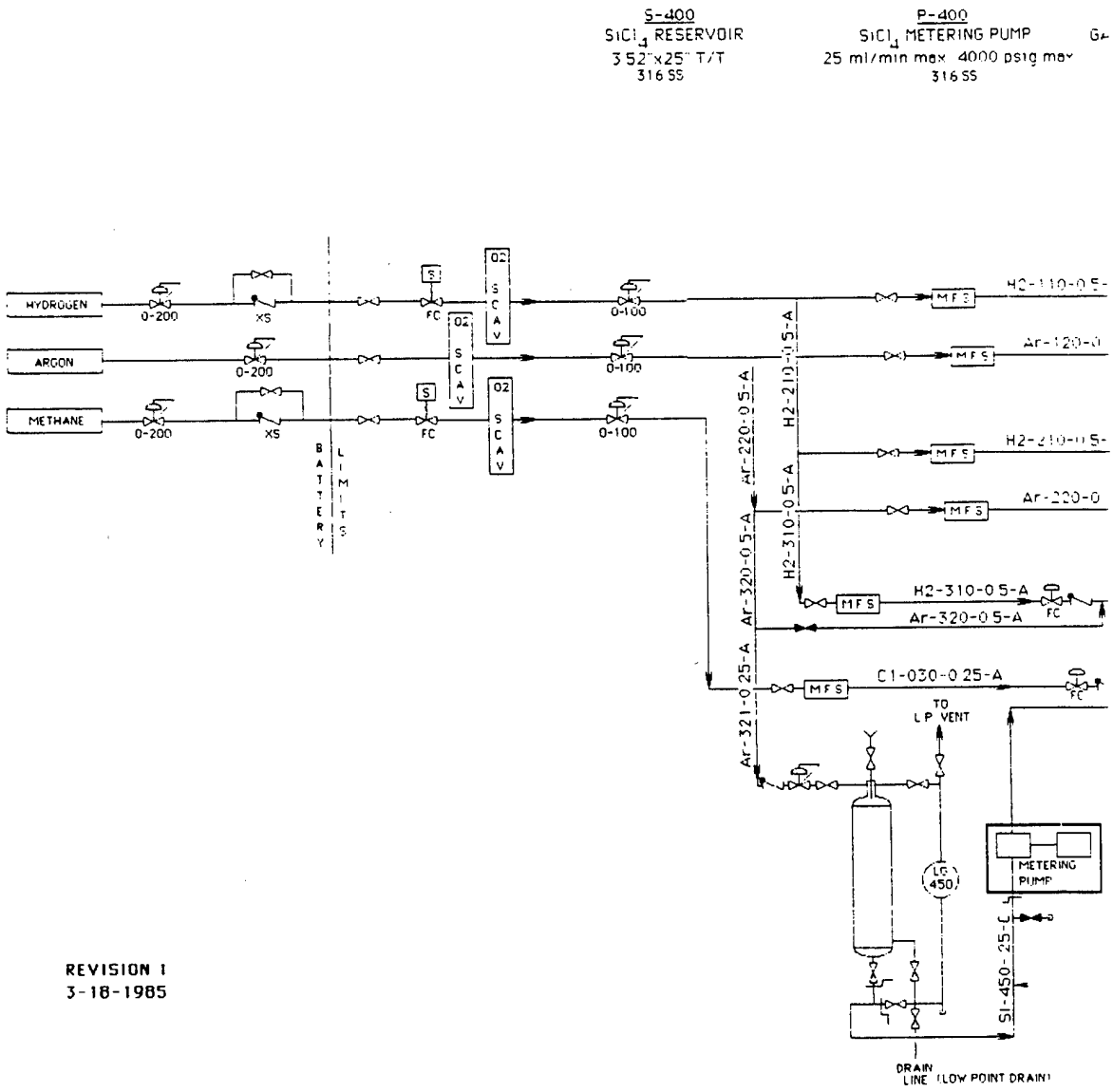

FIGURE II (CONT.)

The gas metering and induction system routes all compressed gases from high pressure cylinders outside the building to the bench scale unit. Hydrogen and argon are supplied from six-cylinder manifolds. Methane is supplied from a single cylinder with a swing spare. All cylinders are equipped with individual shutoff valves, and the manifolds each have a single main shutoff valve. Each gas supply is fitted with a self-contained pressure regulator (PCV 010, 020, and 030) and an additional shutoff valve at the battery limits to the process. The hydrogen and methane supply headers are also fitted with excess flow check valves to prevent large releases of combustible gases in the event of a line rupture or other mechanical failure. A bypass valve is installed around each excess flow check valve to permit releasing the check valve if actuated.

At the process battery limits, each gas supply header is fitted with an oxygen scavenger and a second self-contained pressure regulator (PCV 011, 021, and 023), which are used to set the system operating pressures. In addition, the hydrogen and methane lines are fitted with normally closed solenoid valves that close in the event of a system shutdown or emergency (FZ 010 and 130).

After the regulators, the hydrogen branches into three streams, designated as primary, secondary, and tertiary hydrogen (Streams 5, 8 and 7, respectively). Argon is split into two process streams designated as primary and secondary argon (Stream 6 and 9) as well as a maintenance purge line to the Gas Preheater and an argon supply line to the the silicon supply reservoir (S-400).

The methane, process argon, and process hydrogen streams are individually regulated by Badger Research Control Valves (FCV 110, 120, 210, 220, 310, and 330). Flow rates are controlled using a single-loop PID control scheme employing Brooks Model 5812 mass flow sensors (FT-110, 120, 210, 220, 310, and 330), Moore Digital Controllers (FIC 110, 120, 210, 220, 310, and 330), and Fisher current to pneumatic converters (FY 110, 120, 210, 220, 310, and 330) in conjunction with the flow control valves mentioned. The primary and secondary hydrogen and argon streams are routed to the torch control console, described below.

The tertiary hydrogen and methane gas streams were used as carrier gases to sweep the silicon source into the reaction system. The two gases are mixed together and heated to 375°F in the gas preheater (H-300). The preheater is a 36-inch length of one-inch diameter stainless steel tubing filled with 1/4" stainless steel nuts for enhanced heat transfer. The tube is wrapped with 416 watt silicon rubber heating tape which can reach a maximum temperature of 400°F.

Silicon is supplied to the system in the form of liquid silicon tetrachloride ($SiCl_4$), dimethyldichlorosilane ($(CH_3)_2SiCl_2$) or methyltrichlorosilane (CH_3SiCl_3) from the silicon Reservoir (S-400). The liquid feed is withdrawn from the reservoir by a Whitey metering pump (P-400). As the liquid feed is withdrawn from the reservoir, low-pressure argon (1 psig), let down by a self contained gas pressure regulator (PCV-420), displaces the liquid to exclude atmospheric moisture, which hydrolyzes the silicon materials to form hydrochloric acid. The liquid is metered into a 316 stainless steel atomizing nozzle incorporated into the top of the vaporizer (J-300). The hot tertiary hydrogen/methane mixture atomizes and vaporizes the liquid silicon source, and the resulting vapor is carried to the torch via a heat traced Monel supply line.

Two freestanding consoles house all system instrumentation and shutdown logic. The torch control console was supplied with the torch/power supply system. The system control console was constructed on-site. Each console incorporates discrete shutdown systems which are inter-connected to permit a shutdown of the entire system in an emergency situation. The control logic of both consoles are depicted in the logic ladders included as Figures III and IV.

The torch control console monitors the operation of the torch via current and voltage displays, and includes a rheostat which is used to vary the total DC electric power supplied to the torch. Additionally, the torch control console functions as a gas mixer for primary and secondary torch gases. Primary and secondary hydrogen and argon (Streams 5, 6, 8 and 9) enter the torch control console from the rear. Both hydrogen inlet lines have normally closed solenoid valves (FV 110 and 210) that do not open unless sufficient voltage (80 V) is available to the torch for successful hydrogen operation. Since the main safety logic circuits disable the DC power supply in the event of any upset, these valves exclude combustible gas from the unit in the event of an emergency shutdown. Both primary gas inlets have console- mounted pressure gauges (PI 110 and 120) and gas rotameters (FI 110 and 120). The primary argon inlet (Stream 6) and total primary torch gas (Stream 11) have in-line, low-pressure switches (PSL 120 and 160) which disable the DC power supply, unless minimum pressure and an inferred minimum flow exists in the primary gas to the torch. This interlock system is backed up by low flow shutdown setpoints in the primary gas flow controllers (FSL 110 and 120) upstream of the torch control console.

Secondary argon and hydrogen (Streams 8 and 9) are blended together after passing through their respective gas rotameters (FI 210 and 220). An auxiliary gas feed system is incorporated in the console and includes a separate console-mounted pressure gauge (PI 080, not sown in drawing) and gas rotameter (FI 080). This stream can be diverted to either the primary

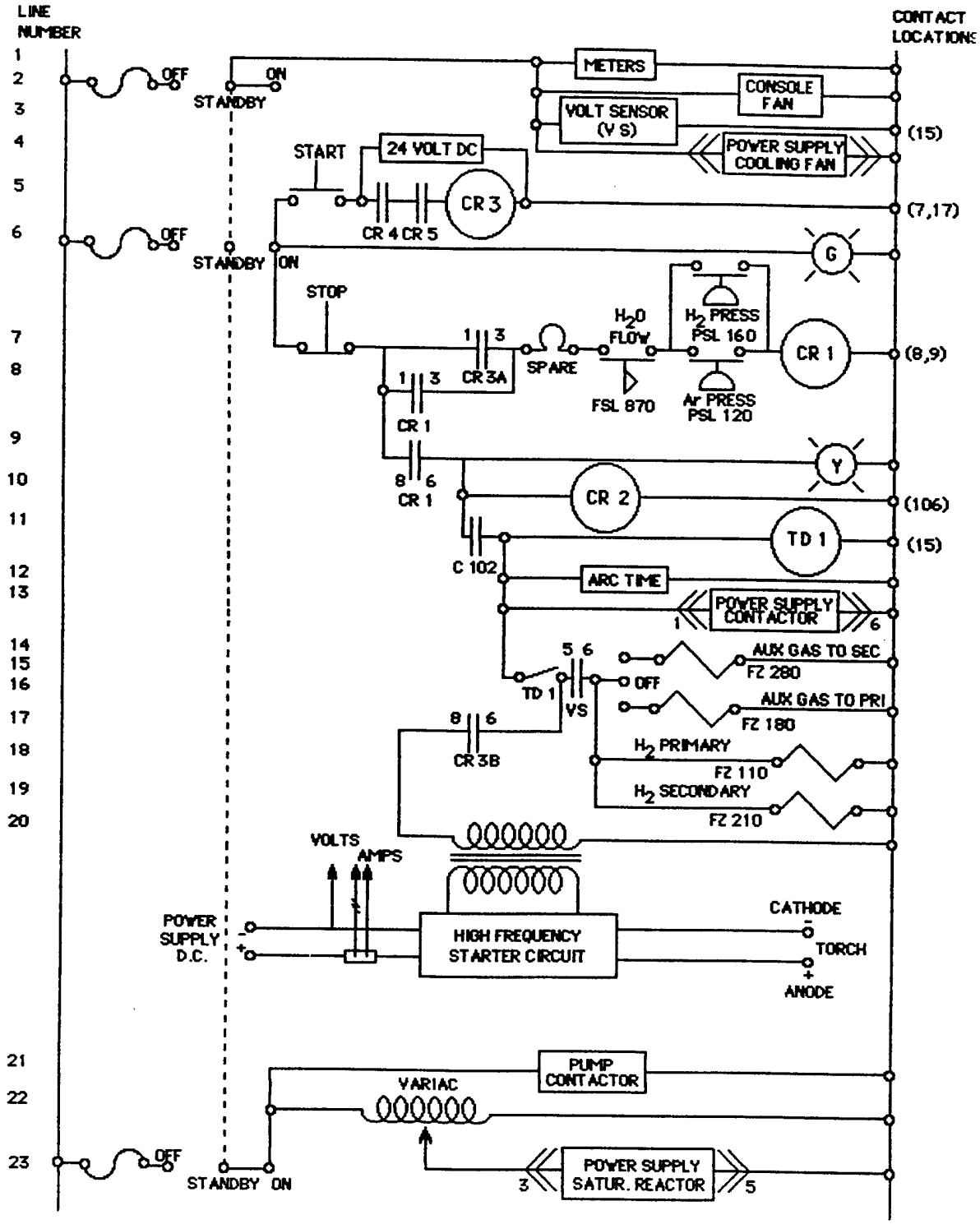

FIGURE III

TORCH CONTROL CONSOLE

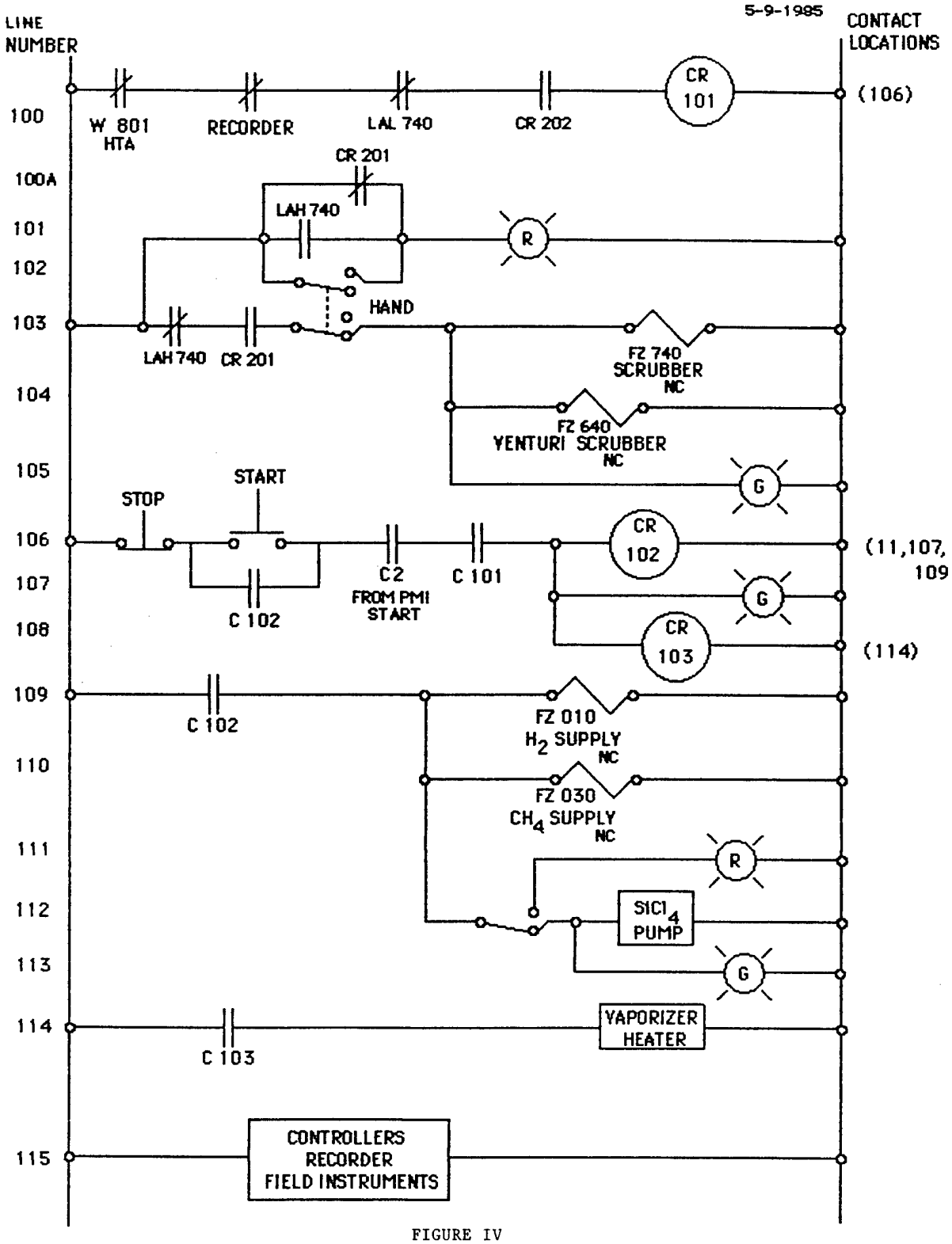

FIGURE IV
SYSTEM CONTROL CONSOLE

or secondary torch gas by electrically opening one of the normally closed solenoid valves (FZ 180 and 280) provided. Since this function was not typically used, block valves were installed to prevent backflow through this system.

The torch control console also includes the closed-loop cooling water monitoring system. A separate closed loop of deionized cooling water is provided to cool the torch. Coolant flows from the 12-gallon closed loop cooling water reservoir (S-800), through the circulating pump (P-800) and to the torch control console. The coolant flows through a water rotameter (FI 870) and the supply temperature is displayed on the console by a digital readout (TI 870). A low flow switch is included in this line to disable the DC power supply when coolant flow is less than 4.5 gallons per minute. The coolant then flows to the torch assembly and returns to the console. The return temperature is displayed on a second digital readout (TI 871) and the coolant is returned to the reservoir after being cooled by once-through cooling water in the torch cooling water chiller (E-800). The once-through cooling water supply is equipped with and anti-backflow check valve and a bypass valve around the heat exchanger. To prevent condensation on the cooling lines, it is sometimes desirable to bypass once-through cooling water around the torch cooling water chiller and allow the closed loop coolant temperature to rise to about 100°F. The total flow of once-through cooling water cannot be reduced, since the spent water is used to cool the reactor/aftercooler (E-500), described previously.

The system control console includes a Westronic DDR-10 multipoint recorder, the Moore digital flow and level controllers (FIC 110, 120, 210, 220, 310, 330 and LIC 740), a West 801 high temperature alarm unit (TSH 581), a watt transducer (JT 360), a Triac controller for the preheater and vaporizer heating tapes, on/off controls for the silicon source metering pump (P 400), and tail gas scrubber water solenoid valves (FZ 640 and 740).

Before disposing of reaction product to flare, it is necessary to remove hydrochloric acid by-products and silicon carbide particulate matter. The cooled gas and solids flow from the dust hopper to the inlet of the Venturi scrubber through a section of one-inch BWG 12 Monel 400 tubing. The tube exits the top of the dust hopper, rises to a point nine feet above grade, makes a long radius 90° bend to horizontal, then doglegs downward to the inlet of the Venturi scrubber. This routing is to avoid possible flooding of the reactor/aftercooler in the event the tail gas scrubber floods. It also assures that the water introduced to the process stream in the Venturi scrubber drains into the tail gas scrubber, rather than into the dust hopper.

The Venturi scrubber is fabricated from a one inch Swagelok union T, a Spraying Systems Whirljet hollow cone water nozzle, and a custom Hastalloy converging/diverging nozzle insert. Process gas enters the T and is intimately mixed with 0.5 gallons per minute of water flowing through the Whirljet nozzle. The mixture is then forced through the converging/diverging nozzle to impact the particulates onto the surface of the water droplets. The resulting mix flows downward and drains into the tail gas scrubber (T 700).

The tail gas scrubber is constructed from an 11-foot section of schedule 40 type 304L stainless steel welded pipe. The pipe is fitted with 150# RF flanges at each end, a three-inch flanged (150# RF) feed nozzle 48 inches from the bottom (Stream 16), a two-inch flanged (150# RF) emergency relief nozzle 54 inches from the bottom (for rupture disk PSE 740, 15 psig burst pressure), a 3000#, 3/4-inch coupling for sight glass and pressure gauge 54 inches from the bottom (LG 740 and PI 740), and a two-inch flanged (150# RF) scrubbing water inlet (Stream 23) twelve inches from the top. The blind flange which serves as the vessel bottom is drilled and tapped for a 1-1/2-inch NPT drain line (Stream 17), a 3/4-inch NPT sight glass connection (LG 740) and a 3/4-inch port for a capacitance level transducer installed in a filtered stillwell (LT 740). The bottom drain line is fitted with a sample connection for the removal of an aliquot sample of the bottoms stream, which is normally sent to the city sewer system on level control. In full open position, level control valve LCV 740 drains the column faster than water can be supplies. The equilibrium sump level is about six inches with no system pressure above the fluid.

The top of the tower is packed with a four-foot bed of 5/8-inch Monel slotted rings washed with spent once-through cooling water coming from the the reactor/aftercooler cooling coils and distributed by three Whirljet hollow cone spray nozzles located eight inches above the packing. Six inches of stainless steel demister pads are above the spray nozzles. Scrubbed overhead gas exits the top of the unit through a 1-1/2-inch carbon steel tubing vent line seal welded to the top flange. A small nitrogen sweep assures positive flow down the flare to the facility thermal oxidizer.

Task II - Development of a Theoretical Model

The previously mentioned proprietary studies conducted by the Carborundum Company before contract activities began resulted in the development of a working model of plasma reactor systems. This preliminary study served to establish an operating regime in several of the critical system parameters for the $SiCl_4/CH_4/H_2/A$ system, including reaction temperature, reactant ratios,

reactant concentration, and mass flowrate. The range of these parameters is given in Table II. Principal conclusions of the prior work were:

A. Thermochemical equilibrium was attained in all instances at residence times of less than 17 milliseconds.

B. Formation of beta silicon carbide powder is favored by the use of reactant mixtures with high hydrogen to carbon ratios.

C. Specific surface area (i.e., particle size) is exponentially dependent upon absolute reactant concentration levels, with lower areas resulting from higher concentrations.

D. Hydrogen is more effective than argon on an equimolar basis in promoting the formation of beta silicon carbide.

E. High purity levels can be achieved in a plasma synthesis reactor.

F. The potential for surface area control (i.e., particle size) is high.

To augment the prior studies, a subcontract was let to International Thermal Plasma Engineering, Inc. for the development of a model of temperature and flow fields in the reactor. A copy of International Thermal Plasma Engineering's final report is attached as Appendix A.

Prior to the modelling work, system operating conditions (reactant and gas flow rates, heat exchanger data, torch power levels) and system geometry (torch exhaust and reactor design) were provided to International Thermal Plasma Engineering. Based upon this data, mathematical models for the computation of flow and temperature fields in the reactor were developed. Numerical models for turbulent as well as laminar flow were developed, and a composite of both models was studied in detail. A model for the thermodynamic and transport properties of mixed gases was also developed. Equilibrium calculations for the $SiCl_4/CH_4/H_2/Ar$ system were also studied. A brief review of reaction kinetics was made, as well as a literature review of nucleation and growth of fine particles in gas phase reactions.

The major conclusions of the study included:

A. The turbulent flow region is limited to the region where the plasma jet enters the reactor for a distance of approximately 100 mm. The inlet jet rapidly decays, such that the axial gas velocity drops to about 140 m/s at a point 190 mm downstream of the reactor inlet.

TABLE II

TYPICAL OPERATING CONDITIONS FOR SURFACE AREA ≤50 M^2/G $SiCl_4$ REACTANTS

Molar Ratios	
:CH_4/Si	1.1 - 2.45
:H/Si	30 - 160
Reaction Temperature	1850 - 3000 (°K)
Plasma Gas	Ar
Reactor Pressure	Atmospheric
Plasma Inlet Temperature	5200 - 11,200 (°K)
Chlorosilane Concentration	0.27 - 1.64 (mole fraction x 10^2)
Mass Flowrate	6.7 - 17.7 (moles/min)

B. The transition from turbulent to laminar flow at the reactor inlet permits significant recirculation of reactant gases and product at the reactor inlet.

C. It is possible that the flow in the entrance recirculation zone is turbulent, with the flow re-attaching to the reactor walls downstream and in laminar flow.

D. The inlet turbulence is not beneficial to the process. Under the assumption of constant reactor wall temperature, between 45 and 65% of the net energy supplied to the reactant gases will be lost to the reactor walls in the ten percent of the reactor length.

E. Higher gas flow rates sustain higher gas temperatures away from the reactor inlet.

Task III - Baseline Characterization and Analytical Method Development

In parallel with construction of the bench scale facility, methodologies to characterize powders were underway. The developed characterization was utilized to access product property control and to monitor process improvements as the project continued.

Initially, two commercially produced silicon carbide powders were to be characterized: H. C. Starck, Inc. (West Germany) A10 Grade; and Carborundum Company submicron alpha silicon carbide. Since both of these powders were alpha phase, it was decided to characterize one beta powder as well, H. C. Stark B10 Grade.

The parameters characterized and the methodologies used included the following:

A. Pressureless Sinterability - percent of theoretical density achieved with and without sintering aids.

B. Surface area - B.E.T. surface analysis.

C. Degree of Agglomeration - tap density.

D. Particle Size Distribution - Horiba particle size analyzer.

E. Phase Distribution - X-ray diffraction.

The results of characterization of the three powders are depicted in Table III.

TABLE III

SUMMARY OF THE CHARACTERISTICS OF THE BASELINE POWDERS

	Starck B-10	Starck A-10	Standard Oil
Chemistry (wt%)			
Total Carbon	30.49	30.30	29.95
Free Carbon	1.83	1.54	0.36
Free Silicon	0.40	0.29	0.09
Oxygen	0.90	0.76	0.27
Iron	0.04	0.03	<0.01
Silicon Carbide[1]	95.50	96.60	98.80
Physical Properties			
Major Phase	Beta	Alpha	Alpha
Median Particle Size (μm)	1.0	1.4	1.2
Surface Area (m^2/g)	15.3	14.3	9.4
Sinterability[2]			
Green Density (g/cm^3)	2.01	2.09	1.67
Fired Density (g/cm^3)	3.03	3.09	3.20

[1] Obtained from carbon balance.
[2] With typical sintering aids.

Task IV - Screening Experiments

Task IV was divided into subtasks for management and reporting purposes.

The first subtask was to characterize the operation of the plasma torch using a hydrogen/argon blend. It should be noted that the original work scope included a short series of experiments to investigate the feasibility of using a hydrogen plasma in lieu of argon. This could be advantageous as hydrogen is a reactant (to scavenge chlorine from the silicon source) and the argon (necessary only as a carrier of energy) could potentially be reduced or eliminated.

As both Standard Oil and the torch vendor, Plasma Materials, Inc., were confident that the torch would operate with a very rich hydrogen to argon blend, it was decided to accomplish this subtask first.

Concurrent with that subtask, careful consideration was given to the choice of the individual variables for the screening experiments. The candidate feedstocks were described in the statement of work, but the values (or range of values) for temperature, carbon/silicon ratio and reactant concentration had to be established.

A matrix of screening experiments was developed to incorporate two levels of each of the variables for each feedstock. The candidate feedstocks are as follows:

Reactant 1: silicon tetrachloride ($SiCl_4$)

Reactant 2: dimethyldichlorosilane [$(CH_3)_2SiCl_2$]

Reactant 3: methyltrichlorosilane (CH_3SiCl_3)

Once the plasma torch had been stabilized on a very rich H_2/Ar blend, silicon feedstock ($SiCl_4$) and methane were added to the system. Several short runs were made, and the powder produced was determined to be beta SiC.

Several debugging problems occurred which aborted many of the initial runs. Some of these problems included the silicon feed pump, the tail gas scrubber level transducer, and a cooling water leak into the plasma torch. All items were satisfactorily resolved.

The torch and reactor system also experienced plugging problems which limited run times; some as short as five minutes. Minor anode configuration changes were made which have since allowed runs up to three hours in

duration. Runs of approximately one-hour duration have generated representative material in sufficient quantities for analysis.

At this point, the work plan called for the initiation of screening experiments; a matrix of 24 variations of temperature, carbon to silicon ratio, and reactant concentration (defined as hydrogen to chlorine ratio). However, a priority was placed upon establishing the consistency and reproducibility of the process. The work plan was modified to first run four prescreening experiments to establish a consistent baseline; then to prioritize the screening experiments (focusing primarily on silicon tetrachloride feedstock). Eight experiments (six using silicon tetrachloride and methane and two using dimethyldichlorosilane) were initially run and the results analyzed. Upon completion of the analytical results of those powders, the remainder of the matrix was completed.

Table IV summarizes the result of the screening experiments. The prime determinants of the quality of the powders produced were: percent SiC, percent free carbon, and percent free silicon.

Based on the results of the screening experiments, methyltrichlorosilane was chosen as the best feedstock to be carried forward to the parametric studies.

Though the other feedstocks may also be suitable, methyltrichlorosilane provided the widest operating window.

Task V - Extended Parametric Studies

This task was intended to further evaluate the process parameters of the feedstock selected at the conclusion of the screening experiments -- methyltrichlorosilane. The parameters to be evaluated included temperature, silicon feedstock flow rate, and hydrogen/chlorine ratio.

One of the first activities for this task was to produce a substantial amount of powder by running methyltrichlorosilane at the best known conditions in order to perform some initial sinterability studies.

Approximately 80 grams of powder were produced, analyzed, and sintering trials were performed.

Analysis of the powder revealed very good chemistry:

Percent SiC	97.5
Percent Free Carbon	0.15
Percent Free Silicon	0.13

TABLE IV

RESULTS OF SCREENING EXPERIMENTS

	No. of Conditions	% SiC	% Free Carbon	% Free Silicon
Silicon Tetrachloride	8	43.9-81.4	2.89-9.32	1.04-3.63
Dimethyl Dichlorosilane	7	46.8-91.2	0.60-4.46	0.16-8.38
Methyl Trichlorosilane	8	76.1-97.9	1.09-3.23	0.03-1.04
Goal		>95.0	<2.0	Minimum

Sintering to 89% and 92% of theoretical density was achieved with normal sintering additives. Though sintering conditions for beta SiC powders had not been optimized, these initial results were considered to have established the ability to sinter the powder produced by this process. Scanning electron micrographs of the powder are shown in Figures V and VI. A photograph of the beta SiC powder and a sintered disc fabricated from it is shown in Figure VII.

The H/Cl ratio could be specifically controlled but temperature could not, nor could it be precisely measured. Therefore, net input power (kw) was varied instead to provide the desired variation in temperature. Also, the flow of feedstock through the system is described by the theoretical rate of SiC production in grams per hour.

A total of 14 sets of unique conditions were run as shown in Table V. These were selected based upon being the most promising areas of the matrix and being within the operating range of the reactor. Powders were produced with a very wide range of operating conditions during the parametric studies. All except one experiment yielded greater than 90% SiC purity. The analytical results for the low 84.8% SiC content had a very poor material balance closure, so that particular number is suspect.

There appeared to be little correlation of the three chosen parameters with the analytical results obtained. However, half of the conditions run gave powders with 95% purity or higher, indicating a wide range of acceptable conditions.

At the completion of the parametric studies, a small sample was prepared for submission to the ORNL Technical Monitor to complete Phase I.

A sinterability trial of this sample of powder achieved 86% of theoretical density. A summary of the characteristics of this powder compared to the baseline powders is shown in Table VI. A photograph of a similar sample of powder with a sintered specimen is shown in Figure VII.

Phase II

Task I - Process Scale-Up

A. Scale

Towards the end of the extended parametric studies, project activities were extended to include scouting experiments to qualify a larger pilot-scale facility with increased production capacity. A number of questions were unresolved as a result of the baseline Phase I activities, and work was conducted to address these issues. The primary questions divided

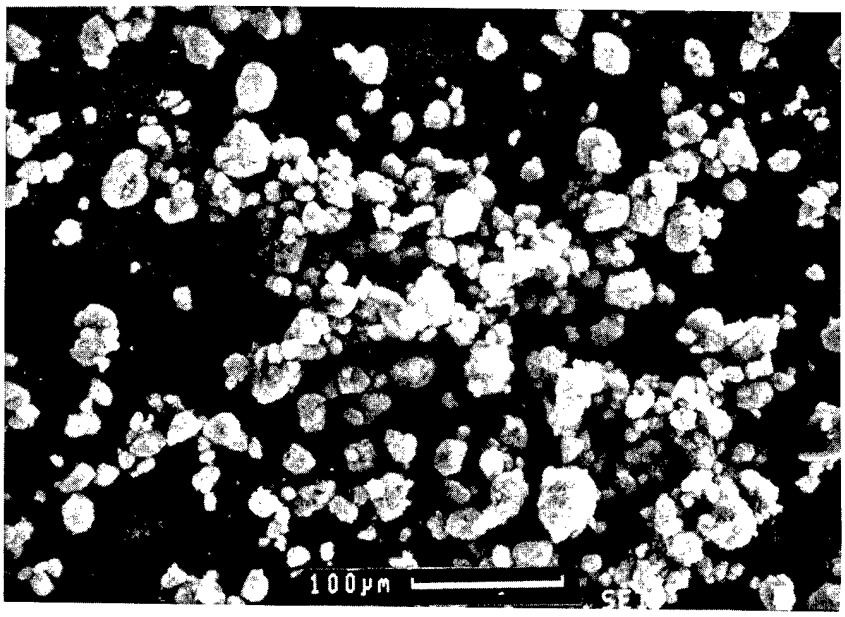

FIGURE V

SCANNING ELECTRON MICROGRAPH OF
TASK V BETA SiC POWDER

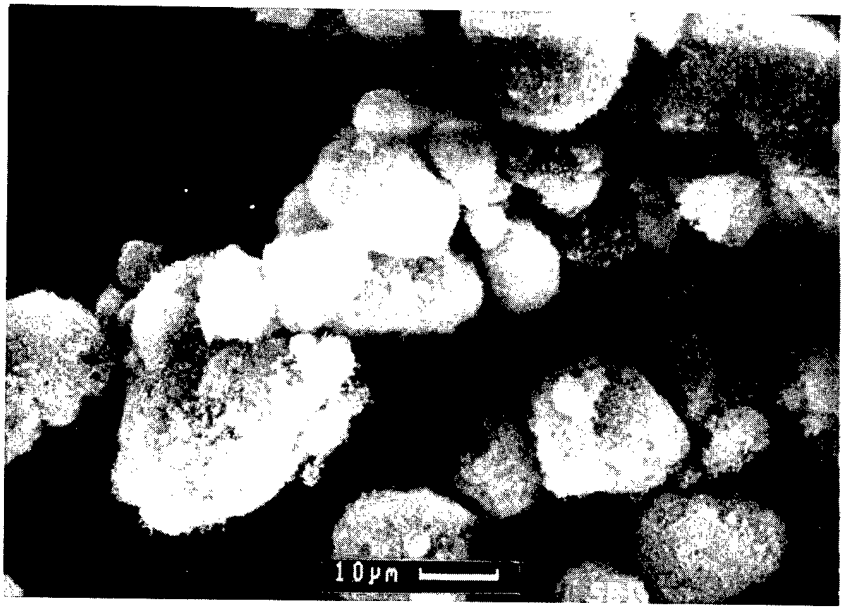

FIGURE VI

SCANNING ELECTRON MICROGRAPH OF
TASK V BETA SiC POWDER

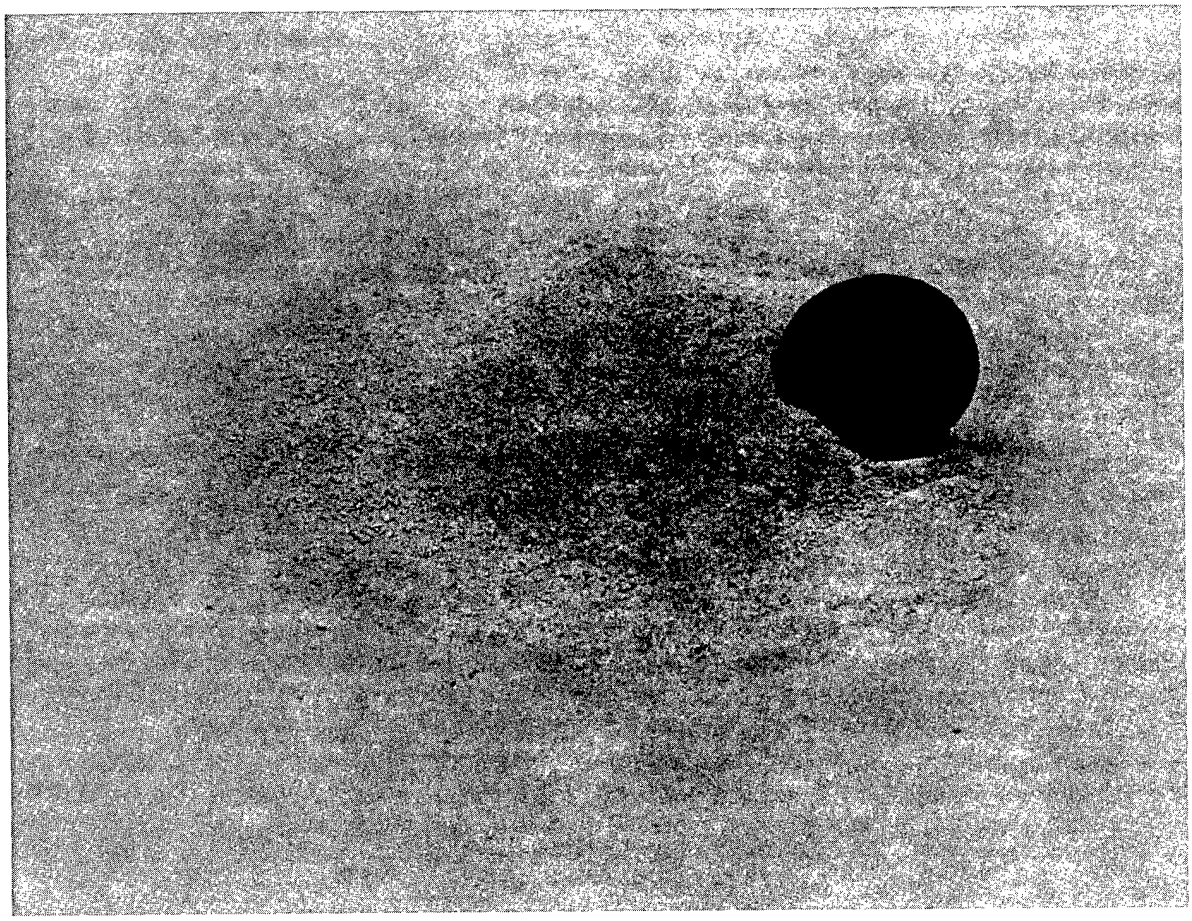

FIGURE VII

A SAMPLE OF POWDER AND SINTERED SPECIMEN

TABLE V

SUMMARY OF PARAMETRIC STUDIES

Total SiC %	Theoretical SiC Production Rate	H/Cl Ratio	Net Input Energy
97.5	High	Medium	High
97.5	Medium	Medium	Low
96.1	Medium	Low	Medium
95.8	Low	High	Low
95.7	High	Medium	Medium
95.3	High	Low	Low
95.2	Medium	High	Low
94.9	Medium	High	High
93.6	Low	Medium	Medium
92.8	High	Low	Low
92.6	Medium	High	Low
92.4	Low	High	Low
91.9	Medium	Medium	High
84.8	Medium	High	Low

TABLE VI

SUMMARY OF THE CHARACTERISTICS OF THE POWDER PRODUCED UNDER THIS SUBCONTRACT COMPARED TO THE BASELINE POWDERS

	Phase I Gas Phase	Starck B-10	Starck A-10	Standard Oil
Chemistry (wt%)				
Total Carbon	29.55	30.49	30.30	29.95
Free Carbon	0.35	1.83	1.54	0.36
Free Silicon	0.09	0.40	0.29	0.09
Oxygen	0.58	0.90	0.76	0.27
Iron	<0.01	0.04	0.03	<0.01
Silicon Carbide[1]	97.33	95.50	96.60	98.80
Physical Properties				
Major Phase	Beta	Beta	Alpha	Alpha
Median Particle Size (μm)	0.75	.10	1.4[1]	1.2
Surface Area (m^2/g)	10.0	15.3	14.3	9.4
Sinterability[2]				
Green Density (g/cm^3)	1.89	2.01	2.09	1.67
Fired Density (g/cm^3)	2.76	3.03	3.09	3.20

[1] Obtained from carbon balance.
[2] With typical sintering aids.

into two general categories: What should the general scaling factor for the larger unit be, and what should be done to address operability issues experienced in Phase I?

The original project scope envisioned silicon carbide powder production rates of 50 to 100 grams per hour in Phase I, with a five to ten-fold scale-up in Phase II. Thus, an ultimate capacity of 250 to 1000 grams per hours was the total project goal. With this target in mind, the original Phase I bench-scale unit was designed and constructed with the requisite flexibility and capability to run at production rates between 50 and 500 grams per hour. This approach would permit the Phase II activities to be performed using a slightly modified version of the Phase I facility.

In the course of Phase I experimental work, it was decided to increase the production rate of the unit. In fact, theoretical production rate became a variable in the parametric study (See Table V). At the conclusion of Phase I, a production rate of 450 grams per hour was achieved, with excellent product powder properties.

Based upon the experience of Phase I, an analysis to determine an appropriate scaling factor for Phase II was executed. The primary issues addressed were: torch and power supply capabilities, heat dissipation in the reactor/aftercooler section, product collection capability, feedstock delivery issues, and effluent treatment and disposal. After internal review and consultation with the project administrator, a seven-fold scale-up factor was chosen. The proposed facility would have a nominal seven pounds per hour production capacity.

B. Effluent Cooling

Operability issues focused on the ability to cool product gases to sufficiently low temperatures to permit removal of the product powders. The initial concept utilized a large recycle of cooled effluent gas to quench the hot reactor effluent. Such a system would cool the effluent gases to a manageably low temperature, then remove the product powder in a relatively cool filter element. The clean gas downstream of the filter could then be cooled with a standard gas/liquid heat exchanger with no fouling problems and the associated decrease in heat exchanger efficiency. Because of the low heat capacity of the hydrogen reactant gas, however, the volumetric requirements for such recycle became prohibitive in terms of compressor horsepower and requisite piping sizes.

An alternate approach was then considered. If cooling of the powder-laden gases was attempted, the product powder would quickly coat the heat exchange surfaces due to thermophoresis. If the powder was allowed to accumulate, the heat exchange surface would quickly become fouled and heat dissipation would drop. Thus, a method for removing the powder from the heat exchange surfaces was required before such a system was considered.

Extending the concept of a cooled reactor to the Phase II facility indicated that a nominal eight-inch diameter reactor tube would be required for adequate heat dissipation. A 12-inch long, 8-inch internal diameter prototype reactor which could be attached to the top of the Phase I reactor was fabricated. This unit was used to determine the viability of such a reactor, as well as to experiment with methods for removing product powder from the cooled reactor walls.

Removal of product powder using mechanical scrapers was considered, but quickly rejected due to the required complexity of the required apparatus. The primary effort focused on pneumatic removal of the powder. It had been noticed that the product powder did not cling tenaciously to the reactor surfaces and could easily be dislodged with a brush or water jet. Compressed gas was chosen as the best candidate for powder removal.

The eight inch prototype reactor was fitted with a single 1/8-inch diameter gas jet entering the midline of the reactor (i.e., six inches from the top of the prototype unit). The jet was orient in a manner that the gas stream entered the reactor vessel exactly tangential to the reactor wall. A 250-milliliter pressure vessel was supplied with 40 psig argon gas at room temperature. This pressure vessel was connected to the gas jet through a normally closed, electrically activated solenoid valve. Using a momentary contact switch and timer circuit, it was possible to pulse argon gas through the jet.

The prototype reactor was mounted, and the system was run for 30 minutes. The reactor was disconnected and opened for inspection. As expected, the walls were coated with a uniform layer of silicon carbide powder approximately two-millimeters thick. The reactor was remounted, and the solenoid valve actuated for 0.5 seconds. After removal, the reactor was re-inspected and all powder was removed from an area defined by an angle of 30 degrees above and below the jet entry point (a 60 degree included angle), extending around the reactor interior for approximately 3/4 of the perimeter.

The prototype reactor was cleaned and remounted. The system was started, and the solenoid pulsed for 0.5 seconds every 15 minutes of powder synthesis. After one hour of operation and four pulses, the prototype reactor was removed and inspected. As before, all material had been dislodged from the reactor wall. No disruption to the operation of the plasma torch was discernible during the test.

Since implementation of tangential gas jets on the pilot-scale unit would require multiple vessel penetrations, welds, and possible leak points, a second method was also explored. Instead of multiple fixed gas jets, a small number of movable gas jets were tested. A ring of 1/2-inch diameter stainless steel tubing was bent into a circle with an outer diameter 1/2 inch smaller than the inside diameter of the prototype reactor. The ring was drilled with twenty holes, each 1/32 inch in diameter. The ring was then welded to a supply tube of 1/2-inch diameter stainless steel tubing. The supply tube was oriented in a manner that permitted the ring to be lowered down the reactor through a packing gland, and would permit the jets to sweep the entire interior surface of the reactor. Argon was supplied to the ring at a rate of 20 standard liters per minute, and the ring stroked the length of the reactor after 15 minute intervals of powder synthesis for a period of one hour (four cycles).

Generally, the powder was cleared from the reactor wall, except for two streaks which, apparently, were due to a plugged gas jet. No apparent wear was noted on the packing gland, but microscopic examinations of the packing was not made. No hydrogen gas leaks were detected by the area combustible gas alarms on the unit. Due to the ease of implementation of the gas ring system, this method was chosen for Phase II, with the fallback position of revamping the reactor tube for tangential jets, if required later.

C. General Considerations

With the issue of gas cooling addressed, the rest of the system had to be designed for the increased capacity required. Increasing the size of the gas metering and induction system, the methyltrichlorosilane delivery system and the tail gas scrubber were straightforward engineering problems. A Piping and Instrumentation Drawing of the Phase II facility is attached as Figure VIII. A heat and material balance of the various process streams is included as Table VII. Instrumentation specification sheets are included in Appendix B.

As mentioned above, the reactor was increases to a nominal eight-inch diameter for heat dissipation considerations. The reactor was constructed from a 72-inch length of schedule 40, 316L stainless steel

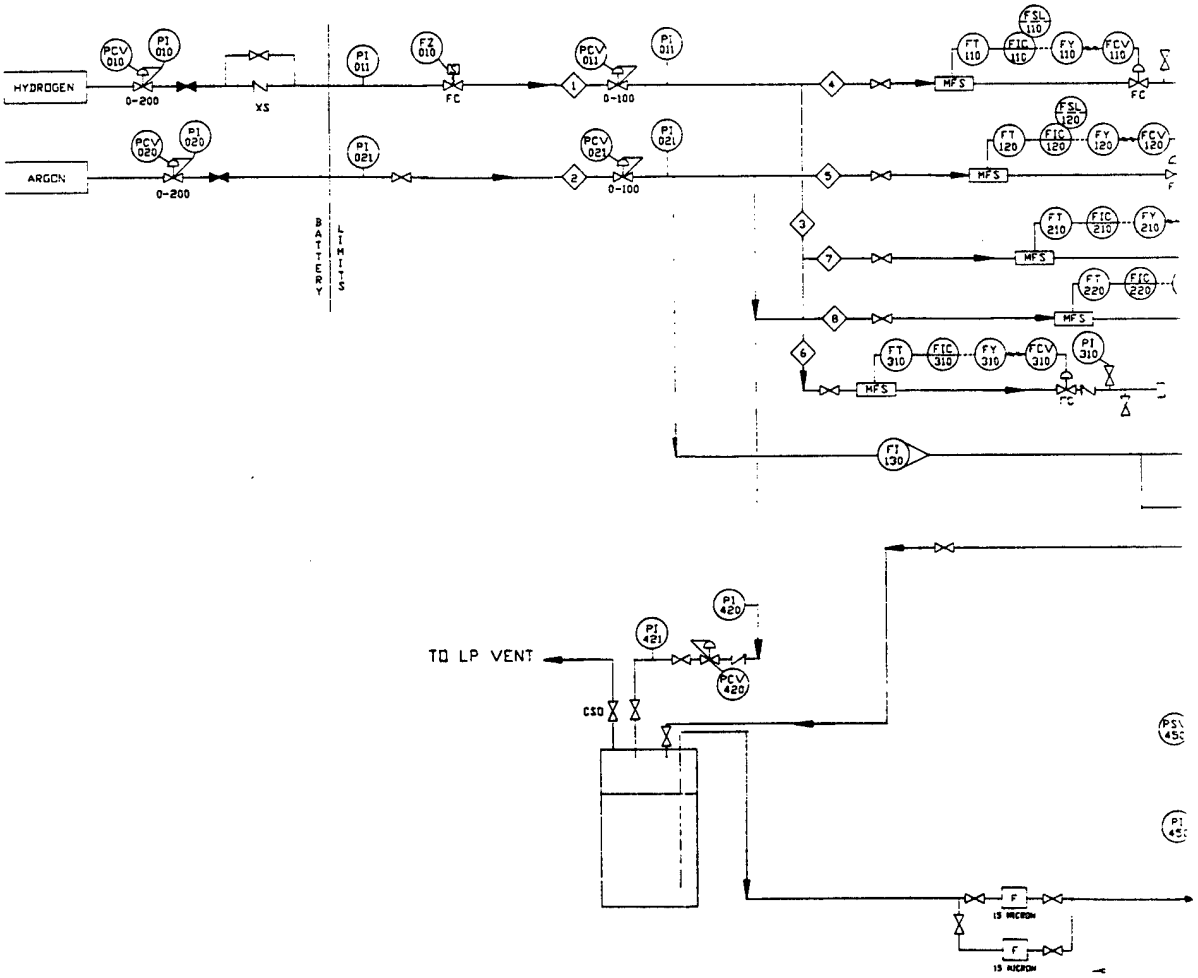
HYDROGEN
ARGON
PCV 010
PI 010
0-200
XS
PI 011
FZ 010
FC
PCV 011
0-100
PI 021
PCV 020
PI 020
PCV 021
BATTERY LIMITS
FSL 110
FT 110
FIC 110
FY 110
FCV 110
MFS
FSL 120
FT 120
FIC 120
FY 120
FCV 120
FT 210
FIC 210
FY 210
FT 220
FIC 220
FT 310
FIC 310
FY 310
FCV 310
PI 310
FI 130
TO LP VENT
PI 420
PI 421
PCV 420
CSO
F
15 MICRON

FIGURE VIII

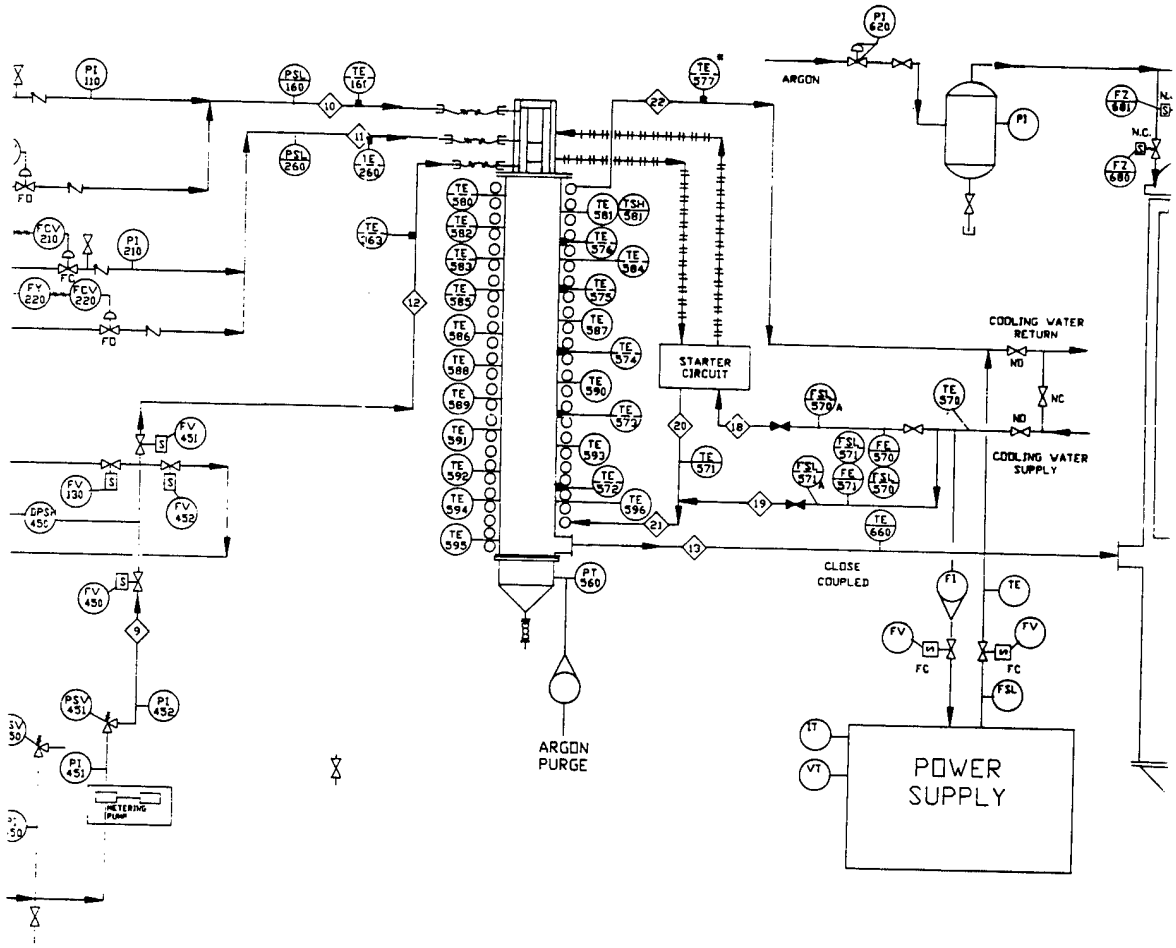

FIGURE VIII (CONT.)

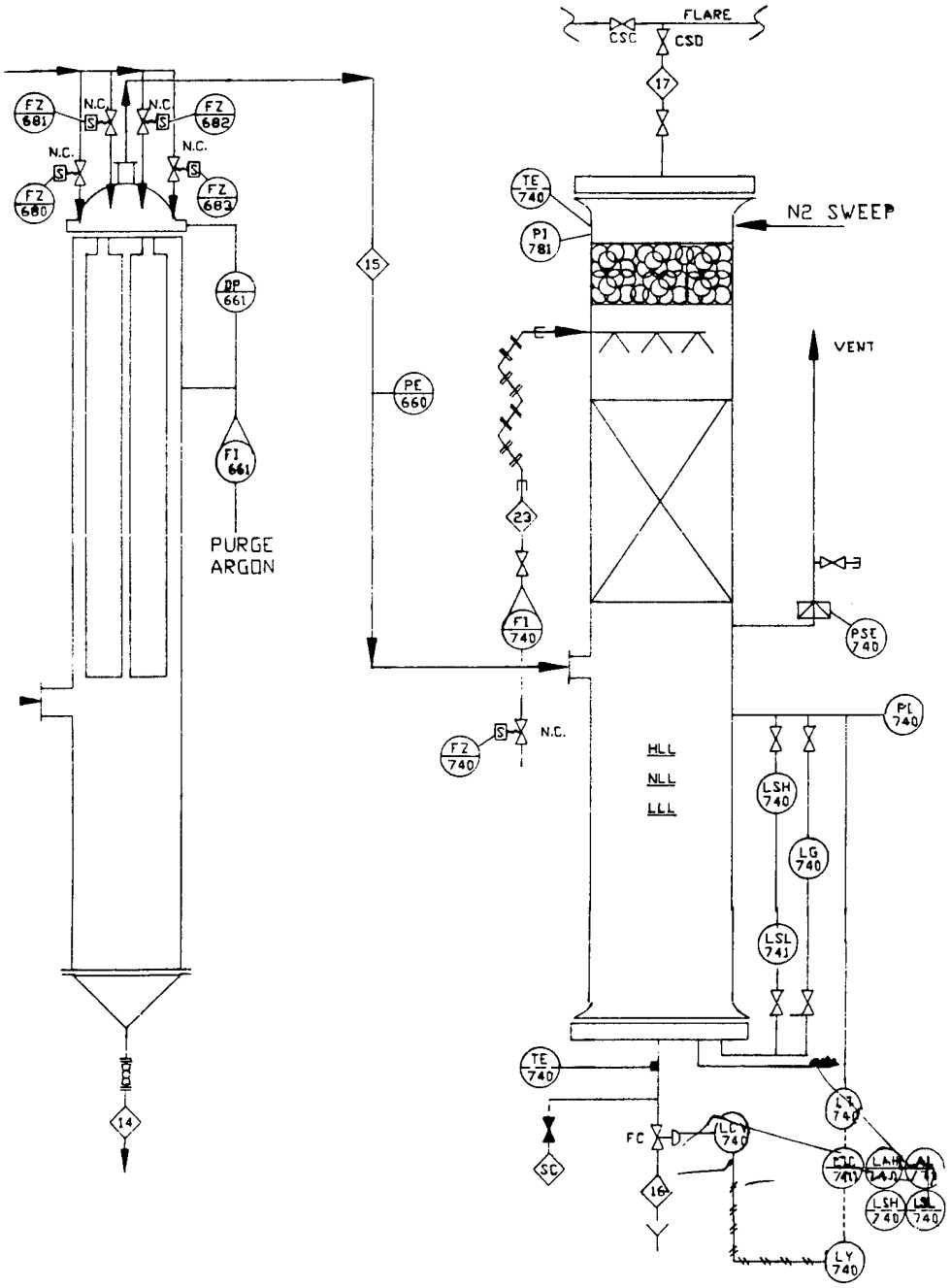

FIGURE VIII (CONT.)

TABLE VII

HEAT AND MATERIAL BALANCE

Species (lb/hr)	Total H_2	2 & 3 Ar	Primary Hydrogen
Argon			
Hydrogen	42.05	37.81	4.86
CH_3SiCl_3			
Silicon Carbide			
Hydrogen Chloride			
Water			
Total	42.05	37.81	4.86
Temperature, °F	70	70	70
Pressure, psia	65	65	65
Mol Frac Vapor	1.00	1.00	1.00
Molecular Wt.	2.02	2.02	2.02
GPM			
SCFH	7614.58	6758.29	564.24
SLM	3594.06	3186.13	407.92

TABLE VII, cont.

Species (lb/hr)	Tertiary Hydrogen	Secondary Hydrogen	Methyltri-Chlorosilane
Argon			
Hydrogen	6.77	24.31	
Ch_3SiCl_3			37.28
Silicon Carbide			
Hydrogen Chloride			
Water			
Total	6.77	24.31	37.28
Temperature, °F	70	79	70
Pressure, psia	65	65	50
Mol Frac Vapor	1.00	1.00	0.90
Molecular Wt.	2.62	2.02	149.47
GPM			0.06
SCFH	2429.61	4820.48	
SLM	1146.87	2039.27	

TABLE VII, cont.

Species (lb/hr)	Tot Primary Gas	Tot Secondary Gas	Tot Tertiary Gas	Reactor Effluent
Argon				
Hydrogen				42.83
Ch_3SiCl_3	4.86	24.31	6.77	
Silicon Carbide				10.00
Hydrogen Chloride				27.28
Water				
Total	4.86	24.31	6.77	80.11
Temperature, °F	70	79	70	70
Pressure, psia	65	65	65	10
Mol Frac Vapor	1.00	1.00	1.00	
Molecular Wt.	2.62	2.62	2.62	3.61
GPM				
SCFH	804.24	4820.48	2429.01	7968.90
SLM	407.92	2039.27	1146.07	3761.70

TABLE VII, cont.

Species (lb/hr)	SiC Product	Reactor Offgas	Tall Gas Scrbr Sott	Effluent Gas	Torch CW Supply
Argon					
Hydrogen		42.03		42.03	
Ch_3SiCl_3					
Silicon Carbide	10.00				
Hydrogen Chloride		27.20	27.05	0.23	
Water			2502.07	7.46	4006.20
Total	10.00	70.11	2530.92	50.52	4066.20
Temperature, °F	300	300	70	70	70
Pressure, psia	19	19	21	19	0
Mol Frac Vapor		1.05	0.05	0.05	0.05
Molecular Wt.	49.01	3.19	18.12	2.20	18.02
GPM					0.06
SCFH		7969.08	5.00	8117.00	
SLM				3031.26	

TABLE VII, cont.

Species (lb/hr)	Add'l Reactor CW	Torch CW Return	Tot RXR CW Supply	Total RXR CW Return
Argon				
Hydrogen				
Ch_3SiCl_3				
Silicon Carbide				
Hydrogen Chloride				
Water	3505.43	4000.20	7511.03	7511.63
Total	3505.43	4000.20	7511.03	7611.63
Temperature, °F	70	70	74.26	110.36
Pressure, psia	65	65	65	25
Mol Frac Vapor	0	0	0	0
Molecular Wt.	10.02	10.02	10.02	10.02
GPM	7.00	0.00	15.00	10.02
SCFH				
SLM				

welded pipe, which has an inside diameter of 7.981 inches. The reactor tube was fitted with eleven 3/4-inch 3000# couplings to permit addition of sight glasses, chemical injection ports, or pressure taps. The entire reactor tube was helically wrapped with four, 50-foot lengths of 5/8-inch diameter soft copper tubing which were manifolded together to provide four discrete cooling zones. A 1-1/2-inch 150# RF flanged nozzle exited the reactor tube six inches from the bottom and connected to the particulate collection system (described below) by a short, flanged spool piece. The entire assembly was coated with Thermon heat conduction concrete to assist in heat transfer to the cooling coils. In addition, a conical bottom piece with a 1-1/2 flange was connected to the reactor to permit product collection.

Due to the nature of the larger system, however, a larger plasma torch and power supply would be required and a more effective particulate collection system would be needed. In addition, a more sophisticated control and data acquisition system would be needed to assure safe operation of the system.

D. Torch

The original scaling studies indicated that 200 kilowatts was a maximum power level attainable by available plasma torches in hydrogen service. Norton was the vendor again chosen to provide the plasma torch. A Model AA-61 gas heater was selected and qualified at 150 kilowatts on pure hydrogen at Norton's facility. A sectional view of the Phase II torch is provided as Figure IX.

E. Power Supply

Norton could not, however, provide a single power supply capable of providing sufficient power for the Phase II work. Alternate power supply vendors were contacted, and Walker Power, Inc., selected to provide a 288 kVA power supply capable of operating at 240, 480, and 986 volts (open circuit) at 1200, 600, and 300 amps, respectively. The power supply was also provided with four 40-millihenry chokes to stabilize the plasma arc. A schematic of the power supply is provided as Figure X. Prior to acceptance of the power supply, an eight-hour "burn-in" using a resistive load was conducted in the vendor's shop. The power supply operated well at all power settings during the testing. The power supply was equipped with water-cooled rectifiers to obviate the need for cooling fans, and the resulting noise of operation. A low flow switch and normally closed, electrically activated solenoid valves on the cooling water supply and return lines were provided to prevent operation of the unit with inadequate cooling.

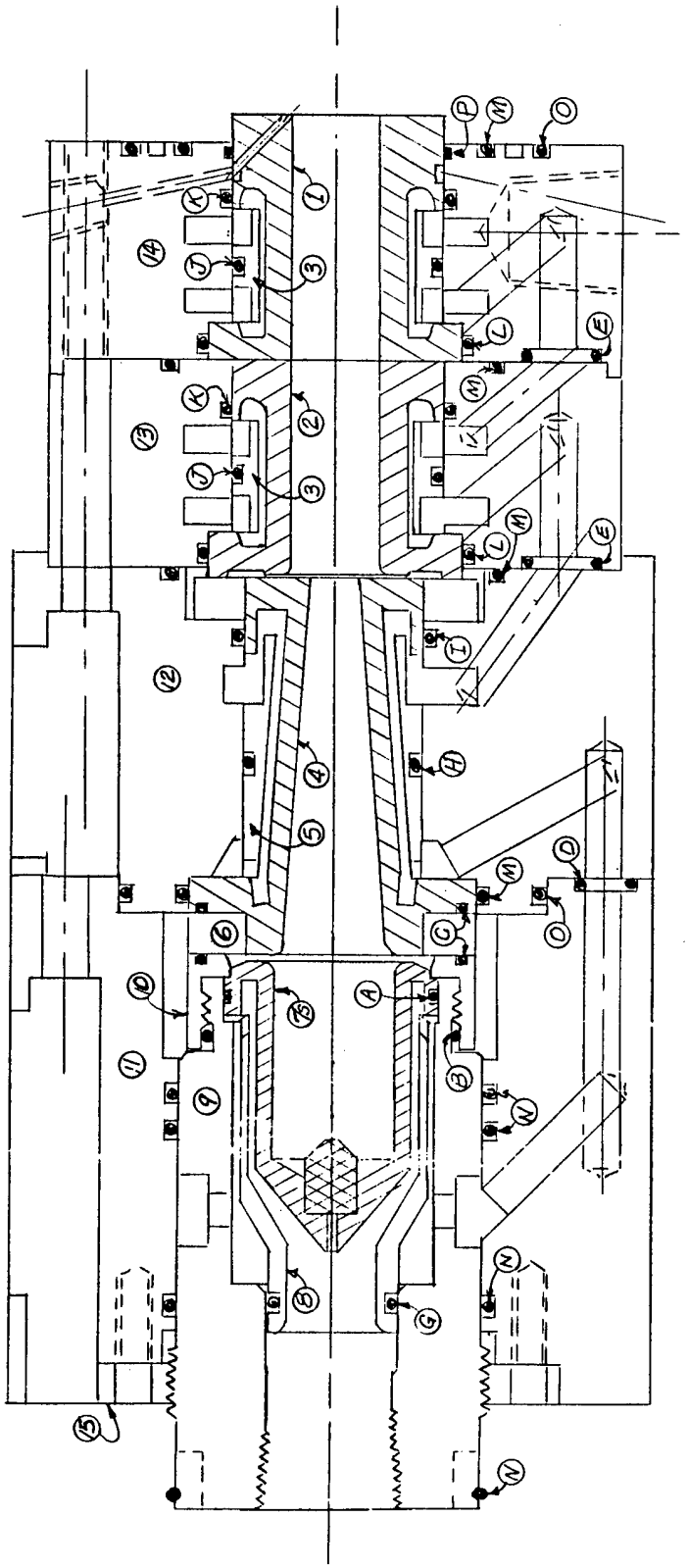

FIGURE IX
A-61E Torch

NORTON COMPANY

A-61E TORCH

Parts List (Refer to Drawing 311B)

		Drawing No.
1.	Downstream Secondary Anode*	310A
2.	Upstream Secondary Anode*	309A
2S.	Special Upstream Secondary Anode* (Extended for single anode operation)	312A
3.	Secondary Anode Water Separator	281A
4.	Primary Anode	278A
5.	Primary Anode Water Separator	180A
6.	Ceramic Insulator	142A
7.	¼ inch Well Cathode	158A
7S.	1¼ inch Well Cathode	144A
8.	Cathode Water Separator	145A
9.	Cathode Holder	146A
10.	Gas Injector	143A
11.	Plastic Rear Body	276B
12.	Primary Anode Body	277B
13.	Upstream Secondary Anode Body	307B
14.	Downstream Secondary Anode Body	308B
15.	Cathode Retainer	153A
16.	Cathode Safety Shield (not shown)	157A

*Several bore diameters available.

O-Rings (Total Number Used)

A.	-028	I.	-124
B.	-030	J.	-125 (2)
C.	-031	K.	-128 (2)
D.	-108 (8)	L.	-132 (2)
E.	-110 (12)	M.	-136 (4)
F.	-115 (2)	N.	-138 (4)
G.	-116	O.	-150 (2)
H.	-122	P.	-029

FIGURE IX
(Continued)

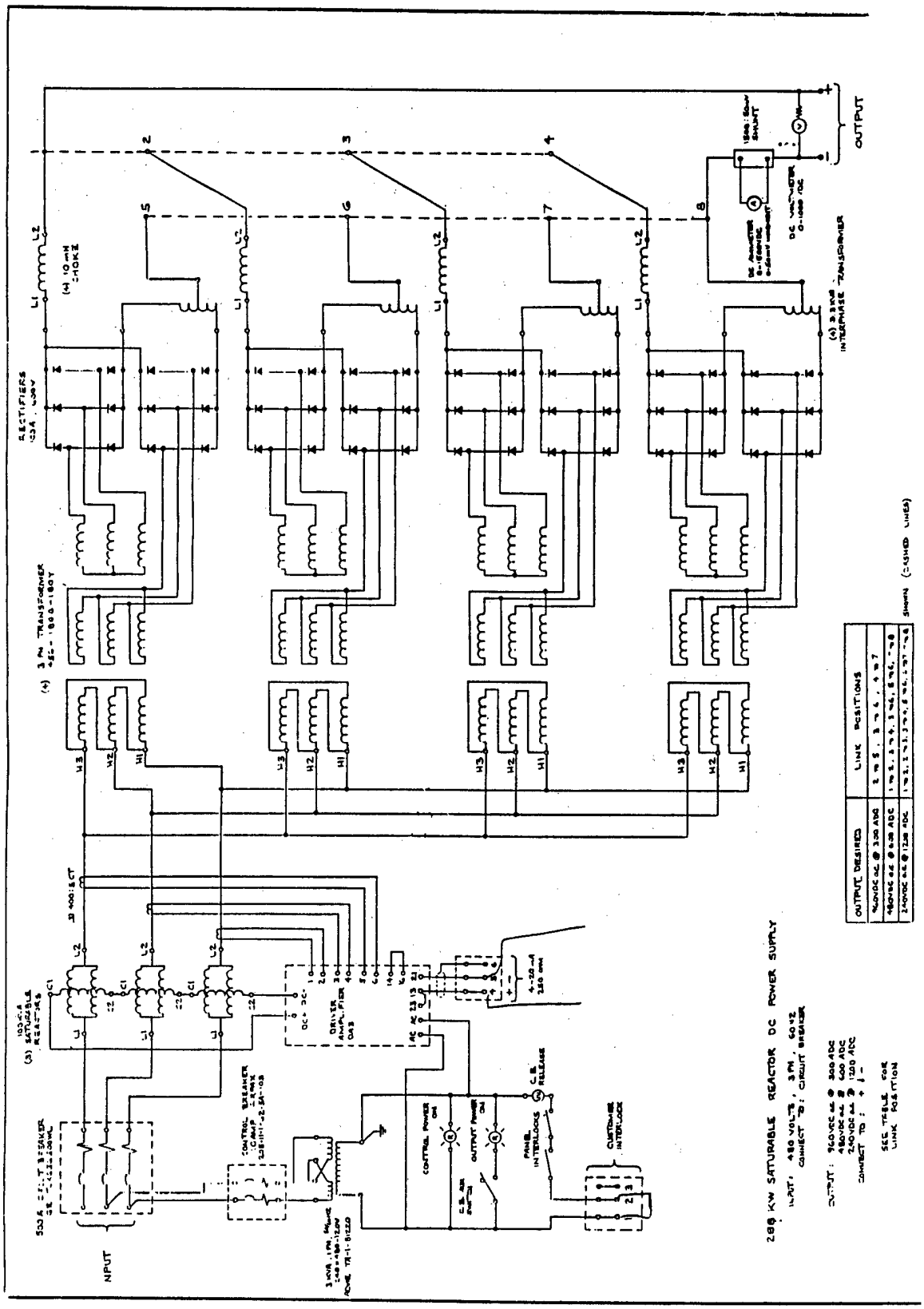
OUTPUT
INPUT
(4) 10 mH CHOKE
(4) 3 PH TRANSFORMER
(4) 3 KVA INTERPHASE TRANSFORMER
DC AMMETER
DC VOLTMETER
DRIVER AMPLIFIER
CONTROL POWER ON
OUTPUT POWER ON
C.B. RELEASE
PANEL INTERLOCKS
CUSTOMER INTERLOCK
OUTPUT DESIRED
LINK POSITIONS
SHOWN (SOLID LINES)

FIGURE X

F. High Frequency Starter Circuit

The torch/power supply system was also equipped with a separate high frequency starter circuit mounted between the power supply output lugs and the power supply cables to the plasma torch. To initiate the plasma, a large potential is developed between the electrodes of the torch and a high frequency signal is injected onto the power supply leads. The high frequency pulse initiates an arc, and the plasma arc stabilizes, driven by the power supply.

Throughout the Phase I activities, the high frequency injection system caused significant problems with process instrumentation, particularly the digital displays for arc current and voltage. To prevent repeated failure of the displays, Faraday cages around the panel displays and relay shunts to short out input lead while the high frequency signal was being injected, were required.

To avoid repeated instrumentation failures, the high frequency injection system was isolated in its own sealed metal box and all control signal supplied to the system, or taken from the system, were filtered and isolated. The system was designed with a "defense in depth" attitude, with input and output transducers totally isolated from the active portions of the circuit by multiple metal bulkheads and filters. A schematic of the high frequency starter system is included as Figure XI.

G. Particulate Collection System

The particulate collection unit is a multi-element metallic filter assembly produced by Fluid Dynamics, Inc. (Note: A diagram of this unit is not included in this report. All vessel drawings and specifications are proprietary information owned by the filter manufacturer and cannot be reproduced in whole or part.) The unit consists of four Hastalloy filter cartridges 2-3/8-inch in diameter and 60 inches long each, providing a total of 12.4 square feet of filter area. The filter media is rated for capture of 99.9% of all particulates greater than 0.1 micron in diameter, and absolute capture of all particulates greater than 0.5 micron in diameter. The four filter cartridges are supported at one end by a one-inch thick, 316 stainless steel tube sheet assembly. Mounted to the tube sheet are four baffles, which partially isolate the filter cartridges from each other. The entire filter/baffle/tube sheet assembly is mounted in a 316 stainless steel pressure vessel. The pressure vessel is constructed of a length of schedule 40 316 stainless steel welded pipe. A 150# RF flange is welded to each end of the pipe such that the face-to-face length of the vessel is 74 inches. A 1-1/2-inch, 150# RF inlet nozzle is positioned eight inches from the bottom of the vessel. The bottom flange is attached to a separate conical section which has

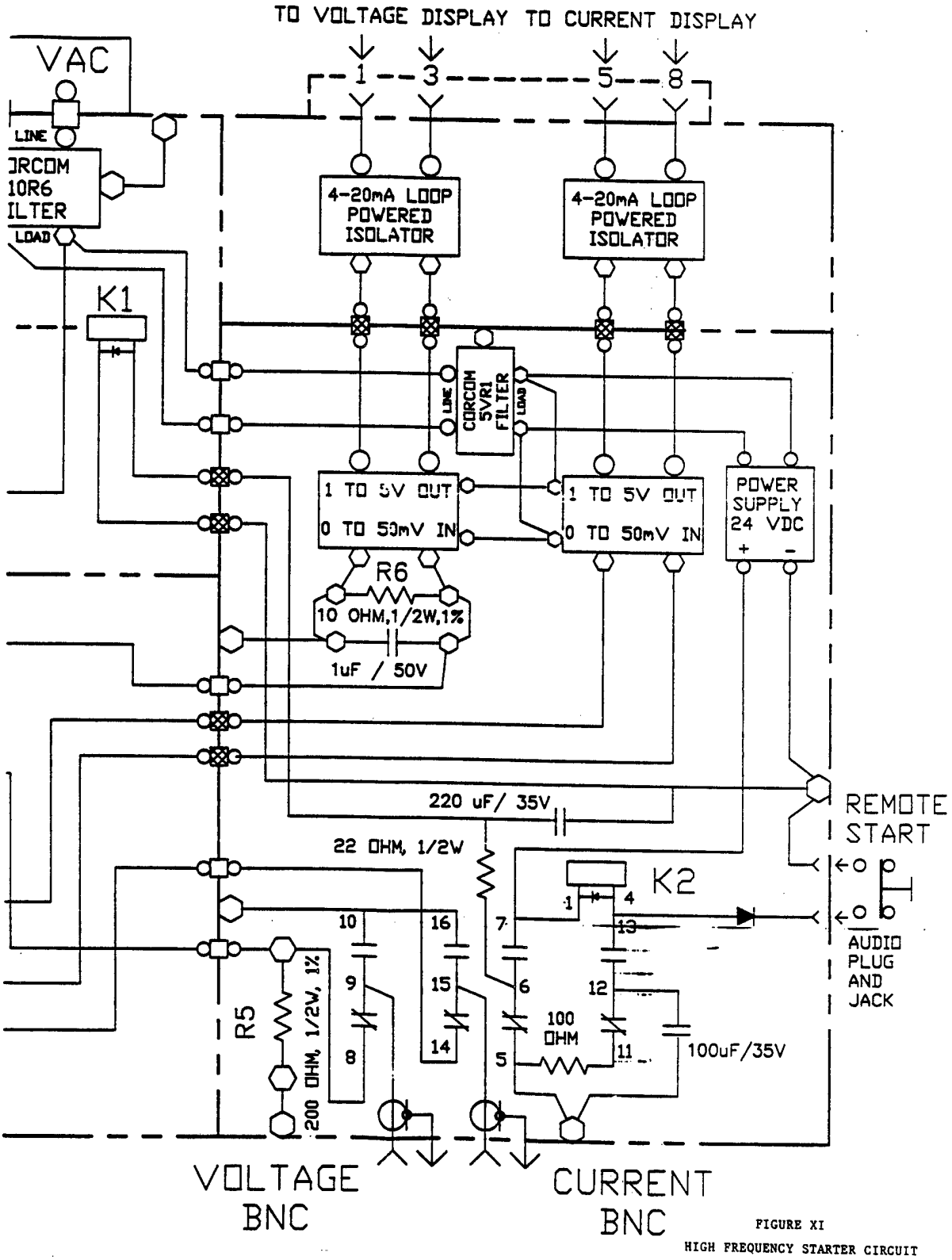

FIGURE XI
HIGH FREQUENCY STARTER CIRCUIT

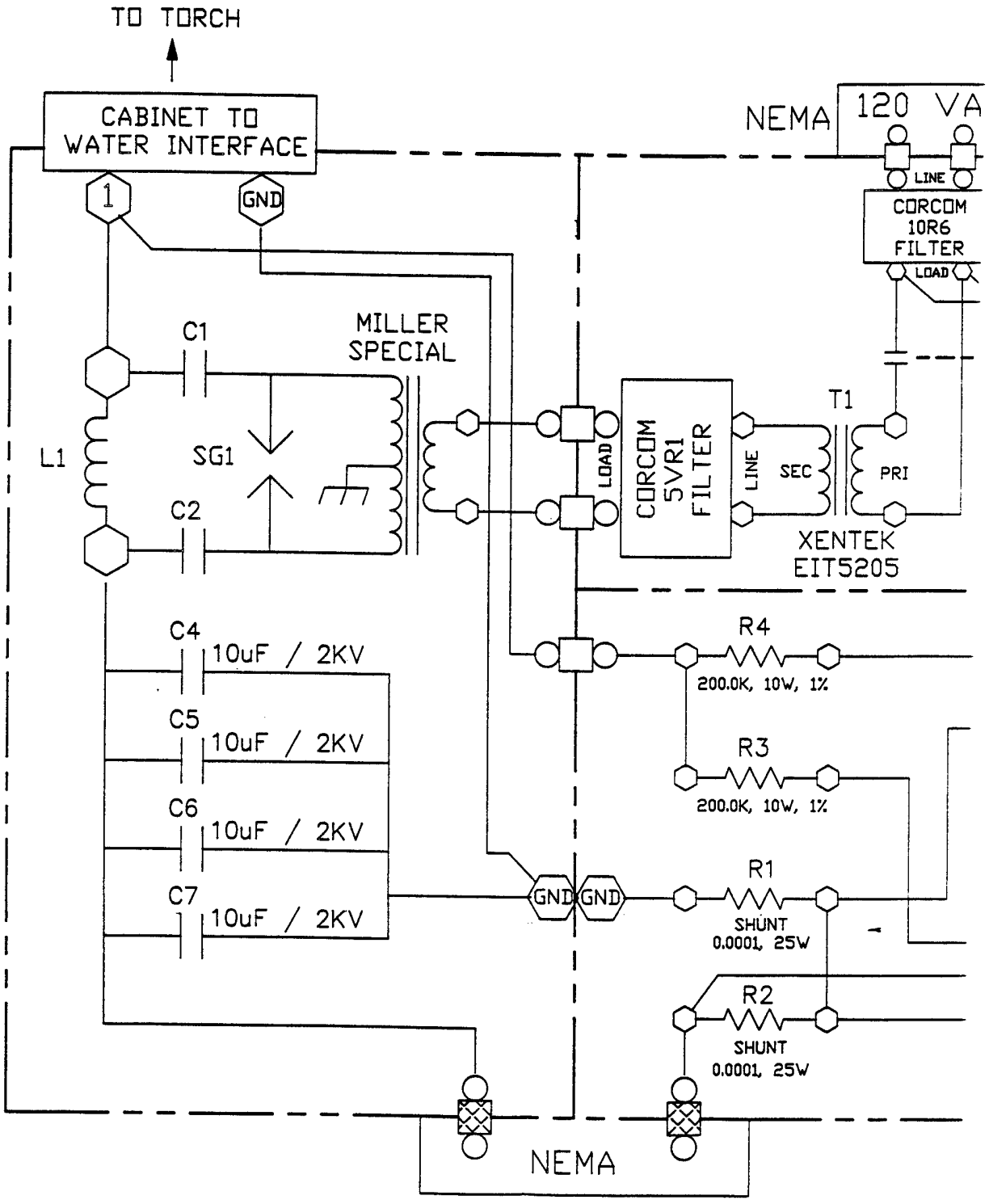

FIGURE XI (CONT.)

NOTES; UNLESS OTHERWISE SPECIFIED:
1. ALL RESISTANCE VALUES ARE IN OHMS
2. ALL DIODES ARE 1N4007

an include angle of 40 degrees and is fitted at the top with a 150# RF flange to mate with the bottom of the main vessel, and a 2-inch, 150# RF flange at the bottom for product removal. The conical bottom section has an overall length of 21-1/4 inches.

The top of the filter vessel is fitted with a second section of schedule 40 316 stainless steel welded pipe fitted with a 12-inch, 150# RF flange to mate with the vessel top. The upper section of pipe is 10 inches long, and fitted with an elliptical head to form a top to the entire filter vessel. Penetrating the elliptical head are four, one-inch diameter schedule 40 welded pipes fitted with 1-inch, 150# RF flanges. These pipes are oriented such that the lower end of each pipe is exactly centered above the exhaust port of each of the four cartridge filters in the tube sheet. The top section is also fitted with a single 1-1/2-inch, 150# RF exhaust nozzle. The overall height of the entire filter unit is 109 inches.

The four, one-inch flanged pipes are, in turn, connected to four normally closed, electrically activated solenoid valves (FZ 680, FZ 681, FZ 682, and FZ 683). The solenoid valves are manifolded together and the manifold connected to a pressure vessel with an internal volume of 2.67 cubic feet. The vessel is filled with argon, which is maintained at a pressure of 75 psig by a self-contained pressure regulator (PCV 620) fed by the main unit argon header upstream of the argon flow control loops.

In operation, particulate-laden gas is introduced to the unit through the 1-1/2-inch feed nozzle in the main section of the vessel. The gas passes through the four filter elements, which retain the particulate matter on the filter surface. The particulate free gas exits the filters through the tube sheet attachment and exits the system through the 1-1/2-inch exhaust nozzle in the top section. The differential pressure across the filter elements is monitored with a differential pressure sensor (DP 661). When the differential pressure reaches an appropriate level, typically between five and ten inches of water pressure, the solenoid valves isolating the filter unit from the argon pressure vessel are opened sequentially for 0.5 seconds, followed by a one second pause. The argon gas pulses through the filter elements in a direction opposite of the original gas flow and dislodges any material on the filter media. The internal baffles prevent the dislodged material from immediately settling on an adjacent, active filter and the solids fall into the conical bottom for removal. The cleaning cycle is triggered by differential pressure, a backup timer set for intermittent cleaning, or manual actuation, on demand of the operator.

Prior to the purchase of the unit, a sample of powder produced in the Phase I activities was qualified by the filter vendor on their test stand to assure adequate filtering capability and media cleaning.

H. Tail Gas Scrubber

The tail gas scrubber for the Phase II facility was similar to the unit used for Phase I, with the following exceptions:

1. The scrubber diameter was increased from eight to fourteen inches.

2. The feed nozzle was increased from a 2-inch to a 3-inch, 150# RF flanged fitting.

3. The wash water was distributed over the packing material by seven Whirljet hollow cone nozzles.

4. The effluent gas nozzle and bottoms liquid nozzle were increased to 2-inch, NPT fittings.

5. Tower sump level was monitored using a differential pressure transducer (LT 740) instead of a capacitance level probe in a stillwell.

Otherwise, the unit's geometry was identical to the Phase I scrubber.

I. Methyltrichlorosilane Supply

Due to the increased quantity of liquid methyltrichlorosilane required by the larger facility, the one-gallon feed tank of the Phase I system had to scaled up significantly. To reduce the hazards associated with transferring methyltrichlorosilane from shipping containers to the process vessel, provisions were made to feed the process directly from a standard 55-gallon shipping drum. The shipping drum was positioned in a hazardous material overpack drum and located in a room adjacent to the process area. A Whitey metering pump, identical to the Phase I unit except for increased volumetric pumping capability, was supplied from the 55-gallon drum through a 15-micron filter. The metering pump was also provided with a high pressure relief valve (PSV 450) that permitted the pump to recirculate if the outlet to the process was plugged or erroneously deadheaded. A back pressure regulator (PSV 451) maintained 35 psig back-pressure on the pump discharge to assure that the pump check valves seated properly.

The discharge of the metering pump enters a manifold of pneumatically actuated shutoff valves with bellows sealed stems (FV 450, FV 451, FV 452, and FV 130). These valves are, in turn, actuated by normally closed, electrically actuated solenoid valves (not shown on drawing) connected to the unit's instrument air header. By selectively opening and closing the pneumatically actuated shutoff valves, methyltrichlorosilane can be routed back to the 55-gallon drum in recycle mode to establish liquid flow, or to the plasma torch for powder synthesis. In addition, by closing the shutoff valve at the pump discharge (FV 450) and opening the shutoff valve to the argon supply header (FV 130), the liquid-filled lines can be blown clear of methyltrichlorosilane for servicing the piping. A differential pressure switch (DPSH 450) prevents this last configuration unless the argon pressure exceeds the methyltrichlorosilane line pressure, and prevents methyltrichlorosilane from flowing back into the argon system. A sweep of argon is maintained through the vapor space of the 55-gallon drum while the unit is in operation to prevent drawing in external air into the supply drum as the liquid is drawn down.

J. Data Acquisition and Process Control

The increased capacity and facility size of the Phase II system required enhanced data acquisition and process control capability. Instead of single-loop control using freestanding digital controllers, the available Bailey 9000 supervisory control system was employed. The Bailey 9000 is a typical distributed process control system which utilizes a central process control computer, but permits access to the process information at various operator stations connected to a plant data base. In addition to providing process control capability, the system also permits collection of various process inputs for operator information or trending for later evaluation. Perhaps the most valuable capability of any distributed process control system is the ability to quickly change tuning parameters of the various control loops, or even completely change the structure of the control logic.

The supervisory computer interfaces with field instrumentation, which provides the required input and output devices necessary for system operation. The supervisory control system is an assembly of functional blocks (AND, OR, SUM, TREND, etc.) which mimic the functions of standard control devices. Figures XII through XXIV depict the control logic of the Phase II system.

All control and data input/output cables were consolidated in three termination boxes mounted on the structural steel of the Phase II system. One termination box was dedicated to digital signals, a second for analog signals, and a third for thermocouples. This design minimized the transfer of digital signal noise onto analog and thermocouple signal

FIGURE XII

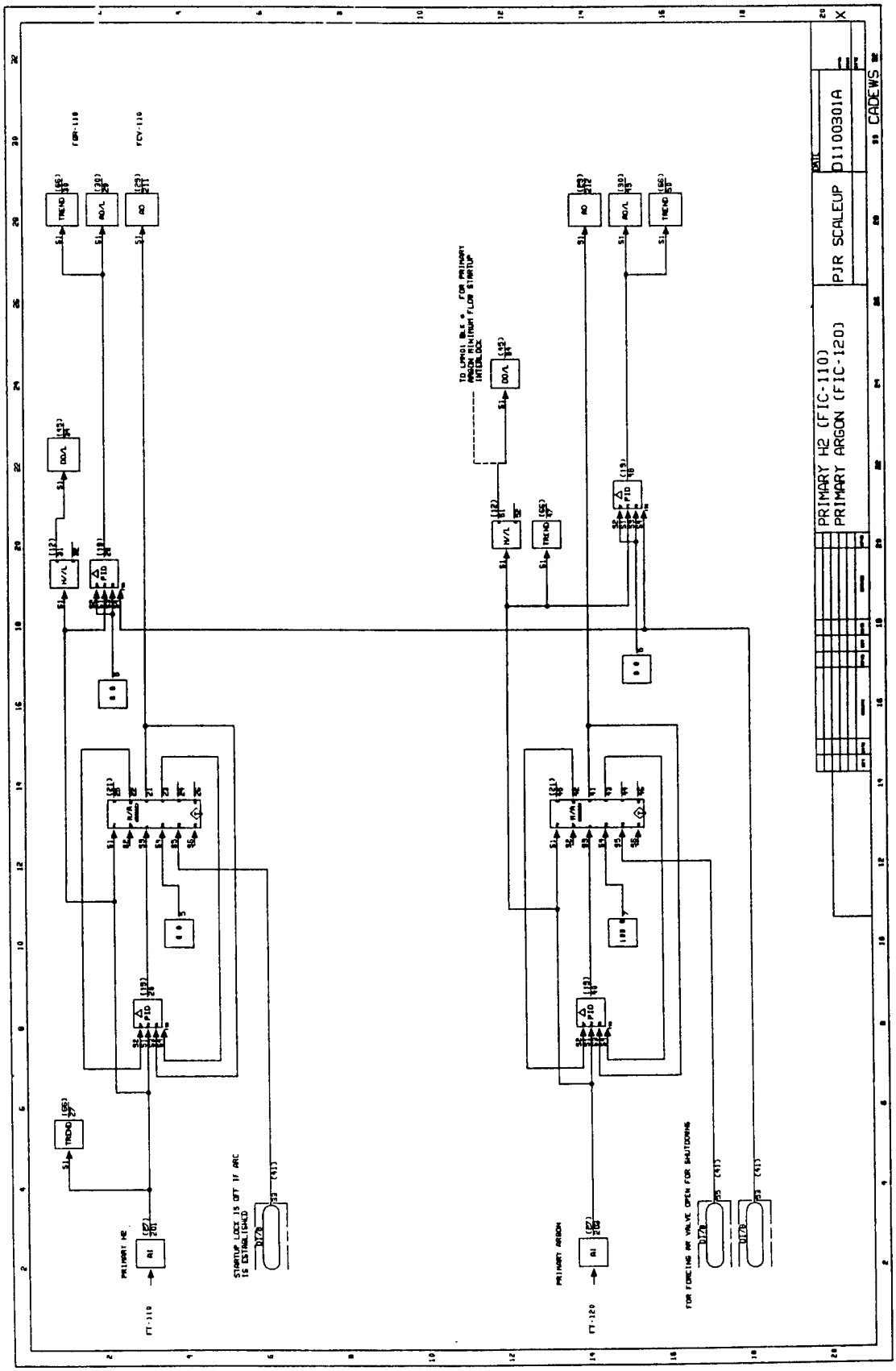
PRIMARY H2 (FIC-110)
PRIMARY ARGON (FIC-120)
PJR SCALEUP
D1100301A
CADEWS
PRIMARY H2
PRIMARY ARGON
FT-110
FT-120
STARTUP LOCK IS OFF IF ARC IS ESTABLISHED
FOR FORCING HV VALVE OPEN FOR SHUTDOWNS
TO LPNOI BLK 6 FOR PRIMARY ARGON MINIMUM FLOW STARTUP INTERLOCK

FIGURE XIII

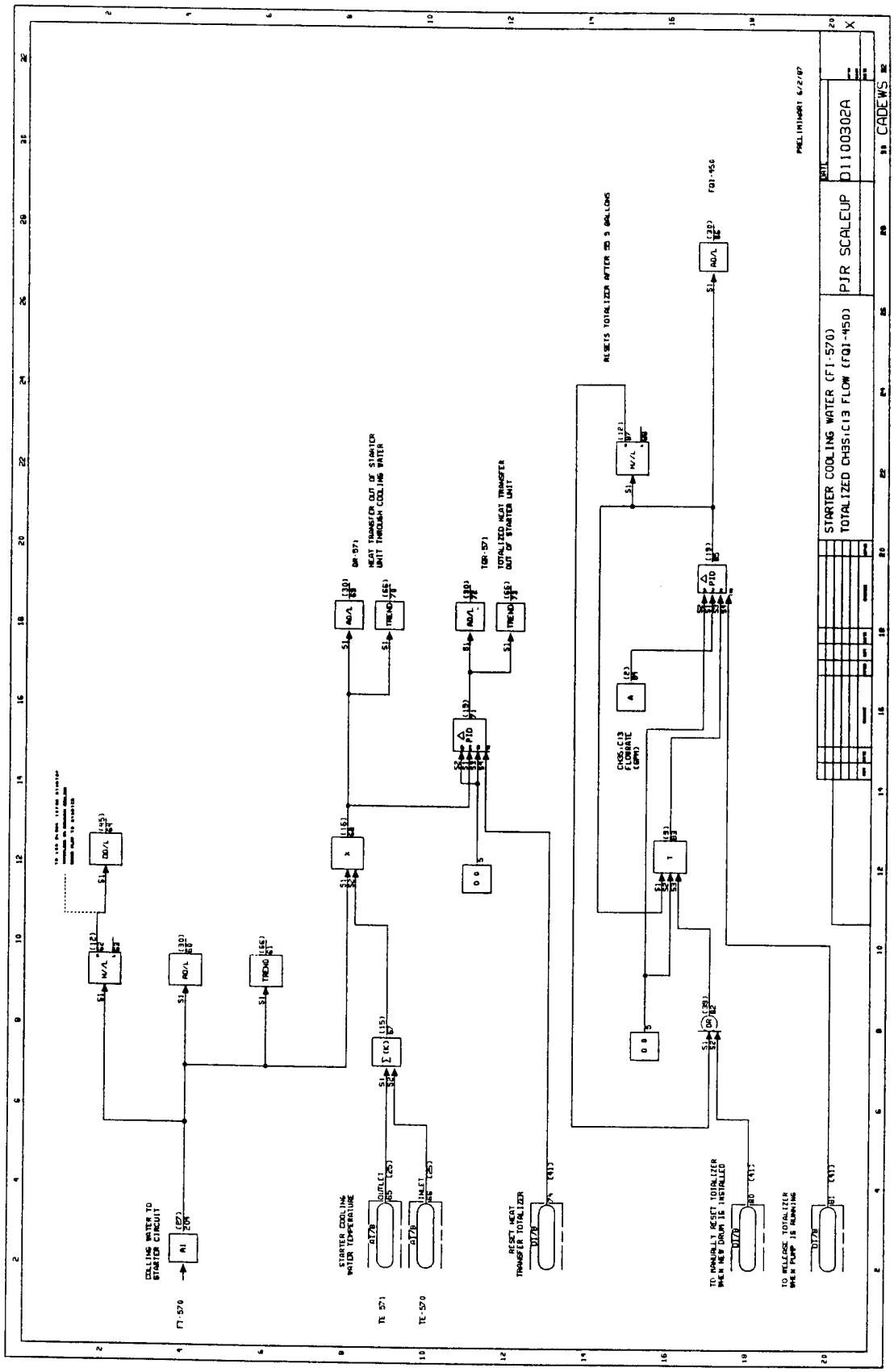
STARTER COOLING WATER (FI-570)
TOTALIZED CH3S:C13 FLOW (FQI-450)
PJR SCALEUP
D1100302A
CADEWS
PRELIMINARY 6/2/97
RESETS TOTALIZER AFTER 55 5 GALLONS
HEAT TRANSFER OUT OF STARTER UNIT THROUGH COOLING WATER
TOTALIZED HEAT TRANSFER OUT OF STARTER UNIT
CHS:C13 FLOWRATE (GPM)
COOLING WATER TO STARTER CIRCUIT
STARTER COOLING WATER TEMPERATURE
OUTLET
INLET
RESET HEAT TRANSFER TOTALIZER
TO MANUALLY RESET TOTALIZER WHEN NEW DRUM IS INSTALLED
TO RELEASE TOTALIZER WHEN PUMP IS RUNNING
FI-570
TE-571
TE-570

FIGURE XIV

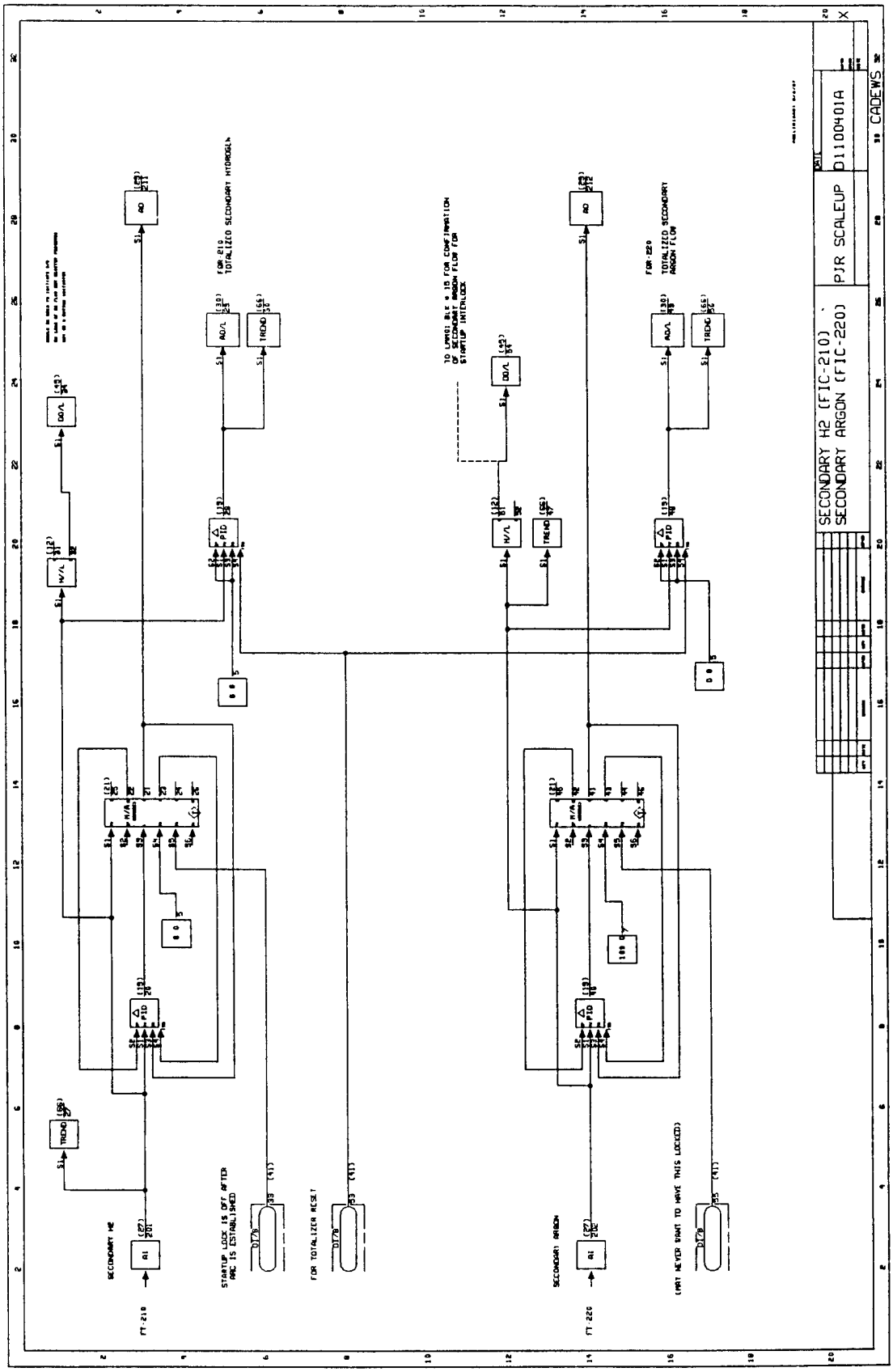
SECONDARY H2 (FIC-210)
SECONDARY ARGON (FIC-220)
PJR SCALEUP
D1100401A
CADEWS
FOR-210
TOTALIZED SECONDARY HYDROGEN
FOR-220
TOTALIZED SECONDARY ARGON FLOW
TO LOWER BLK # 15 FOR CONFIRMATION OF SECONDARY ARGON FLOW FOR STARTUP INTERLOCK
STARTUP LOCK IS OFF AFTER ARC IS ESTABLISHED
FOR TOTALIZER RESET
(PART NEVER START TO HAVE THIS LOCKED)
SECONDARY HE
SECONDARY ARGON
FT-210
FT-220

FIGURE XV

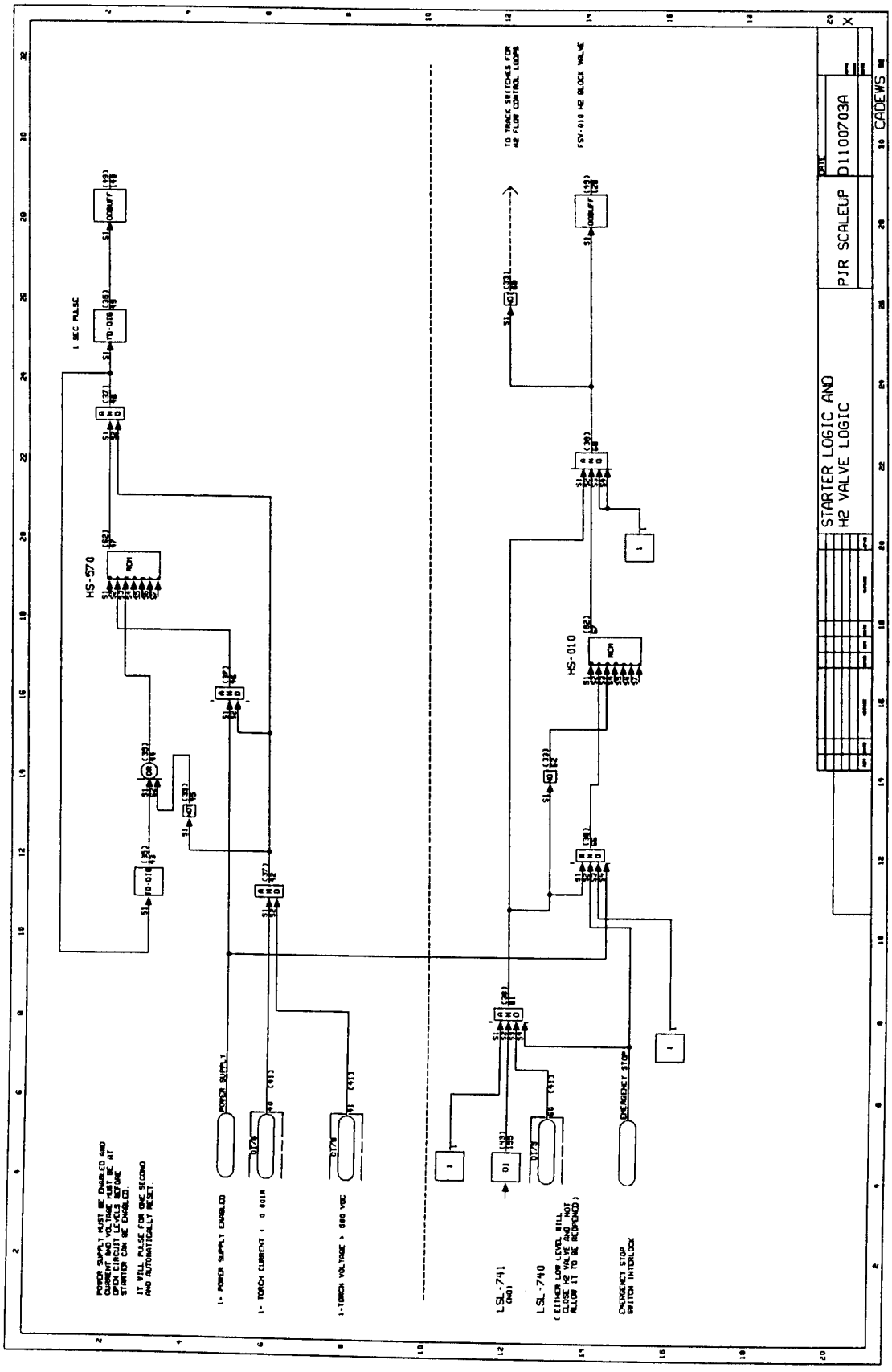
STARTER LOGIC AND
H2 VALVE LOGIC
PJR SCALEUP
D1100703A
CADEWS
HS-570
HS-010
1 SEC PULSE
TO TRACK SWITCHES FOR H2 FLOW CONTROL LOOPS
FSV-010 H2 BLOCK VALVE
POWER SUPPLY MUST BE ENABLED AND CURRENT AND VOLTAGE MUST BE AT STARTER CIRCUIT LEVELS BEFORE STARTER CAN BE ENABLED
IT WILL PULSE FOR ONE SECOND AND AUTOMATICALLY RESET
1- POWER SUPPLY ENABLED
1- TORCH CURRENT < 0.001A
1-TORCH VOLTAGE > 600 VDC
LSL-741
LSL-740
(EITHER LOW LEVEL WILL CLOSE H2 VALVE AND NOT ALLOW IT TO BE REOPENED)
EMERGENCY STOP
EMERGENCY STOP BUTTON INTERLOCK

FIGURE XVI

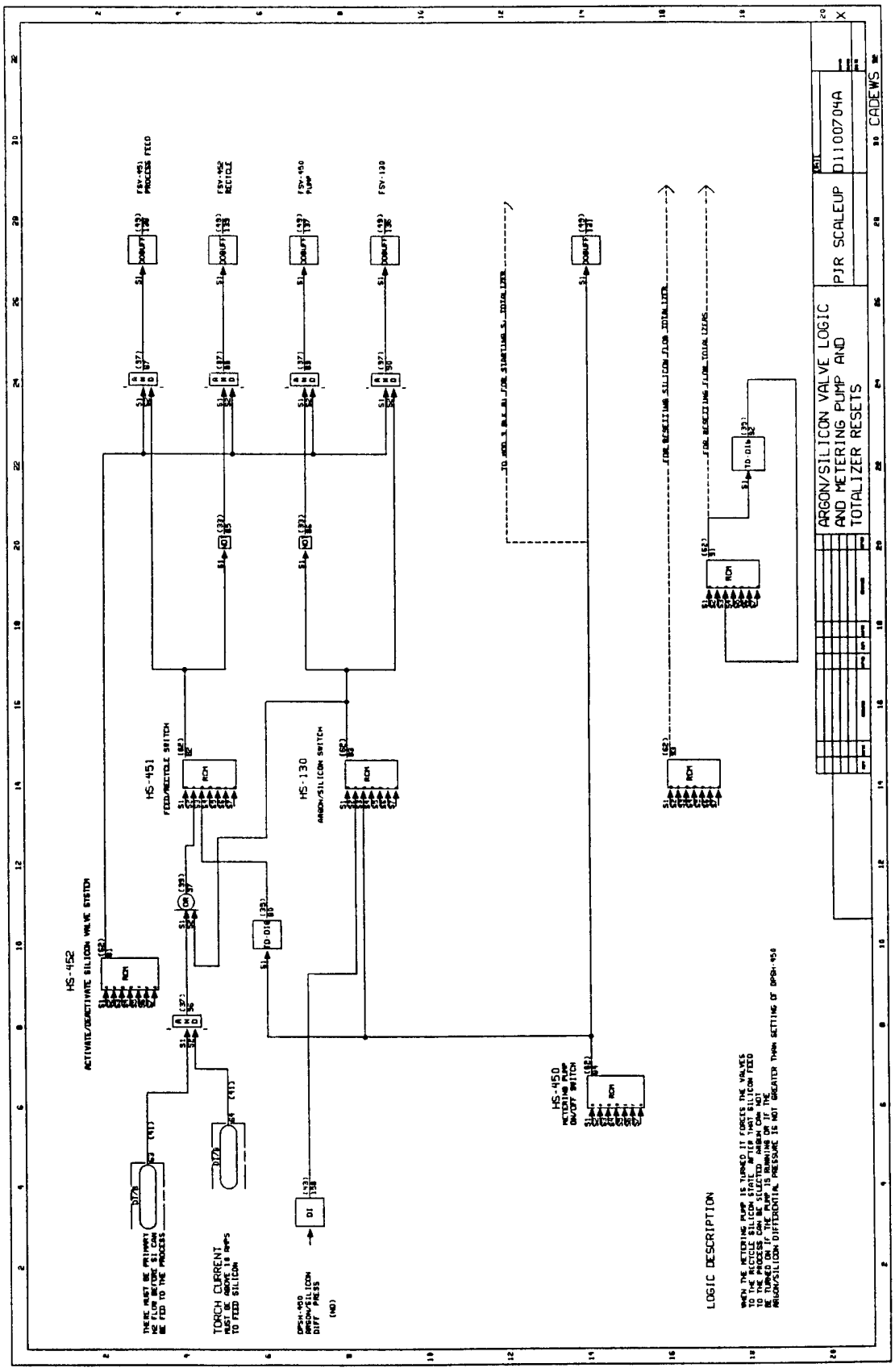
ARGON/SILICON VALVE LOGIC
AND METERING PUMP AND
TOTALIZER RESETS
PJR SCALEUP
D1100704A
CADEWS
HS-452
ACTIVATE/DEACTIVATE SILICON VALVE SYSTEM
HS-451
FEED/RECYCLE SWITCH
HS-130
ARGON/SILICON SWITCH
HS-450
METERING PUMP
ON/OFF SWITCH
FSV-451
PROCESS FEED
FSV-452
RECYCLE
FSV-450
PUMP
FSV-130
TORCH CURRENT
MUST BE ABOVE 18 AMPS
TO FEED SILICON
DPSH-450
ARGON/SILICON
DIFF PRESS
(HD)
LOGIC DESCRIPTION

FIGURE XVII

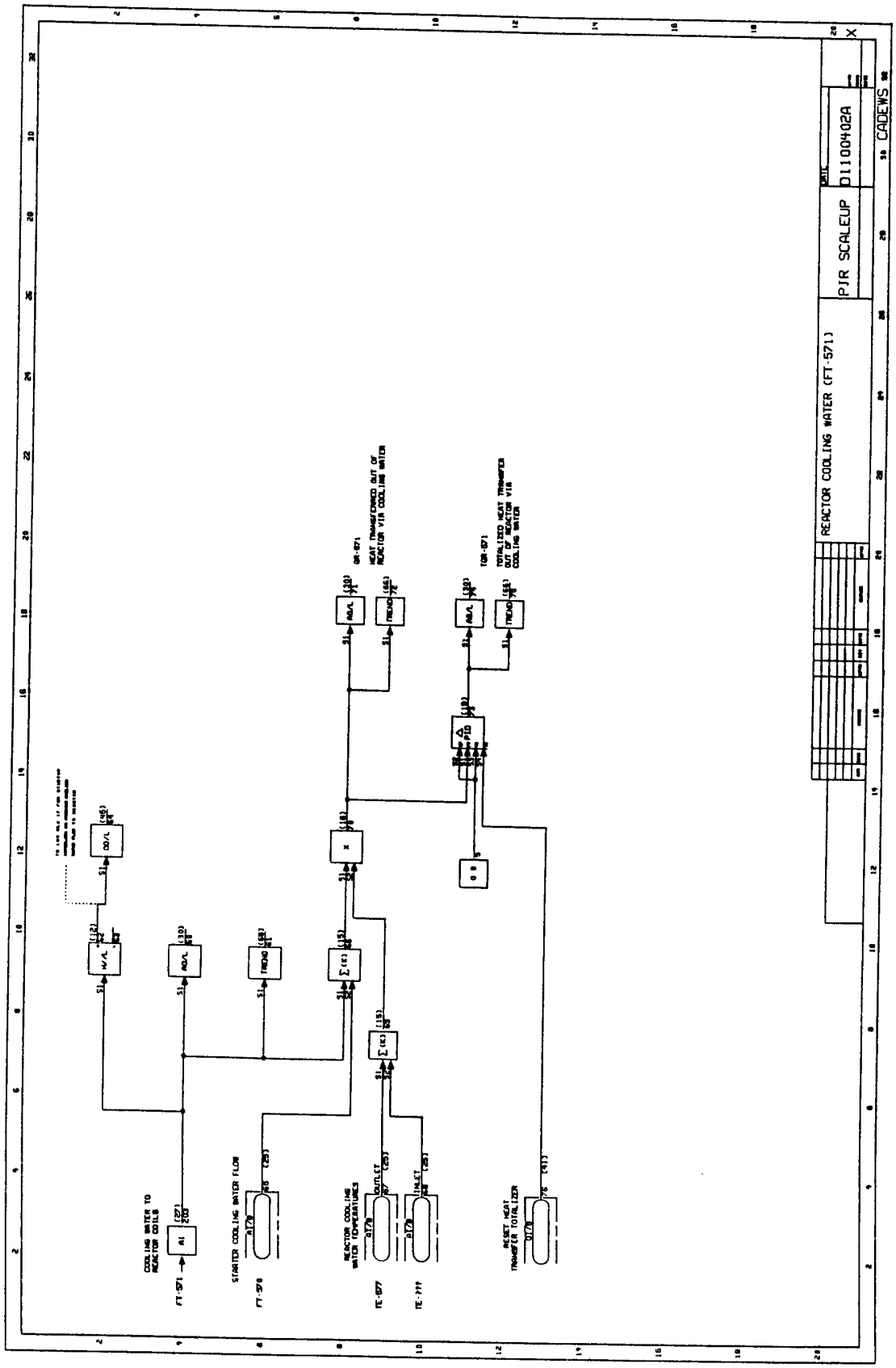
REACTOR COOLING WATER (FT-571)
PJR SCALEUP
D1100402A
CADEWS
COOLING WATER TO REACTOR COILS
FT-571
STARTER COOLING WATER FLOW
FT-570
REACTOR COOLING WATER TEMPERATURES
OUTLET
INLET
TE-577
TE-???
RESET HEAT TRANSFER TOTALIZER
HEAT TRANSFERRED OUT OF REACTOR VIA COOLING WATER
TOTALIZED HEAT TRANSFER OUT OF REACTOR VIA COOLING WATER
TREND
AVG

FIGURE XVIII

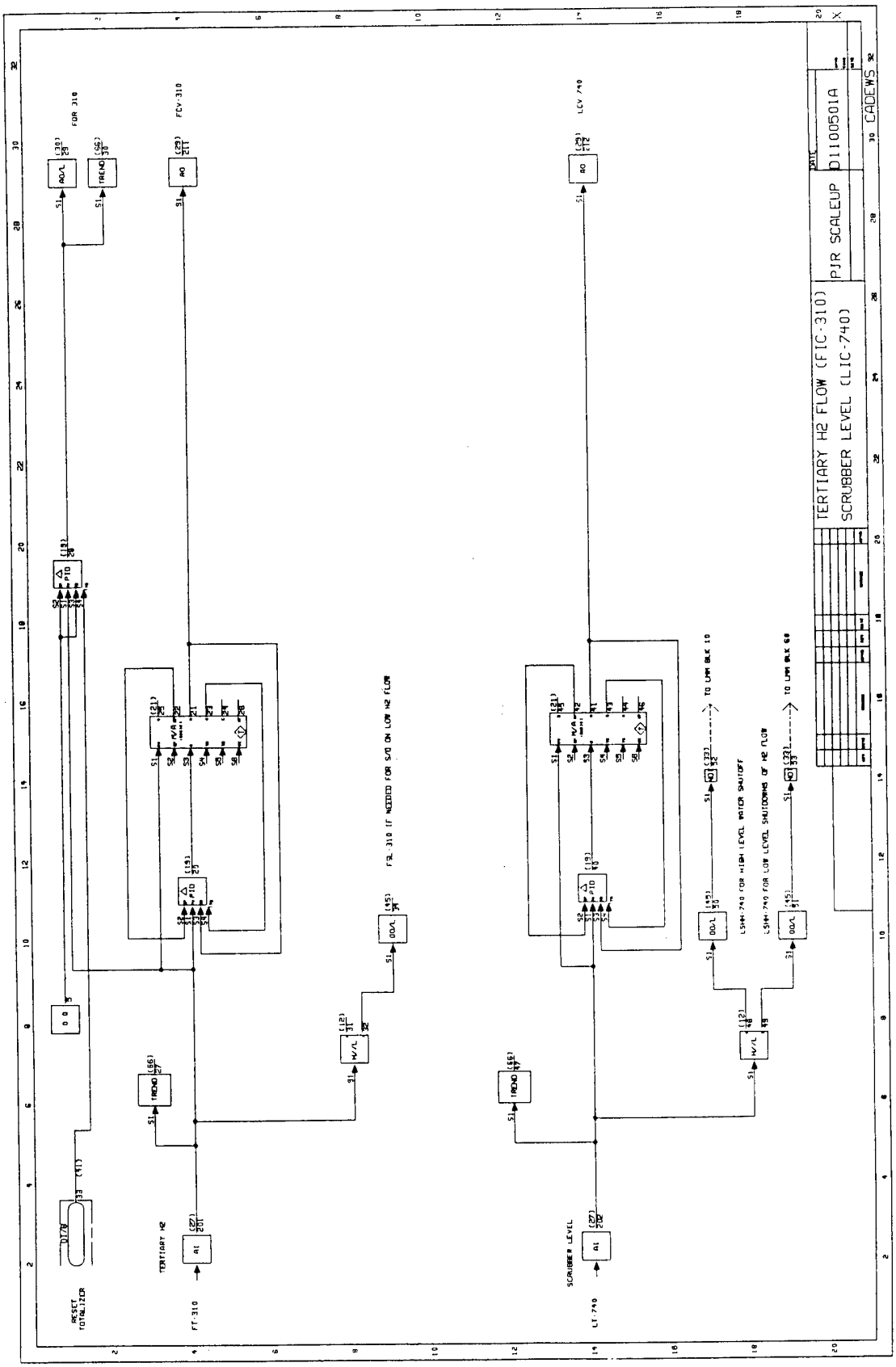

FIGURE XIX

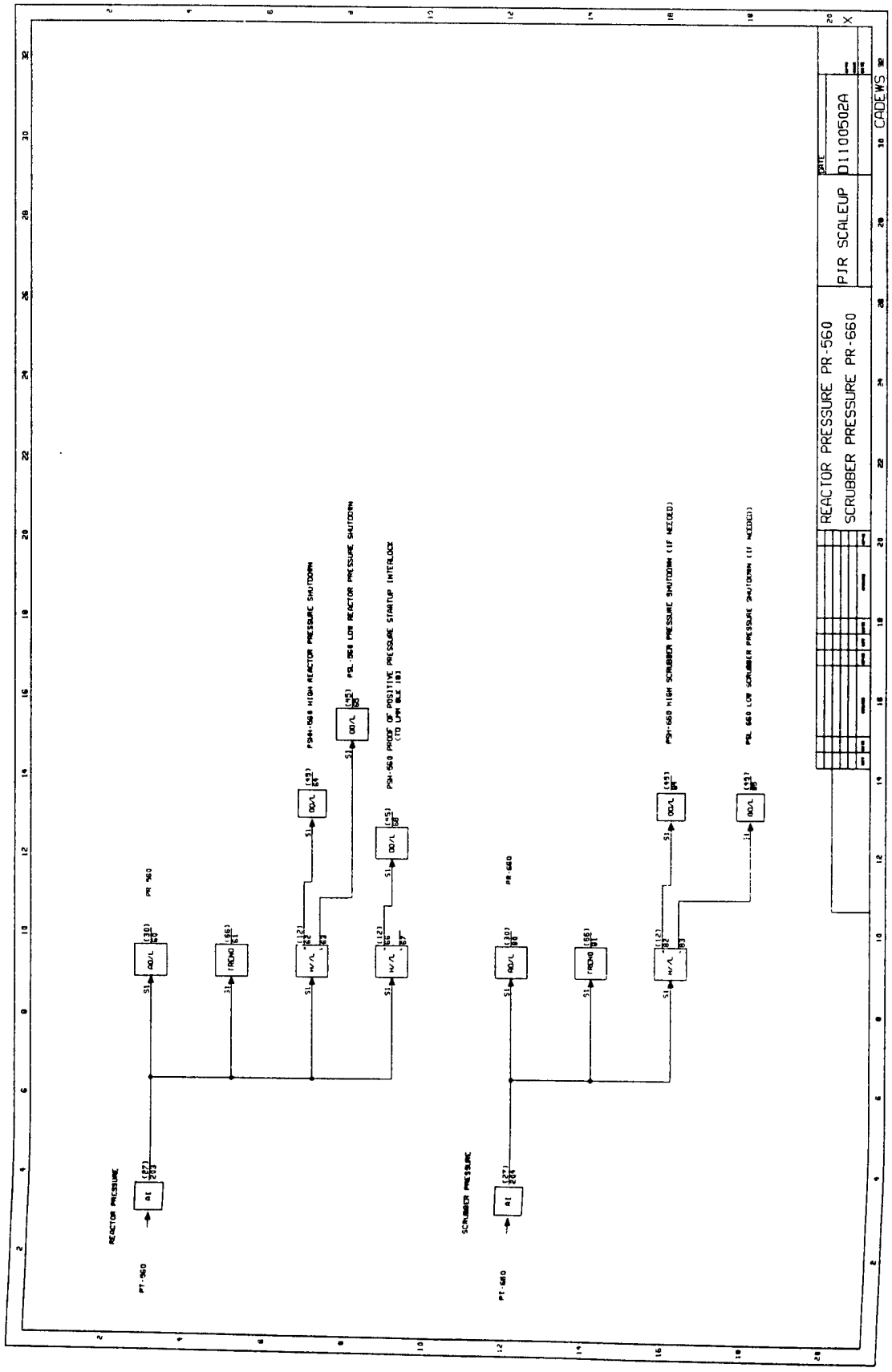
REACTOR PRESSURE PR-560
SCRUBBER PRESSURE PR-660
PJR SCALEUP
D1100502A
CADEWS
REACTOR PRESSURE
SCRUBBER PRESSURE
PT-560
PT-660
PSH-560 HIGH REACTOR PRESSURE SHUTDOWN
PSL-560 LOW REACTOR PRESSURE SHUTDOWN
PSH-560 PROOF OF POSITIVE PRESSURE STARTUP INTERLOCK
(TO LPM BLK 101)
PSH-660 HIGH SCRUBBER PRESSURE SHUTDOWN (IF NEEDED)
PSL 660 LOW SCRUBBER PRESSURE SHUTDOWN (IF NEEDED)

FIGURE XX

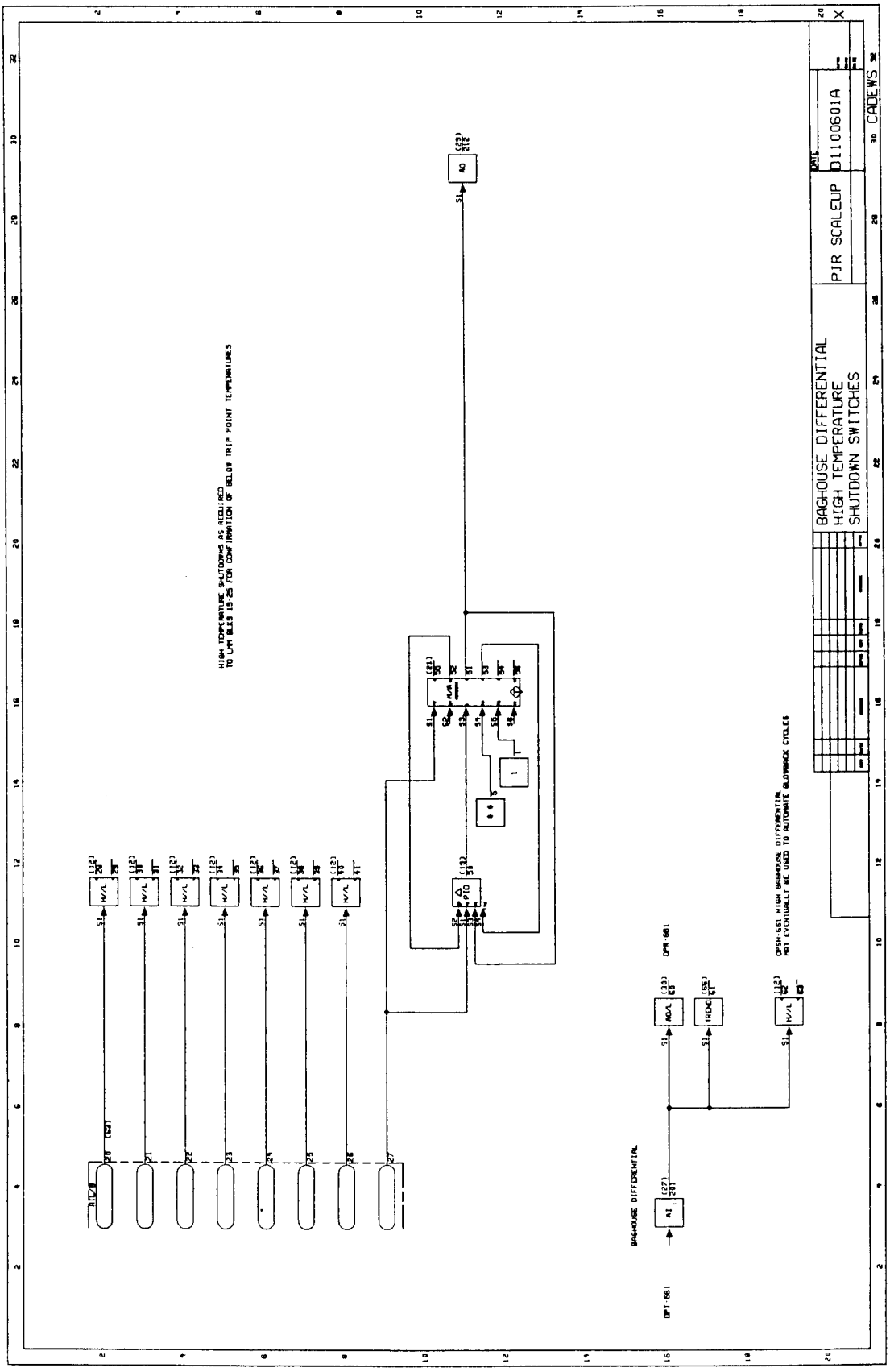
BAGHOUSE DIFFERENTIAL
HIGH TEMPERATURE
SHUTDOWN SWITCHES
PJR SCALEUP
D1100601A
CADEWS
HIGH TEMPERATURE SHUTDOWNS AS REQUIRED
TO LAH BLS 19-25 FOR CONFIRMATION OF BELOW TRIP POINT TEMPERATURES
BAGHOUSE DIFFERENTIAL
DPT-661
DPA-661
OPEN-661 HIGH BAGHOUSE DIFFERENTIAL
MAY EVENTUALLY BE USED TO AUTOMATE BLOWBACK CYCLES

FIGURE XXI

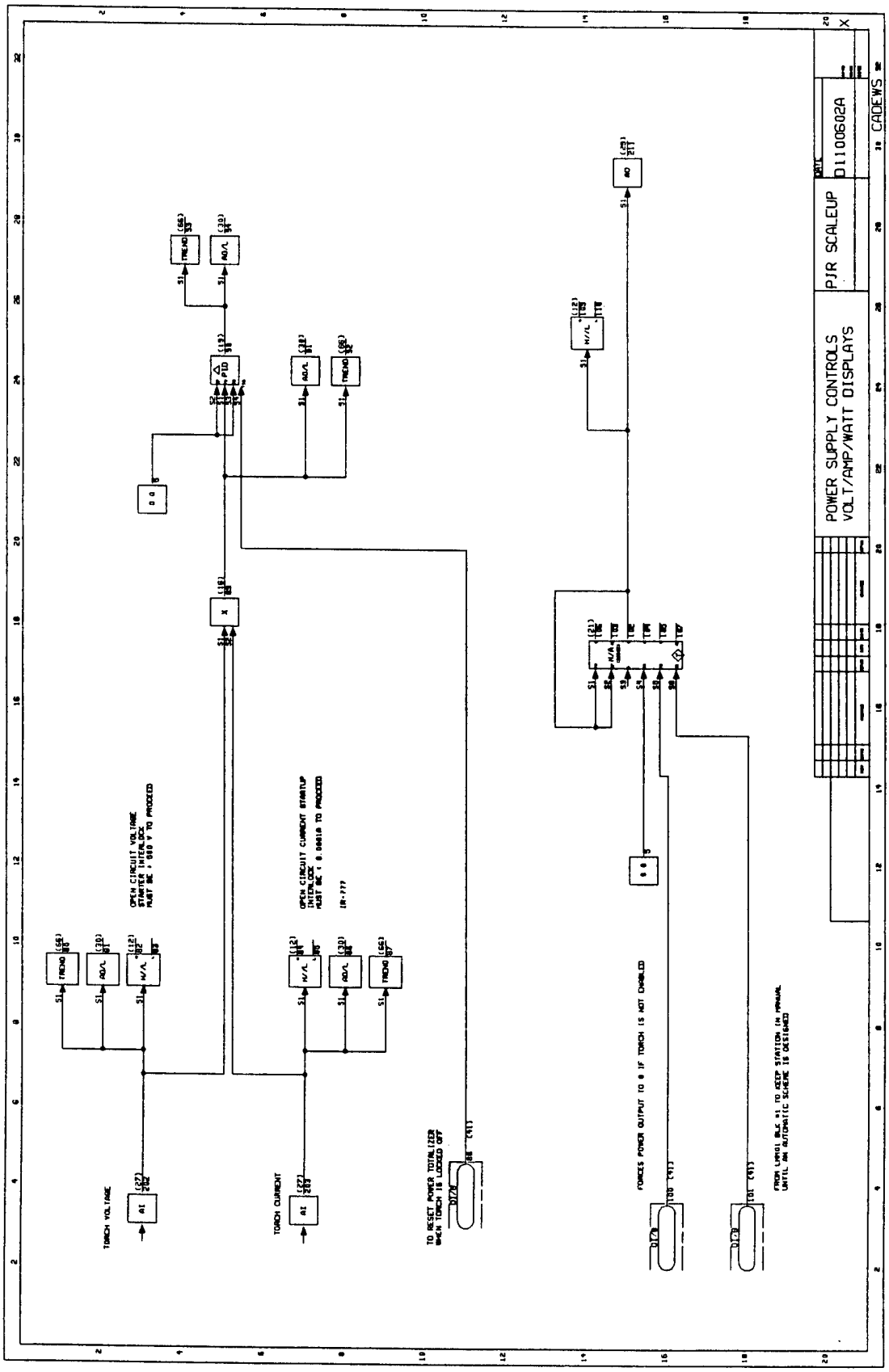
POWER SUPPLY CONTROLS
VOLT/AMP/WATT DISPLAYS
PJR SCALEUP
D1100602A
CADEWS
TORCH VOLTAGE
TORCH CURRENT
OPEN CIRCUIT VOLTAGE
STARTER INTERLOCK
OPEN CIRCUIT CURRENT STARTUP
INTERLOCK
TO RESET POWER TOTALIZER
FORCES POWER OUTPUT TO 0 IF TORCH IS NOT ENABLED
FROM LMPOI BLK #1 TO KEEP STATION IN MANUAL
UNTIL AN AUTOMATIC SCHEME IS DESIGNED

FIGURE XXII

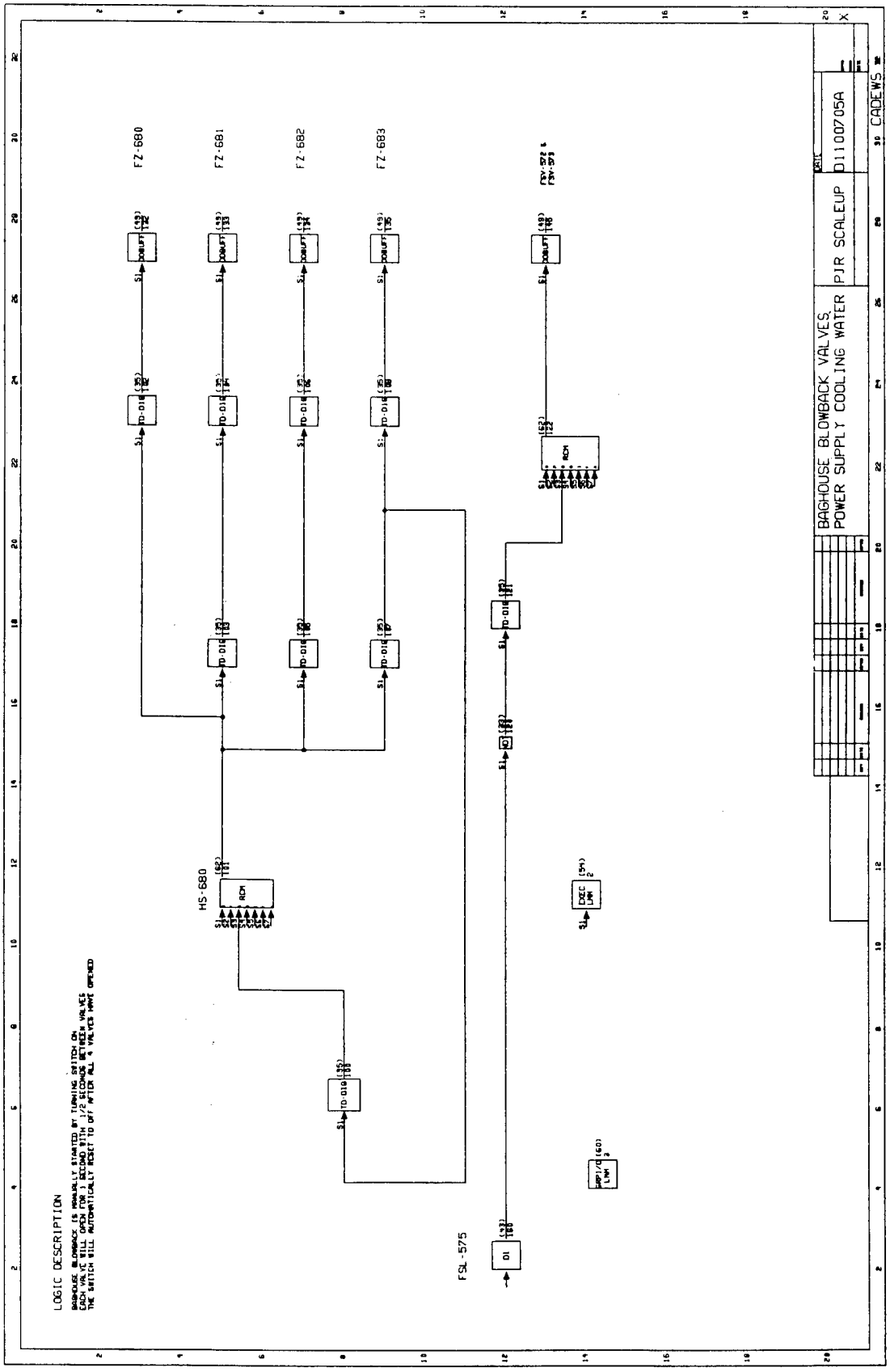
LOGIC DESCRIPTION
BAGHOUSE BLOWBACK IS MANUALLY STARTED BY TURNING SWITCH ON
EACH VALVE WILL OPEN FOR 1 SECOND WITH 1/2 SECOND BETWEEN VALVES
THE SWITCH WILL AUTOMATICALLY RESET TO OFF AFTER ALL 4 VALVES HAVE OPENED
FZ-680
FZ-681
FZ-682
FZ-683
HS-680
FSL-575
BAGHOUSE BLOWBACK VALVES
POWER SUPPLY COOLING WATER
PJR SCALEUP
D1100705A
CADEWS

FIGURE XXIII

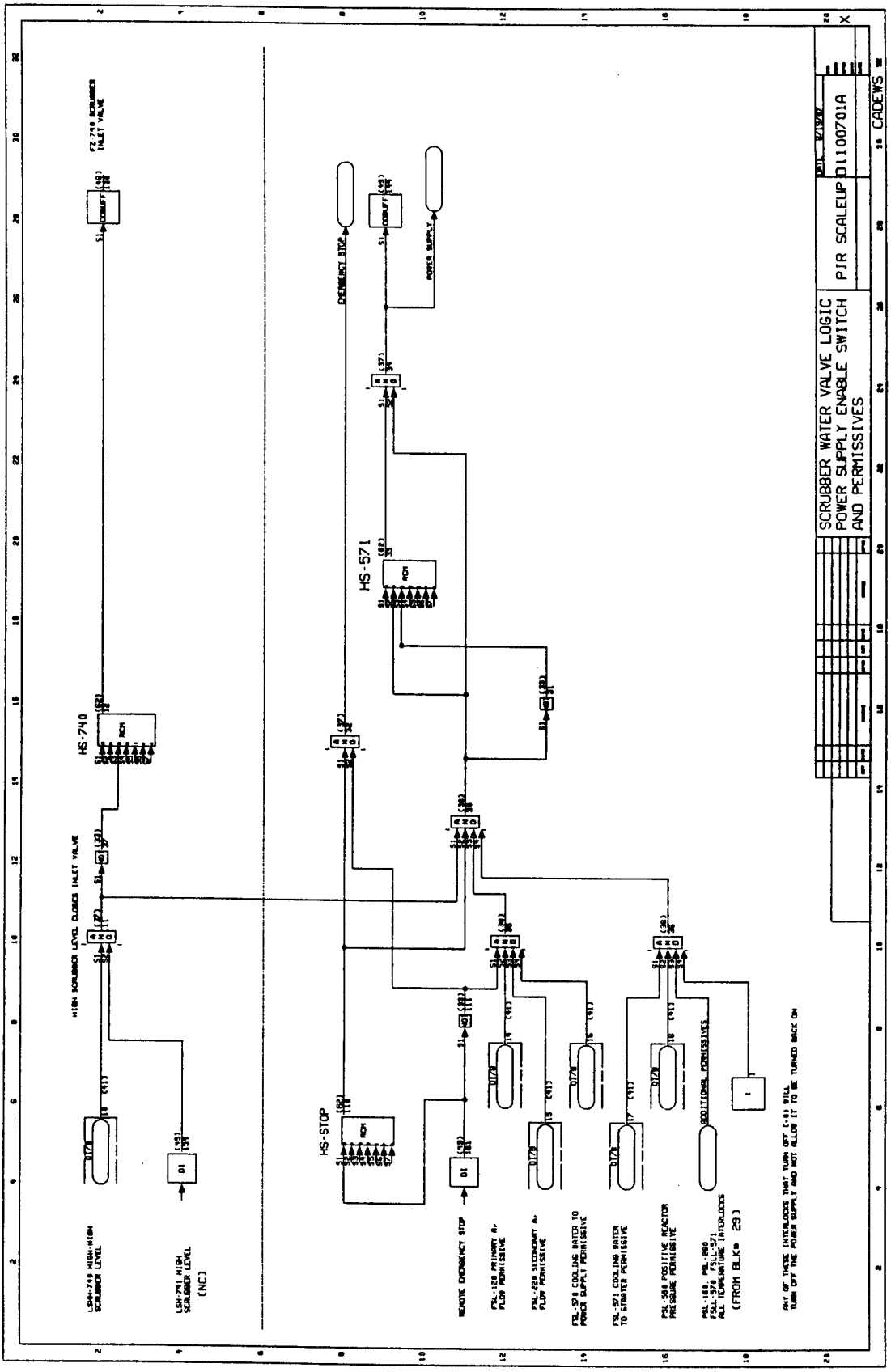

FIGURE XXIV

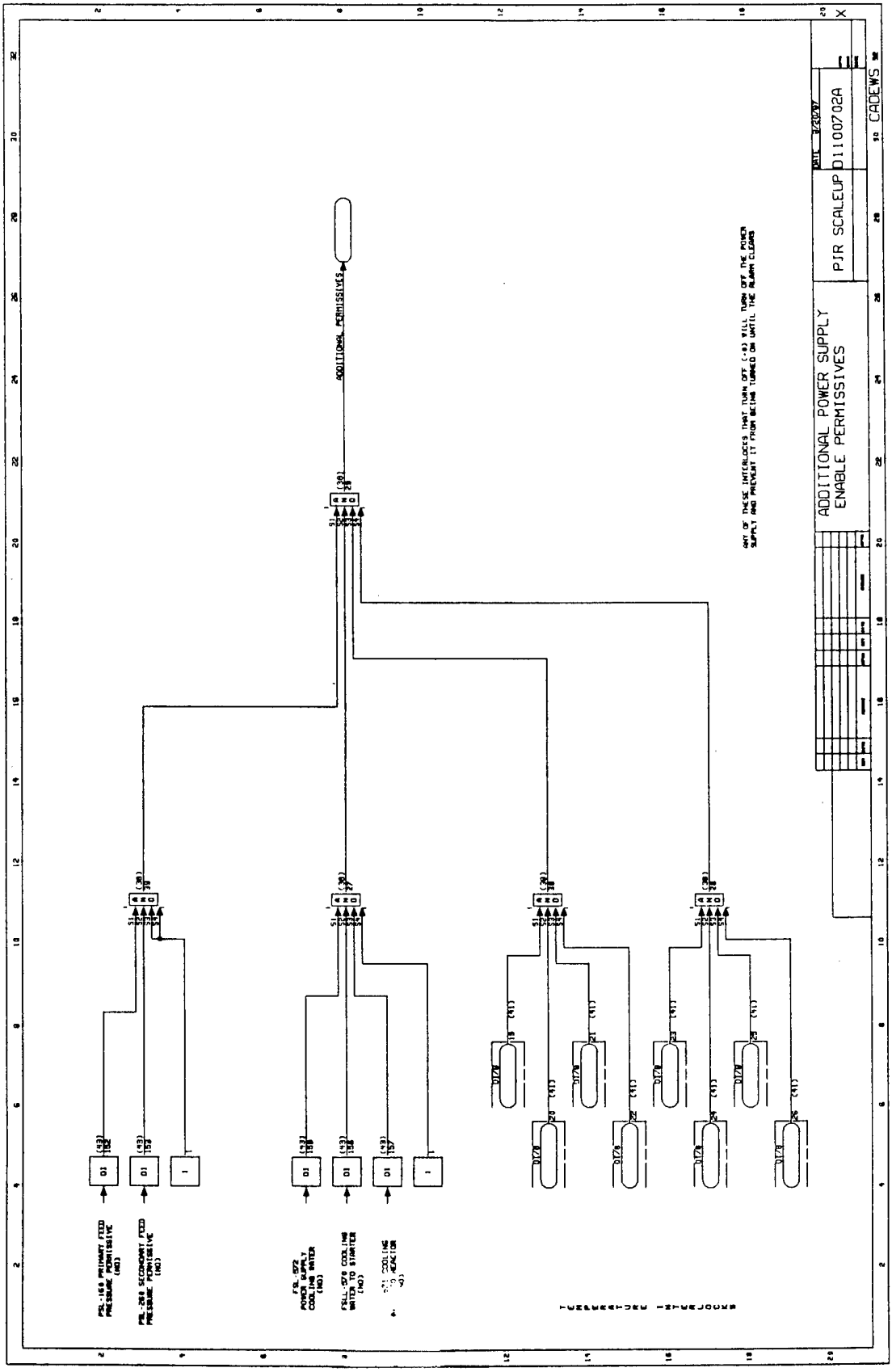
ADDITIONAL POWER SUPPLY
ENABLE PERMISSIVES
PJR SCALEUP
D1100702A
CADEWS
ADDITIONAL PERMISSIVES

lines. All field wiring was enclosed in cable trays, conduit, or flexible shielding. Connection cables between the termination boxes and the supervisory computer were routed in rigid conduit. Termination designations for the three termination boxes are depicted in Figures XXV, XXVI, and XXVII.

A separate area safety monitoring system was also installed on the Phase II unit. Combustible gas detectors were located above the gas induction system to identify any system hydrogen leaks. Fire detectors were located in the ceiling above the unit. Both systems were connected to the area alarm network. A free-standing chlorine monitor with a local alarm was also mounted on the unit to warn of any leakage of methyltrichlorosilane.

Task II - Confirmatory Experiments and Limited Production

A. Commissioning Exercises

Commissioning the Phase II facility was an extended and trying endeavor. The operation of the system was hampered by poor torch operability, product quality issues, and low product yields. Only the product quality issues were fully resolved.

Subsystems were qualified individually, and no significant problems were encountered with the gas and liquid feed systems, controls, cooling systems, or effluent handling. Significant problems surfaced in the power supply, and later in the particulate collection system.

The torch/power supply subsystem was tested using argon as the plasma gas and no methyltrichlorosilane feed. Argon torch operation is much less sensitive than hydrogen operation, but a stable plasma arc could not be established and maintained. Instead, severe erosion of the torch internals were experienced on every startup attempt. The gas metering system was recalibrated to assure appropriate gas flows, and additional attempts made with identical results. The potential problem areas were narrowed to four possibilities: the AA-61 torch was defective in some manner, the use of plant cooling water instead of deionized water was detrimental to torch operation, the power supply was defective in some manner, or the high frequency starter circuit was affecting torch operation.

The Phase I facility was pressed into service as a test stand for the Phase II subsystems. The AA-61 torch was reconfigured to resemble the Phase I AA-60 torch by fitting the new torch with a longer cathode bar. The reconfigured AA-61 torch was then mounted in the Phase I unit and operated using all Phase I support equipment. The torch started and

FIGURE XXV

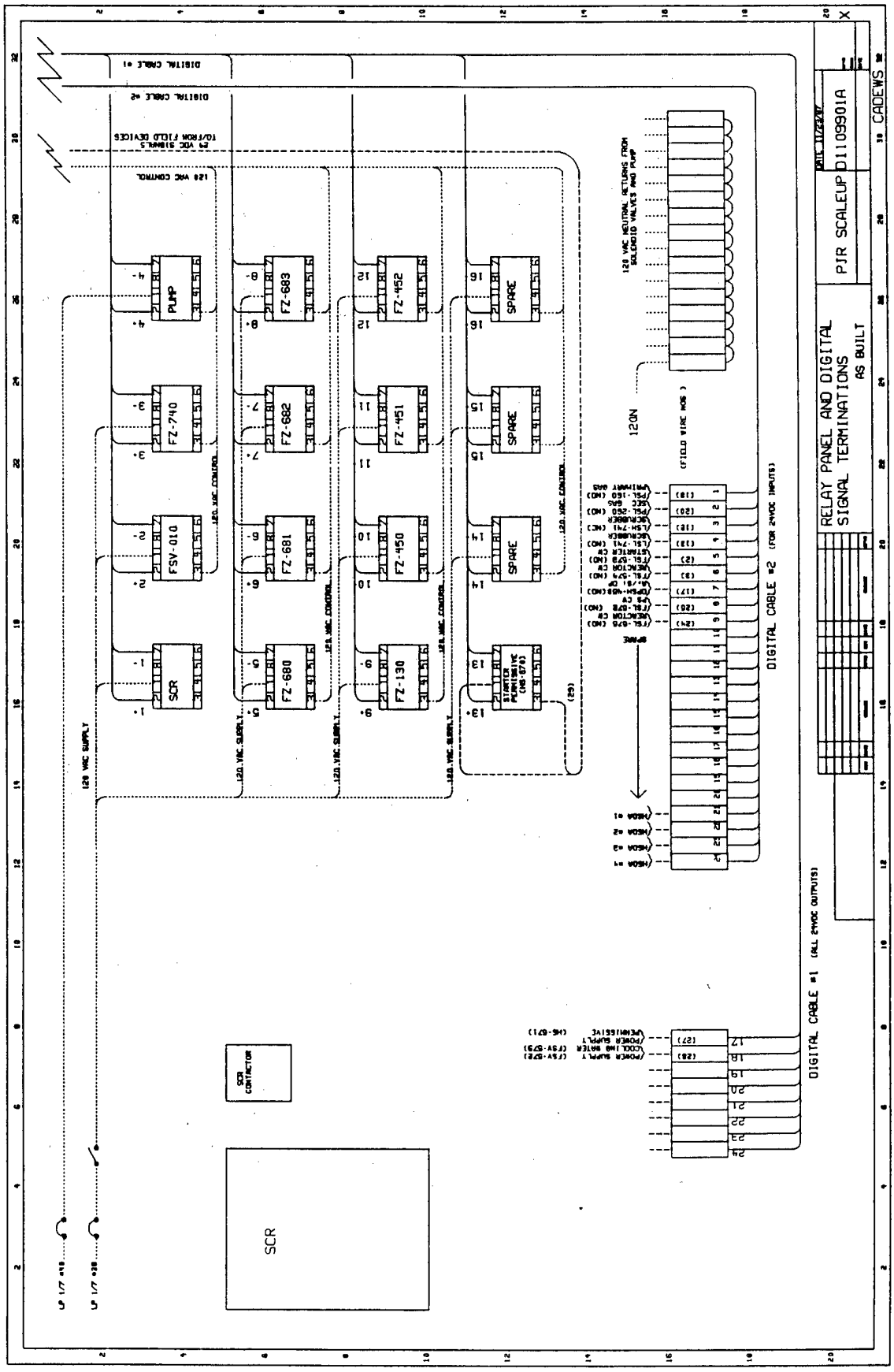
RELAY PANEL AND DIGITAL
SIGNAL TERMINATIONS
AS BUILT
PJR SCALEUP
D1109901A
CADEWS
DIGITAL CABLE #1
DIGITAL CABLE #2
120N
SCR
SCR CONTACTOR
PUMP
FZ-740
FSV-010
SCR
FZ-683
FZ-682
FZ-681
FZ-680
FZ-452
FZ-451
FZ-450
FZ-130
SPARE
SPARE
SPARE
STARTER FEEDBACK (CAB 070)
120 VAC SUPPLY
120 VAC CONTROL

FIGURE XXVI

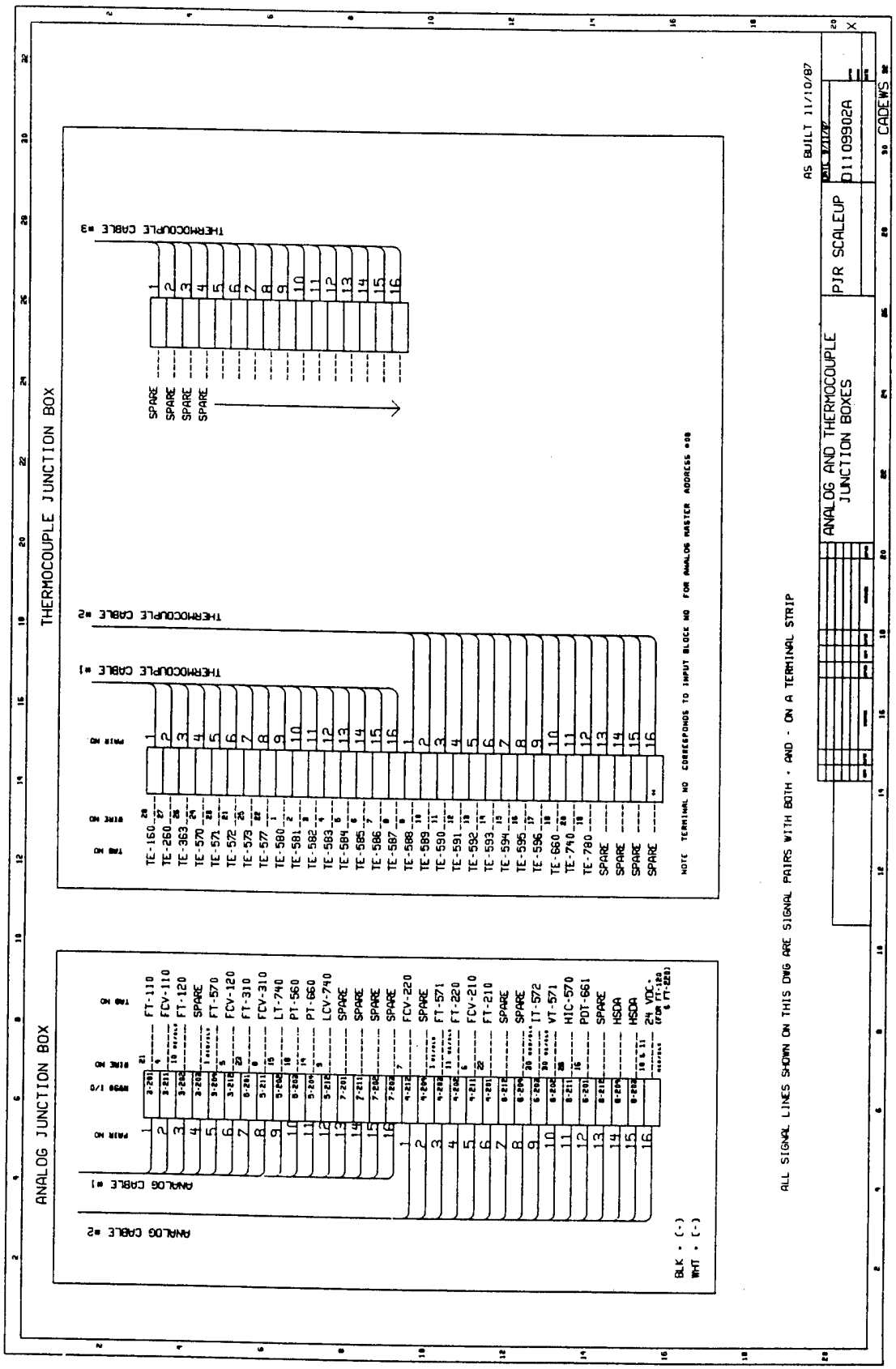
ANALOG JUNCTION BOX
ANALOG CABLE #1
ANALOG CABLE #2
BLK - (-)
WHT - (-)
THERMOCOUPLE JUNCTION BOX
THERMOCOUPLE CABLE #1
THERMOCOUPLE CABLE #2
THERMOCOUPLE CABLE #3
NOTE TERMINAL NO CORRESPONDS TO INPUT BLOCK NO FOR ANALOG MASTER ADDRESS #08
ALL SIGNAL LINES SHOWN ON THIS DWG ARE SIGNAL PAIRS WITH BOTH + AND - ON A TERMINAL STRIP
AS BUILT 11/10/87
ANALOG AND THERMOCOUPLE JUNCTION BOXES
PJR SCALEUP
D1109902A
CADEWS

FIGURE XXVII

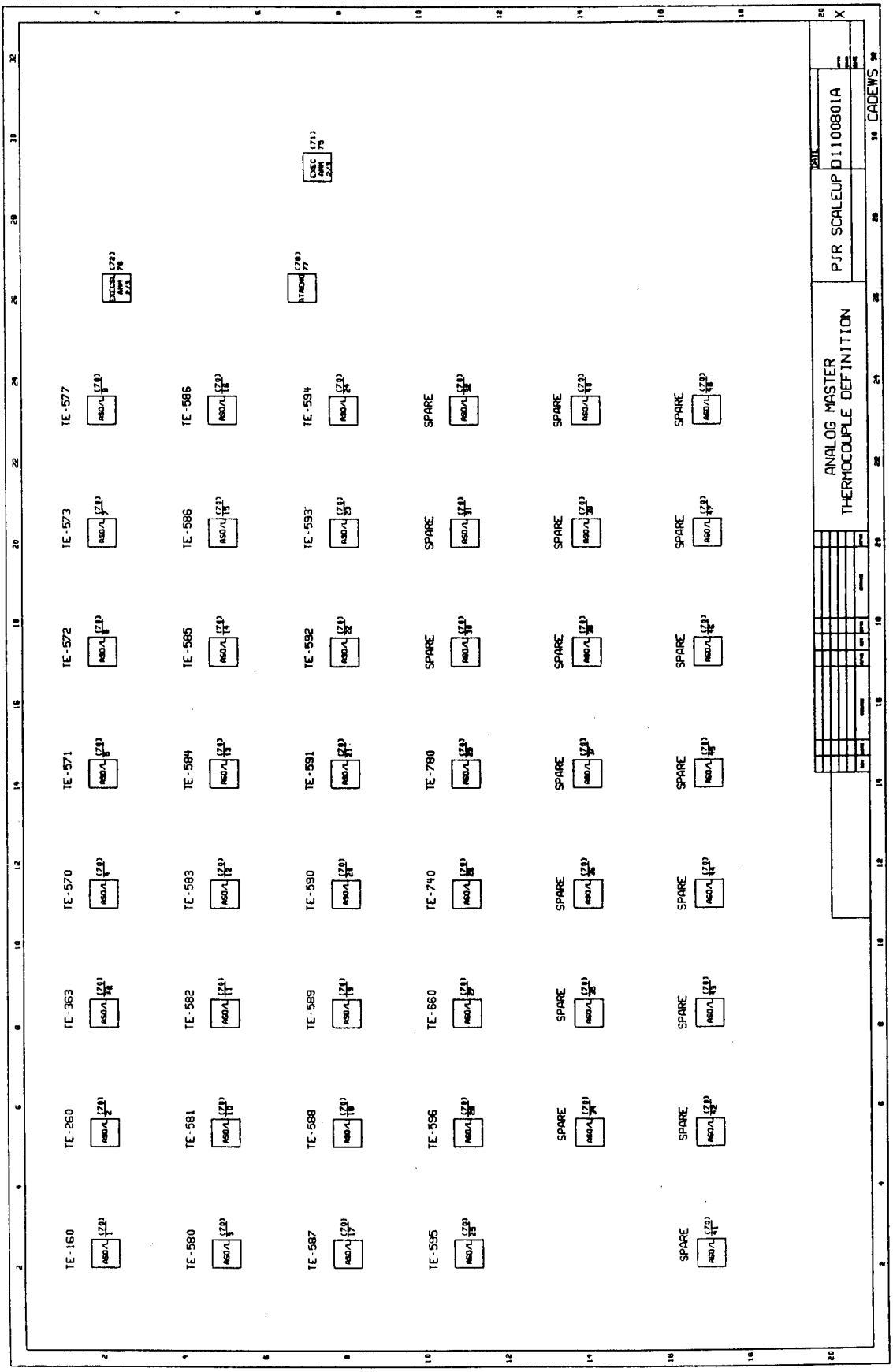

operated smoothly on both argon and hydrogen. The torch was removed, disassembled, and inspected. No wear was noted.

The torch was reassembled and mounted on the Phase II system. After three attempts to start the torch were unsuccessful, the torch was remove, disassembled, and inspected. As in previous attempts, the internal erosion was severe. The torch was dropped as a potential problem area and efforts focused on the other candidates.

The reconfigured AA-61 torch was rebuilt and remounted on the Phase II system. A pair of conductors was run between the Phase I power supply and the Phase II facility and connected to the torch system. The Phase II power supply was isolated from the system. The torch started and ran smoothly on argon at identical conditions as previously run on the Phase I system. The torch was again inspected, and no damage was noted. Since the new high frequency starter system and plant cooling water was used for this test, attention focused on the power supply to identify the difficulty.

The internal controller in the Phase II power supply was examined, and it was discovered that the controller output was not linear with controller input. The 4-20 mA input signal required a 50% signal before a 10% output signal was generated. Since all initial tests were conducted at a 20% setting, the power supply was effectively shut off on every occasion. The severe torch damage was thus even more puzzling.

To minimize the potential problem areas, the internal controller was disconnected and a manual rheostat control installed. The rebuilt AA-61 torch was tested again, and ran for 20 minutes on argon before the system was shut down in a normal manner. Upon inspection, however, the torch was severely eroded, indicating the problem still persisted. The question of time dependence of the damage was then addressed.

A rebuilt torch was mounted and operated for two seconds. Upon inspection the torch was damaged again, indicating that operation of the system did not have a significant affect, but either startup or shutdown damaged the torch. Shutdown transients were particularly suspect due to the increased inductive force provided by the four 40-millihenry chokes installed in the new power supply. Isolating the chokes was considered, but deferred as being potentially hazardous due to the confined space in the power supply enclosure and the potential for shorting out the power supply due to inadequate conductor spacing. It should be noted that experimental activities with a 960 volt, 300 amp DC power supply

designed to operate at an effective dead short is an extremely sensitive activity and had to be performed in a very methodical, considered manner to prevent possible lethal consequences. An examination of the power supply schematic will indicate that a minimum of 400 amps current draw at the main breaker is required to shut down the power supply, and thus affords no personnel protection in the event of a poorly designed test.

In lieu of isolating the chokes, a high speed data acquisition system was installed to monitor the current and voltage transients upon torch startup and shutdown. The system consisted of a Data Precision D6000 waveform analyzer driven by a Compaq 386. The system was capable of collecting a waveform "snapshot" of four thousand data points at a rate of up to one million points per second. The waveform was then downloaded to the Compaq's hard drive for later examination. A strip chart recorder was installed in parallel with the high speed system to monitor macroscopic system changes. A rebuilt torch was mounted and the torch started for two seconds, then shut down.

The results were a revelation. The high speed system went off scale, and stayed off scale for the entire data collection period (0.002 seconds after startup), indicating 1000+ amps current through the torch. The stripchart recorder, installed merely to identify gross transients, told the entire story; the current rose to over 2000 amps upon torch startup, and decayed to 200 amps (normal torch operating current) in a linear manner over a period of 750 milliseconds. No shutdown transient was noted. The startup transient, expected to last no more than half a cycle, was lasting over half a second, resulting in extreme damage to the torch.

Since the transient was so unexpectedly slow, the internal controller was investigated as a possible solution. The time constant of the controller was more than adequate to respond to the excursion noted. The input/output curve was calibrated and the unit reactivated. A torch test with the controller output similar to the manual rheostat was established and the torch was started. The system shut down immediately. A recorder connected to the controller output to monitor any possible induced setpoint increase showed that the controller shut down the output control signal as soon as the torch began to draw current. The torch was again damaged, and required a rebuild.

The power supply vendor was contacted, and indicated that the controller was typically used for furnace power supplies and would shut down if it detected a short in the output. Since the power supply

vendor also manufactured the controller, it was possible to identify the circuit that caused this response, and the unit was modified in the field.

A repeat of the test was made, and power supply did not shut down. The high current transient was noted again, even though the controller should have taken control action to prevent it. Consultation with internal and external power supply specialists, as well as the power supply manufacturer, indicated that a current surge on startup might induce a current in the control windings of the saturable reactor of the power supply, which would then respond by increasing output in response to the erroneous, induced signal. Parasitic resistors in series with the saturable reactor and controller output were then installed to dampen this effect. Further tests indicated that this approached diminished the transient somewhat, but not enough to prevent torch damage.

The output of the saturable reactors to the main power supply transformers were then tapped to permit the installation of large resistors between the two unit to reduce any induced signal. A 13-kw resistor was installed using the taps and the system tested again, with no better results.

Additional efforts to correct the startup transient were unsuccessful, and it was determined that all further project activities would proceed using the Phase I power supply and the Phase II torch reconfigured for operation at the reduced power level available. This course of action necessitated a reduction in the target production rate of silicon carbide powder. Using the Phase I power supply, a theoretical yield of two to three pounds of powder per hour was possible (less than half the original target rate).

B. Shakedown Runs

The production of silicon carbide powder was begun using the new facility and the Phase I power supply. A few short runs were made with no methyltrichlorosilane feed to identify stable torch operating conditions. The torch tended to run more stably at higher gas enthalpy levels, and the first synthesis attempts were made at elevated current and voltage levels (See Table VIII) since the system exhibited better operability characteristics and the Phase I work indicated that the methyltrichlorosilane system was relatively insensitive to torch conditions. Four runs were made in this series, with poor product results.

As shown in Table IX, the product from the first four runs had high surface areas (31 to 64 m^2/g), high free carbon levels (2.8 to 4.7 wt%) and low levels of silicon carbide in the product (81 to 93% calculated

TABLE VIII

PHASE II RUN OPERATING CONDITIONS

	Shakedown Runs								Confirmatory Runs				Production Runs					
RUN	1	2	3	4	5	6	7	8	9	10	11	12	13	14	15	16	17	18
Total H_2 (slm)	204	101	58	51	134	165	170	165	148	150	152	145	149	148	145	152	150	148
Total Ar (slm)	91	96	53	56	50	48	50	51	50	50	50	44	49	51	50	51	50	50
CH_3SiCH_3 (ml/min)	30.0	30.0	30.0	30.0	21.34	21.34	21.34	21.34	21.34	21.34	21.34	21.34	21.34	21.34	21.34	21.34	21.34	19.09
Volts	140	195	137	141	146	145	144	145	159	154	161	134	147	147	121	123	127	131
Amps	207	207	144	147	145	154	178	156	148	152	133	150	138	133	151	158	157	152
Torch Cooling (kW)		22.2	13.8	11.9	16.4	15.2	19.0	15.8	16.0	15.9	14.0	15.4	16.7	16.2	13.7	15.5	15.0	15.0
Net Power to Gas (kW)		18.1	5.87	8.85	4.77	7.11	6.59	6.82	7.56	7.52	7.37	4.74	3.59	3.35	4.53	3.96	4.94	4.91

TABLE IX
PHASE II PRODUCT CHARACTERIZATION

		Shakedown Runs								Confirmatory Runs				Production Runs							
RUN	PHASE 1	1	2	3	4	5	6	7	8	9	10	11	12	13	14	15	16	17	18	Baghouse Up To Run 16	Baghouse Runs 17, 18
Surface Area (m^2/g)	10.0	64.7	31.0	59.2	62.0	195.	107.	170.	100.	29.8	25.8	26.1	29.2	22.5	26.2	21.7	33.2	20.1	24.3	29.7	20.3
Total C w/o	29.55	29.30	30.75	29.32	28.96	21.98	25.60	-	-	30.24	29.80	29.85	29.96	29.72	29.49	28.76	29.40	29.33	29.37	24.82	28.65
Free C w/o	0.35	4.2	2.8	3.5	4.71	0.2	0.1	-	-	1.06	1.67	1.27	0.67	0.48	0.38	0.24	0.40	0.31	0.12	0.34	0.08
Calc SiC w/o	97.3	83.9	93.4	86.2	81.0	72.7	85.2	-	-	97.5	94.0	95.5	97.8	97.7	97.2	95.3	96.9	96.9	97.7	81.8	95.4
Free Si w/o	0.09	0.32	0.19	0.15	0.68	-	-	-	-	0.10	0.21	0.14	0.07	0.10	0.08	1.75	0.46	0.10	0.20	1.03	0.19
GOI w/o	-	-	1.55	2.55	-0.22	14.7	9.38	-	-	2.96	0.36	2.86	3.45	4.11	1.76	2.39	4.48	1.15	1.90	2.27	2.43
Oxygen w/o	0.58	3.88	1.35	1.55	2.81	-	-	-	-	1.64	1.82	0.93	0.43	0.37	0.42	0.63	0.77	0.39	0.36	5.46	.92
Nitrogen w/o		0.03	0.09	0.07	0.01	-	-	-	-	0.07	0.05	0.07	0.04	0.048	0.031	0.014	0.065	0.057	0.14	0.058	0.24
Iron w/o	<0.01	0.3	0.05	0.04	0.03	-	-	-	-	0.16	0.12	0.12	0.05	0.04	<0.01	<0.01	0.03	<0.01	0.03	.66	<0.01 (ES)
Aluminum w/o		0.08	0.02	0.01	<0.01	-	-	-	-	0.06	0.04	0.05	<0.005	<0.005	<0.01	<0.01	<0.01	<0.01	<0.01	<0.01	<0.01 (ES)
Copper-PPM		[950.	1000	400	<50	-	-]			[<50	100	<50]	<28.	<0.5	<30.	<0.5	<0.5	<0.1	<0.1	<0.5	<0.1 (NAA)
			By ES								By ES										
NF Lab #		159	233	279	304	396	405			630	630	630	691	692	713	748	05	044	052	07	052

SiC). In addition, very low recovered product yields were experienced, which was attributed to the undersized product powder passing through the filter elements and being washed down the drain in the tail gas scrubber bottoms stream.

It was decided to benchmark the Phase II system on the best operating point defined by the Phase I parametric study. To permit methyltrichlorosilane feedrates identical to Phase I work, the liquid metering pump was changed out with the same pump used for the Phase I studies. A series of four more runs was then made.

The results of the benchmark runs were more distressing than the first four runs. As described in Runs 5 through 8 in Table IX, the product powder had extremely high surface areas (between 100 and 195 m^2/g), which was an order of magnitude greater that the Phase I products. Because of the high surface areas, the materials were not even fully characterized. Again, low recovered product yields were attributed to the very fine particle size of the product powders.

Referring to the temperature and flow field model developed in Phase I, it was noted that the transition from turbulent to laminar flow in the bench scale reactor permitted appreciable recirculation of reactant gases and products at the entrance to the reactor vessel. The recirculation might also contribute to cooling of the plasma plume, degrading the synthesis reaction. It was decided to install a baffle at the reactor inlet to confine the plasma and reactants until sufficient mixing and reaction had occurred and minimize the recirculation effect.

A cylindrical graphite insert eight-inches long, with an internal diameter of 2.0 inches and walls 0.25-inches thick was fabricated and installed at the reactor inlet port. Plasma gas and methyltrichlorosilane entered the reactor along the center line of the insert, and then into to the eight-inch diameter reactor vessel. A third series of four runs was then conducted.

The results of the third series, designated "Confirmatory Runs," are shown as Runs 9 through 12 in Table IX. The surface area dropped to 25 to 30 m^2/g, and the product purity met or exceeded the best Phase I material. The system ran very smoothly, with no unscheduled shutdowns or other difficulties. Product powders were collected and submitted for detailed sintering studies.

C. Sintering Studies

The beta-SiC powders were processed in several ways prior to sintering. In all cases, however, boron and carbon were added as sintering aids.

The boron addition was elemental boron manufactured by Callery Chemical Company. Properties of the material are:

- Particle Size - Submicron (1500A) and amorphous
- Surface Area - 80 m^2/gm
- Purity - 99+%
- Impurities
  - C <0.01%
  - N_2 <0.02%
  - O_2 ~0.1% (as packaged
  - Other less than spectrographic analysis detection limit of 10 ppm

The carbon addition was a liquid phenolic resin manufactured by Reichold Chemicals, Inc. Properties of this material are:

- Density - 1.185 to 1.195 g/cm^3
- Char Yield - 44%

Figure XXVIII describes the powder beneficiation steps used as indicated in Table X, Powder Processing Matrix.

Vibratory grinding was done in a polymer-lined vibratory mill containing 100 gms of beta-SiC powder, 2200 gms of sintered SiC grinding media, 250 ml of distilled water, and 5 to 10 drops of a wetting/dispersion agent. Grinding time was eight hours.

Screening was done initially through a course 20 mesh sieve to remove the grinding media from the slurry and subsequently through a 500 mesh sieve. The powder was allowed to settle and the water was decanted.

Drying was done in an oven at 80°-90° for eight hours in air.

Oxidation of dried powder to remove excess carbon was done in a crucible heated to 800°C for four hours in an air atmosphere furnace.

Acid treatment of the oxided powder to remove SiO_2 was done by leaching 30 g of the powder in a solution of 30 ml HF/HNO_3 mixture, 100 ml of distilled water for two hours at room temperature while mixing with a magnetic stirrer. The slurry was transferred to a 1-gallon

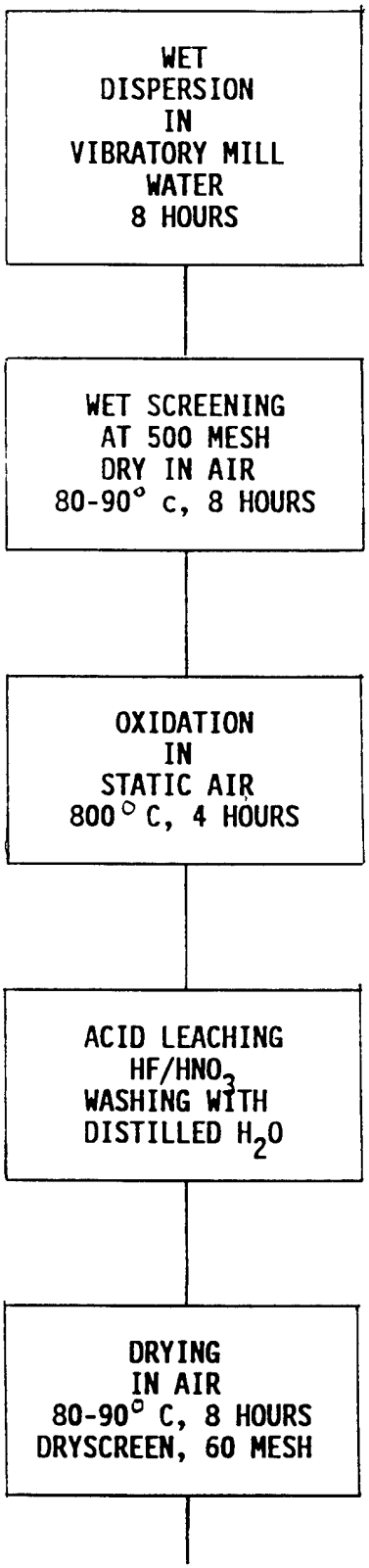

FIGURE XXVIII

Beneficiation of Beta Silicon Carbide Powder

TABLE X

SINTERING QUALIFICATIONS OF BETA SILICON CARBIDE

Powder Processing Matrix

Sintering Conditions: Continuous Tube Furnace

2130°C, 1/4 inch/min., 45 min. in hot zone

POWDER LOT NO.	R&D NO. A-88	VIBROTARY MILLING (hrs.)	PROCESSING CONDITIONS WET SCREEN (Mesh Size)	OXIDATION 800°C/4hrs	ACID TREATMENT HF/HNO_3	SINTERING ADDITIVES Wt% B	Wt% C	GREEN DENSITY at 16000 psi (%)	SINTERING DENSITY Sample (%)	Standard (%)
12	691	---	---	---	---	0.5	2.0	55.2	85.2*	92.6
						0.5	4.0	55.8	86.1	
11	630	---	---	---	---	0.5	2.0	58.1	83.6	85.6
10	630	---	---	---		0.5	2.0	53.2	78.4	98.1
13	692	---	---	---	---	0.5	2.0	57.4	85.9*	92.6
13	692	---	---	X	X	0.5	2.0	54.2	82.6	95.8
						0.5	4.0	57.2	86.1	95.8
13	692	---	400	---	---	0.5	2.0	55.9	84.4	97.3
13	692	---	400	X	X	0.5	2.0	54.2	82.6	95.8
						0.5	4.0	57.2	86.1	95.8
13	692	9	500	---	---	0.5	2.0	49.8	49.9	96.5
						0.5	4.0	51.5	49.3	96.5
14	713	8	500	X	---	0.5	2.0	49.6	48.1	96.5
						0.5	4.0	49.5	46.8	96.5
14	713	8	500	X	X	0.5	2.0	56.3	96.0	97.1
						0.5	4.0	59.3	97.1	97.1
15**										
16**										

** Sintering Qualifications Not Complete. Will Be Added as Available

* Sintered at 2100° for 30 Minutes, All Others at 2130°C for 60 Minutes. All in Argon.

container where the powder was repeatedly washed with water (five minutes agitation), settled, and decanted until a pH of 5 to 5.5 was reached.

Drying was again done in air at 80 to 90°C.

The beta-SiC powders were then prepared for pressing into test specimens. The following composition was mixed for 15 to 20 minutes with a magnetic stirrer:

Beta-SiC Powder	27.25 g (95.5%)
Resin	1.36 g (2% C) or
Resin	2.73 g (4% C)
Callery Boron	0.15 g (0.5%)
Acetone	50 ml

This slurry was allowed to air dry and then was screened through a 60 mesh sieve. The screened powder was pressed at 20,000 psi into 1-1/4 inch diameter sample discs.

Standard sample discs were prepared from Betarundum SiC (beta-SiC) batch 0195, acid treated.

Sintering tests were conducted in either a laboratory Astro furnace or a Harper tube furnace.

The dry-pressed beta-SiC green sample was placed in a closed graphite crucible. The crucible was fed into a laboratory Astro furnace and went through the sintering profile shown in Figure XXIX. The heating rate between room temperature and 1600°C is 27°C/min and a sample was held at 1600°C for 30 minutes. Then, the heating rate was adjusted to 15°C/min and a temperature of 2125°C was held for the pre-set time.

For the sintering tests in the tube furnace, the hot zone was maintained at 2130°C. Disk samples along with beta-SiC standard samples in a crucible were fed at a rate of 1/4 inch/min, so that it required about 60 minutes to pass through the hot zone. All the sintering tests were done in argon gas.

The sintering results for as-received and beneficiated beta-SiC powder lots are all shown in Tables X and XI. Under the conditions indicated, which are not all considered optimum for beta-SiC, as-received powder lots sintered to greater than 91% of theoretical density, and beneficiated powder lots sintered to 97% of theoretical density.

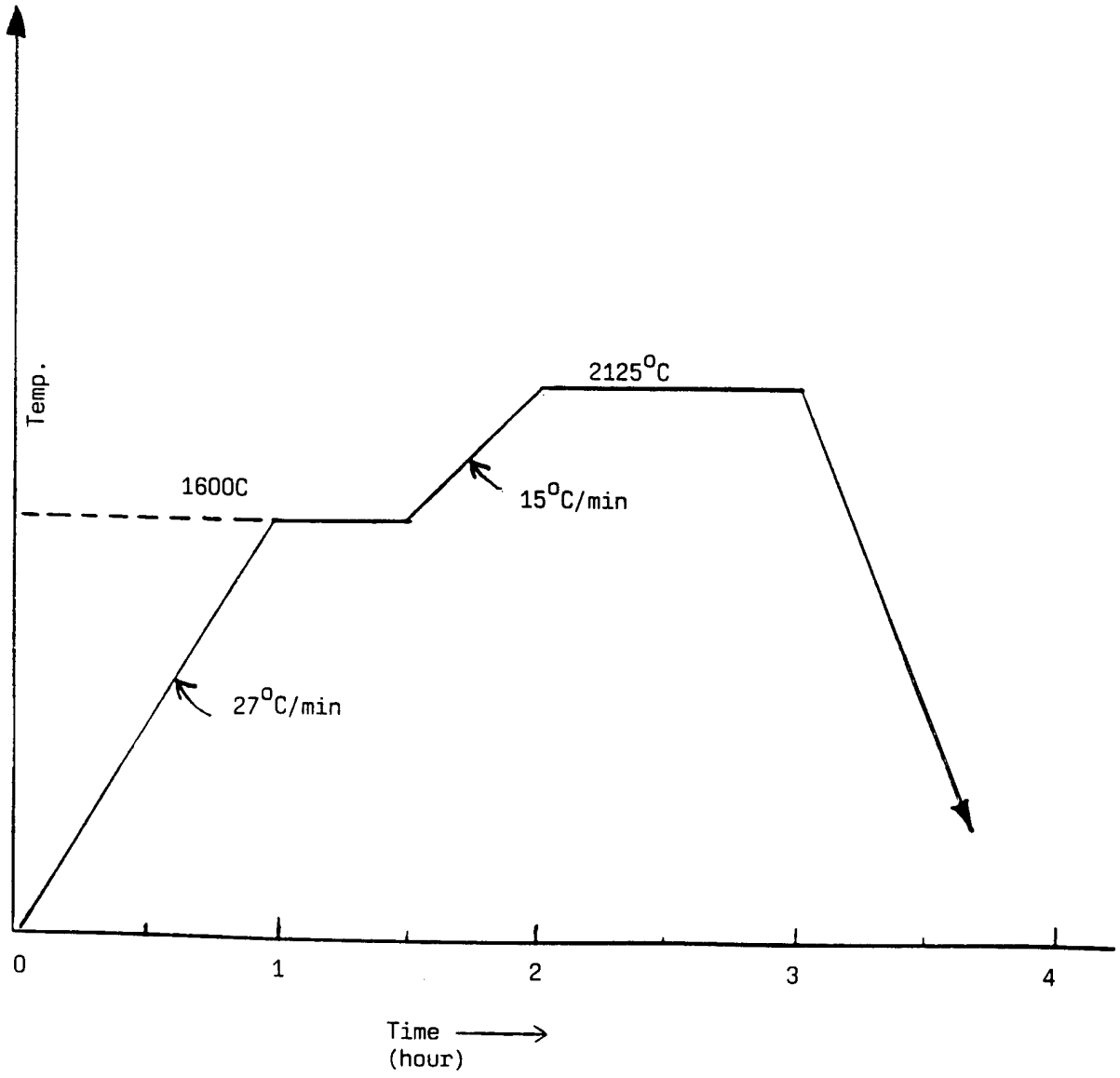

FIGURE XXIX: Laboratory Astro Sintering Schedule

TABLE XI

SINTERING QUALIFICATION OF BETA SILICON CARBIDE

Sintering Condition Matrix (as received powder)

Laboratory Astro Furnace - Batch Operation

Argon Atmosphere

POWDER LOT NO.	R&D NO. A88-	SINTERING ADDITIVES Wt. % B	Wt. % C	GREEN COMPACTION DENSITY (%)	SINTERING CONDITIONS Temp. (°C)	Hold Time (min)	SINTERING DENSITY Sample (%)	Standard (%)
9	630	0.5	2.0	54.9	2,060	90	82.1	92.3
10	630	0.5	2.0	53.6	2,060	90	79.7	92.3
11	630	0.5	2.0	58.2	2,080	45	84.8	95.3
10	630	0.5	2.0	58.1	2,080	45	85.1	95.7
12	691	1.0	4.0	57.2	2,050	90	85.3	
12	691	1.0	4.0	57.3	2,125	30	91.2	
12	691	1.0	4.0	56.8	2,200	30	79.8	
12	691	1.0	4.0	55.8	2,125	60	86.1	
12	691	0.5	2.0	55.2	2,100	30	85.2	92.6
13	692	0.5	2.0	57.4	2,100	30	85.9	92.6
14	713							
15*								
16*								
17*								

*Sintering Qualifications Not Completed. Will Be Added As Available.

Microstructures of a sintered sample from Lot #14 are shown in Figure XXX. These and the sintered densities compare favorable with the sintered samples prepared from Phase 1 powders.

D. Production Runs

Concurrent with the sintering studies, a series of four, five-hour production runs was made to produce powder for additional sintering investigations and to provide material to Oak Ridge National Laboratory for their evaluation. The operating conditions of these runs are tabulated in Table VIII, and the product powder characterization is included as Table IX. The runs were replicates of Run 13, and the system operated as smoothly as in the previous tests. Similar to previous runs, the recovered product yield was exceptionally low and particulate material was evident in aliquot samples withdrawn from the liquid bottoms of the tail gas scrubber.

A fifth production run was terminated after 10 minutes of methyltrichlorosilane feed due to excess reactor pressure. The normal 8 to 10 psig reactor pressure abruptly rose to 30 psig and the filter element blowback attempted to go into continuous blowback mode. The reactant gas flow was stopped and the filter blowback system cycled a number of times to dislodge any filter cake. When gas flow was re-established, the pressure again climbed to 25 psig before the gas supply was discontinued. A second attempt to clear the filter elements with the blowback system was also unsuccessful.

The filter unit was disconnected and the filter elements removed for inspection. All four filter elements were coated with a 1/4- to 3/8-inch thick layer of silicon carbide powder. The material was easily removed with a plastic bristle brush followed by a water wash using a garden hose-type nozzle. Upon inspection, it was discovered that a weld in the filter media of one element had failed and gap of approximately 1/4 inch by 12 inches long had developed. The space between the filter media and the metal cage which supported the media from inside was packed solid with powder, and powder was observed in the inside of the filter element to the height of the gap.

It is speculated that the filter failed early in the test program and was masked by the other difficulties encountered and the small particle size of the initial product powders. The three square inch gap in the filter media was more than adequate for easy passage of all reactant and product gases, as well as most product powder. Because no differential pressure developed across the filter media, the blowback cycles were not frequent enough to loosen the powder that gradually accumulated. A portion of the powder that passed through the gap in the media salted

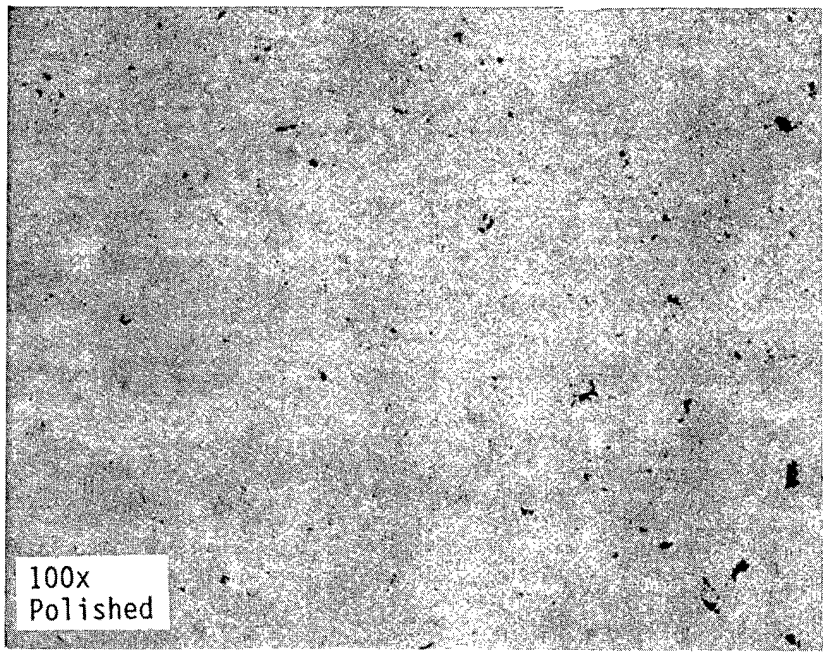

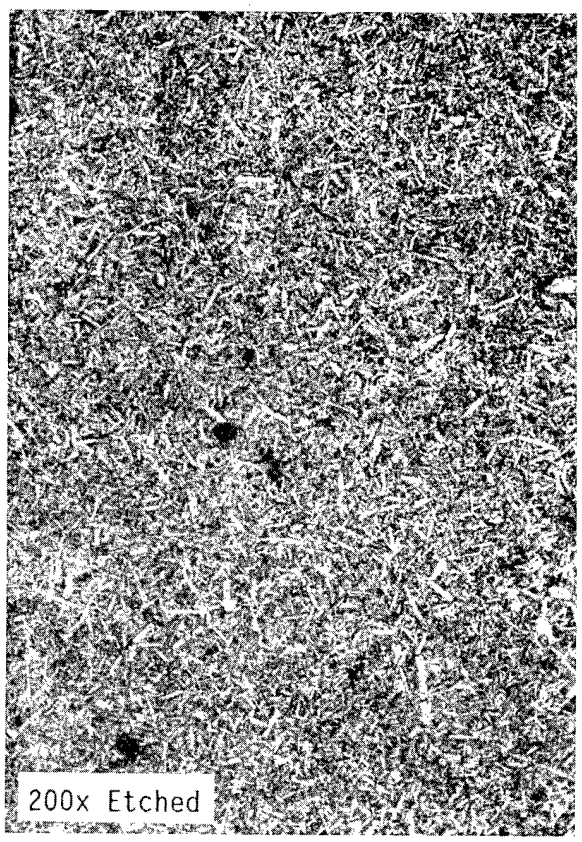

FIGURE XXX: The polished and etched microstructures of Oak Ridge powder Lot No. 14 A88-713 with 0.5%B and 4%C sintered at 2130°C for 60 min in argon to a density of 97.1% of theoretical density.

out of the gas stream and accumulated in the bottom of the filter element. When a sufficient volume of powder accumulated to close off the gap, the differential pressure rose abruptly. Because of the thick layer of powder on the filters and the compaction of the filter cake by the small amount of reactant gases that passed through the cake, the blowback system could not dislodge the material.

Task III - Flowsheet Development and Economic Analysis

The target production rates of the Phase II facility were used as the basis for the economic evaluation of the process. Based on a 50,000 pound per year product yield, 95% product recovery, and an 80% service factor for the facility, the heat and material balances developed for the pilot scale unit may be used. See Figure VIII and Table VII.

The production costs of product silicon carbide powder were categorized as variable costs (Table XII); fixed capital costs, based on the actual construction costs of the pilot scale unit and required offsites (Table XIII); a calculation requiring a 15% return on capital employed (Table XIV); and fixed operating costs (Table XV).

The total product cost is estimated to be $20.60 per pound of recovered silicon carbide powder, with a range between $19.60 and $21.55 based on December, 1988, current costs (Table XVI). The estimate range is due to a ±40% cost estimate of fixed capital costs. These estimates do not include the costs of any required product beneficiation for specific process requirements.

The key cost components of the estimate are hydrogen gas consumption (36% of total cost) and manpower charges, which include wages, administration, plant overhead and benefits (34% of total costs). Materials, excluding hydrogen, account for only 18% of total cost, and employed capital 7 to 16% of product costs.

These estimates indicate that significant economies of scale can be realized by increasing production rates, which would lead to a significant reduction in labor costs on a per-pound-produced basis. Since the intermediate scale was not successfully demonstrated in this project, extrapolation to a 300,000 to 500,000 pound per year process was not possible with any degree of precision. It is reasonable, however, to consider a cost reduction in excess of $3 per pound a possibility for such a facility.

TABLE XII

PROCESS ECONOMICS
VARIABLE COSTS

Resource	Cost Per Pound Recovered Product
Hydrogen	$7.50
Methyltrichlorosilane+	2.70
Electricity	.50
Cooling Water/Misc.	.50
Total Variable Costs	$11.20

* December, 1988

\+ Nominal 99% Purity

TABLE XIII

PROCESS ECONOMICS
FIXED CAPITAL COSTS

BASIS: 50,000 lb/yr Silicon Carbide Product Make

Inside Battery Limits
- Reactant Metering and Induction System
- Torches, Power Supply, Controls
- Product Recovery
- Process Instrumentation and Controls

$400,000 (+/- 40%)

Outside Battery Limits
- Feedstock/Product Storage
- Environmental Systems (Flare)
- Offices
- Shipping/Receiving

$400,000 (+/- 40%)

TABLE XIV

PROCESS ECONOMICS
RETURN ON CAPITAL EMPLOYED

BASIS: 50,000 pounds per year silicon carbide product make
$800,000 total fixed capital (+/- 40%)
15% return on investment

Fixed Capital Costs: $2.40 per pound

Range: $1.44 to $3.36 per pound

TABLE XV

PROCESS ECONOMICS
FIXED OPERATING COSTS

Resource	Cost Per Year
Operators*	$174,000
Local Administration+	40,000
Plant Overhead**	87,000
Payroll Burden++	47,000
Total Fixed Operating Costs	$348,000
Fixed Operating Costs Per Pound	$6.96

* One shift position; three shifts per day; $37,000 per year per operator; 4.7 factor for shift coverage and absences.
\+ At 23% of hourly payroll.
** At 50% of hourly payroll.
++ At 27% of hourly payroll.

TABLE XVI

PROCESS ECONOMICS
TOTAL PRODUCT COST

Resource	Cost Per Pound Recovered Product
Total Variable Costs	$11.20
Total Fixed Capital Costs*	2.40
Total Fixed Operating Costs	7.00
Total Product Cost	$20.60
Product Cost Range	$19.60 to $21.55

* Range: $1.44 to $3.36 per recovered pound silicon carbide

At any scale greater than the bench scale unit developed for the Phase I work, locating the production unit at or near a hydrogen production unit is indicated. Since well over a third of the product cost can be attributed to hydrogen consumption and large quantities of hydrogen effluent results from the processing, recovery is a definite economic incentive. A stand-alone hydrogen purification facility to process waste gases and recycle would be prohibitively expensive except for a huge silicon carbide production unit. More reasonably, the silicon carbide plant could be located in close proximity to an existing hydrogen purification plant with excess capacity, and return spent gas for recovery. Since the actual consumption of hydrogen gas is relatively small, about 0.08 pound hydrogen per pound silicon carbide produced, costs could be driven into the $10 to $15 per pound range.

CONCLUSIONS

High purity, high surface area, pressureless sinterable silicon carbide powders can be produced using a hydrogen rich thermal plasma and methyltrichlorosilane as a carbon and silicon source. Produced powder can be pressureless sintered to 91% of theoretical density with no additional treatment, or to 97% of theoretical if beneficiated by post-processing. The thermal plasma process is amenable to process scale-up until torch power levels exceed 200 kilowatts. Thereafter, multiple torch systems, possibly with a common product collection train, must be considered. Great care should be taken when specifying and selecting the torch/power supply subsystem to avoid extreme current transients. Economic evaluations indicate that silicon carbide powders can be produced for approximately $20 per pound at a scale of 50,000 pounds per year, and potentially at $15 per pound at a larger scale with an inexpensive supply of hydrogen, or an available hydrogen purification facility.

APPENDIX A

COMPUTER MODELLING OF THE GAS PHASE SYNTHESIS OF SILICON CARBIDE IN D.C. PLASMA REACTOR

FINAL REPORT

COMPUTER MODELLING OF THE GAS-PHASE SYNTHESIS OF SILICON CARBIDE IN A D.C. PLASMA REACTOR

by

M.I. Boulos, P. Fauchais and E. Pfender

Prepared under the terms of contract agreement # RJ42954 of March 1985
with Sohio Chemicals & Ind. Products Engineering Materials Sector,
Niagara Falls, N.Y.

EXECUTIVE SUMARY

An investigation was carried out of the different fundamental phenomena which playes an important role in the synthesis of ultrafine silicon carbide powders in a d.c. plasma jet reactor. This involved the following specific studies.

- The development of an appropriate mathematical model for the computation of the flow and temperature fields in the reactor. An important feature of this model is that it involved both turbulent and laminar flow regimes in the main reactor chamber. The turbulent flow region was limited to the entrance region of the reactor where flow separation occurs accompanied by the development of a strong recirculatory flow. Between 50-60% of the energy of the plasma was lost to the reactor wall in this region.

- Thermodynamic calculations of the equilibrium composition of a gas mixture of H_2-Ar-Ch_4-$SiC\ell_4$ at atmospheric pressure over the temperature range between 300 and 6000 K. The results obtained using the Gibbs free energy minimization technique are given in both graphical and tabulated form for the following gaseous mixture initial molar composition H_2 = 0.566, Ar = 0.337, CH_4 = 0.019 and $SiC\ell_4$ = 0.038.

- An analysis of the chemical kinetics of the homogeneous reactions occuring in the plasma. This study was however limited to the the $SiC\ell_4$ + H_2 system.

- A literature review of nucleation and growth theory of fine particle formation by gas phase reactions. This covered such topics as homogeneous nucleation and particle growth by condensation and different coagulation mechanisms.

ACKNOWLEDGMENT

Contributions to this study has been made by the following persons.

Dr. Javad Mostahimi, Dept. of Chemical Engineering, Université de Sherbrooke, who has been responsible for the development of the computer code for the calculation of the flow and temperature fields in the plasma reactor.

Dr. B. Pateyron, Université de Limoges, who has been responsible for the computation of the equilibrium composition of the reaction mixture as function of temperature.

Dr. M.E. Couder, Université de Limoges, who has been responsible for the Chemical kinetics study.

1. INTRODUCTION

Over the last few years there has been a growing interest in the use of thermal plasma technology for the synthesis of ultrafine powders of refractory ceramics such as oxides, nitrites and carbides of silicon, aluminum, titanium, tungsten...etc. Most studies have been carried out using d.c. and r.f. plasma generators at different power levels up to 100-150 kW. In a few cases, such as for the production of TiO_2 pigment by the combustion of $TiC\ell_4$ in an oxygen plasma, commercial level operation has been achieved on the MW level.

The present investigation is mainly concerned with the synthesis of ultrafine silicon carbide powders in a d.c. plasma jet through the reaction of silicon tetrachloride with methane according to the following simplified chemical reaction route.

$$SiC\ell_4 + CH_4 \rightarrow SiC + 4HC\ell$$

The work presented in this report has been carried out as part of a larger research program undertaken by Sohio Chemicals with the objective of developing the scientific and technological bases for the scale-up and the eventual commercial production of silicon carbide powders using the plasma route. Three areas of research has been addressed in parallel in this study at the Université de Sherbrooke in Quebec, The Université de Limoges in France and at the University of Minnesota. These dealt respectively with the following tasks.

- The development of an appropriate mathematical model for the computation of the flow and temperature fields in the plasma jet reactor.

- Computation of the equilibrium composition as function of temperature for the H_2-Ar-CH_4-$SiC\ell_4$ system and the study of the chemical kinetics of possible reactions occuring in the plasma process for the same system.

- Literature review of work carried out in the area of aerosol particle nucleation and growth which could be pertinent to the modelling of the overall reactor/condensor system.

In this report the results obtained for each of these studies are presented separately in sections 2-5. An overall summary of the principal finding and recommendations for futher work are presented in section 6.

2. MATHEMATICAL MODEL FOR THE CALCULATION OF THE FLOW AND TEMPERATURE FIELDS IN THE PLASMA JET REACTOR

2.1 INTRODUCTION

This section deals with the development of an appropriate mathematical model for the calculation of the flow and temperature fields in the plasma jet reactor. A schematic of the reactor and its principal dimensions are given in Figure 2.1. This consisted essentially of a d.c. plasma torch of a nominal power of 45 kW. At the exit of the torch, the plasma gas, Q_1, composed of an Ar/H_2 mixture, is introduced into a mixing chamber in the form of a cylindrical channel, 66.0 mm long and 8.0 mm i.d., in which the secondary, Q_2, and tertiary, Q_3, gases are injected. These are composed respectively of Ar/H_2, and Ar/CH_4 mixtures. At the end of the mixing chamber, the gases immerge into a cylindrical, water-cooled, reactor chamber with an internal diameter of 48.0 mm and 1800 mm long. A summary of the nominal operating conditions as indicated in the original work statement of March 29, 1985, is given in the 1st column of Table 2.1. The maximum gas flow rates in this case are as follows:

Primary gas, Q_1

H_2 = 100 slm
Ar = 100 slm

Secondary gas, Q_2

H_2 = 100 slm
Ar = 100 slm

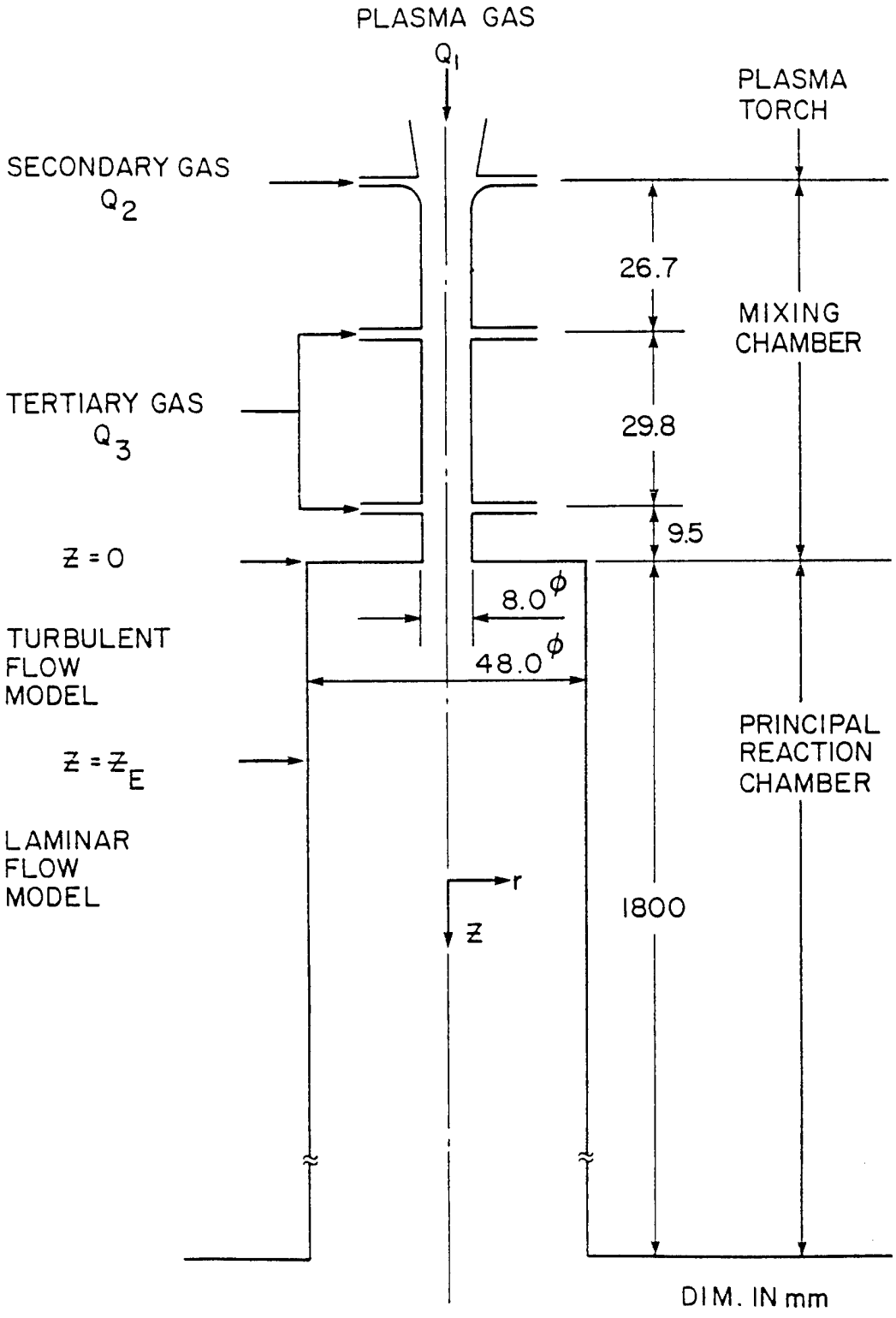

2.1 Schematic and principal dimensions of the plasma jet reactor.

Table 2.1

Parameter	Operating condition in the original work statement March 29, 1985	New set of operating conditions Oct. 10, 1985
Gas flow rate (slm)		
Argon	200.-	15.0
Hydrogen	300.-	75.0
CH_4	10.-	-
$SiCl_4$	20.-	-
Total	530.-	90.-
Gross torch power (kW)	50.-	20.-
New power in the plasma (kW)	30.-	10.-

Tertiary gas, Q_3

H_2 = 100 slm
CH_4 = 10 slm
$SiC\ell_4$ = 150 g/m

On October 10th 1985, the above stated operating conditions were revised downwards to be more in line with the actual operating conditions used in the experimental study at Sohio Chemical Laboratories. The new set of conditions on which the final model development work is based are given in the second column of Table 2.1. For the sake of simplicity, as far as the computation of the necessary thermodynamic and transport properties of the reaction mixture is concerned, the gaseous at the inlet of the reactor was treated as being composed solely of a mixture of Ar/H_2 as indicated in Table 2.1.

The modelling work developed in the context of this study is limited to the principal reaction chamber, Figure 2.1, and involved the following principal assumptions.

- Axisymmetric system of coordinates with two-dimensional flow and temperature fields.
- Plasma in local thermodynamic equilibrium.
- Optically thin plasma.
- Negligible viscous dissipation.

While the first set of operating conditions, Table 2.1, gave rise to turbulent flow through the reactor, it become increasingly evident that, with the reduction of the gas flow rates and the plasma power that the flow in the main reactor tube is most likely to be laminar rather than turbulent while the flow in the entrance region of the reactor remains fully turbulent. The presence of both

turbulent and laminar flow regimes in different regions of the same reactor added obviously to the complexity of the modelling task since both turbulent and laminar flow models had to be developed.

In this section a separate description is given of each of these two models followed by a discussion of typical results obtained under different operating conditions.

2.2 TURBULENT FLOW MODEL

The turbulent flow model of the d.c. plasma jet reactor is based on the solution of the Navir- Stokes equations after Reynolds averaging. The turbulence model used is the standard k-ε model in conjunction with the wall functions in regions close to the solid boundaries.

2.2.1 Governing equations

The equations for the conservation of mass, momentum, energy and for the production and dissipation of turbulence, can be written in cylindrical coordinates as follows:

Continuity

$$\frac{1}{r}\frac{\partial}{\partial r}(r\rho v) + \frac{\partial}{\partial z}(\rho u) = 0 \qquad (2\text{-}1)$$

momentum

$$\rho\left(v\frac{\partial u}{\partial r} + u\frac{\partial u}{\partial z}\right) = -\frac{\partial P}{\partial z} + 2\frac{\partial}{\partial z}\left(\mu_{eff}\frac{\partial u}{\partial z}\right) + \qquad (2\text{-}2)$$

$$\frac{1}{r}\frac{\partial}{\partial r}\left\{r\,\mu_{eff}\left(\frac{\partial u}{\partial r} + \frac{\partial v}{\partial z}\right)\right\} - \frac{\partial}{\partial z}\left(\frac{2}{3}\rho k\right)$$

$$\rho \left(v \frac{\partial v}{\partial r} + u \frac{\partial v}{\partial z}\right) = - \frac{\partial P}{\partial r} + \frac{2}{r} \frac{\partial}{\partial r} \left(\mu_{eff}\, r \frac{\partial v}{\partial r}\right) + \frac{\partial}{\partial z} \left\{\mu_{eff} \left(\frac{\partial v}{\partial z} + \frac{\partial u}{\partial r}\right)\right\}$$

$$- 2 \frac{\mu_{eff}\, v}{r^2} - \frac{\partial}{\partial r} \left(\frac{2}{3} \rho k\right) \qquad (2\text{-}3)$$

Energy

$$\rho \left(v \frac{\partial h}{\partial r} + u \frac{\partial h}{\partial z}\right) = \frac{1}{r} \frac{\partial}{\partial r} \left\{r \left(\frac{\mu}{\sigma_\ell} + \frac{\mu_t}{\sigma_t}\right) \frac{\partial h}{\partial r}\right\} + \qquad (2\text{-}4)$$

$$\frac{\partial}{\partial t} \left\{\left(\frac{\mu}{\sigma_\ell} + \frac{\mu_t}{\sigma_t}\right) \frac{\partial h}{\partial z}\right\}$$

Turbulence production and dissipation

$$\rho \left(v \frac{\partial k}{\partial r} + u \frac{\partial k}{\partial t}\right) = \frac{1}{r} \frac{\partial}{\partial r} \left\{r \left(\mu + \frac{\mu_t}{\sigma_k}\right) \frac{\partial k}{\partial r}\right\} + \qquad (2\text{-}5)$$

$$\frac{\partial}{\partial z} \left\{\left(\mu + \frac{\mu_t}{\sigma_k}\right) \frac{\partial k}{\partial z}\right\} + \rho G - \rho \varepsilon$$

$$\rho \left(v \frac{\partial \varepsilon}{\partial r} + \frac{\partial \varepsilon}{\partial z}\right) = \frac{1}{r} \frac{\partial}{\partial r} \left\{r \left(\mu + \frac{\mu_t}{\sigma_\varepsilon}\right) \frac{\partial \varepsilon}{\partial r}\right\} + \qquad (2\text{-}6)$$

$$\frac{\partial}{\partial z} \left\{\left(\mu + \frac{\mu_t}{\sigma_\varepsilon}\right) \frac{\partial \varepsilon}{\partial z}\right\} + \rho C_1 \frac{\varepsilon G}{k} - C_2 \frac{\rho \varepsilon^2}{k}$$

with

$$G = \nu_t \left\{2\left[\left(\frac{\partial u}{\partial z}\right)^2 + \left(\frac{\partial v}{\partial r}\right)^2 + \left(\frac{v}{r}\right)^2\right] + \left(\frac{\partial u}{\partial r} + \frac{\partial v}{\partial z}\right)^2\right\} \qquad (2\text{-}7)$$

where

μ_{eff} = $\mu + \mu_t$

μ = molecular viscosity

$\mu_t = C_D \frac{\rho k^2}{\varepsilon}$ = turbulent viscosity

and

$C_D = 0.09$, $\sigma_k = 1.0$, $\sigma_\varepsilon = 1.3$, $\sigma_t = 1.0$

$C_1 = 1.43$, and $C_2 = 1.92$ (2.1)

$\sigma_\ell = \frac{\mu C_p}{k}$ is the laminar Prandtl number

The heat and momentum fluxes close to solid boundaries, however, cannot be predicted correctly by the above equations. For this purpose the Prandtl mixing length theory is used [2.1,2.2].

The fluxes of heat and momentum to the walls of reactor are assumed to obey the following relations:

$$\frac{u_p}{(\tau/\rho)_w} C_D^{\frac{1}{4}} k_p^{\frac{1}{2}} = 2.5 \ln \left[E \frac{Yp}{\nu} (C_D^{\frac{1}{2}} k_p)^{\frac{1}{2}}\right] \qquad (2\text{-}8)$$

$$\frac{(T_p - T_w) C_p \rho C_D^{\frac{1}{4}} k_p^{\frac{1}{2}}}{q_w''} = 2.5 \sigma_t \ln \left[E \frac{Yp}{\nu} (C_D^{\frac{1}{2}} k_p)^{\frac{1}{2}}\right] \qquad (2\text{-}9)$$

$$+ \sigma_t \frac{\Pi/4}{\text{Sin } \Pi/4} (2.5 A)^{\frac{1}{2}} \left(\frac{\sigma_\ell}{\sigma_t} - 1\right) \left(\frac{\sigma_t}{\sigma_\ell}\right)^{\frac{1}{4}}$$

where,

u_p is the average velocity at point P parallel to the wall

τ_w is the shear stress at the wall

q''_w is the heat flux to the wall

E is a function of the wall roughness ≈ 9.0 for smooth walls

A is Van Driest's constant = 26.0 for smooth walls

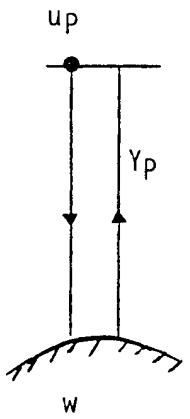

solid wall

Let

$$y^+ \equiv \frac{y_p}{\nu} \left(C_D^{\frac{1}{2}} k_p\right)^{\frac{1}{2}} \qquad (2\text{-}10)$$

and

$$\tau_w = - \mu_w \frac{du}{dy} = \mu_w \frac{up}{yP} \qquad (2\text{-}11)$$

$$q''_w = - \lambda_w \frac{dT}{dy} = \frac{Tp - Tw}{y_p} \qquad (2\text{-}12)$$

Using (8) and (9) the expressins for μ_w and λ_w can be evaluated as:

$$\mu_w = \frac{\mu\, y^+}{2.5\, \ln\,[E\, y^+]} \tag{2-13}$$

$$\lambda_w = \frac{\mu\, C_p\, y^+}{2.5\, \sigma_t\, \ln\,[E\, y^+] + \sigma_t \dfrac{\Pi/4}{\operatorname{Sin}\frac{\Pi}{4}} (2.5A)^{\frac{1}{2}} \left(\frac{\sigma_\ell}{\sigma_t} - 1\right)\left(\frac{\sigma_t}{\sigma_\ell}\right)^{\frac{1}{4}}} \tag{2-14}$$

Assuming E=9.0, σ_t=1.0, A=26.0:

$$\mu_w = \frac{\lambda_w}{Cp} = \frac{\mu\, y^+}{2.5\, \ell n[9\, y^+] - 8.95(1-\sigma_\ell)\sigma_\ell^{-1/4}} \tag{2-15}$$

for $y^+ > 11.5$ the values of μ_w and λ_w should be calculated according to 2-15 [1-2].

2.2.2 Boundary conditions

u, v, h, k, ε inlet conditions

$u = v = k = \varepsilon = 0$ and $h = h_w$ on the solid boundaries

$$\frac{\partial u}{\partial r} = \frac{\partial h}{\partial r} = \frac{\partial k}{\partial r} = \frac{\partial \varepsilon}{\partial r} = v = 0 \quad \text{on the axis of symmetry} \tag{2-16}$$

$$\frac{\partial \rho u}{\partial z} = \frac{\partial v}{\partial z} = \frac{\partial k}{\partial z} = \frac{\partial \varepsilon}{\partial z} = \frac{\partial h}{\partial z} = 0 \quad \text{at the exit}$$

2.2.3 Numerical method

The numerical method used here is the finite volume solution procedure of Patankar and Spalding [2.3]. The solution domain is discretized into a non-uniform rectangular mesh. The finite difference equations for each variable are derived by approximate integration of their corresponding differential equations for each control volume, thus ensuring the preservation of their conservation properties. The nodes are arrange in such a way that the velocities are located midway between the pressures that drive them (see Fig. 2-2). The resultant finite-difference equations connect each nodal value of variable, ϕ, to its four nearest neighbours by linear algebraic relations. Thus for node P:

$$A_P \phi_P = \sum_n A_n \phi_n + S_\phi (P) \qquad (2\text{-}17)$$

where

A_n are coefficients representing convection and diffusion

$A_P = \sum_n A_n$ where the summation extends over the neighboring points

$S_\phi(P)$ is the integrated source term.

The obtained set of algebric equations are solved by an interative scheme along successive grid lines using a Tri-Diagonal Matrix Algorithm (TDMA). A Pressure perturbation equation of a form similar to that of Eq. (2-17), can be derived combining the discretized continuity and momentum equations. The solution of this equation yields the updated pressures which drive the velocities in the direction of satisfying continuity.

The non-uniform rectangular meshes allow for grid refinement where gradients are steep. A hybrid differencing scheme combining the advantages of both upwind and central differencing is employed to

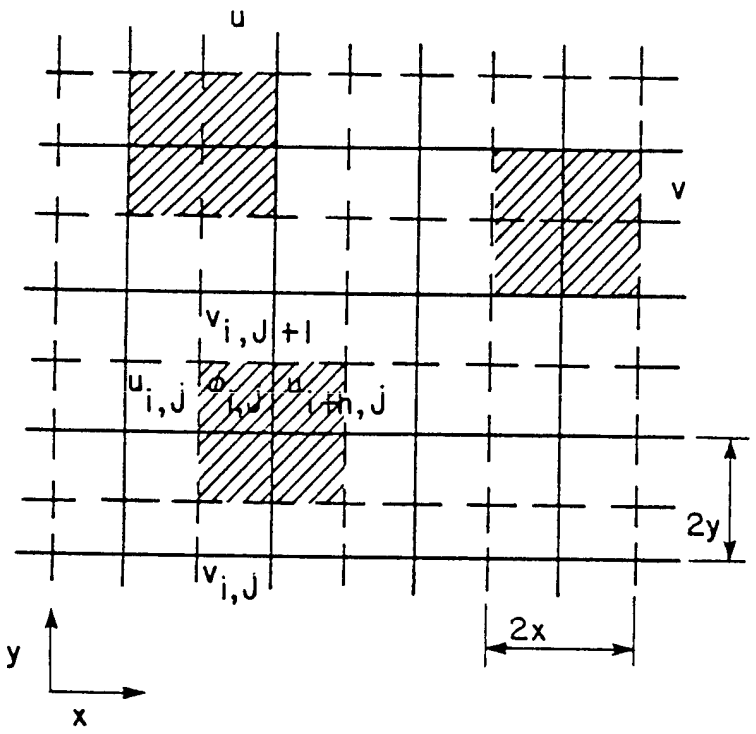

2.2 Staggered rectangular grid system illustrating the ϕ (i.e. G,h,k,ε) as well as the u and v control volumes.

ensure the stability at all Péclet numbers (i.e. $\rho u_i \partial x_i / \mu_{eff}$) and to reduce the effect of false diffusion which are the greatest when streamlines are at 45° with respect to the grid lines.

2.2.4 Results and discussion

Preliminary computations were carried out for the torch geometry given in Fig. 2-1 with the following inlet and wall conditions for an argon plasma at atmospheric pressure.

$$u_i = 3890 \quad m/s$$
$$T_i = 8000 \quad K$$
$$T_w = 500 \quad K$$
$$k_i = 0.005\ u_i^2$$
$$\varepsilon_i = 0.10\ k_i^2$$

These correspond to a torch operating with a total argon flow rate of 500 ℓ/min at a net power dissipated in the plasma of 50 kW. It should be pointed out that because further computations are to be carried out at considerably lower flow rates and power levels, the fact that the flow under the above stated operating conditions was supersonic was intentionally overlooked and compressibility effects neglected.

Typical results obtained for the reactor entrance region (z=200 mm) with a 14 x 25 grid system (25 in the z direction) are given in figures 2-3,2-6. These show the variation of u,T,k, and ε on the axis of symmetry. Because of the high turbulence mixing, the inlet jet decays very rapidly at the entrance region, so that the axial velocity has dropped to about 140 [m/s] at z=190 [mm] (Fig. 2-3). However after the sharp decay at the entrance region, the rate at which the velocity decreases depends on the temperature of the argon gas. Figure 2-4 shows that at the end of the reactor section (L=190 mm) the gas cools down at a rate of about

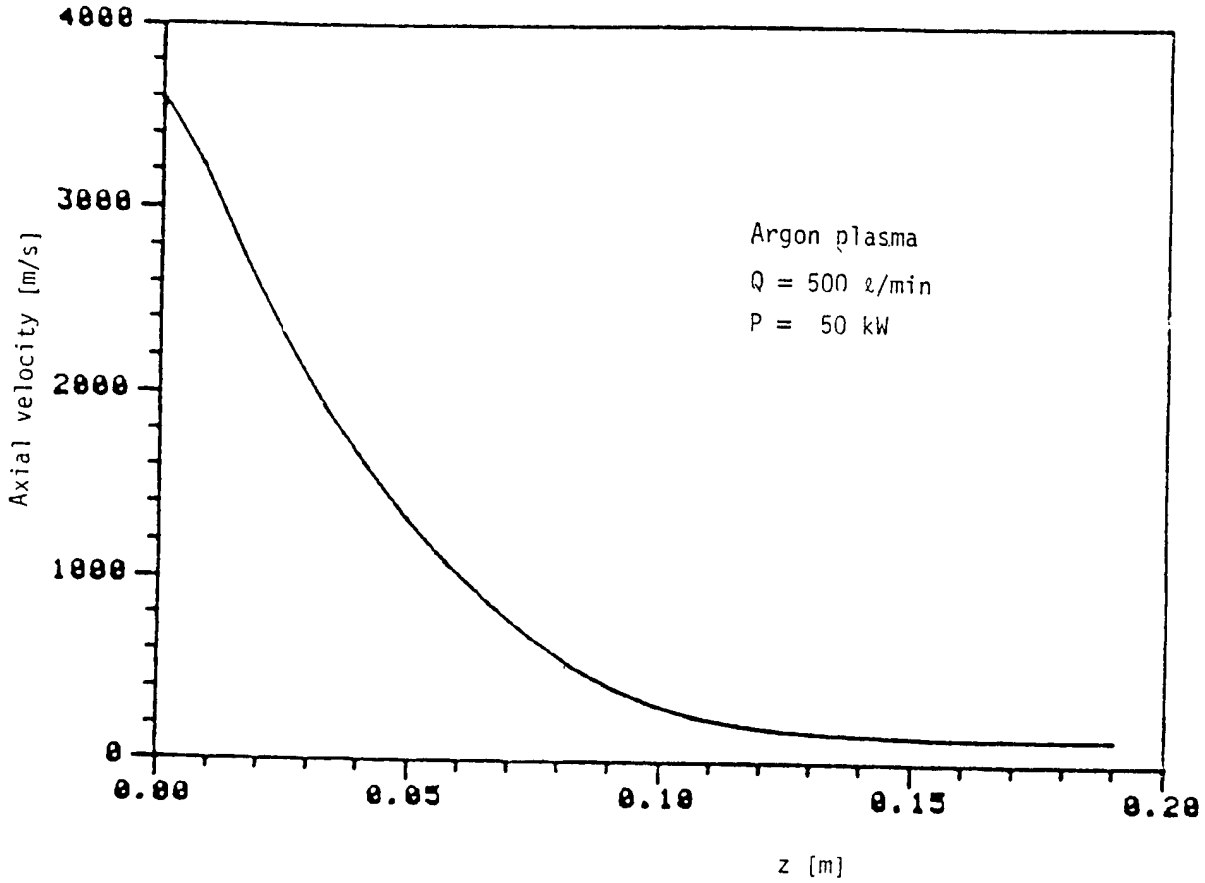

2.3 Axial variations of velocity along the centerline of the reactor.

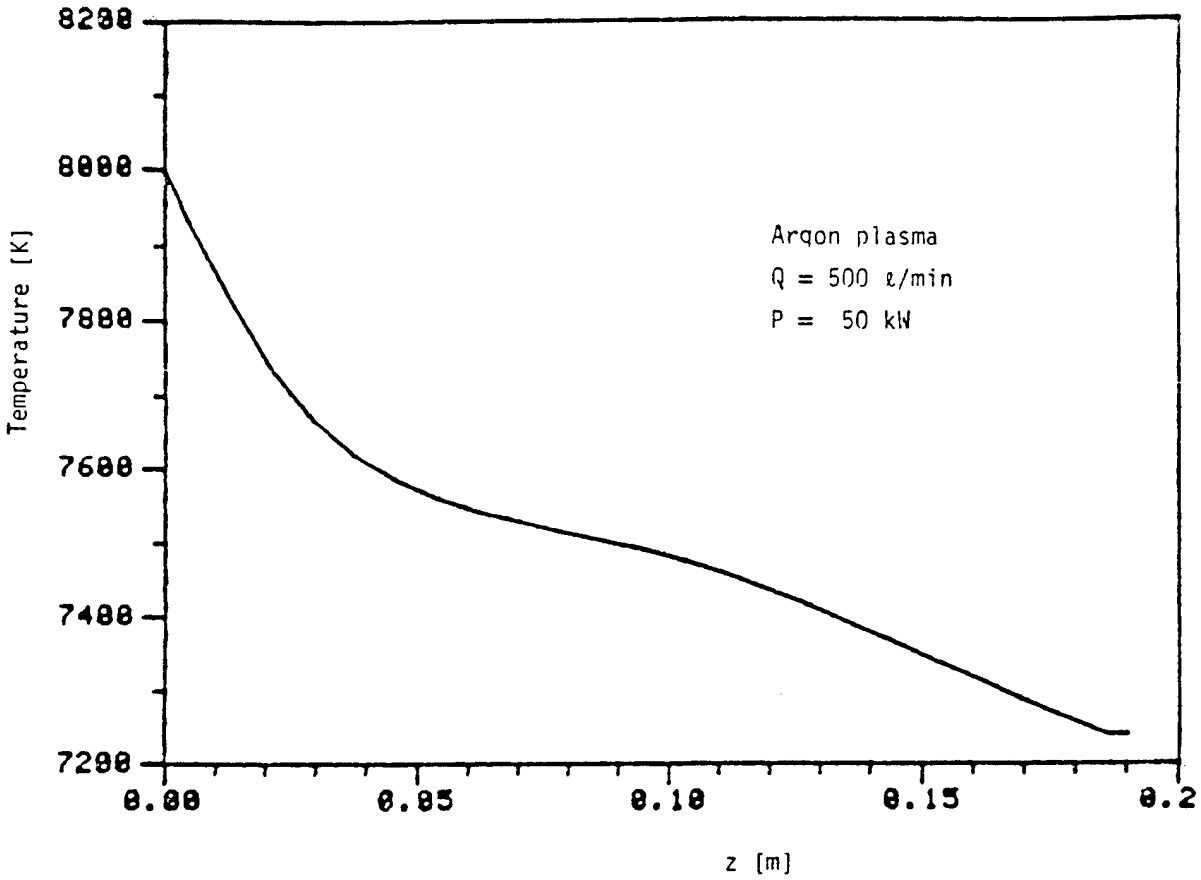

2.4 Axial variation of temperature along the centerline of the reactor.

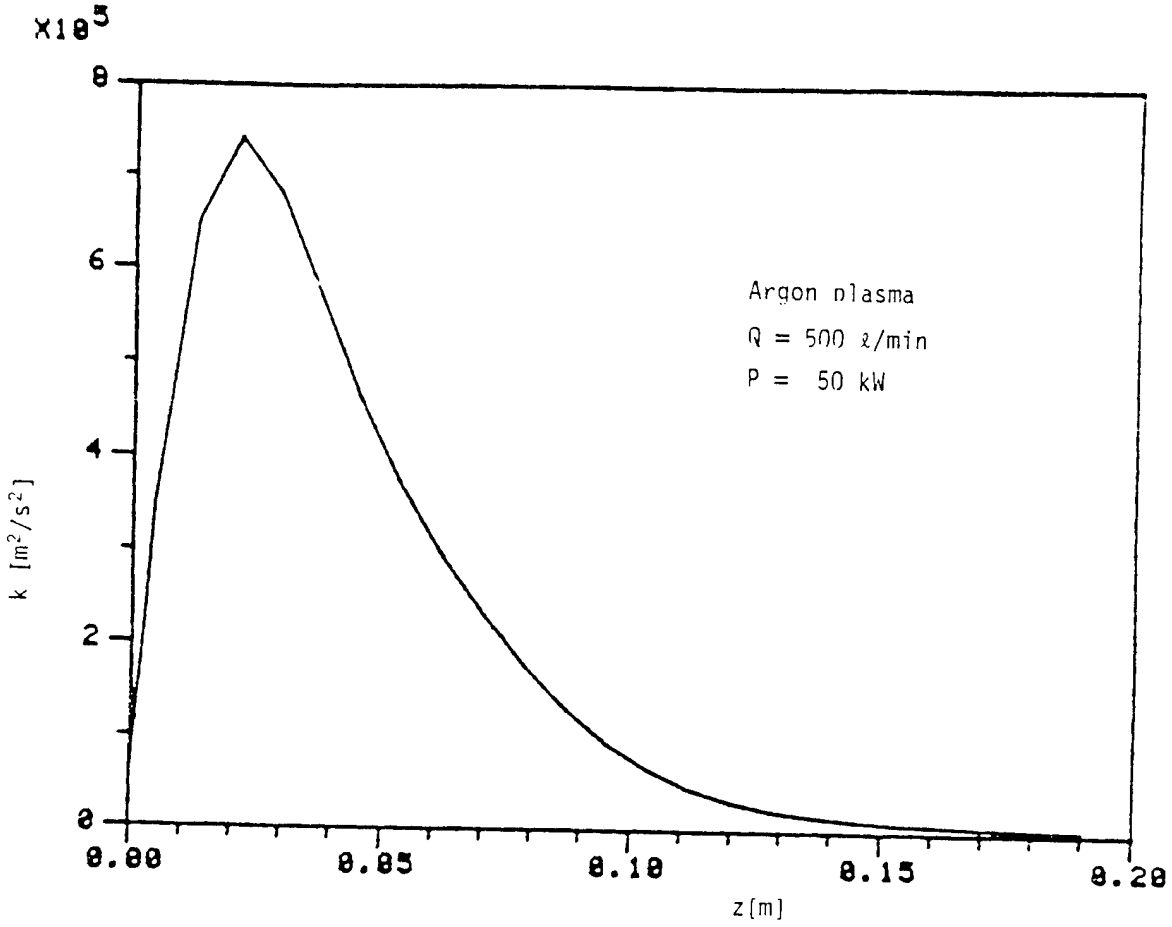

2.5 Axial variation of k along the centerline of the reactor.

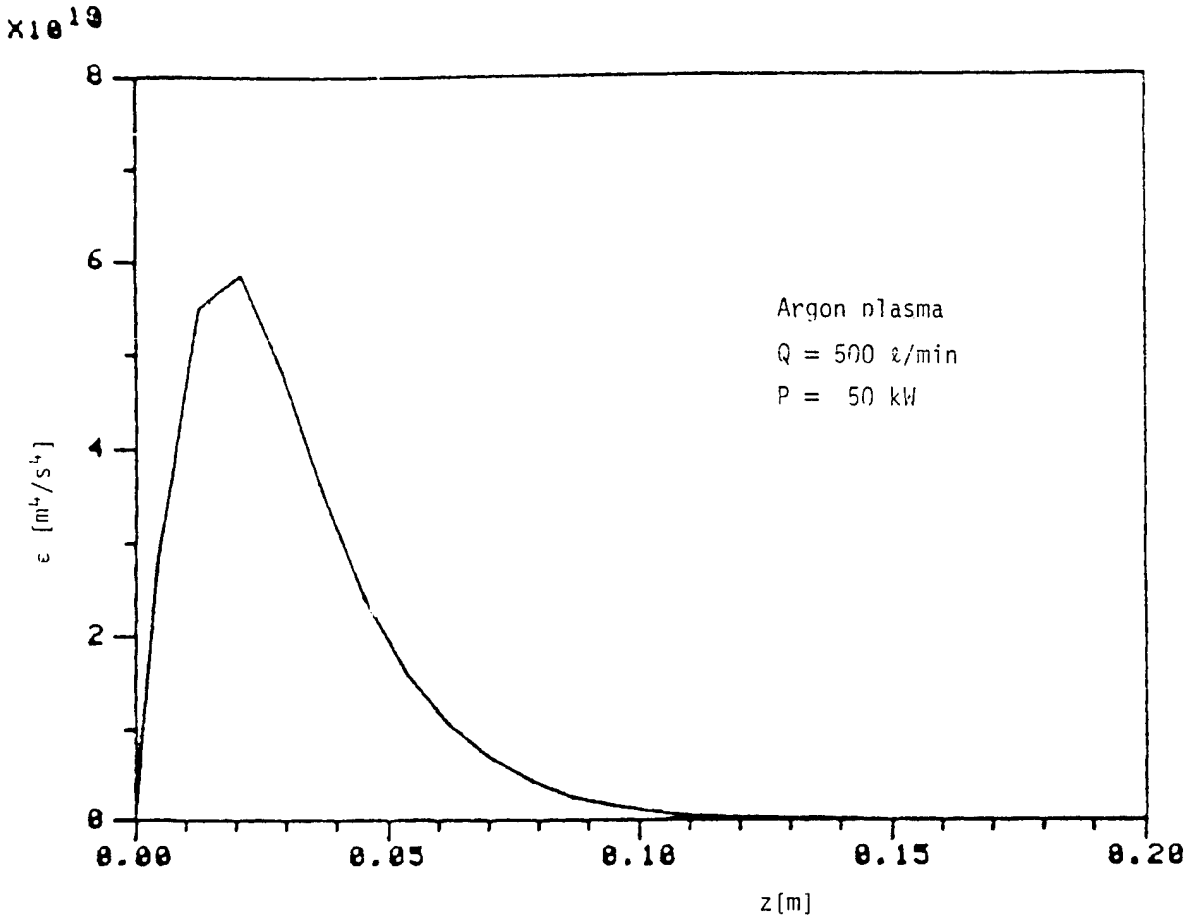

2.6 Axial variations of ε along the centerline of the reactor.

4 000 K/m. The axial variation in the production and dissipation of turbulence is shown in Figures 2-5 and 2-6 respectively. The maximum lies close to the entrance region (approximately 20 mm from the inlet). Since the level of turbulence downstream of the reactor is considerably less than that in the immediate neighbourhood of the entrance region, the values of k and ε drop sharply at z=190 mm. Figures 2-7 and 2-8 show the radial distribution of temperature and axial velocity for different axial positions. The temperature profile is almost flat over most of the radius. This is largely due to the high level of turbulent mixing in this region. The same type of profile is also seen for the velocity. As expected, the gradients of the temperature and velocity are very large near the wall.

Two principal problems are noted based on this set of priliminary computations. The first is the excessive computer storage required to carry out the computations for the full length of the reactor. The second is the possible variaton of the flow regime in the reactor with the reduction of the gas flow rates and the plasma power.

As to the problem of variations of the flow regime in the reactor, on the other hand, this was a complex one which necessitated the development of a second computer model for the laminar region of the flow as described in section 2.3.

The problem of computer storage was overcome by performing the computations for short successive segments of the reactor using the field at the exit of any such segments as the inlet condition for the next segment. The process was repeated untill the total length of the reactor was covered.

Computations were also carried out using the turbulent flow model for the same reactor geometry for argon at 400 K with a total gas flow rate of 1600 ℓ/min. The corresponding Reynolds number of the flow based on the reactor diameter was 10^5. The reactor wall tem-

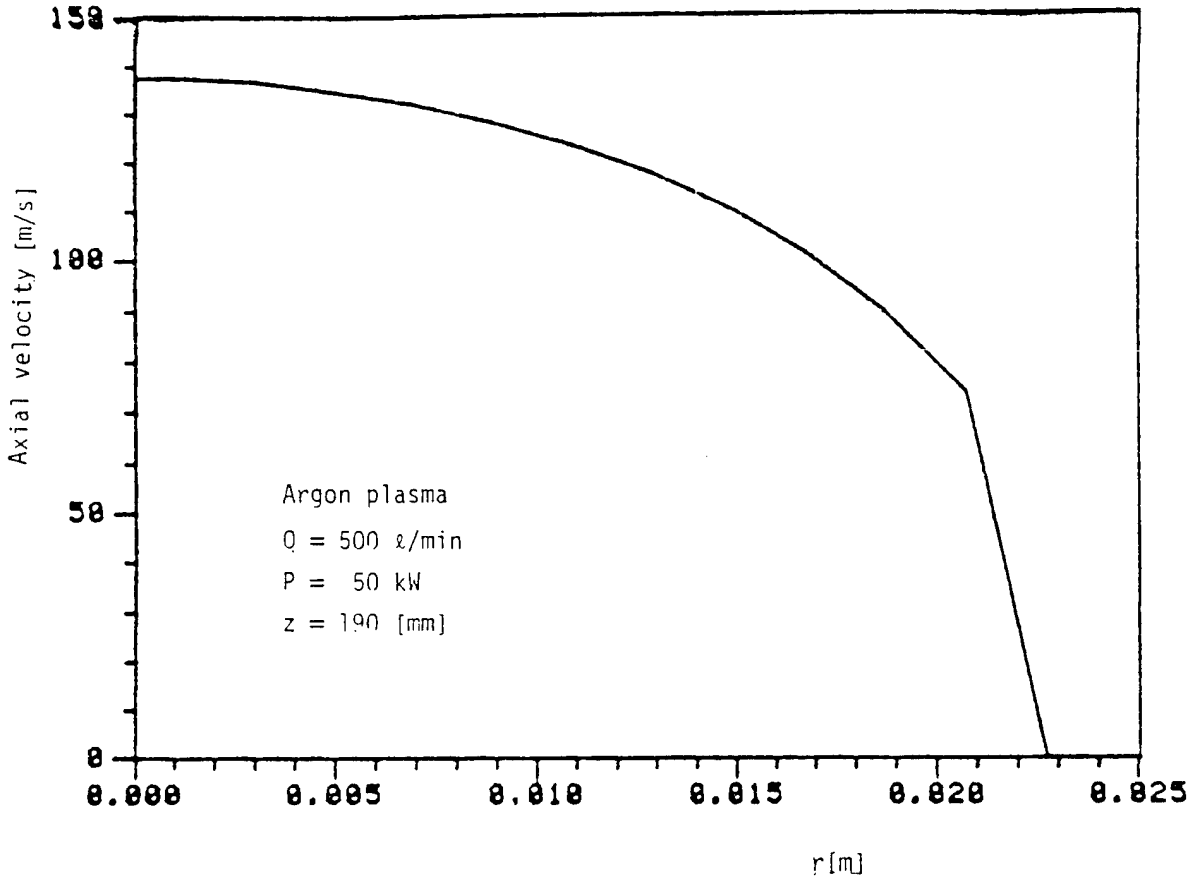

2.7 Radial variation of the axial velocity at z=190 mm.

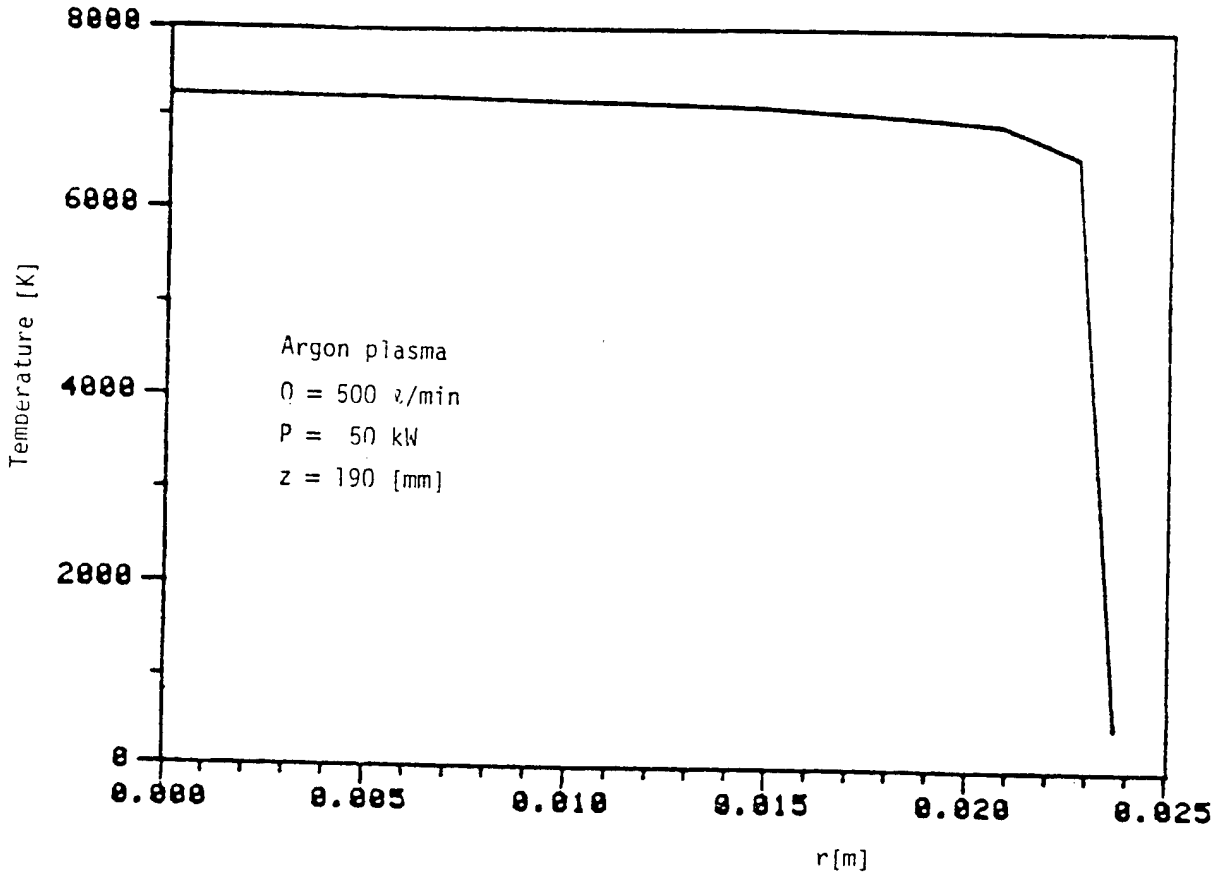

2.8 Radial variation of the temperature at z=190 mm.

perature was fixed at 305 K. The intensity of turbulence at the inlet of the reactor was assumed to be 10%. Typical results are given in Figures 2.9-2.12.

Because of the high level of turbulent mixing, the axial velocity along the centerline is noted to drop rapidly over the first 100 mm of the reactor as shown in Figure 2.9. The subsequent slight increase of the velocity along the centerline further downstream, can be attributed to the development of the velocity profile. As shown in Figure 2.10, this gradually approaches that of a fully developed turbulent flow at a distance of about 600 mm from the inlet of the reactor which corresponds to a (Z/d) value of 30.0. The corresponding temperature profiles along the axial and radial directions in the reactor are given in Figures 2.11 and 2.12 respectively.

2.3 LAMINAR FLOW MODEL

The laminar flow model is based on essentially the same assumptions as those stated in section 2.1.

2.3.1 Governing equations

Continuity

$$\frac{1}{r}\frac{\partial}{\partial r}(\rho\, r\, v) + \frac{\partial}{\partial z}(\rho\, \mu) = 0 \qquad (2\text{-}18)$$

Momentum

$$\rho\left(v\frac{\partial u}{\partial r} + u\frac{\partial u}{\partial z}\right) = -\frac{\partial p}{\partial z} + \partial\frac{\partial}{\partial z}\left(\mu\frac{\partial u}{\partial z}\right) + \frac{1}{r}\frac{\partial}{\partial r}\left[\mu r\left(\frac{\partial u}{\partial r} + \frac{\partial v}{\partial z}\right)\right] + \rho g \qquad (2\text{-}19)$$

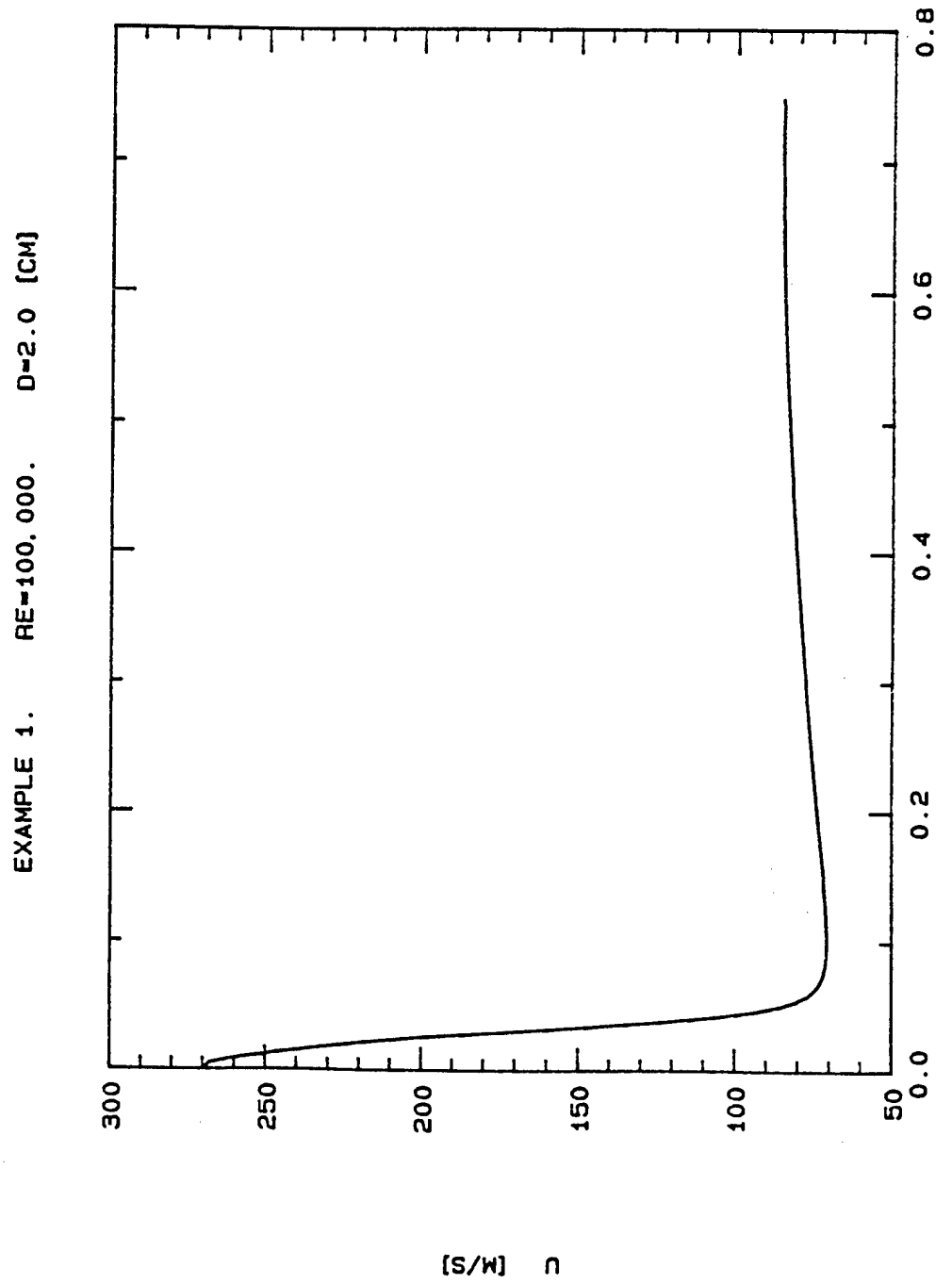

2.9 Centerline velocity profile along the axis of the reactor for an argon flow at 400 K.

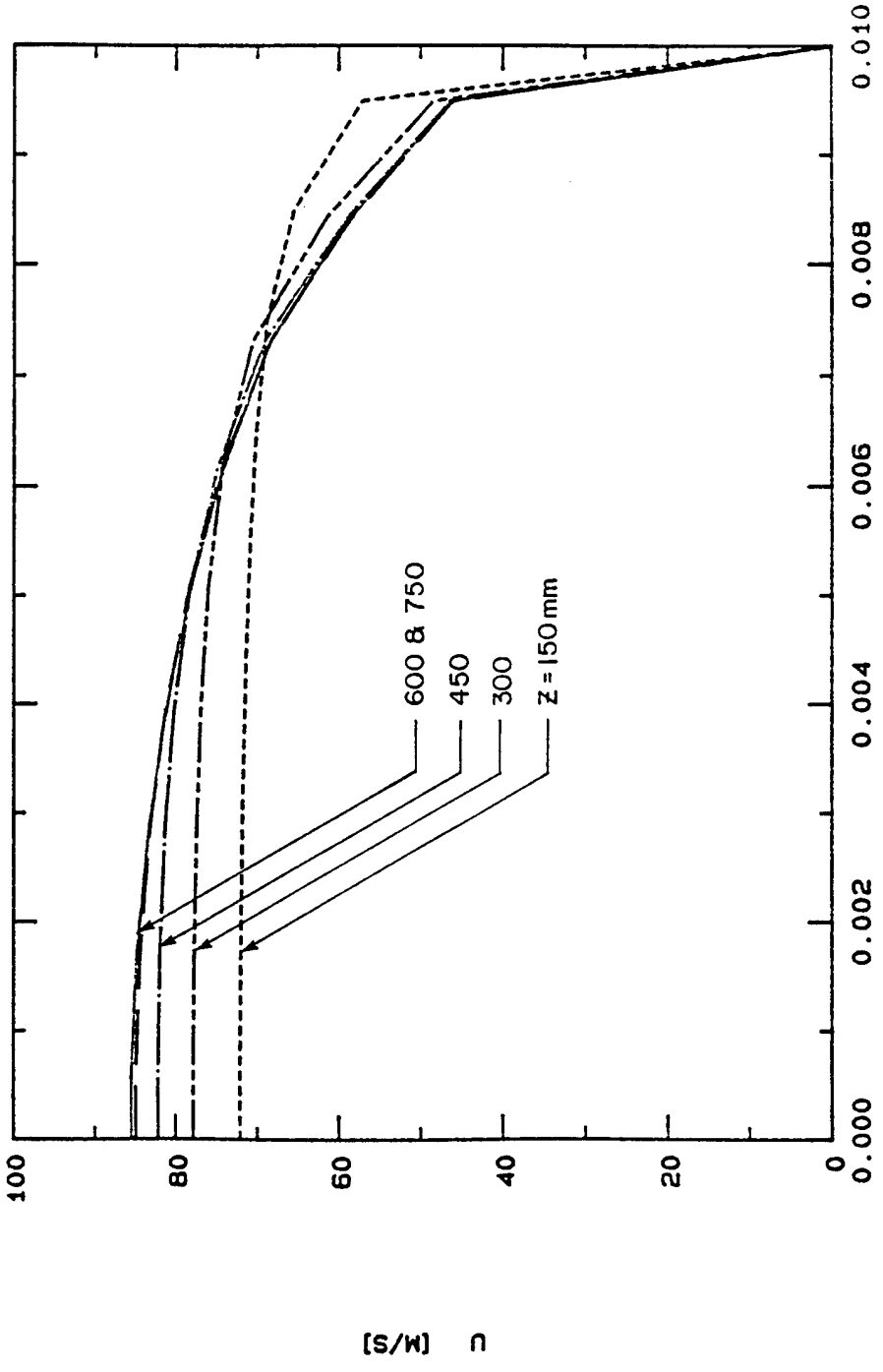

2.10 Radial velocity profiles at different distances from the reactor inlet for an argon flow at 400 K.

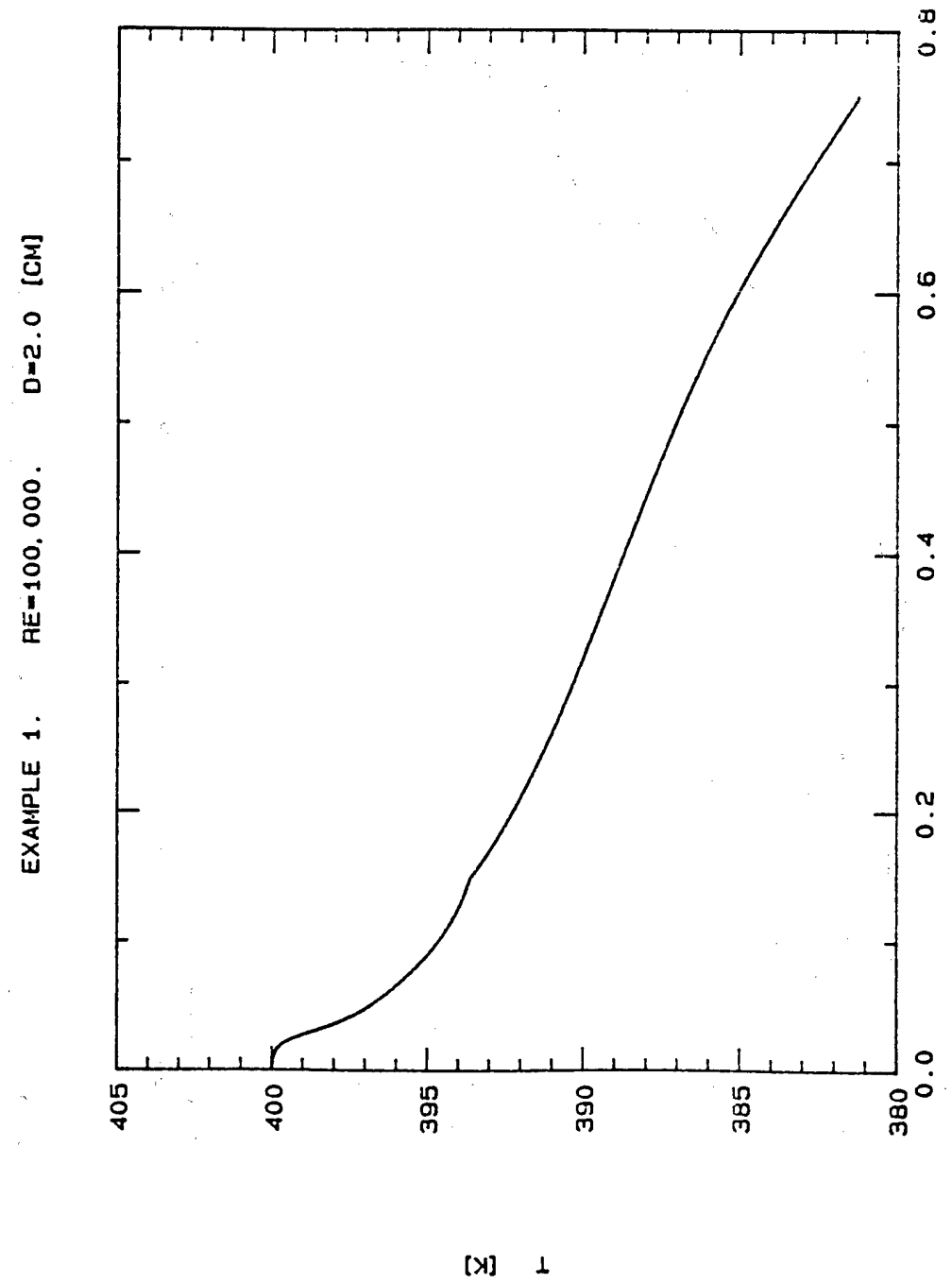

2.11 Centerline temperature profiles along the axis of the reactor for an argon flow at an inlet temperature of 400 K. Tw=350 K.

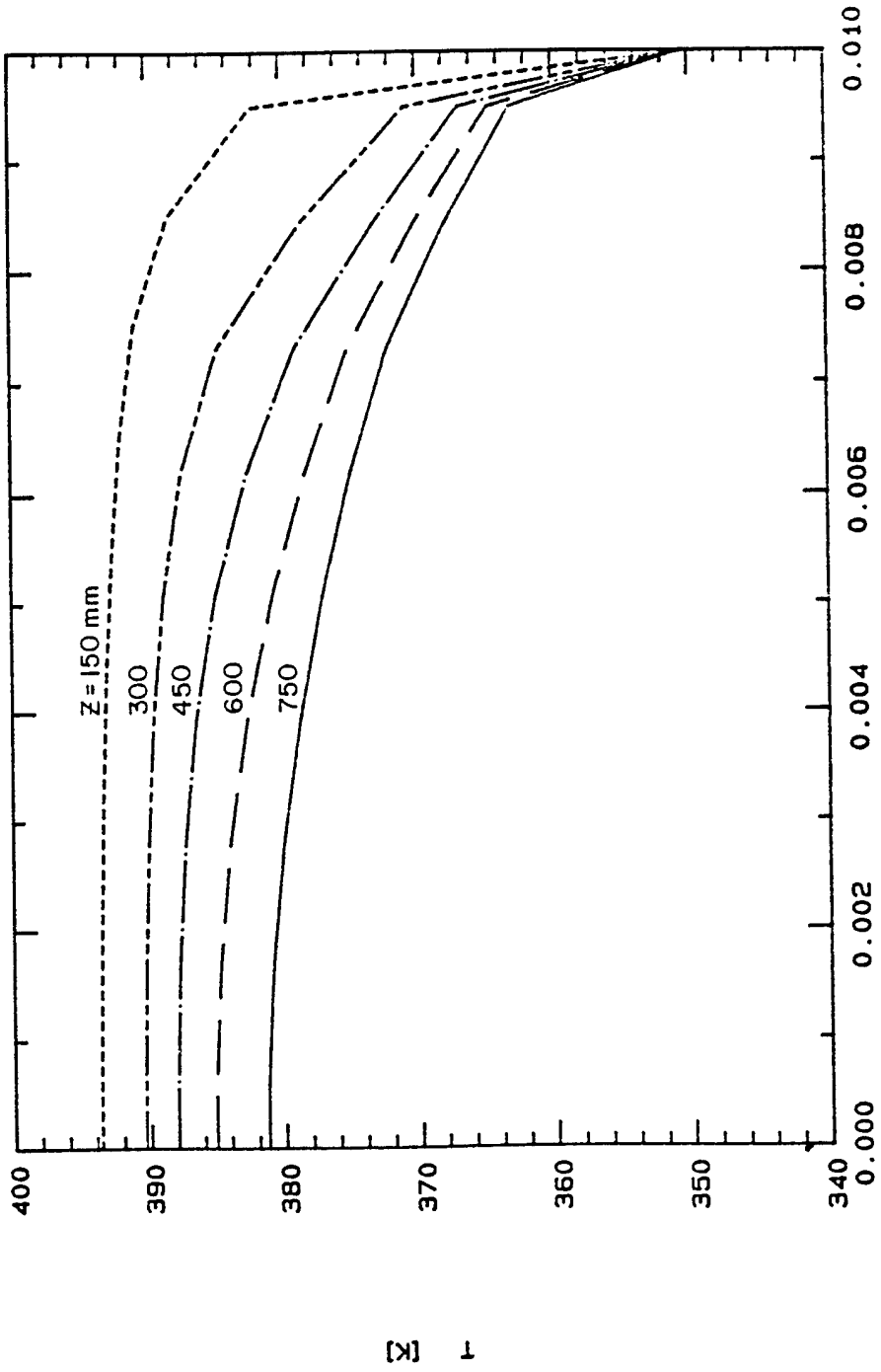

2.12 Radial temperature profiles at different distances from the reactor inlet for an argon flow at an inlet temperature of 400 K. Tw=350 K.

$$\rho \left(v \frac{\partial v}{\partial r} + u \frac{\partial v}{\partial z}\right) = - \frac{\partial p}{\partial r} + \frac{2}{r} \frac{\partial}{\partial r} \left(\mu r \frac{\partial v}{\partial r}\right) + \frac{\partial}{\partial z} \left[\mu \left(\frac{\partial u}{\partial r} + \frac{\partial v}{\partial z}\right)\right] \qquad (2\text{-}20)$$

Energy

$$\rho \left(v \frac{\partial h}{\partial r} + u \frac{\partial h}{\partial z}\right) = \frac{1}{r} \frac{\partial}{\partial r} \left(r \frac{k}{Cp} \frac{\partial h}{\partial r}\right) + \frac{\partial}{\partial z} \left(\frac{k}{Cp} \frac{\partial h}{\partial z}\right) \qquad (2\text{-}21)$$

Where ρ, v, u, p, h are the density, radial velocity, axial velocity, pressure and enthalpy respectively; μ is the viscosity, k is thermal conductivity, Cp is specific heat at constant pressure, and g is the accelaration of gravity; r and z are the radial and axial coordinates respectively.

2.3.2 Boundary conditions

Equations 2-18 - 2-21 are subject to the following boundary conditions:

a) Inlet conditions

$$u, v, p, h \quad \text{given} \qquad (2\text{-}22\text{-}a)$$

These values are specified from the computed results of the turbulent flow model for the entrance region.

b) Wall conditions

$$u = v = 0$$

$$T = Tw \quad \text{given wall temperature} \qquad (2\text{-}22\text{-}b)$$

c) Axis of symmetry

$$v = \frac{\partial u}{\partial r} = \frac{\partial h}{\partial r} = 0 \qquad (2\text{-}22\text{-}c)$$

d) Exit

$$\frac{\partial v}{\partial z} = \frac{\partial (\rho u)}{\partial z} = \frac{\partial h}{\partial z} = 0 \qquad (2\text{-}22\text{-}d)$$

2.3.3 Numerical method

The numerical method used in this case was that based on the finite difference approximations of the partial differential equations according to the SIMPLER computer code (2.3).

2.3.4 Results and discussion

Preliminary computations using the laminar computer model were carried out to determine the characteristics of the flow in the recirculation region close to the reactor inlet. The point of flow attachment predicted using this laminar flow code as function of the flow Reynolds number based on the step height ($Re_h = \rho \bar{u}_i H/\mu$), is given in Figure 2.13. Experimental data compiled by Eckert [2.4] finds that for $Re_h > 520$. The shear flow at the entrance region becomes turbulent. Since for the present geometry and operating conditions, the Reynolds number based on the step height is about 1600 (Figure 2.14), it is quite possible that flow in the entrance recirculation region is turbulent, while that donwstream of the point of reattachment is laminar.

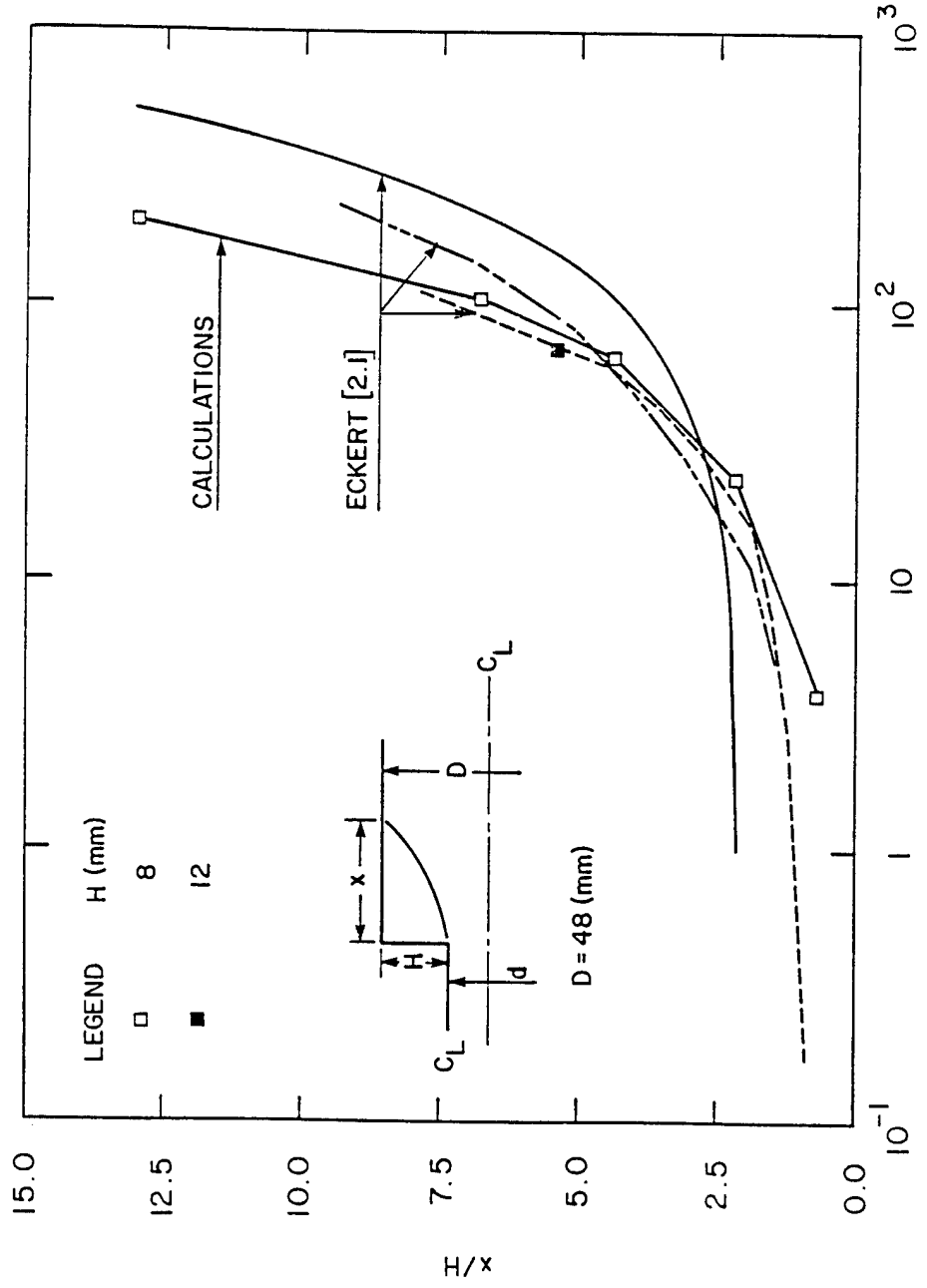

2.13 Vortex reattachment point as function of the Reynolds number based on the step height.

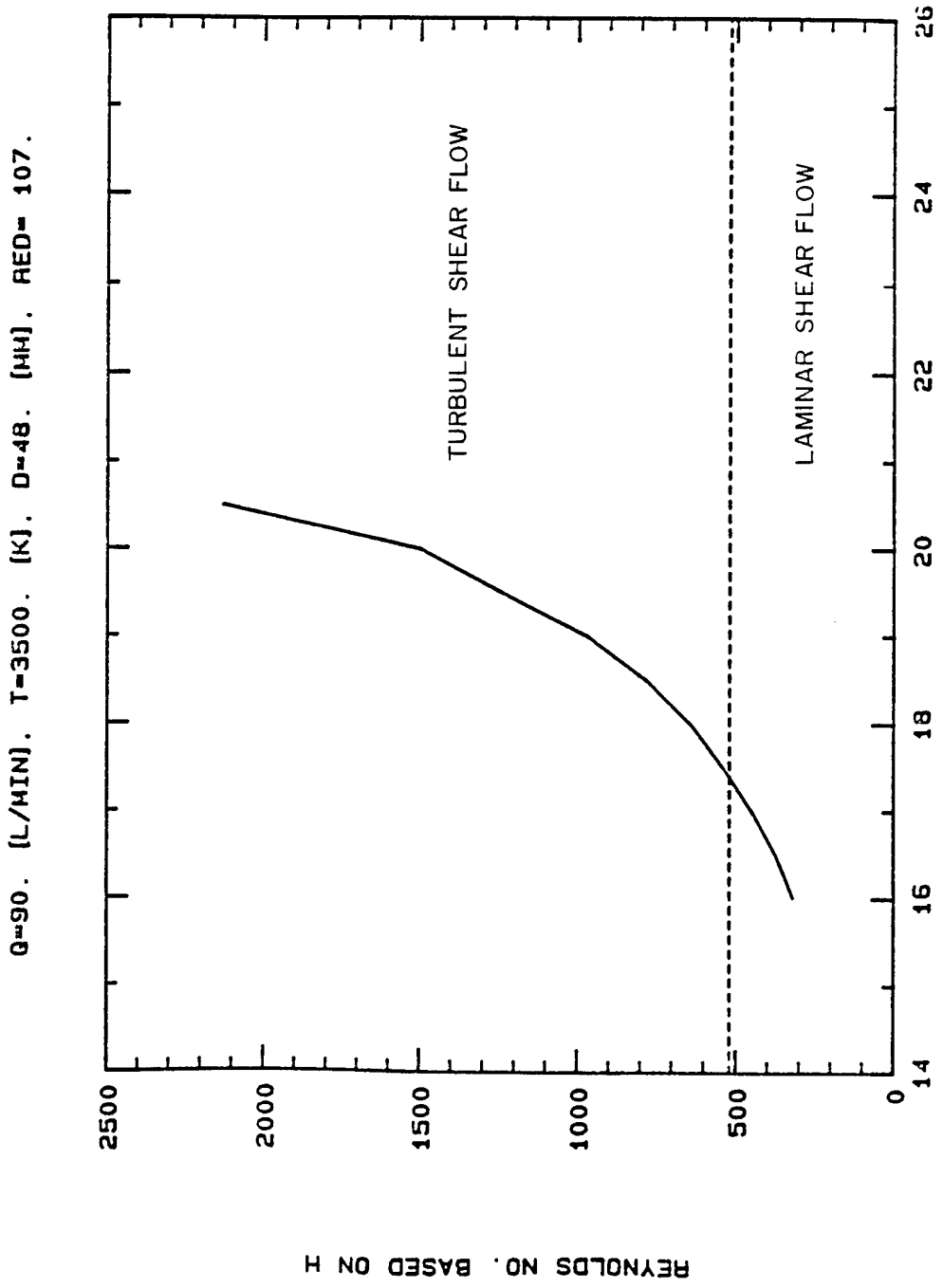

2.14 Flow regions for the entrance region of the present reactor geometry.

2.4 THERMODYNAMIC AND TRANSPORT PROPERTIES FOR GAS MIXTURES

As mentioned earlier in section 2.1 the plasma reactor was operated using an $Ar/H_2/CH_4/SiC\ell_4$ mixture. In order to be able to carry out the computations of the flow and temperature fields in the reactor under realistic conditions it was necessary to know as closely as possible the thermodynamic and the transport properties of the reaction mixture as function of temperature.

Since Argon and hydrogen were by far the principal constituents of reaction mixture, the thermodynamic and transport properties of the gases mixture was estimated based on those of pure argon and hydrogen only using the so called "mixture rules" (2.5).

For a mixture of non-reacting gases, the procedure is as follows:

a) Viscosity and thermal conductivity

$$\mu = \sum_{i=1}^{n} \frac{x_i}{A_i} \mu_i$$

$$k = \sum_{i=1}^{n} \frac{x_i}{A_i} k_i \qquad (2\text{-}23)$$

Where μ and k are the viscosity and thermal conductivity of the mixture, n is the number of species, x_i is the mole fraction of the i^{th} species, μ_i and k_i are the corresponding viscosity and thermal conductivity of the i^{th} species, and A_i is given by:

$$A_i = \sum_{j=1}^{n} x_j \, \phi_{ij}$$

where (2-24)

$$\phi_{ij} = \frac{1}{8} \left(1 + \frac{M_i}{M_j}\right)^{-\frac{1}{2}} \left[1 + \left(\frac{\mu_i}{\mu_j}\right)^{\frac{1}{2}} \left(\frac{M_j}{M_i}\right)\right]^2$$

M is the atomic/molecular mass of the species.

b) density and specific heat at constant pressure

$$\rho = \sum_{i=1}^{n} x_i \rho_i$$
$$\rho C_p = \sum_{i=1}^{n} x_i \rho_i C_{p_i} \qquad (2\text{-}25)$$

Where ρ is the density and C_p is the specific heat at constant pressure.

The results given in Figures 2.15 - 2.18 include separate curves for pure argon, pure hydrogen and an intermediate mixture containing 83.3% (molar) H_2 which corresponds to the plasma gas composition used.

2.5 RESULTS OBTAINED USING THE TURBULENT/LAMINAR CODE

In order to cope with this turbulent-laminar transition in the reactor, the flow and temperature fields for the entrance region of the reactor (length about 150 mm) were computed using the turbulent code, while the laminar code was used to calculate the flow and temperature fields further downstream.

Typical results obtained for the conditions specified on the RHS column of Table 2.1 are given in Figure 2.19. These show a jet attachment at a distance of approximately 80 mm from the reactor inlet. The inlet turbulent intensity in this case was assumed to be 0.32. Because of the strong backflow and high level of mixing, the temperature profiles in the inlet region are rather flat.

Figures 2.20 - 2.22 show the centerline velocity and temperature profiles in the reactor. While the inlet velocity of the plasma jet is 302 m/s, the average velocity at the exit of the reactor, (z = 1.8 m) drops down to 1.94 m/s. Over the same distance the temperature drops from 3550 K to 442 K as shown in Figure 2.22. Figures 2.23 - 2.26 show the radial velocity and temperature profiles at different axial positions in the reactor. The reactor wall temperature was assumed to be 350 K.

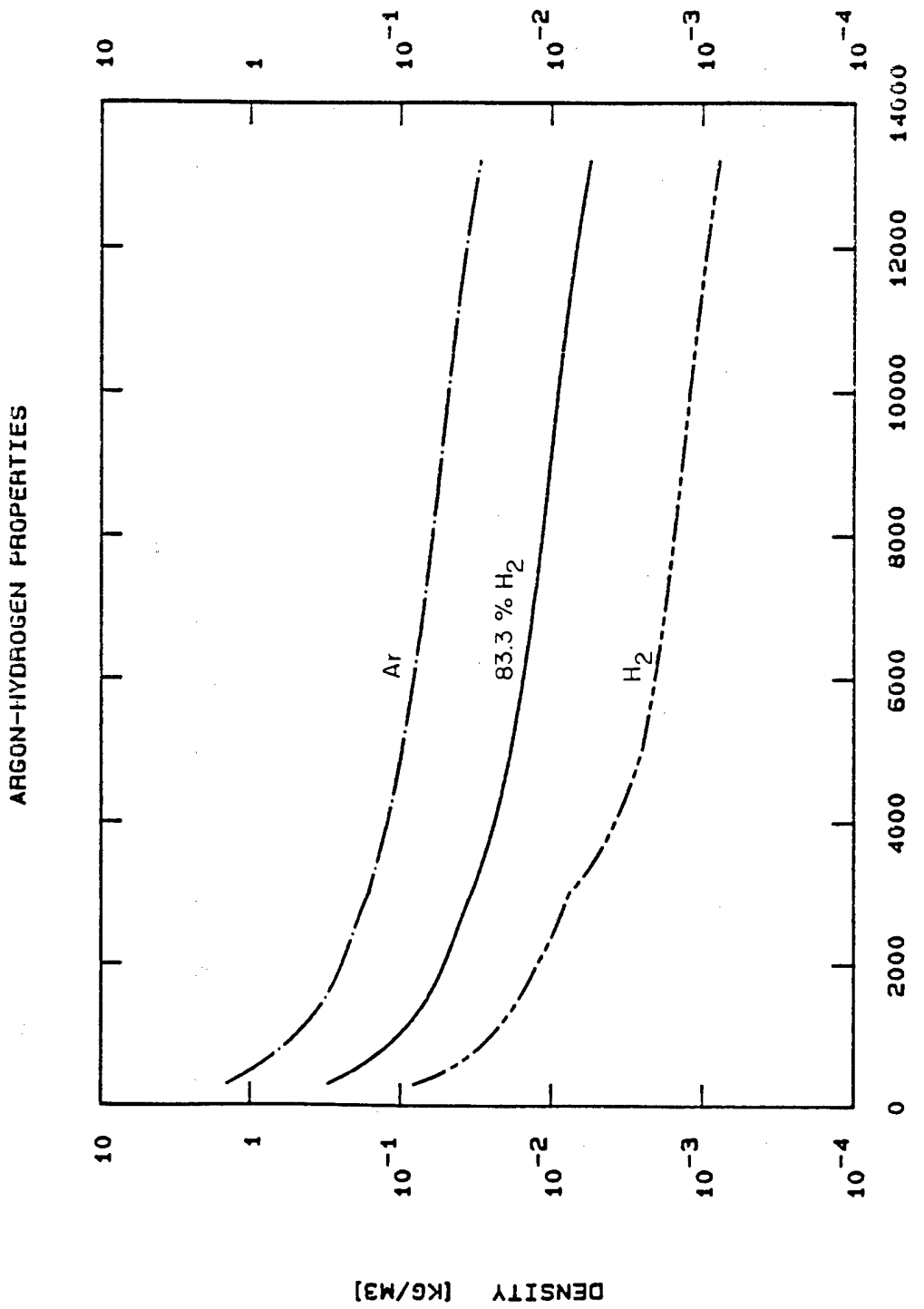

2.15 Density of Ar/H_2 mixtures under atmospheric pressure.

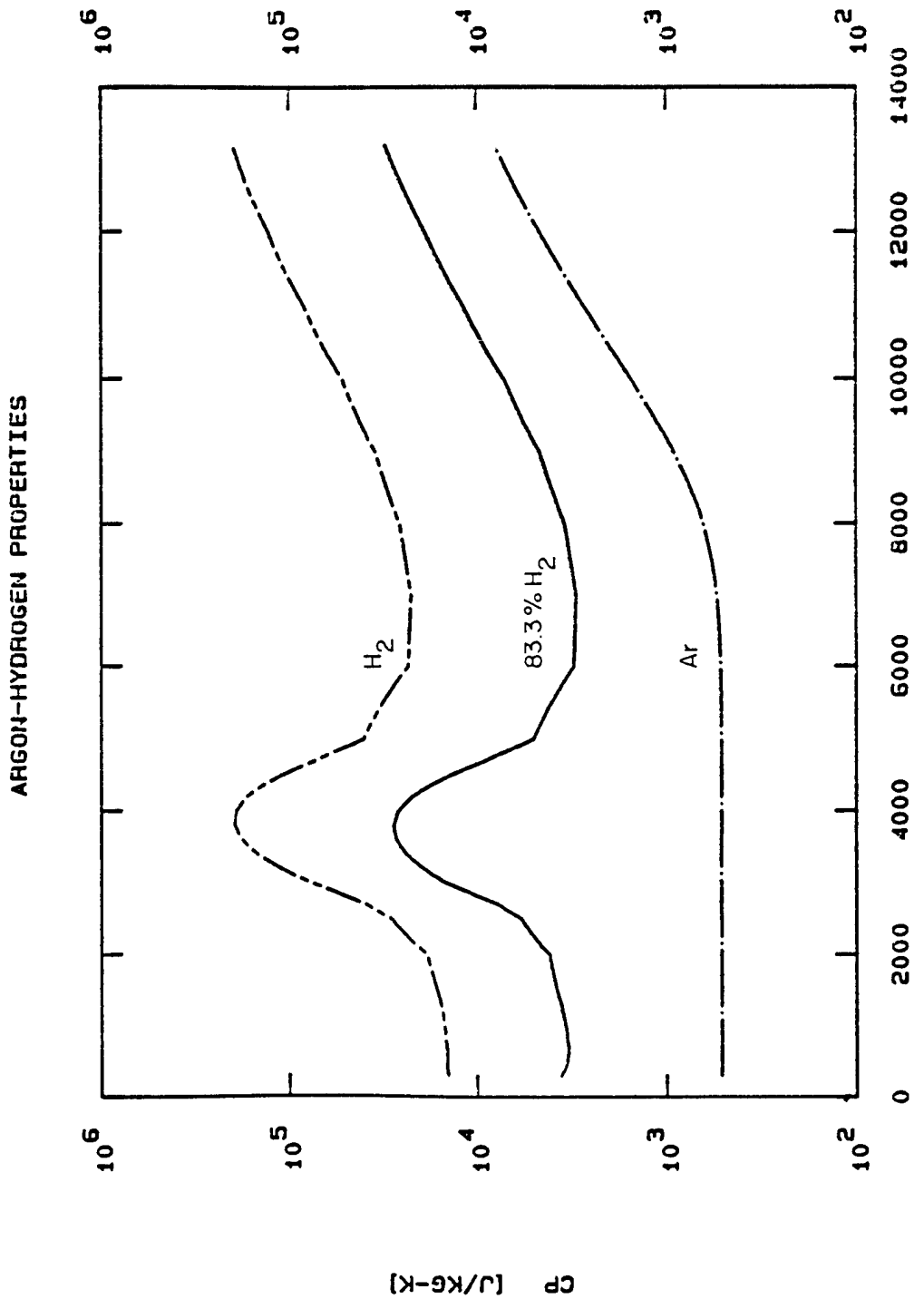

2.16 Specific heat at constant pressure of Ar/H_2 mixtures under atmospheric pressure.

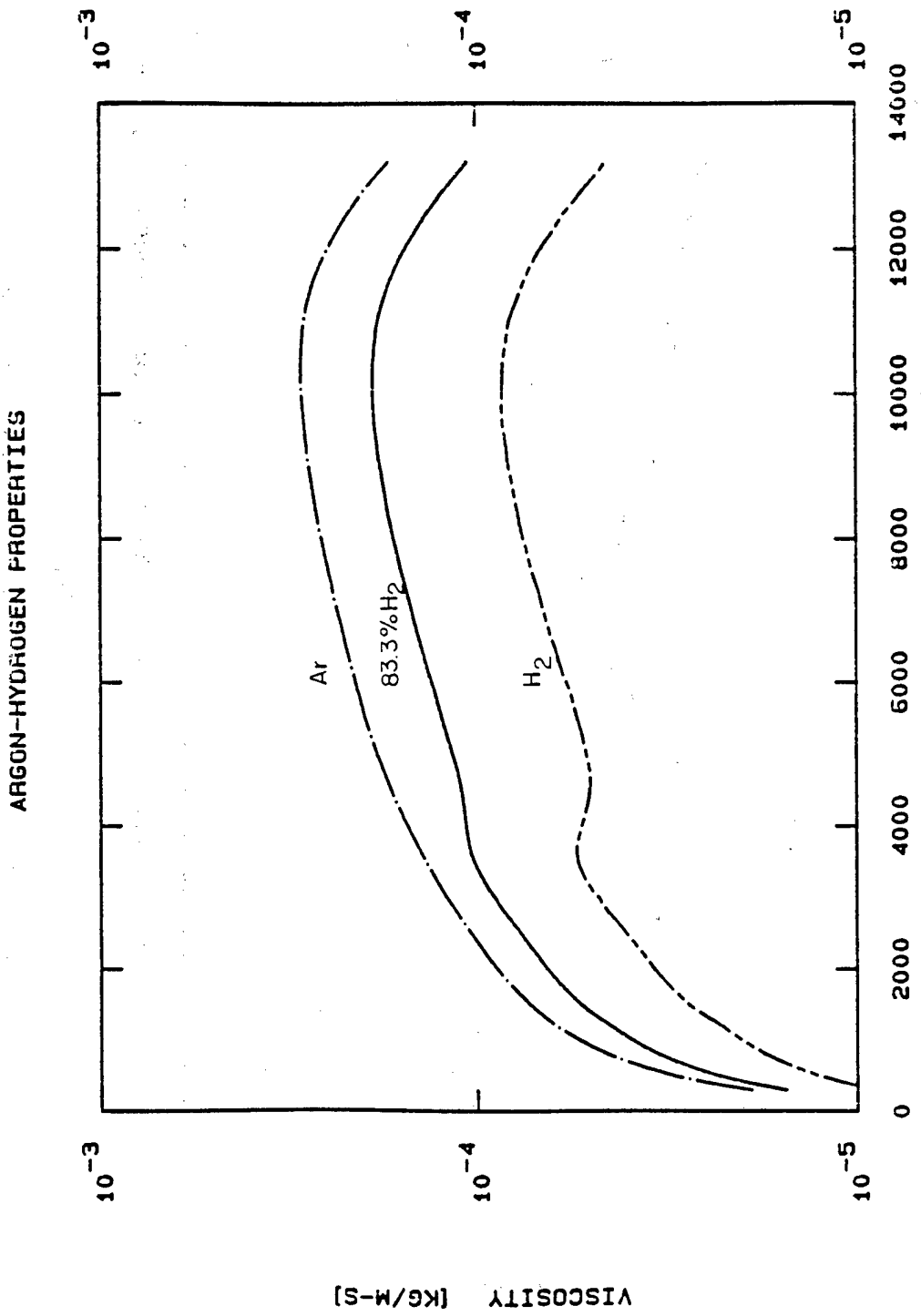

2.17 Viscosity of Ar/H_2 mixtures under atmospheric pressure.

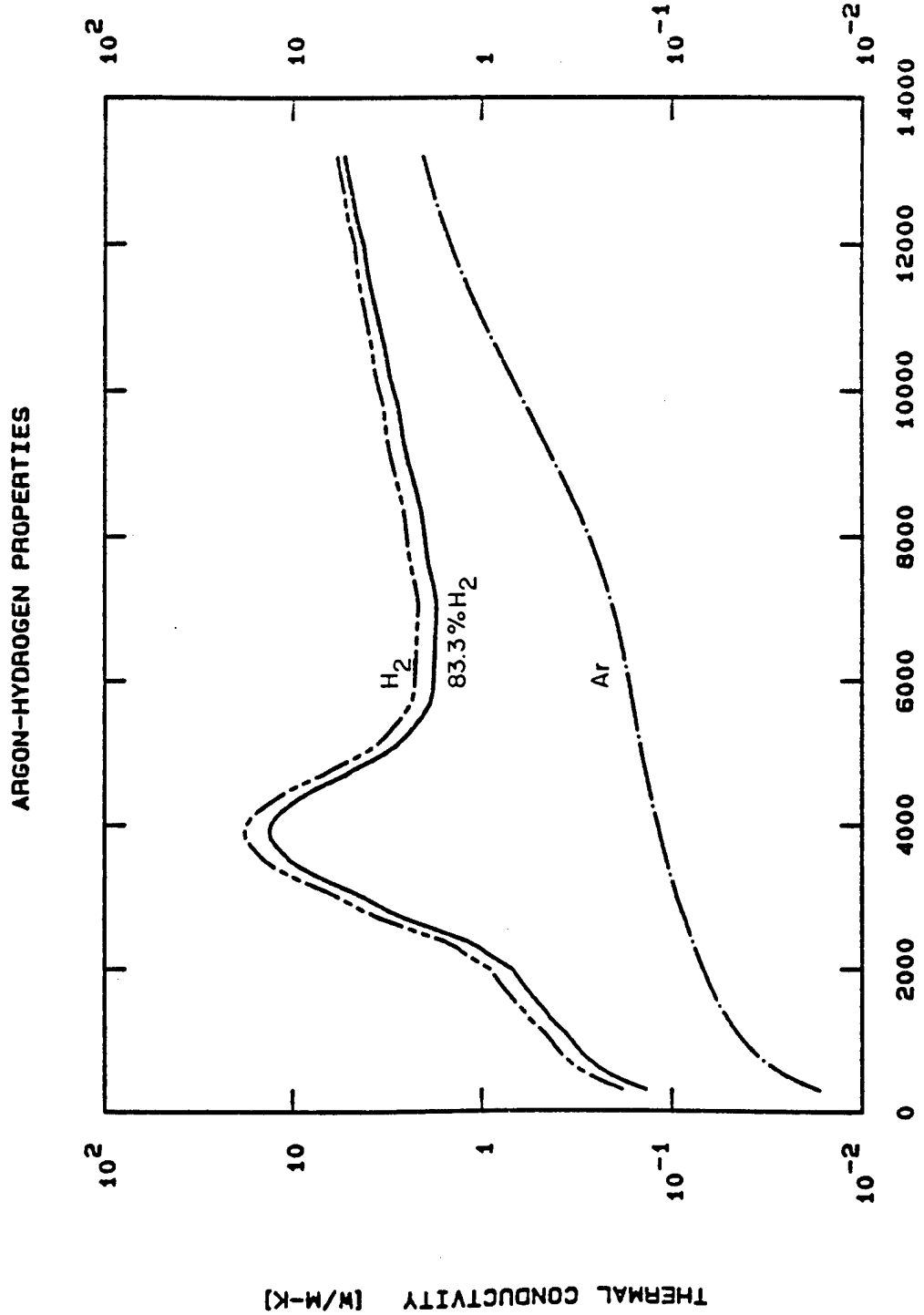

2.18 Thermal conductivity of Ar/H_2 mixtures under atmospheric pressure.

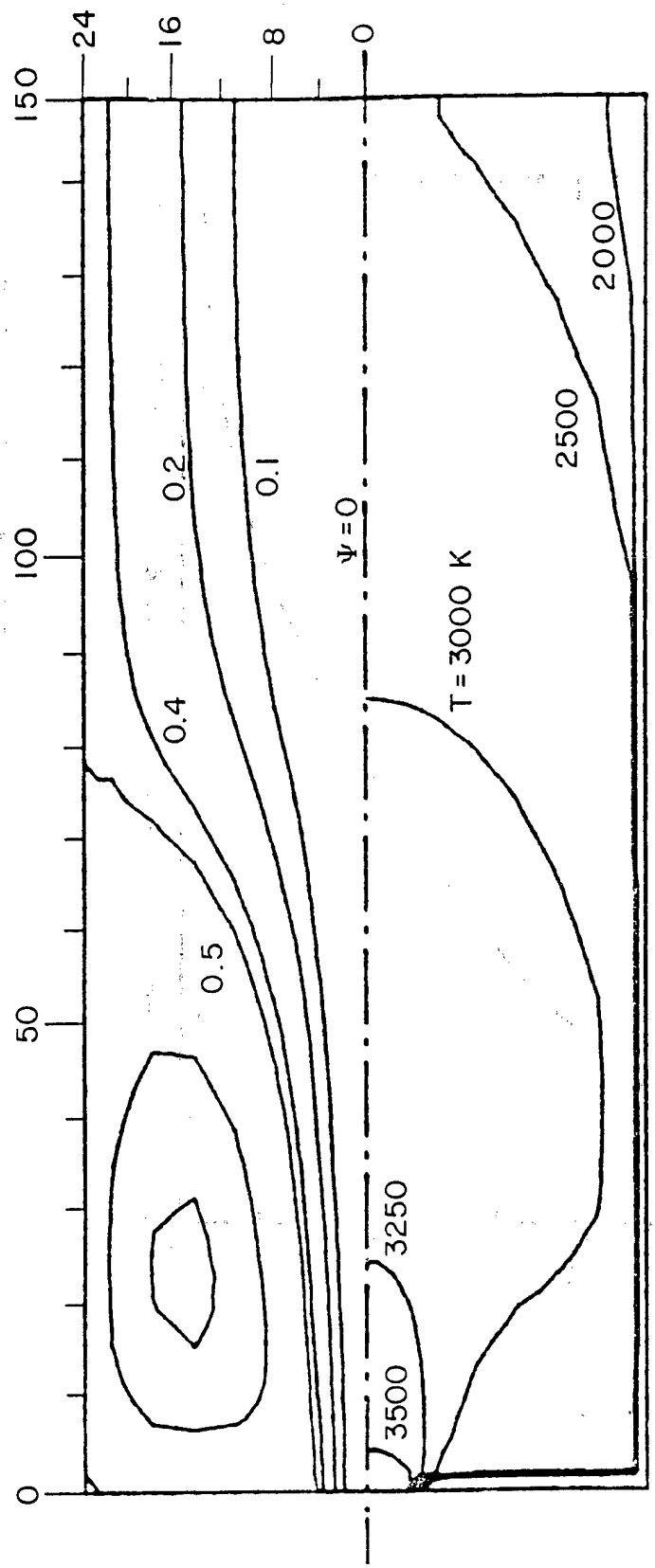

2.19 Flow (top) and temperature (bottom) fields in the inlet section of the reactor (dimensions in mm).

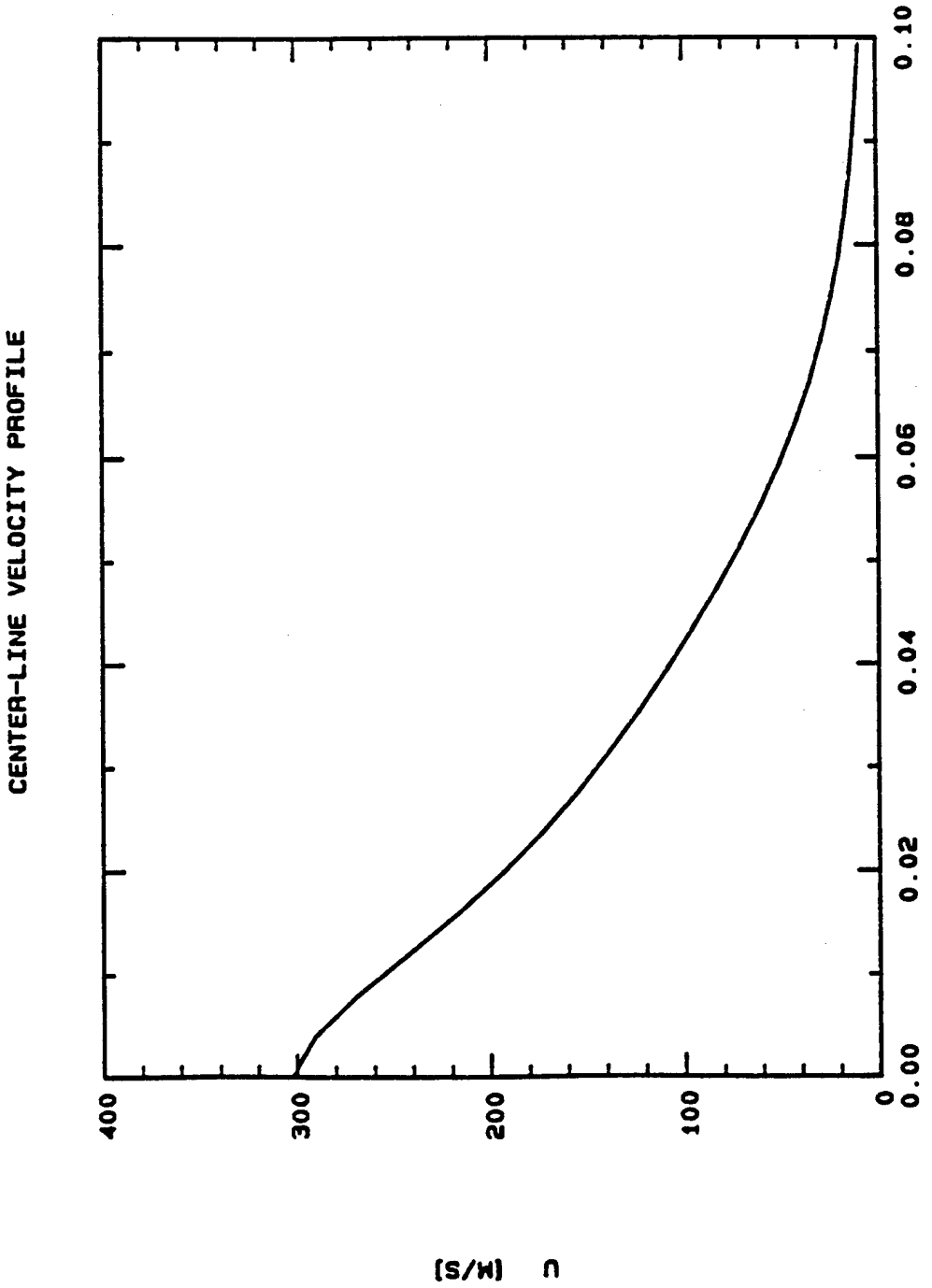

2.20 Centerline velocity profile in the entrance region of the reactor.

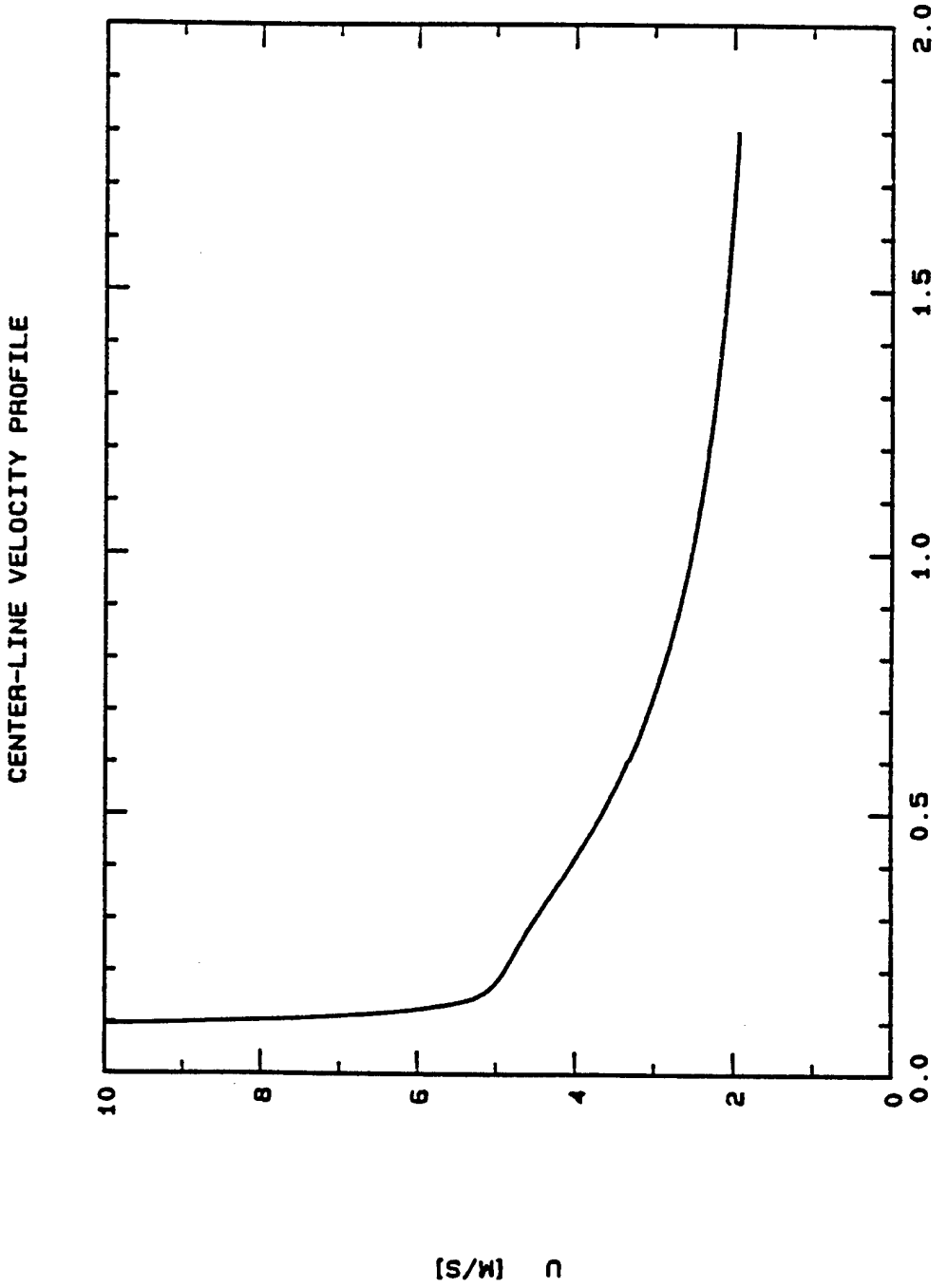

2.21 Centerline velocity profile along the full length of the reactor.

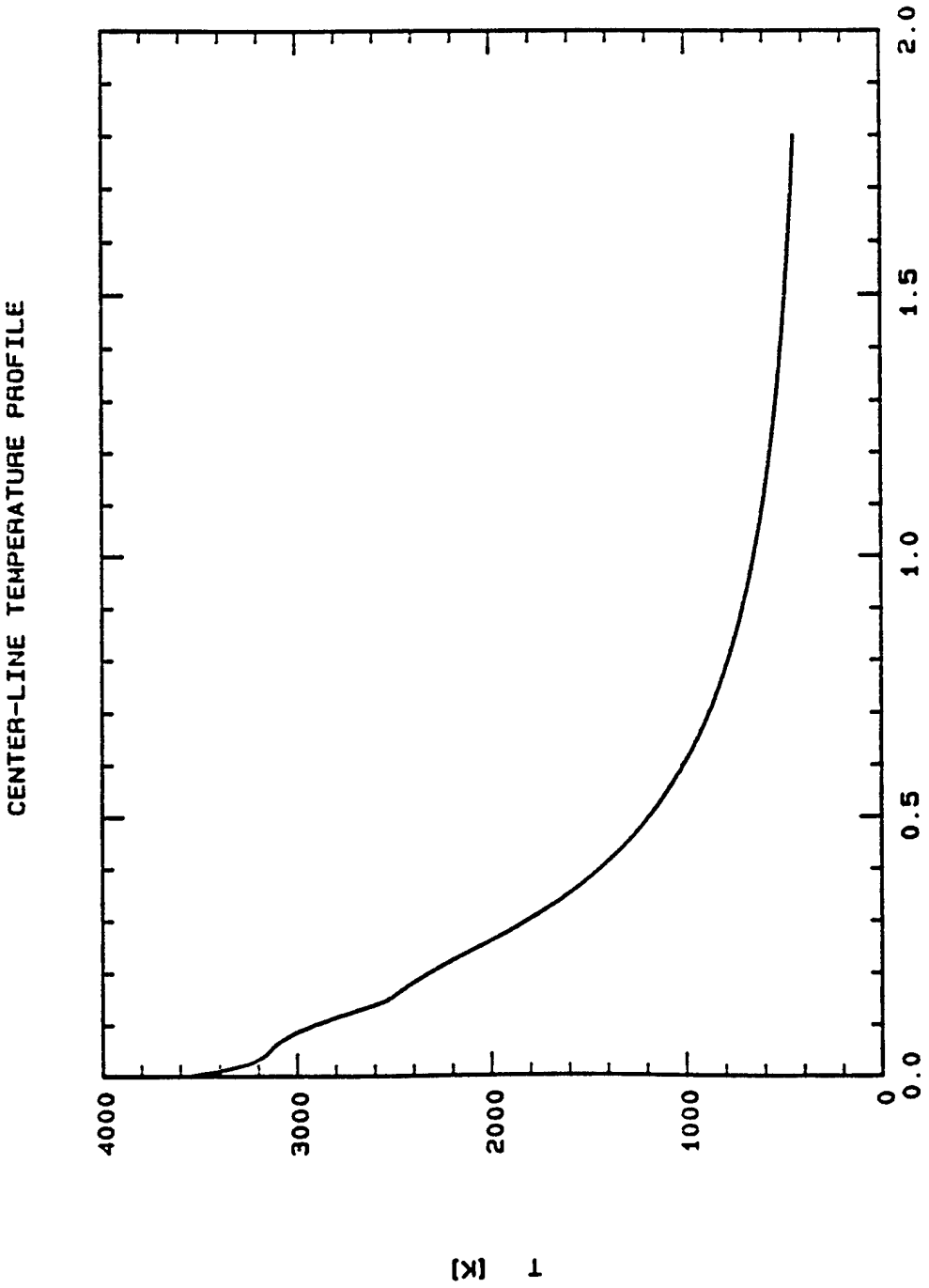

2.22 Centerline temperature profile along the full length of the reactor.

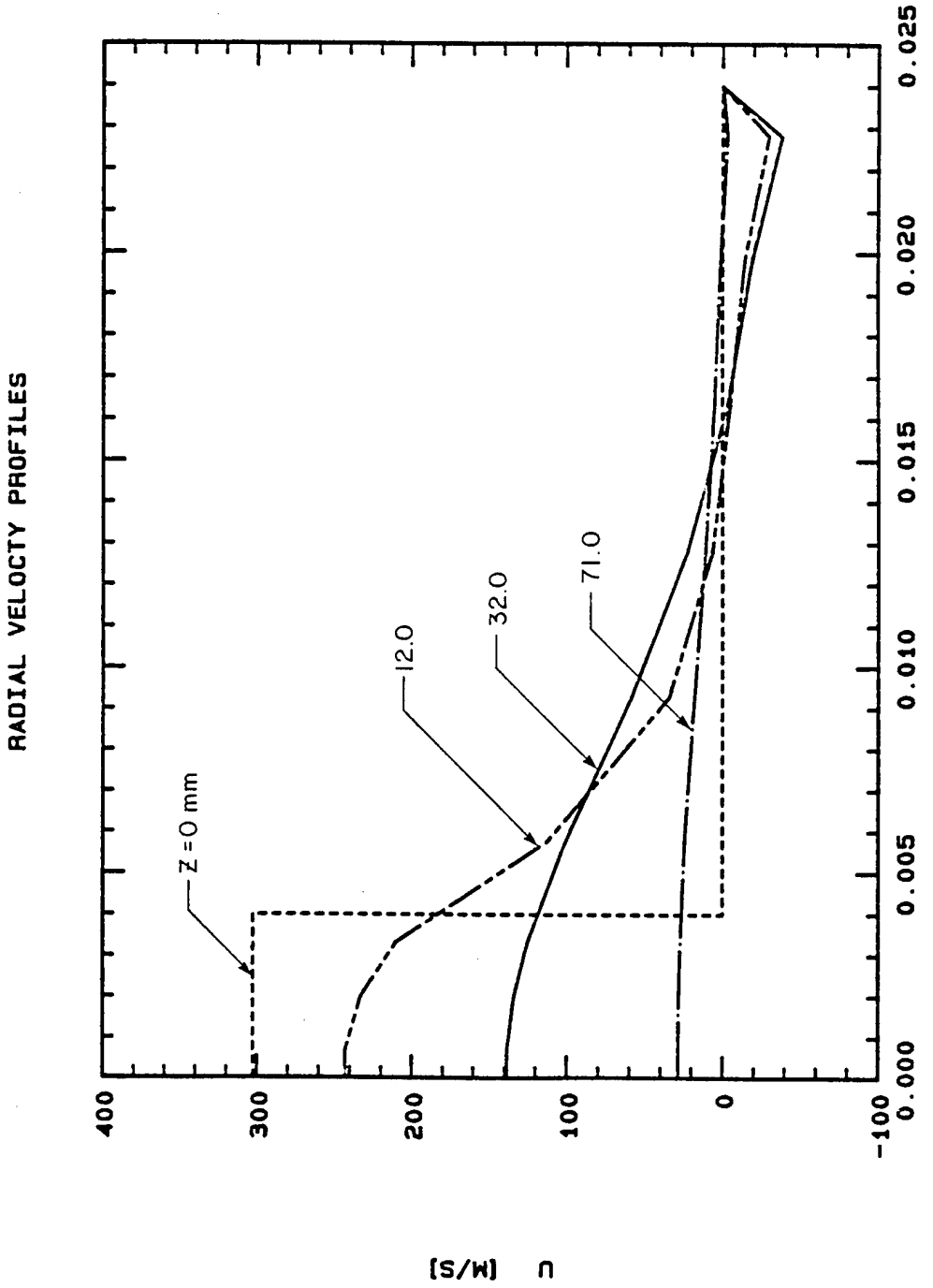

2.23 Radial velocity profiles over the entrance region of the reactor.

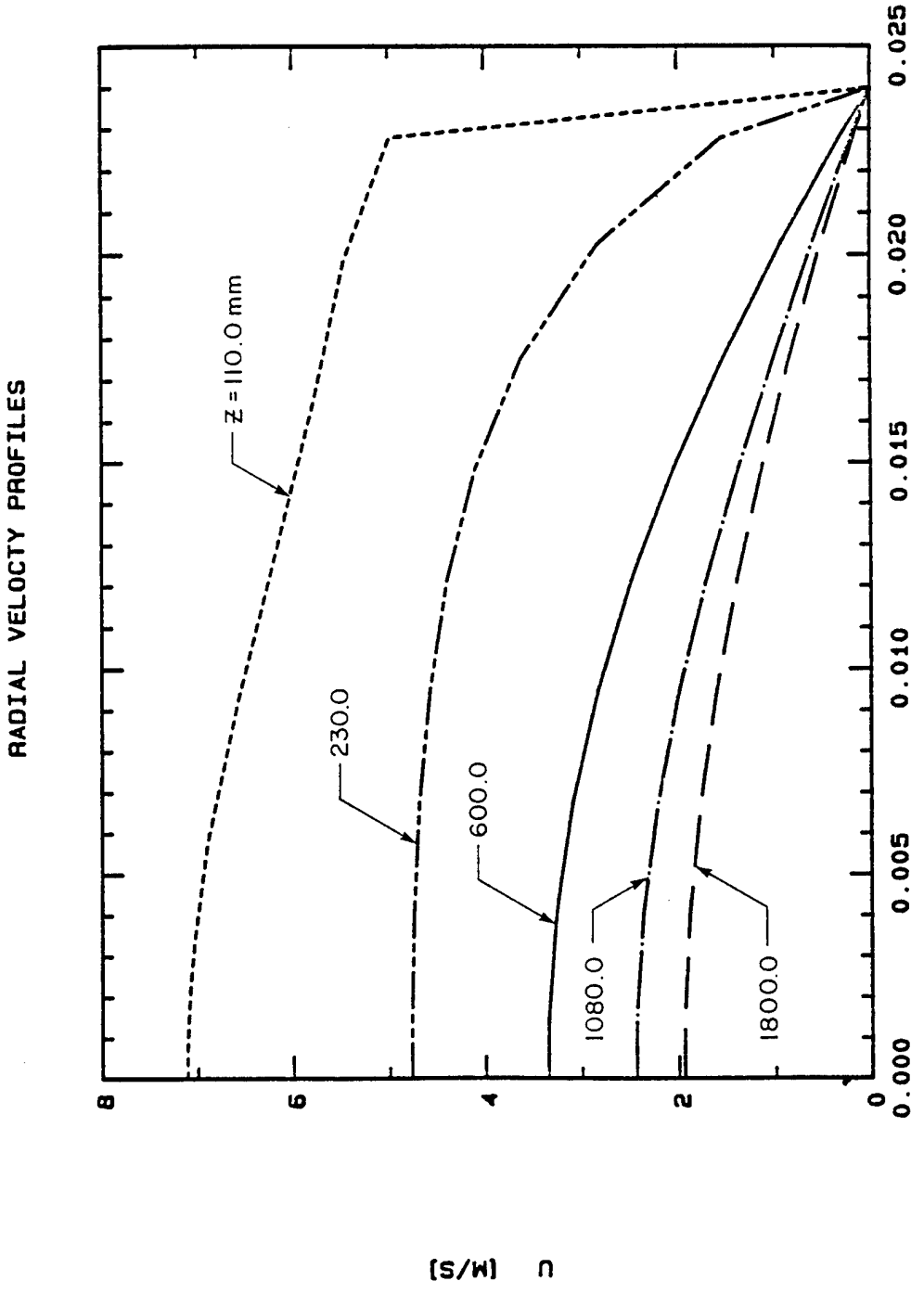

2.24 Radial velocity profiles at different levels in the reactor.

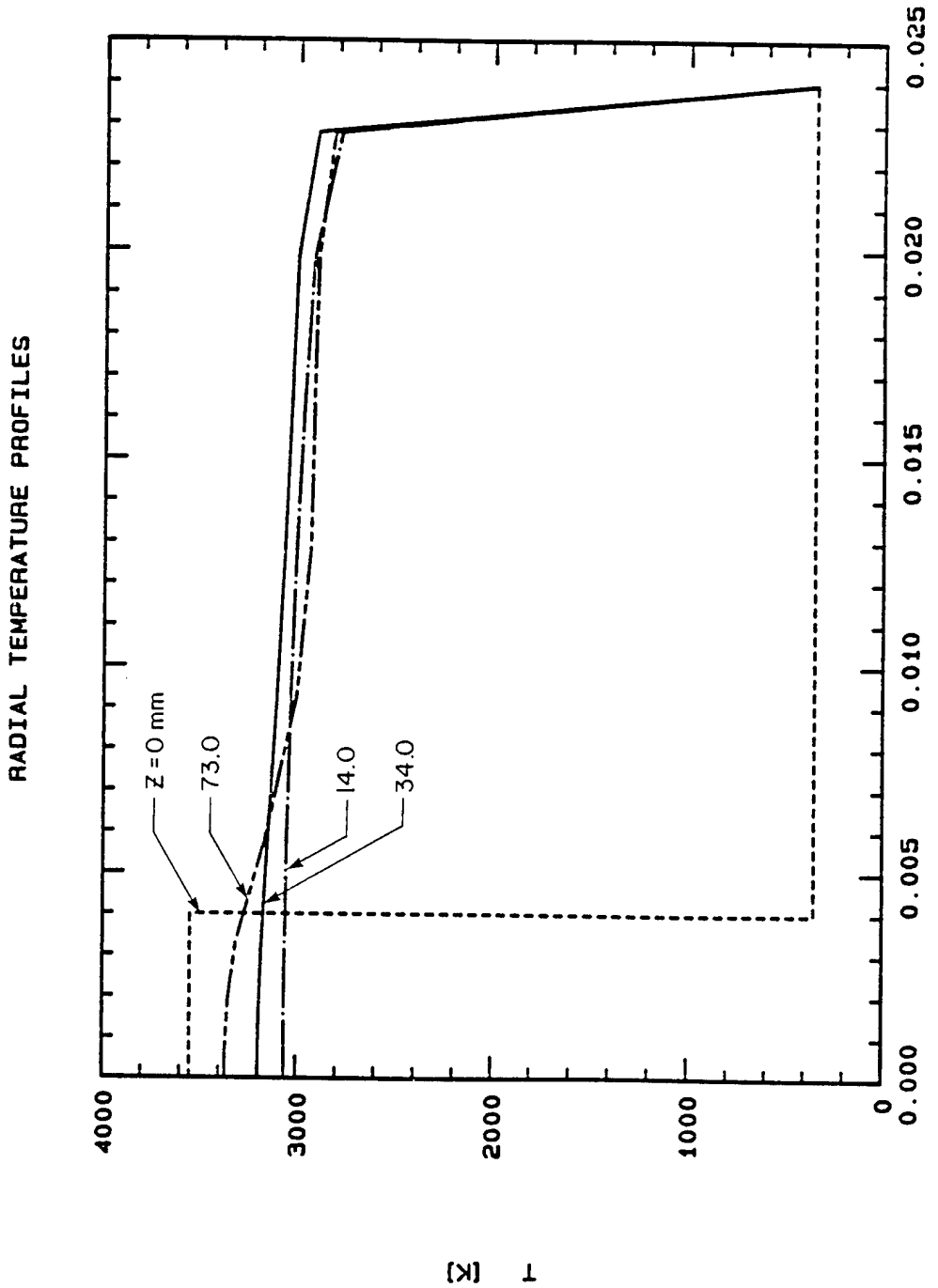

2.25 Radial temperature profiles over the entrance region of the reactor.

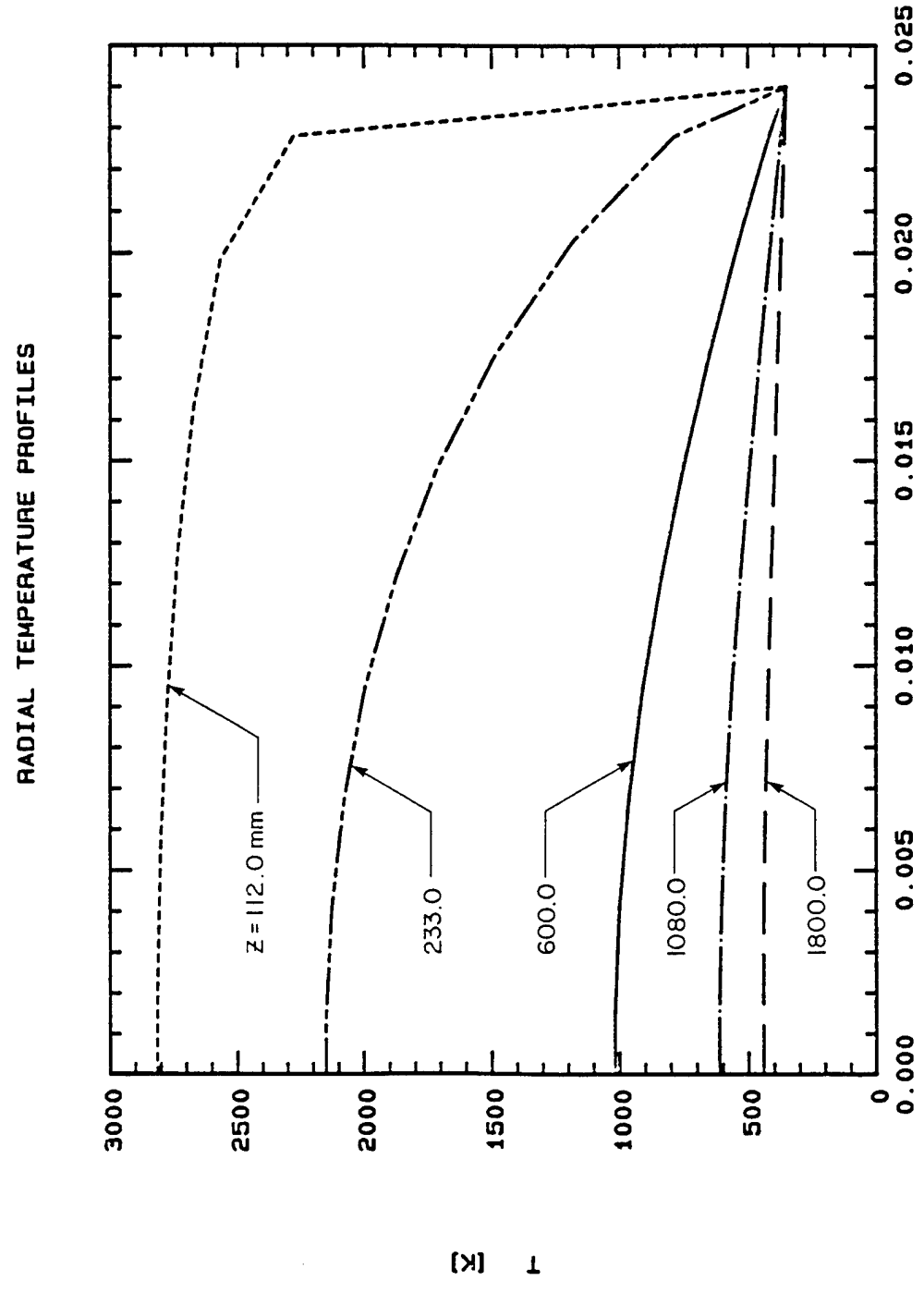

2.26 Radial temperature profiles at different levels in the reactor.

The wall heat flux distribution is shown in Figure 2.27. The maximum heat flux occurs close to the entrance region and is about 4×10^5 w/m^2. At z = 1.8 m the heat flux is less than 10^3 w/m^2.

Further computations were carried out for five different sets of operating conditions which are given in Table 2.2. Also included are the Reynolds numbers of the flow for the jet, Re_d, for the step, Re_h, and for the reactor Re_D. These were defined as follows.

jet; $$Re_d = \frac{4\dot{m}}{\pi\mu d}$$

Step; $$Re_h = Re_d \cdot \left(\frac{H}{d}\right)$$

Reactor; $$Re_D = \frac{4\dot{m}}{\pi\mu D}$$

Where
- $\dot{m}$ Mass flow rate of the reaction mixture
- μ Dynamic viscosity
- d Nozzle diameter
- D Reactor internal diameter
- H Step high at the reactor inlet (H = 0.5 (D-d)), see Fig. 2.13

The results are presented as follows:

First the effect of wall temperature on the temperature and flow field is discussed, i.e. a comparison is made between cases a.1, a.2 and a.3.

Secondly, the effect of inlet power on the flow and temperature fields are presented, and finally the effect of the flow rate on these fields is given.

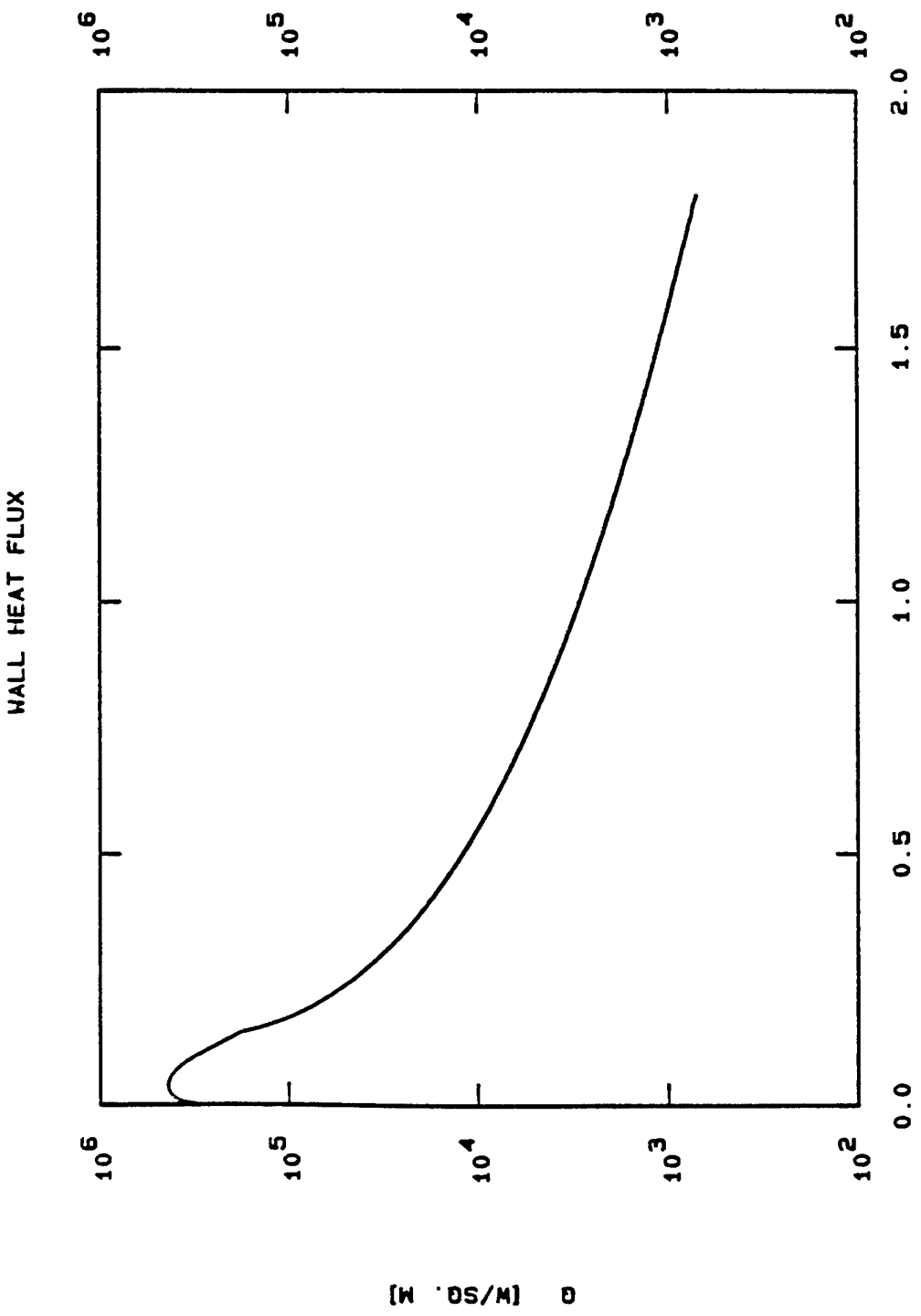

2.27 Wall heat flux along the full length of the reactor.

Table 2.2 Summary of the operating conditions for which computations were carried out using Ar/H_2 as reaction mixture with 83.3% by volume H_2

Case	Q_{Ar} (slm)	Q_{H_2} (slm)	P_{net} (kW)	To (K)	Tw (K)	Re_d	Re_h	Re_D	
								inlet	exil
a.1	15.0	75.0	10.0	3550	350	640	1600	107	560
a.2	15.0	75.0	10.0	3550	500	640	1600	107	480
a.3	15.0	75.0	10.0	3550	1000	640	1600	107	280
b.1	15.0	75.0	3.0	2300	350	910	2275	150	560
b.2	30.0	150.0	10.0	2900	350	1500	3740	250	1130

Typical results of the flow and temperature fields at the entrance region are shown in Figure 2.28. The reattachment point for the cases considered here occur at approximately 75 mm from the entrance of the reactor. This region is characterized by a high level of turbulent mixing and the radial variations in the gas temperature is rather small over a large part of the cross section.

Figures 2.29 and 2.30 show a comparison of the radial temperature and velocity profiles between cases a.1, a.2 and a.3. For $z < 100$ mm, the temperature profiles are flat and drop sharply at the wall (Fig. 2.29), on the other hand. When the flow becomes laminar, these profiles develop into the standard parabolic profile For $z = 1800$, the gas temperature is almost the same as the wall temperature. The gas velocities show a similar pattern, except that for $z < 75$ mm, a strong recirculation zone develops near the reactor wall (Fig. 2.30).

Figure 2.31 shows the axial temperature profile along the centerline of the reactor. The entrance region is characterized by a sharp drop in temperature due to high heat transfer to the wall. The wall heat flux distribution is shown in Figure 2.32. The maximum heat flux occurs close to the inlet region and is close to 10^6 w/m^2 for these cases. The heat flux will then drops, however, to less than 10^3 w/m^2 at $z = 1800$ mm, the lowest heat flux is obtained for case a.3, i.e. for the case with highest wall temperature. It is important to note that between 50% to 65% of the inlet power is lost to the wall in the inlet region of the reactor $z < 150$ mm. This high value of losses over such a short distance is mainly due to the high turbulence in this region.

Since such a power loss could result in a considerable drop in processing efficiency, special care should be taken to avoid flow separation and the development of a turbulent recirculatory flow in the entrance region. This could be achieved either by decreasing the reactor diameter or the use of a gradually diverging nozzle to expand the plasma jet to the reactor diameter.

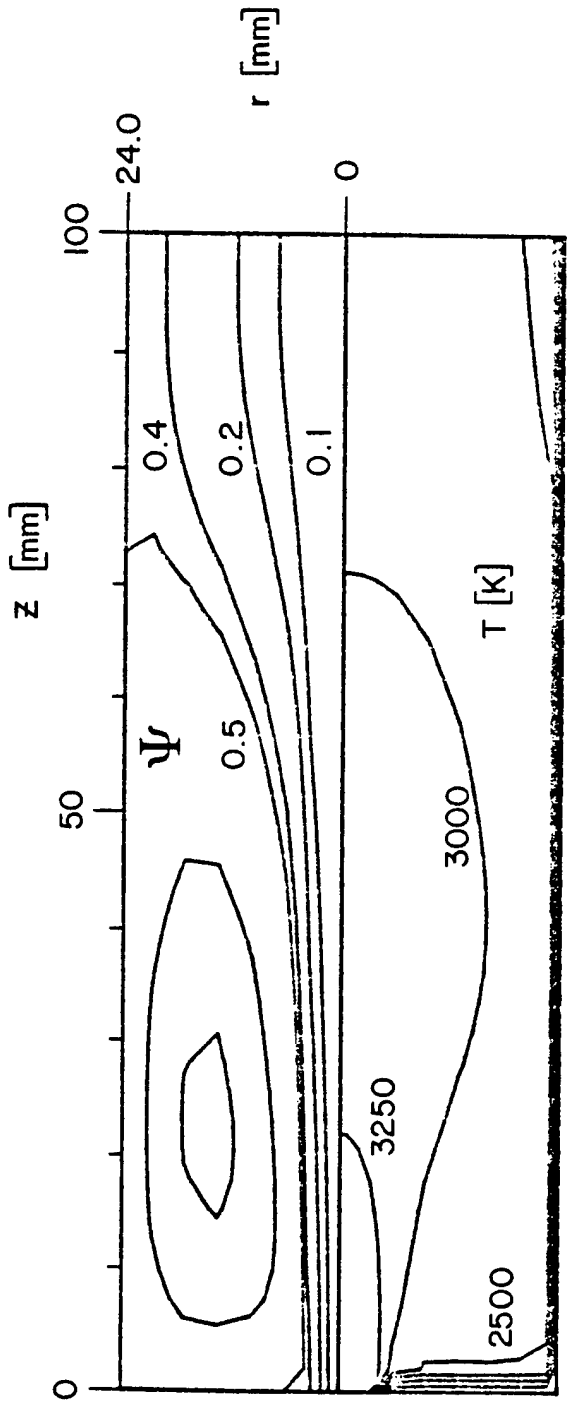

2.28 Streamlines and temperature isocontours in the entrancew region of the reactor (z<100 mm) for case a.2.

COMPARISON OF TEMPERATURE PROFILES

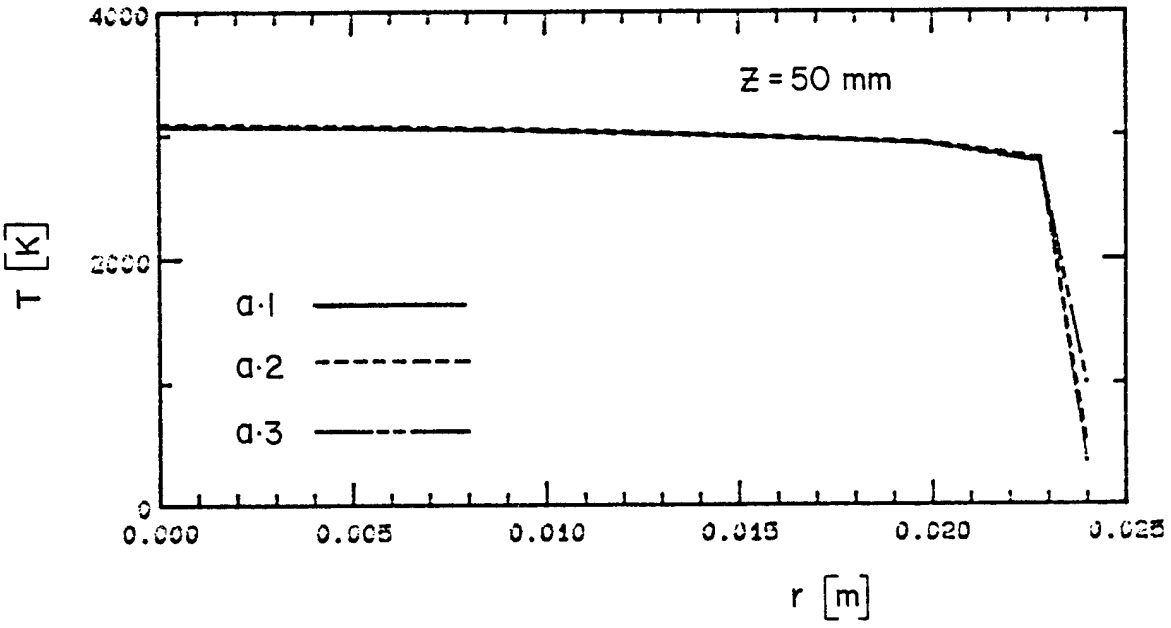

a

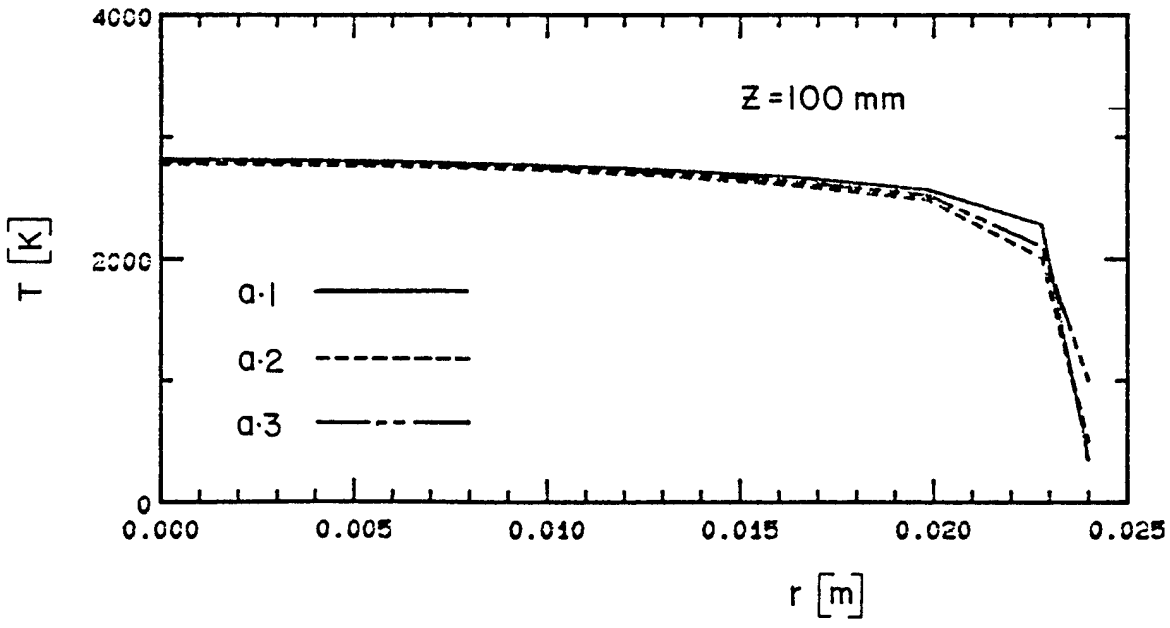

b

2.29 Radial temperature profiles at different levels in the reactor for cases a.1, a.2 and a.3.

a)	z = 50 mm	e)	z = 900 mm
b)	z = 100 mm	f)	z = 1200 mm
c)	z = 300 mm	g)	z = 1500 mm
d)	d = 600 mm	h)	z = 1800 mm

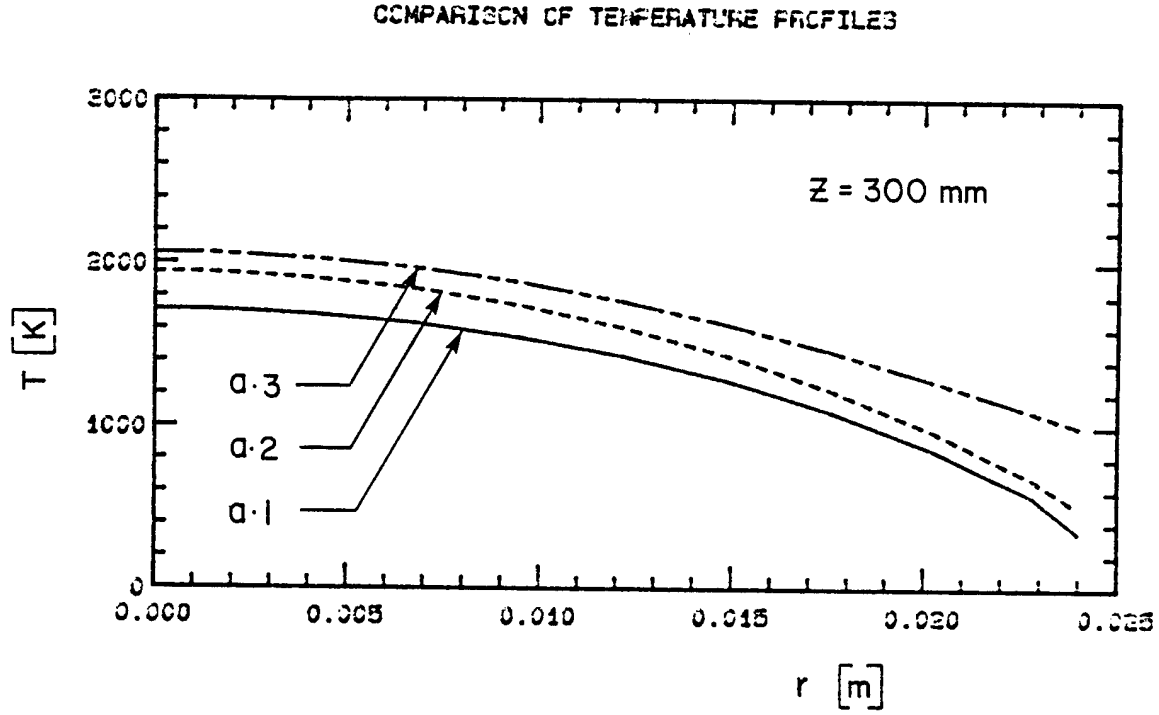

c

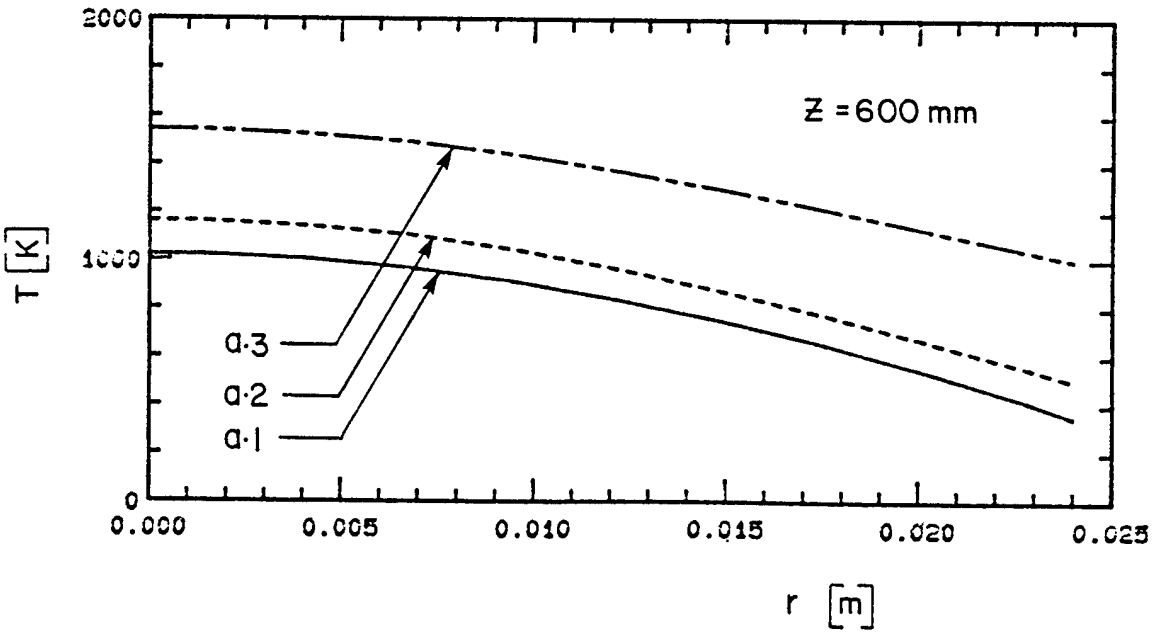

d

Fig. 29 (cont.)

COMPARISON OF TEMPERATURE PROFILES

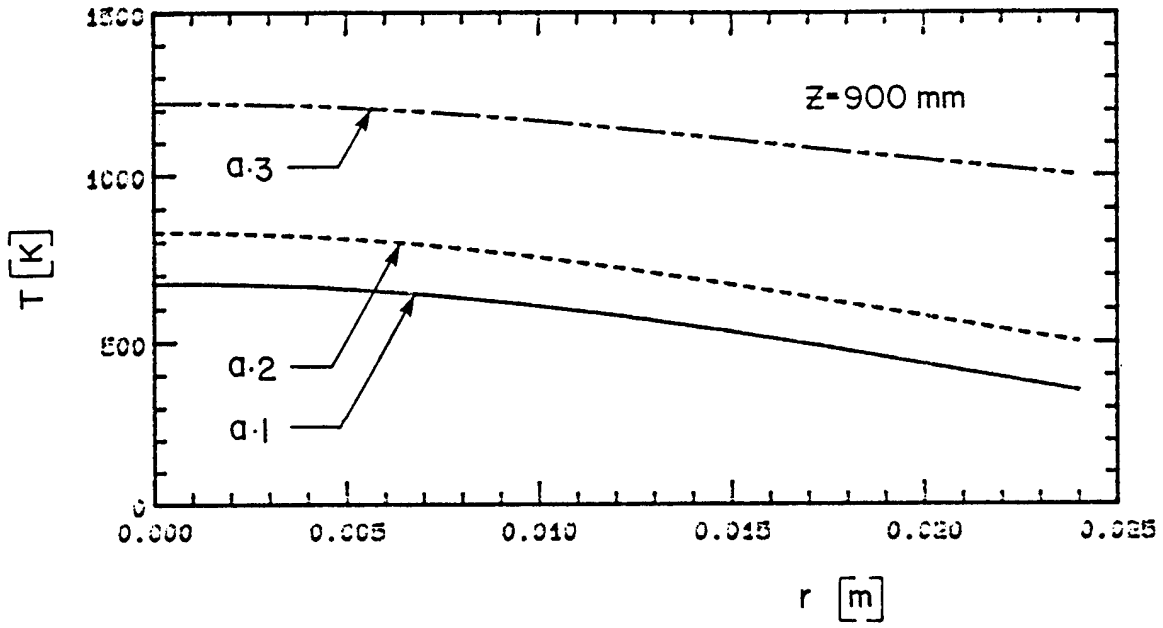

e

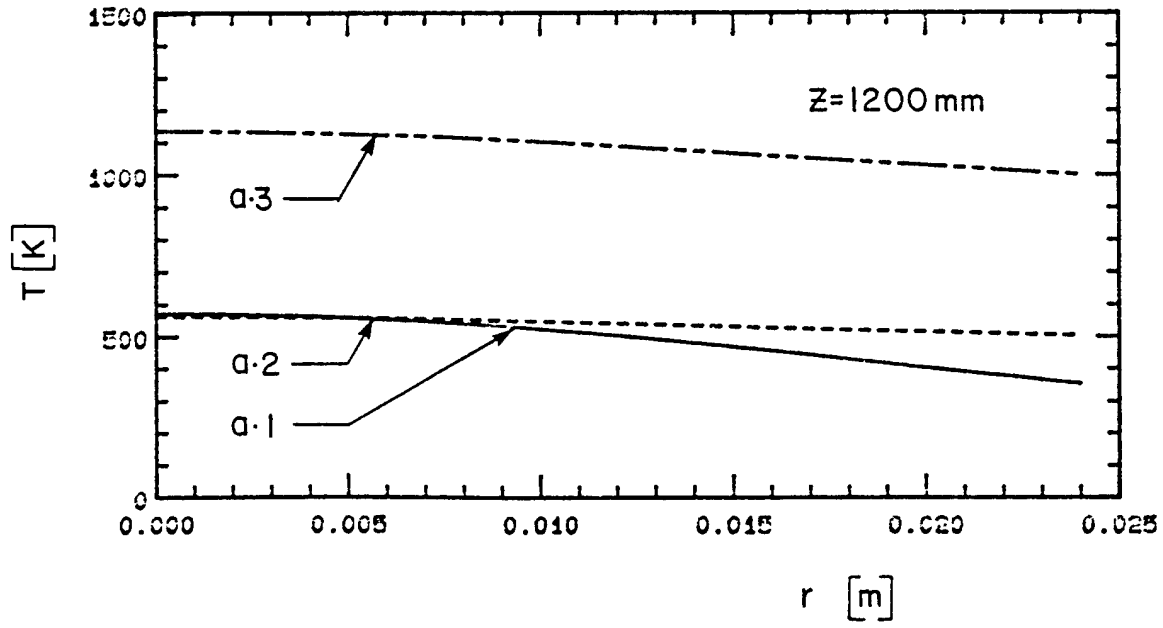

f

Fig. 29 (cont.)

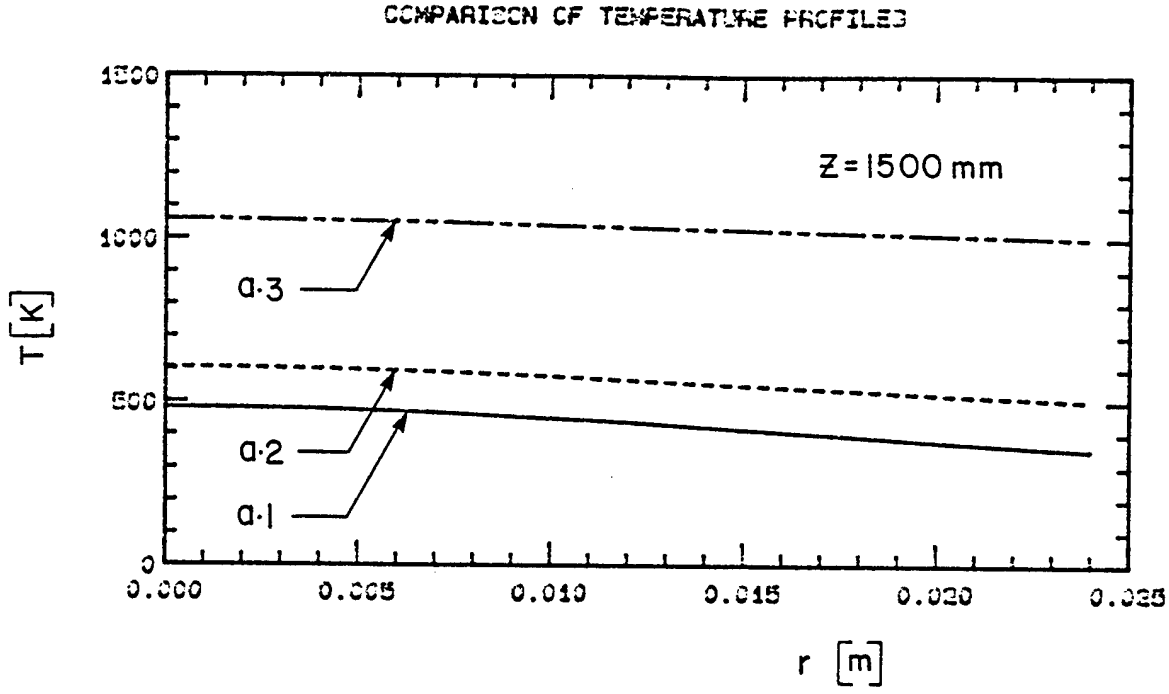

g

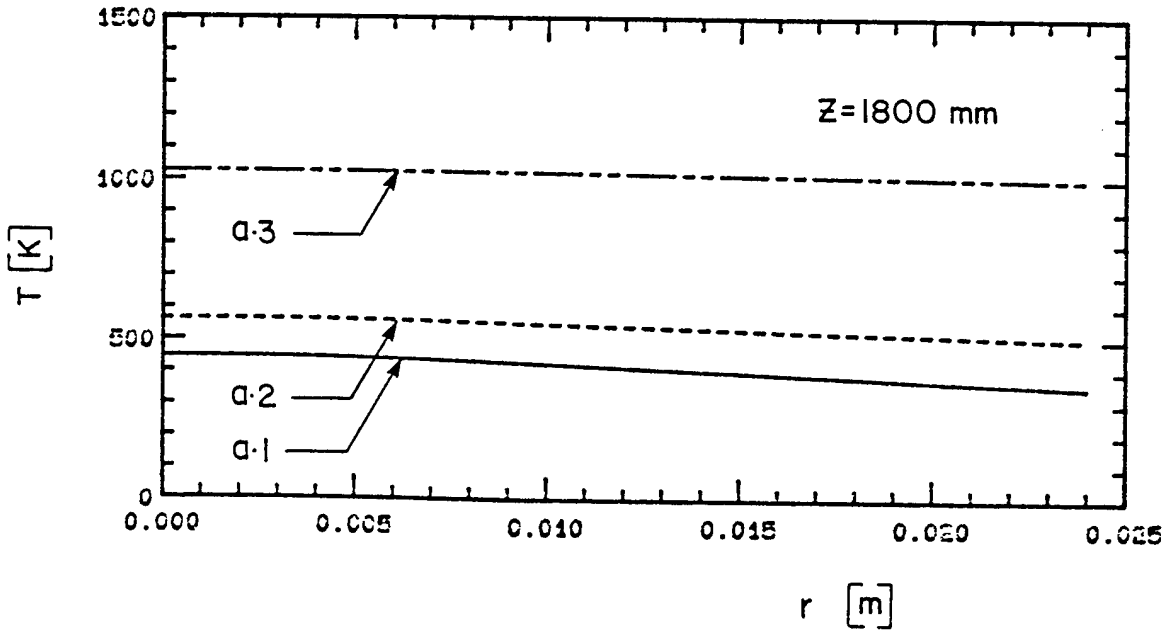

h

Fig. 29 (cont.)

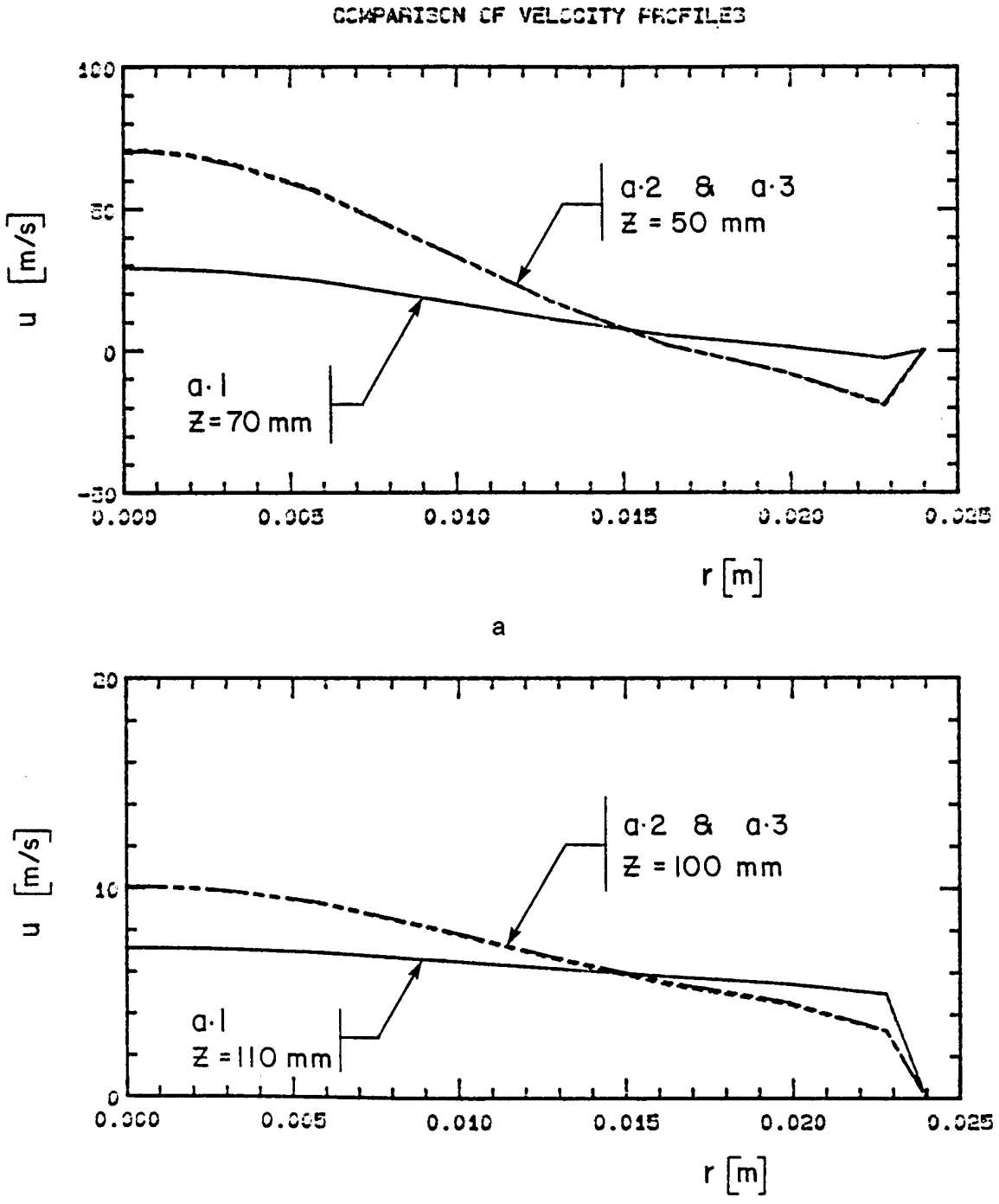

2.30 Radial velocity profiles at different levels in the reactor for cases a.1, a.2 and a.3.

a) z = 50 & 70 mm
b) z = 100 & 110 mm
c) z = 300 mm
d) d = 600 mm
e) z = 900 mm
f) z = 1200 mm
g) z = 1500 mm
h) z = 1800 mm

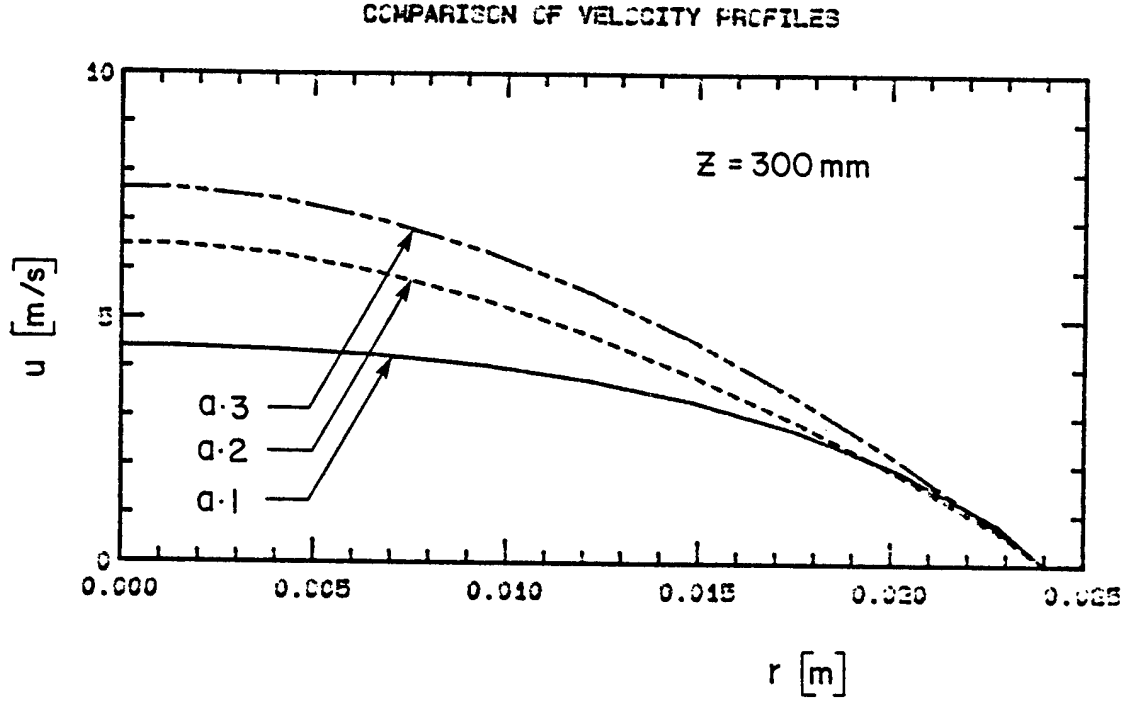

c

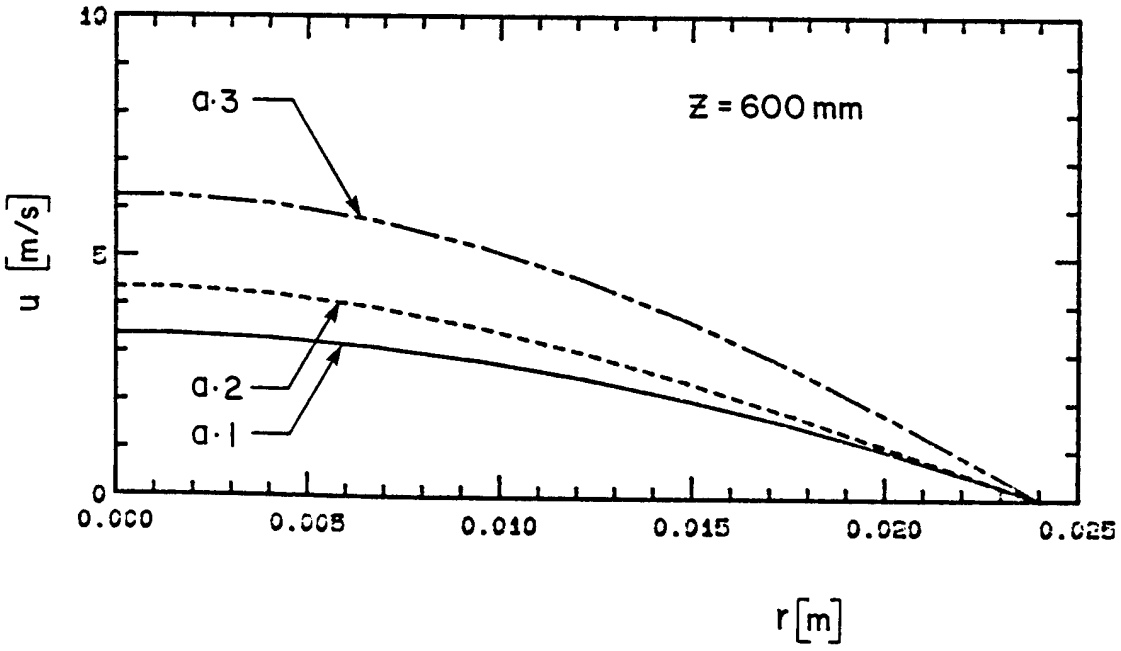

d

Fig. 30 (cont.)

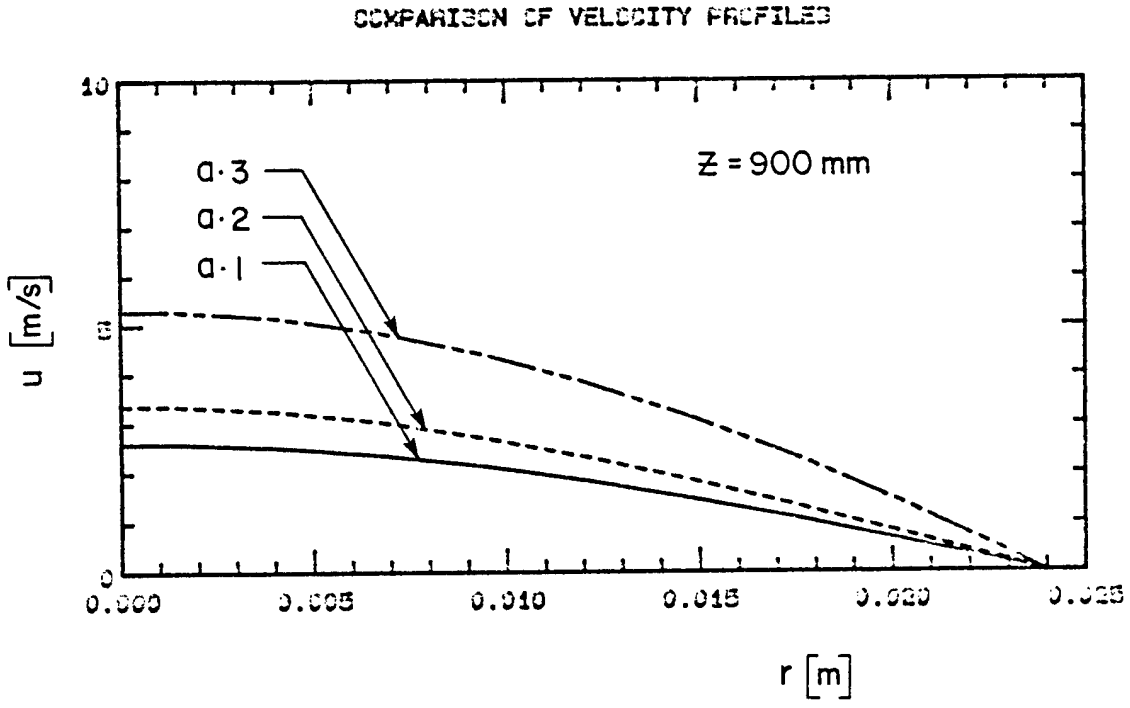

e

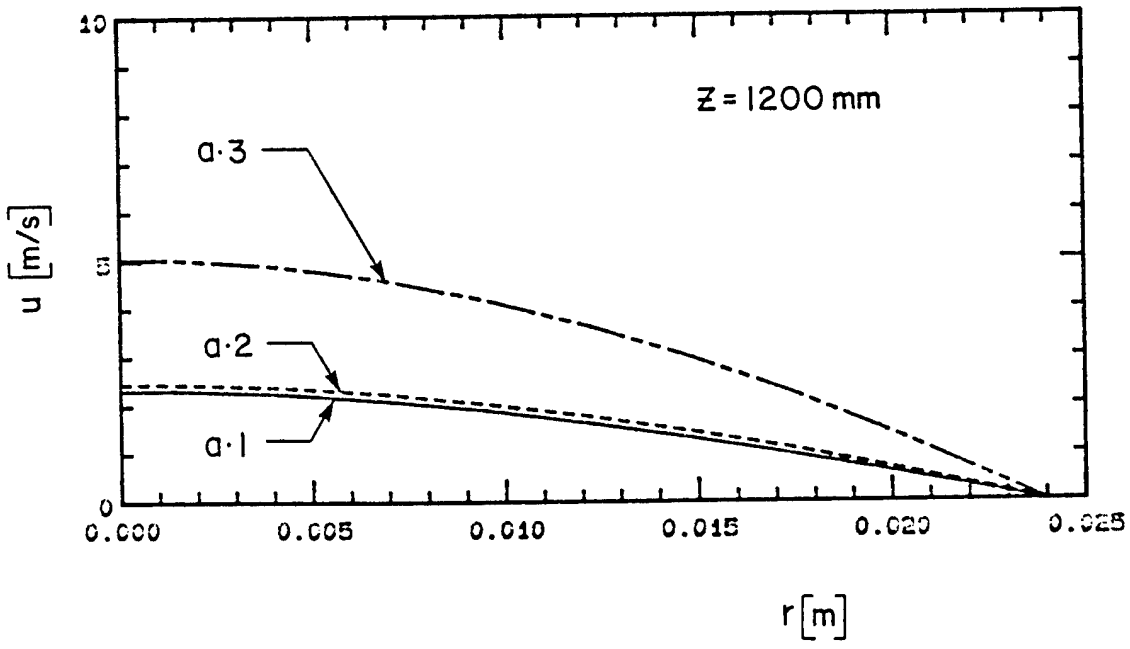

f

Fig. 30 (cont.)

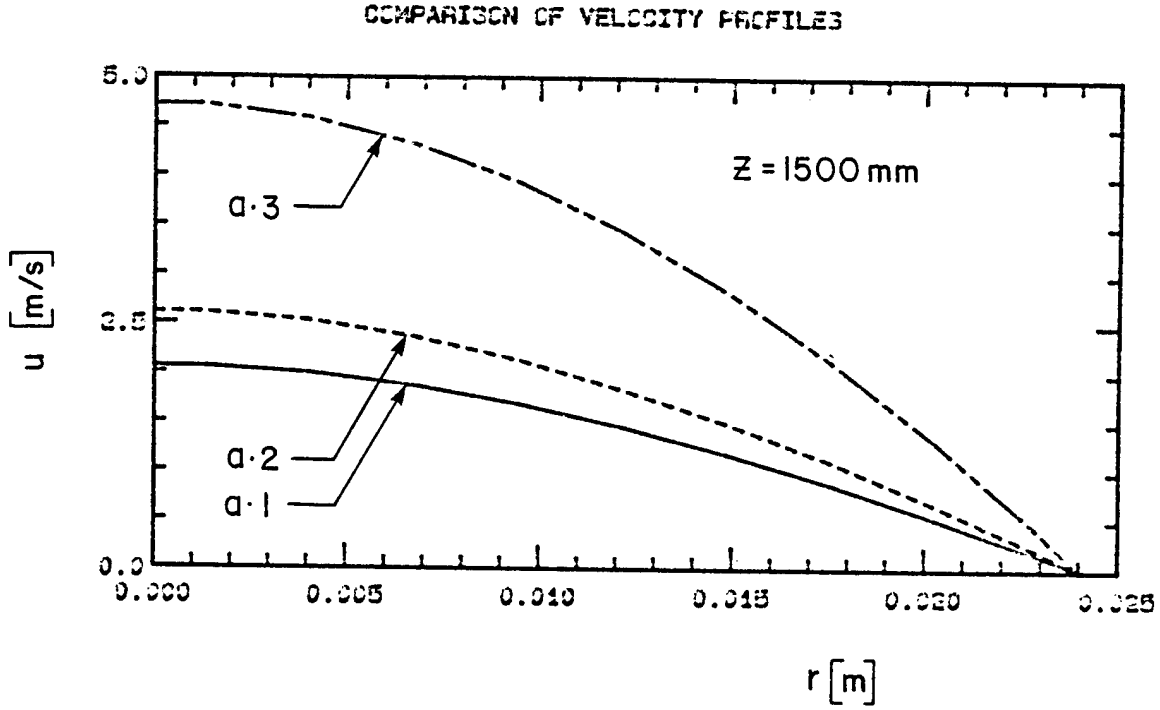

g

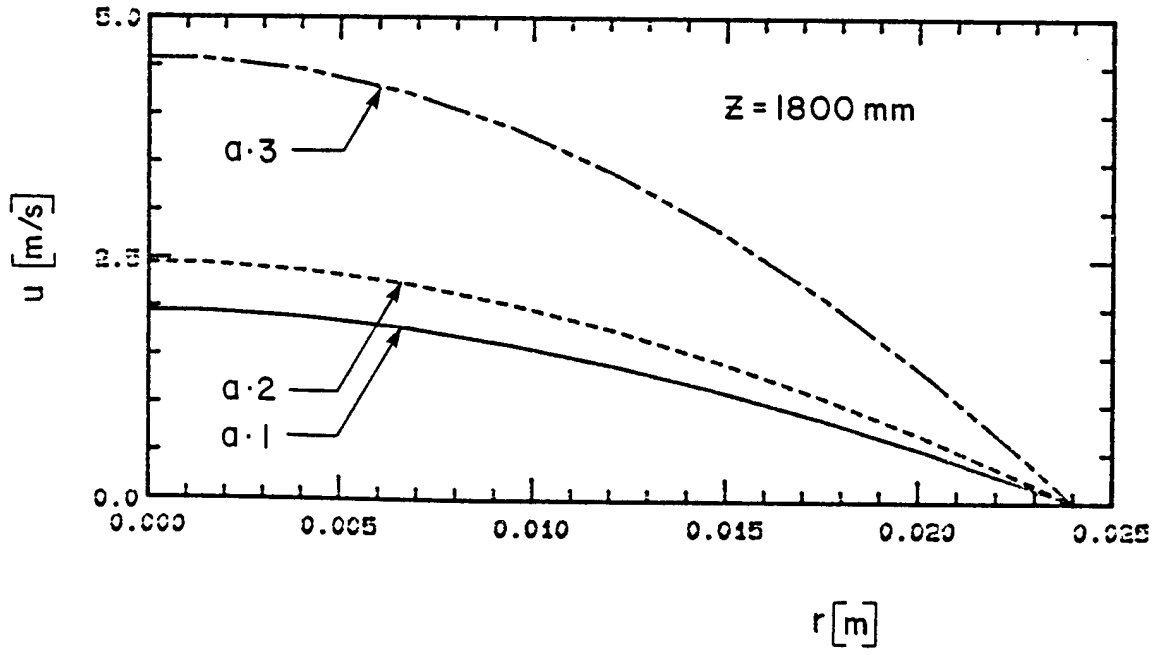

h

Fig. 30 (cont.)

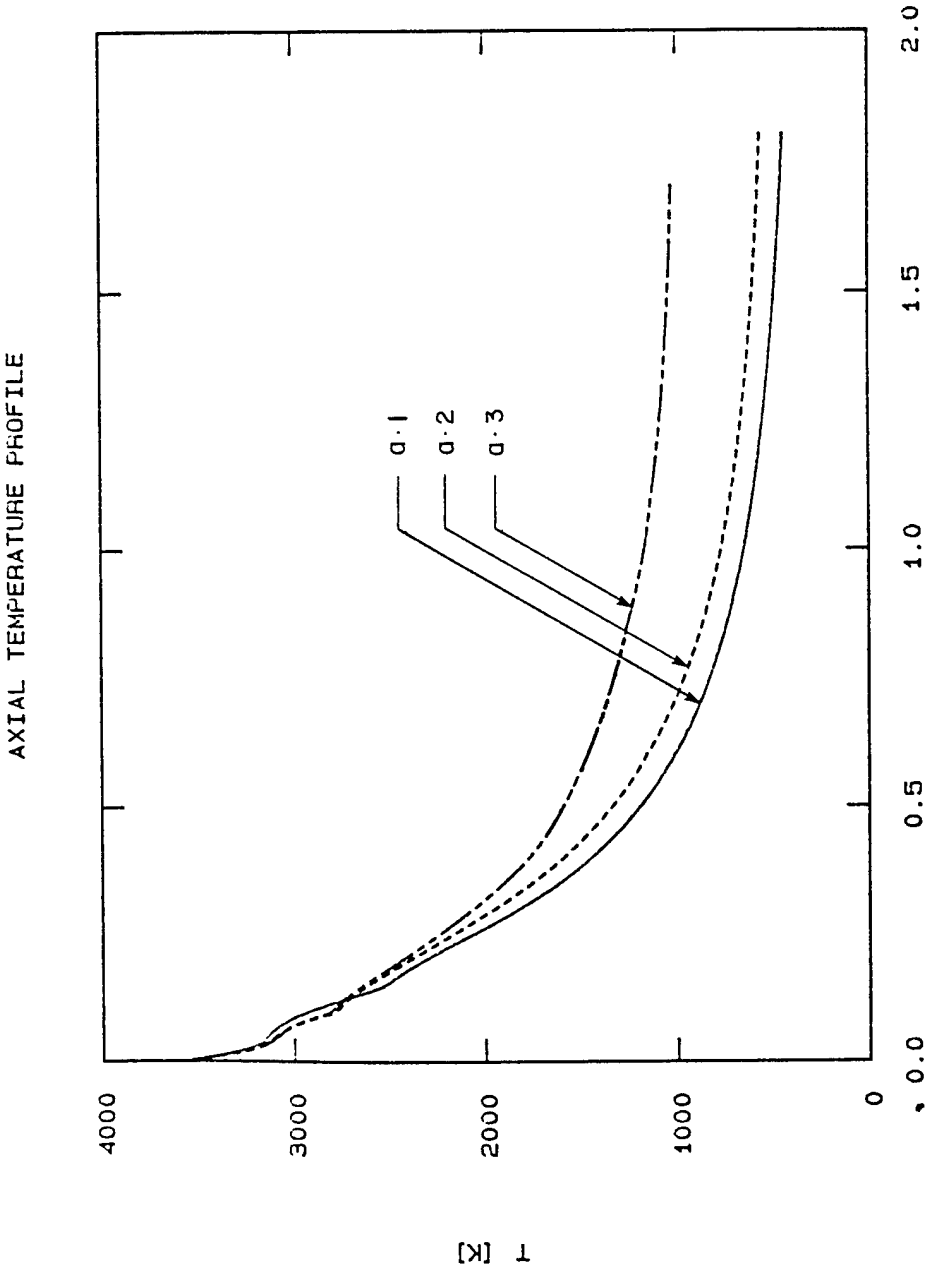

2.31 Axial temperature profile along the centerline of the reactor for cases a.1, a.2 and a.3.

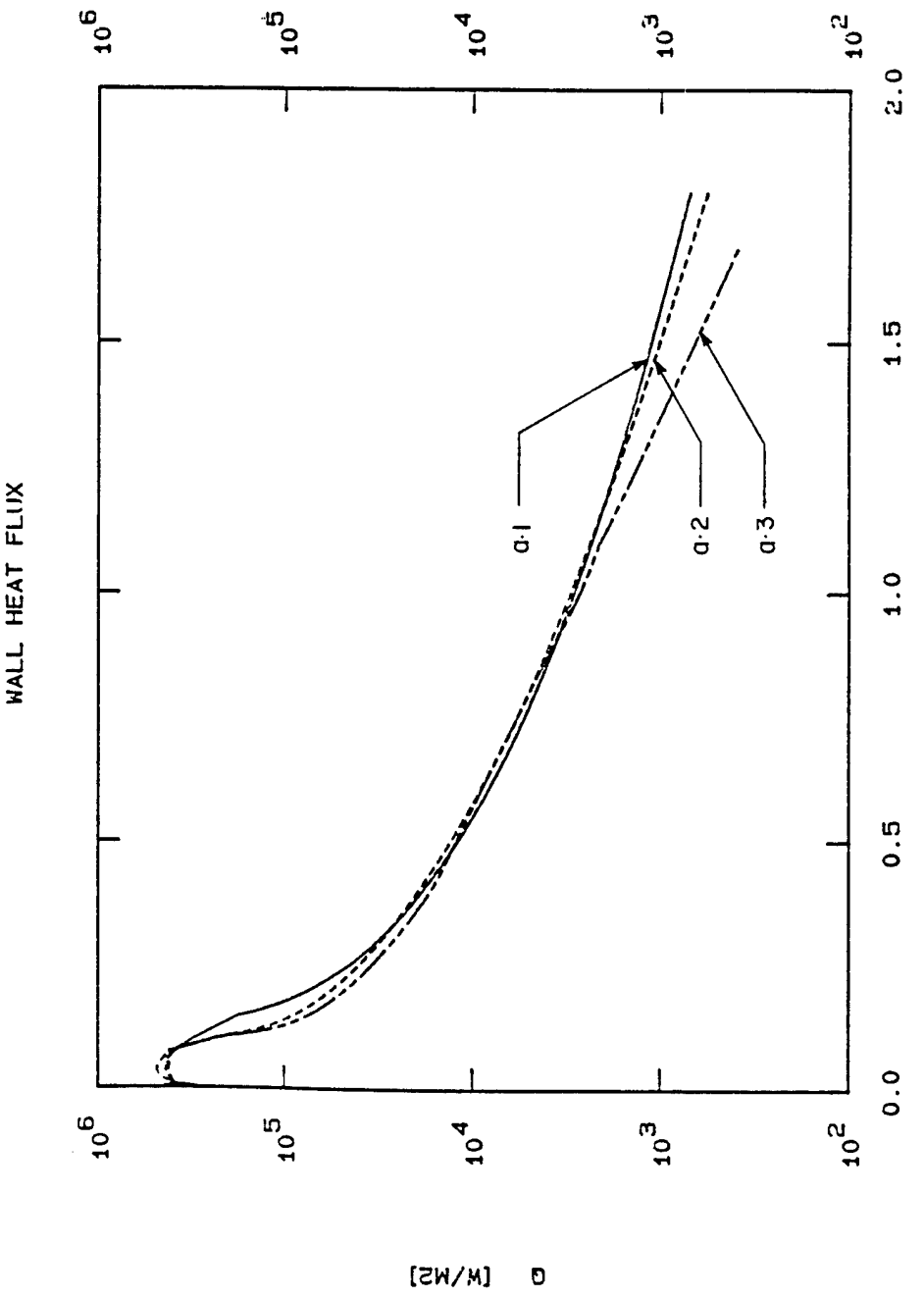

2.32 Heat flux to the reactor wall for cases a.1, a.2 and a.3.

Figure 2.33 shows the streamlines and temperature isocontours for case b.1. The inlet gas temperature in this case is 2300 K. The flow field is similar to the previous cases, i.e. a large recirculation at the entrance and the reattachment point is around 75 mm from the inlet. Figures 2.34 and 2.35 show a comparison of radial temperature and velocity profiles between cases a.1 and b.1 at different axial positions.

While for case a.1, the inlet gas temperature is 1200 K higher than that for case b.1, the difference dropps to only 20 K at z=1800 mm. The gas velocity distribution follows the same pattern (Fig. 2.35). Figures 2.36 and 2.37 show a comparison of the temperature and velocity profiles along the centerline of the reactor for cases a.1 and b.1. The rate at which the temperature drops for case a.1 is considerably higher than that for case b.1. The wall heat flux distribution for the two cases (Fig. 2.38) shows the higher heat losses associated with case a.1.

Finally for case b.2, while the net torch power is similar to that of a.1, 10 kW the total gas flow rate is doubled to 180 lpm. This results in the drop of the inlet average gas temperature to 2900 K. Figures 2.39 and 2.40 show the radial temperature and axial velocity profiles at different axial positions for cases a.1 and b.2. Although the inlet temperature for case a.1 is higher by 650 K than that for case b.2, the gas temperature at the exit of the reactor is more than 250 K higher for case b.2 compared to that for case a.1. This could be attributed to the fact that for a fully developed pipe flow with constant wall temperature, the bulk temperature varies according to the equation;

$$T_b - T_w \sim \exp\left(-\frac{2Nu}{RePr}\frac{z}{R}\right) \qquad (2\text{-}26)$$

where z is the axial position, R is the radius, Nu is the Nusselt number, Pr is the Prandtl number and Re is the Reynolds number.

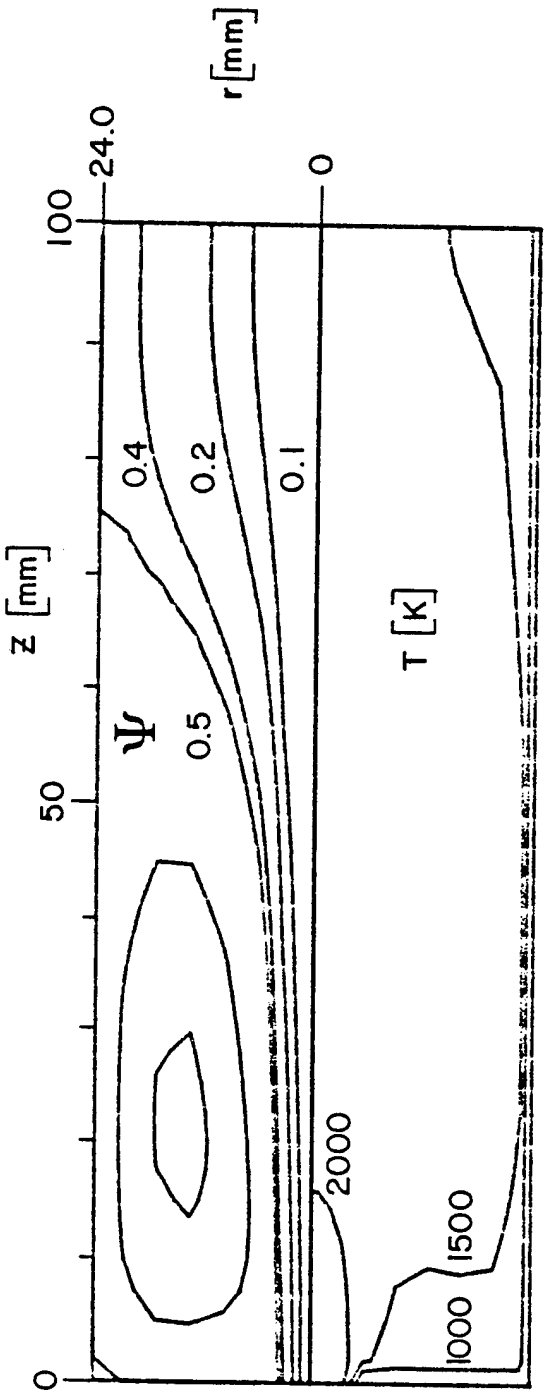

2.33 Streamlines and temperature isocontours in the entrance region of the reactor (z<100 mm) for case b.1.

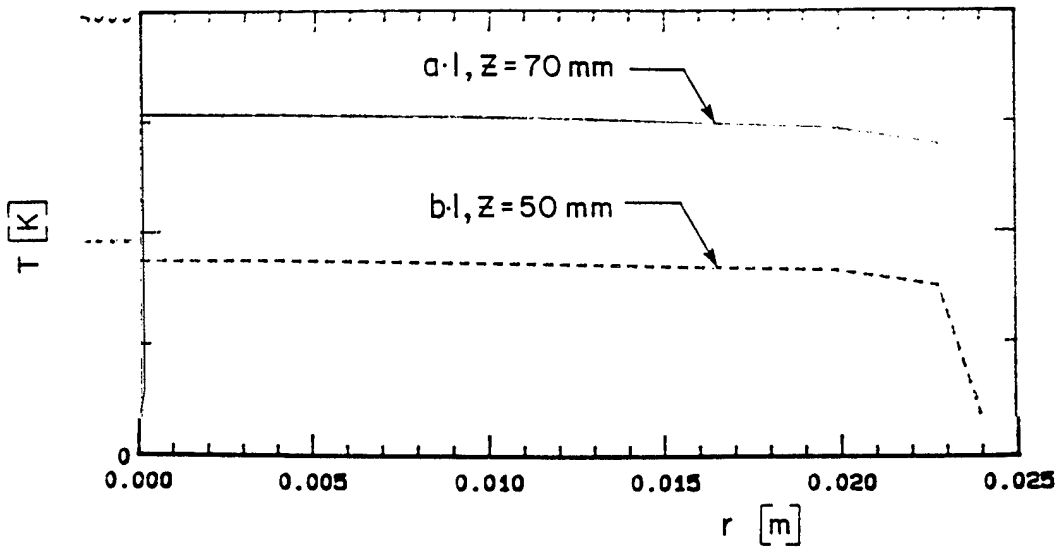

a

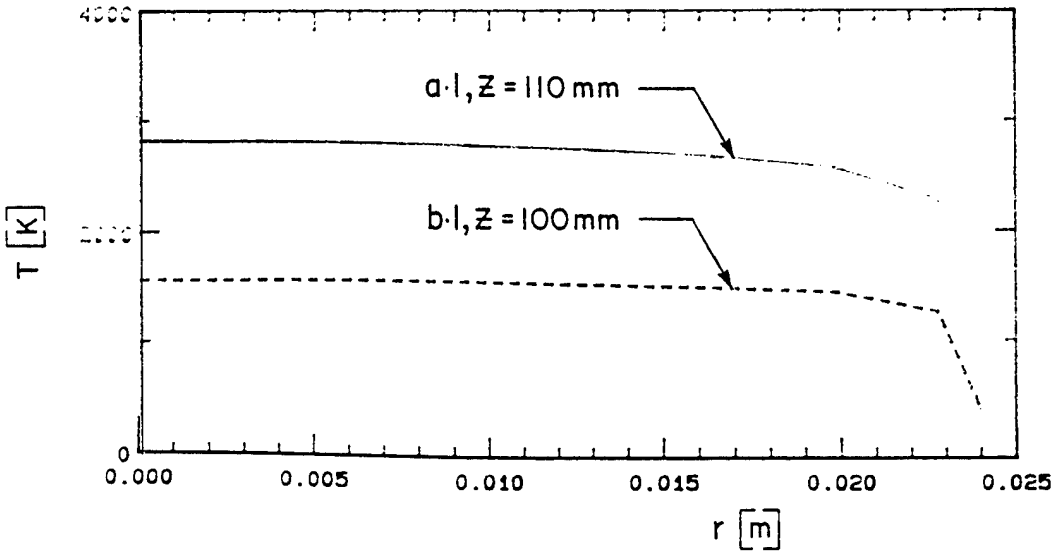

b

2.34 Radial temperation profiles at different levels in the reactor for cases a.1 and b.1.

a) z = 50 mm
b) z = 100 mm
c) z = 300 mm
d) d = 600 mm
e) z = 900 mm
f) z = 1200 mm
g) z = 1500 mm
h) z = 1800 mm

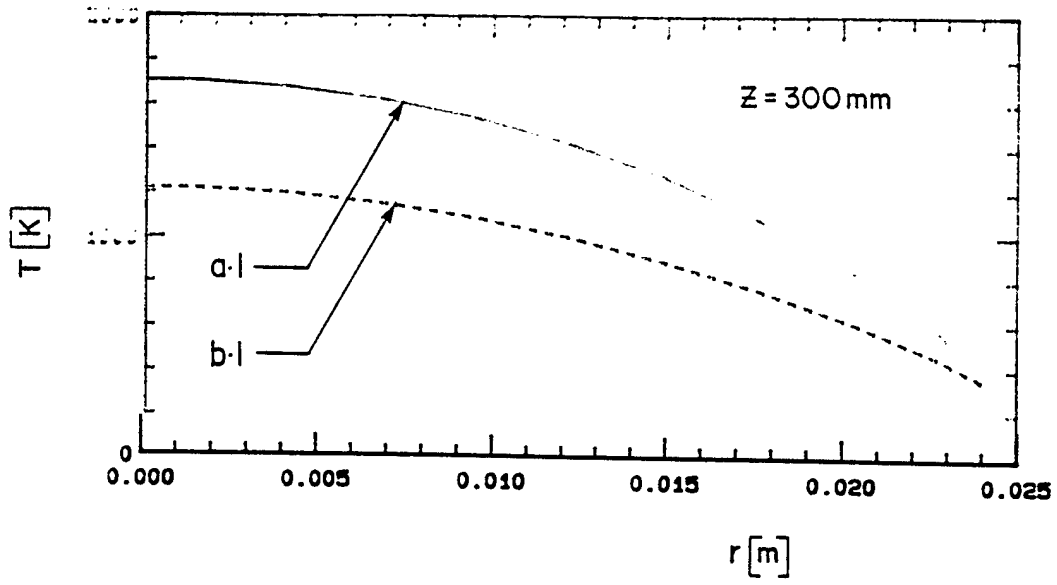

c

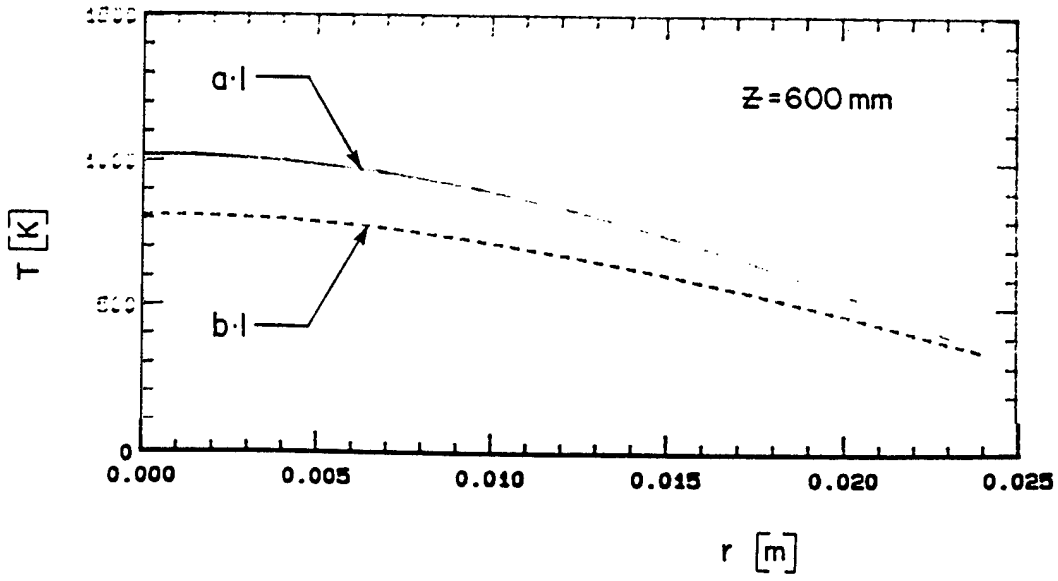

d

Fig. 2.34 (cont.)

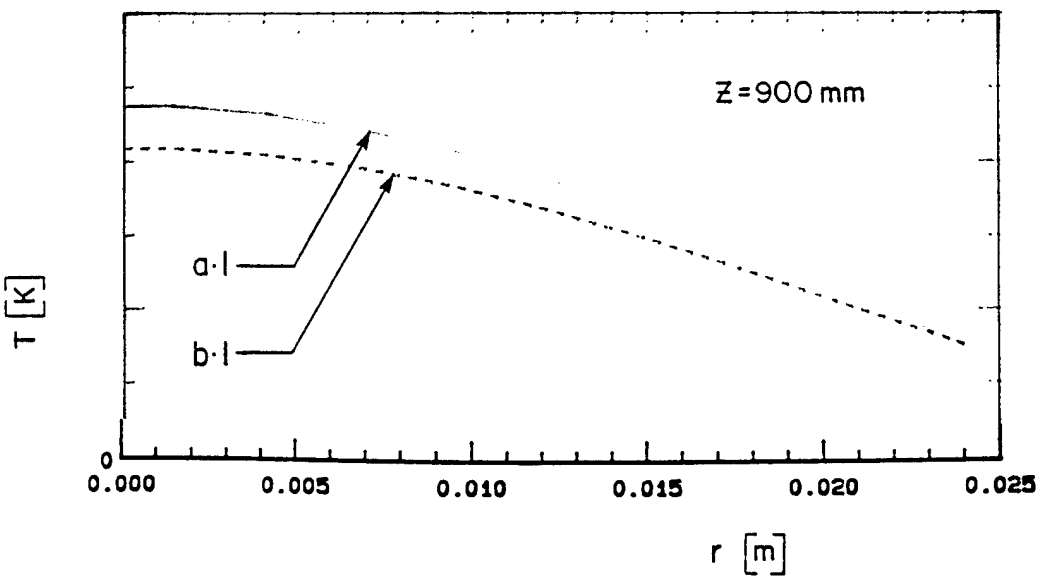

e

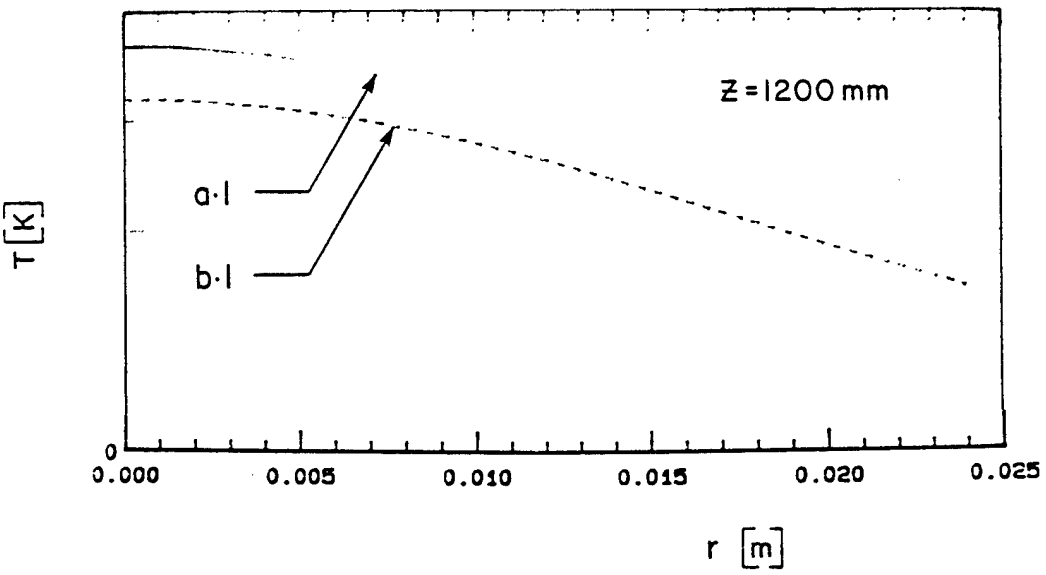

f

Fig. 2.34 (cont.)

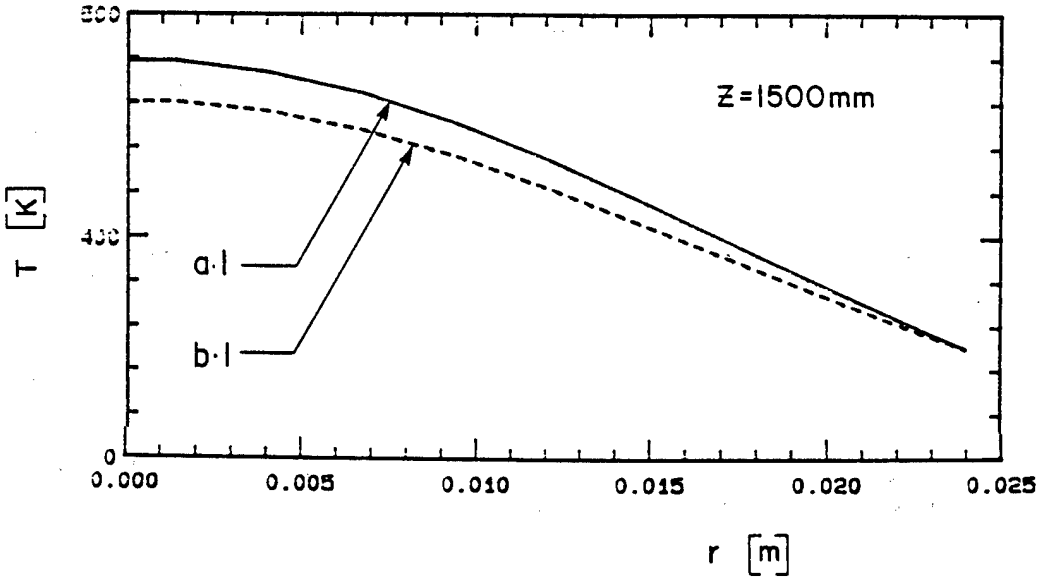

g

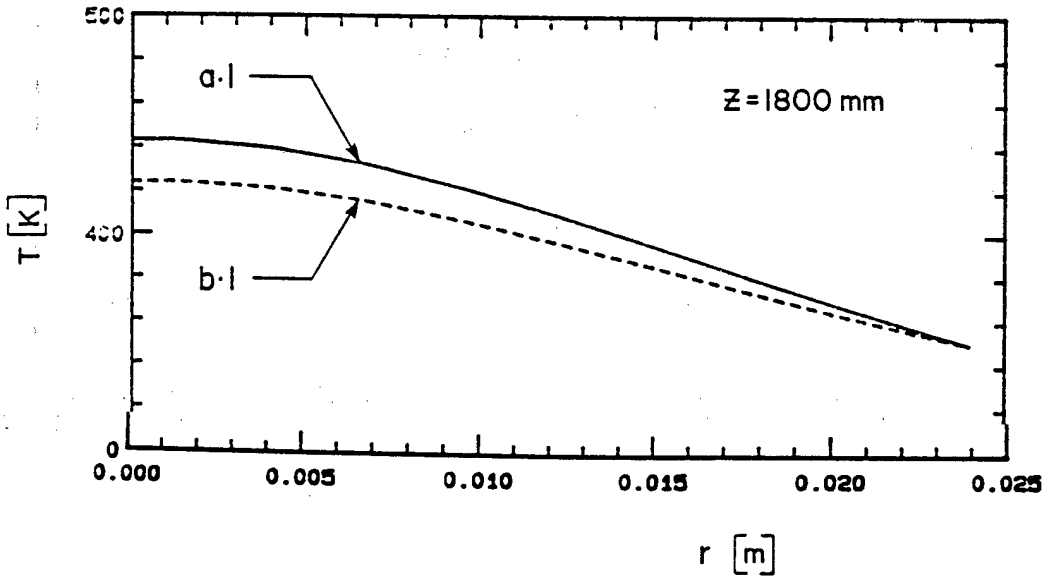

h

Fig. 2.34 (cont.)

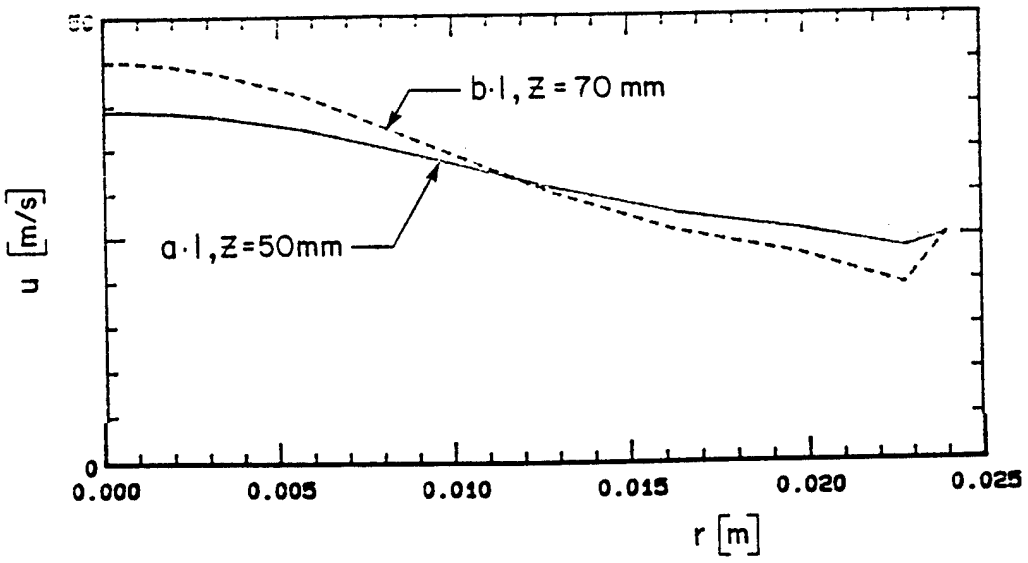

a

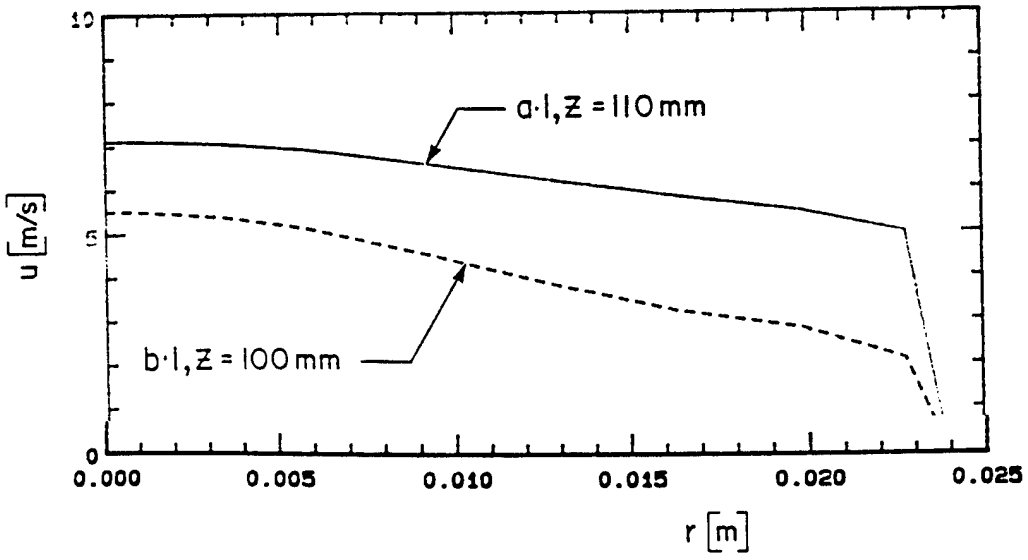

b

2.35 Radial velocity profiles at different levels in the reactor for cases b.1 and b.2.

a) z = 50 mm
b) z = 100 mm
c) z = 300 mm
d) d = 600 mm
e) z = 900 mm
f) z = 1200 mm
g) z = 1500 mm
h) z = 1800 mm

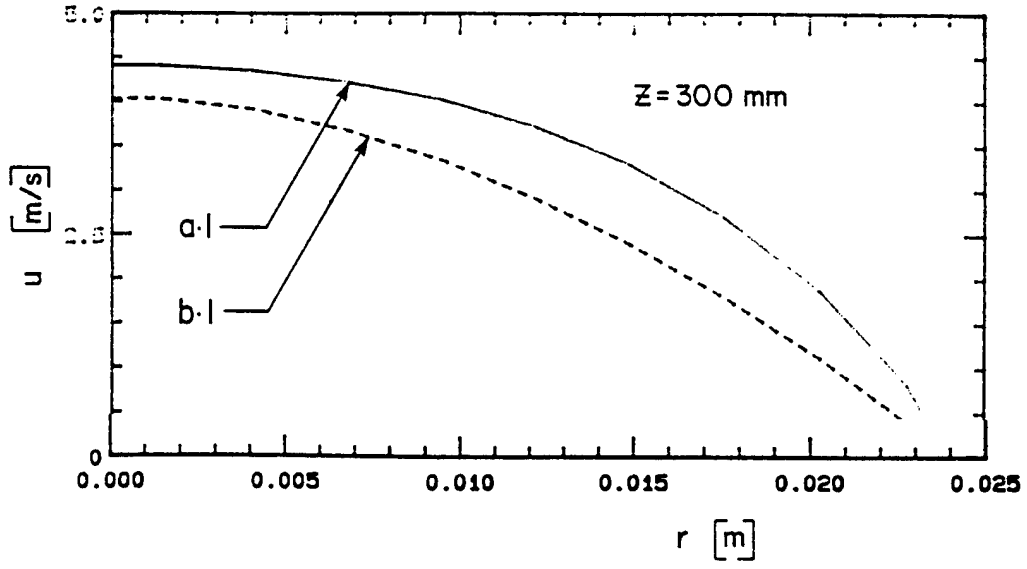

c

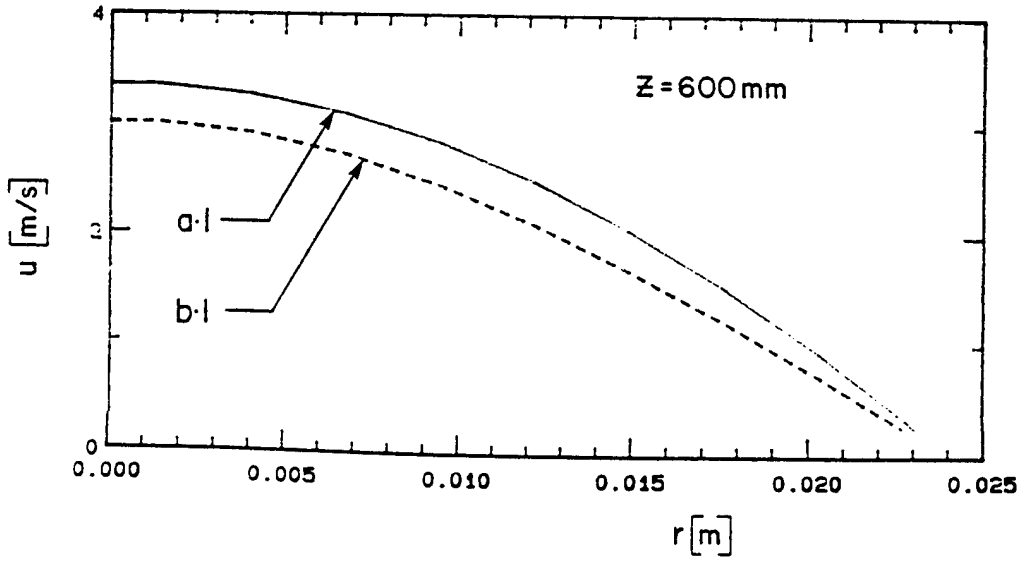

d

Fig. 2.35 (cont.)

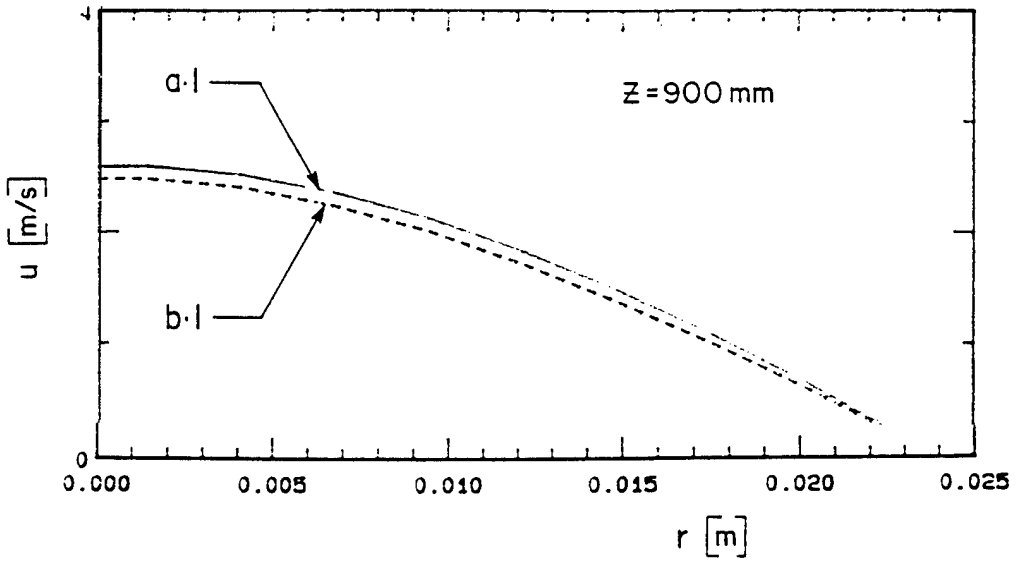

e

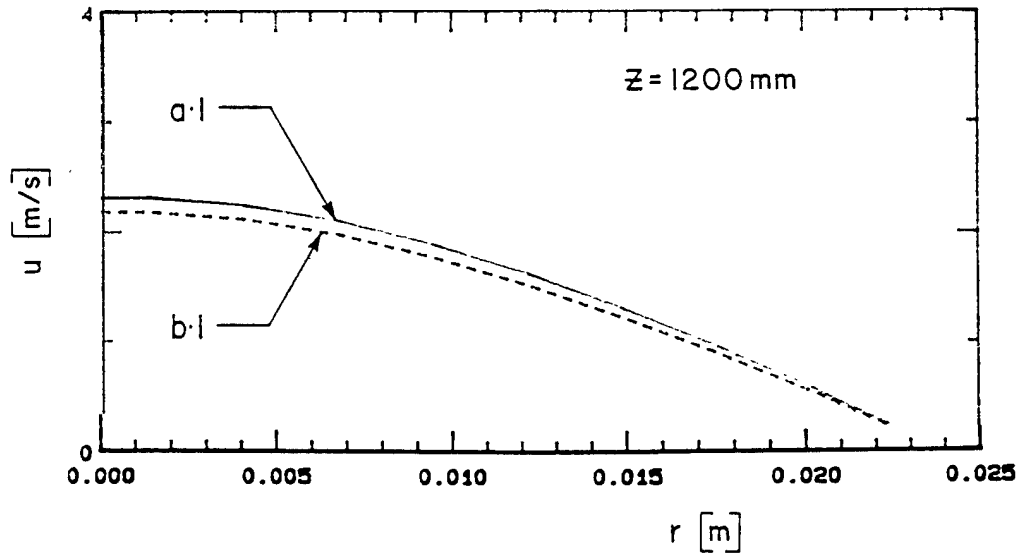

f

Fig. 2.35 (cont.)

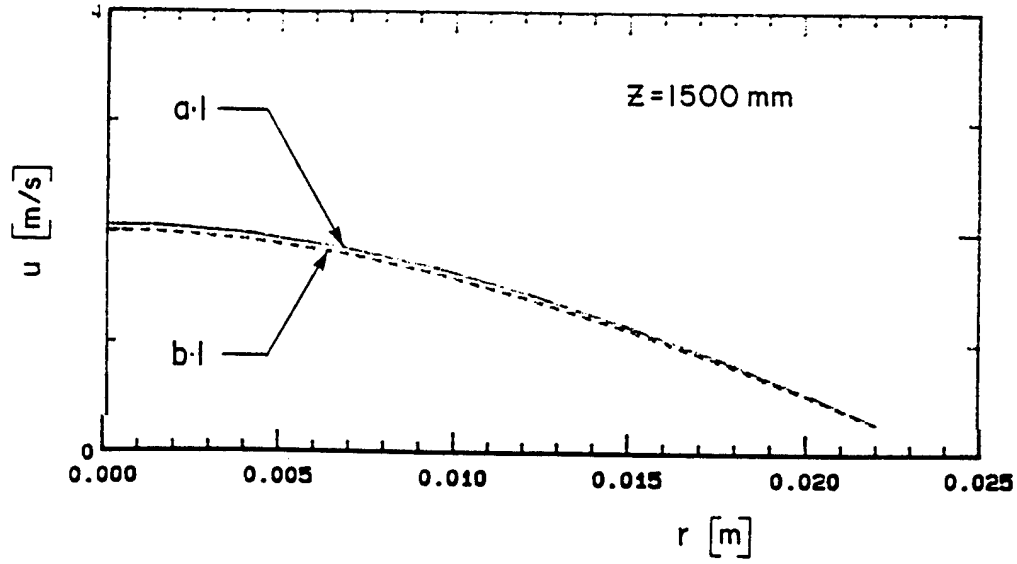

g

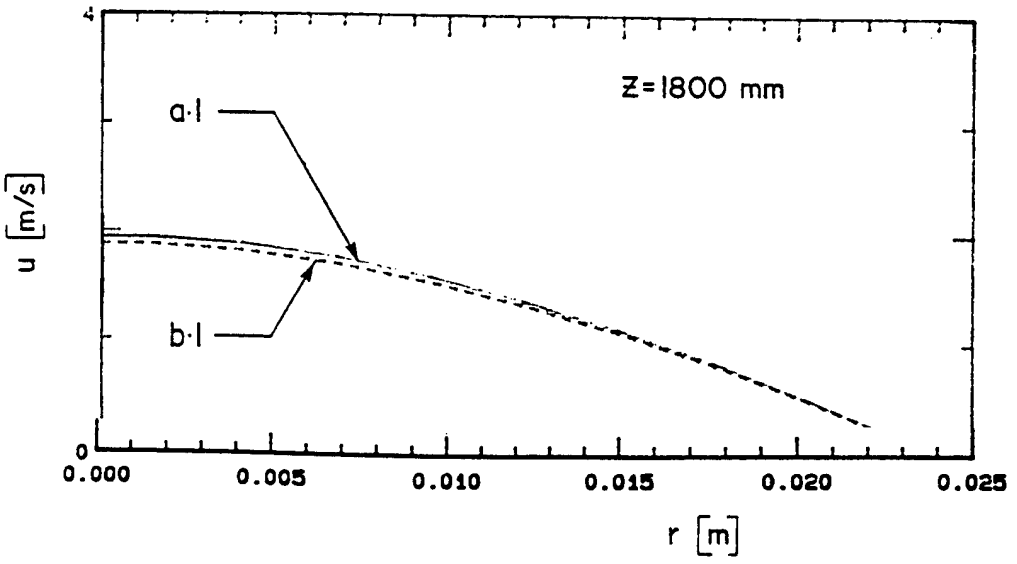

h

Fig. 2.35 (cont.)

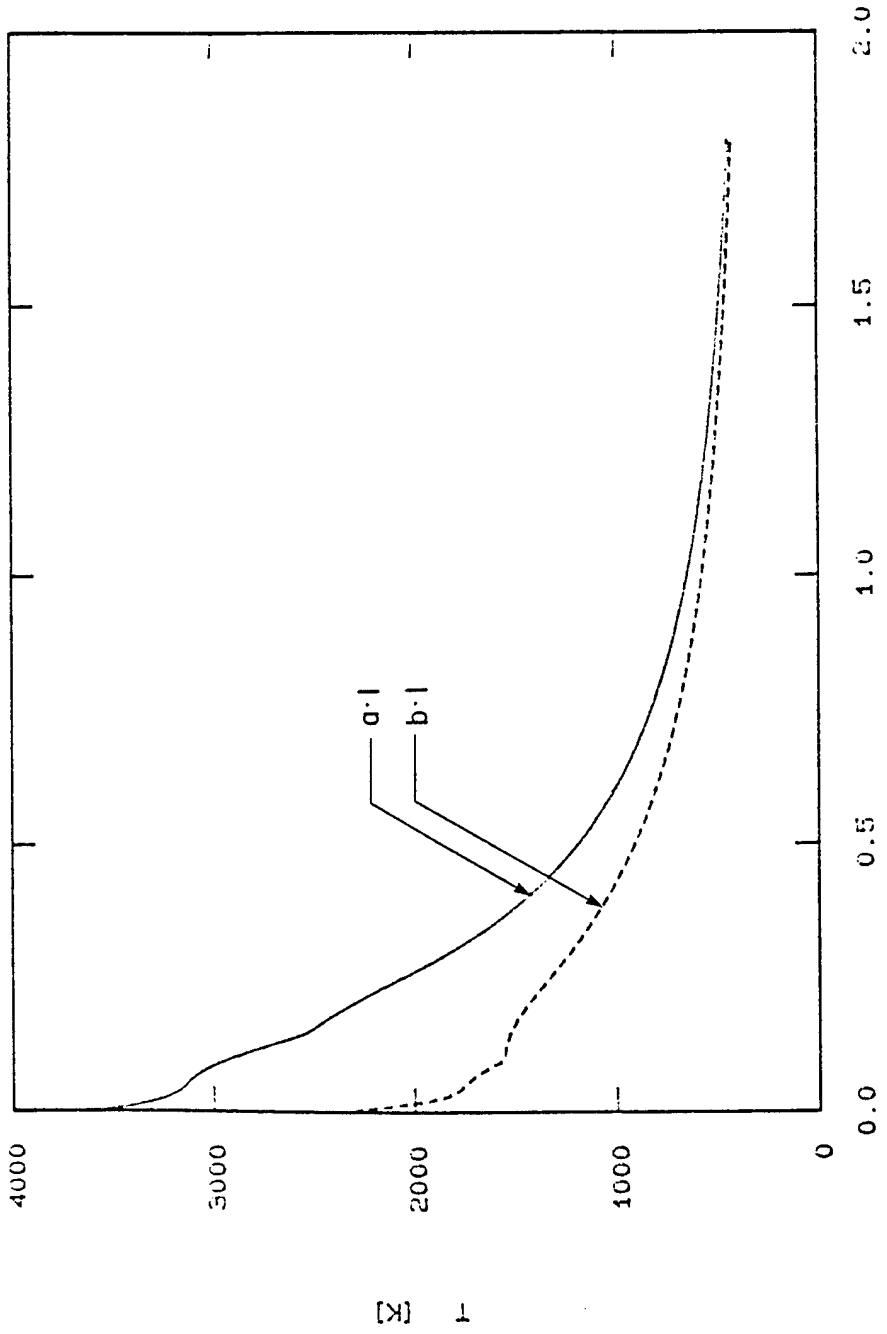

2.36 Axial temperature profiles along the centerline of the reactor for cases a.1 and b.1.

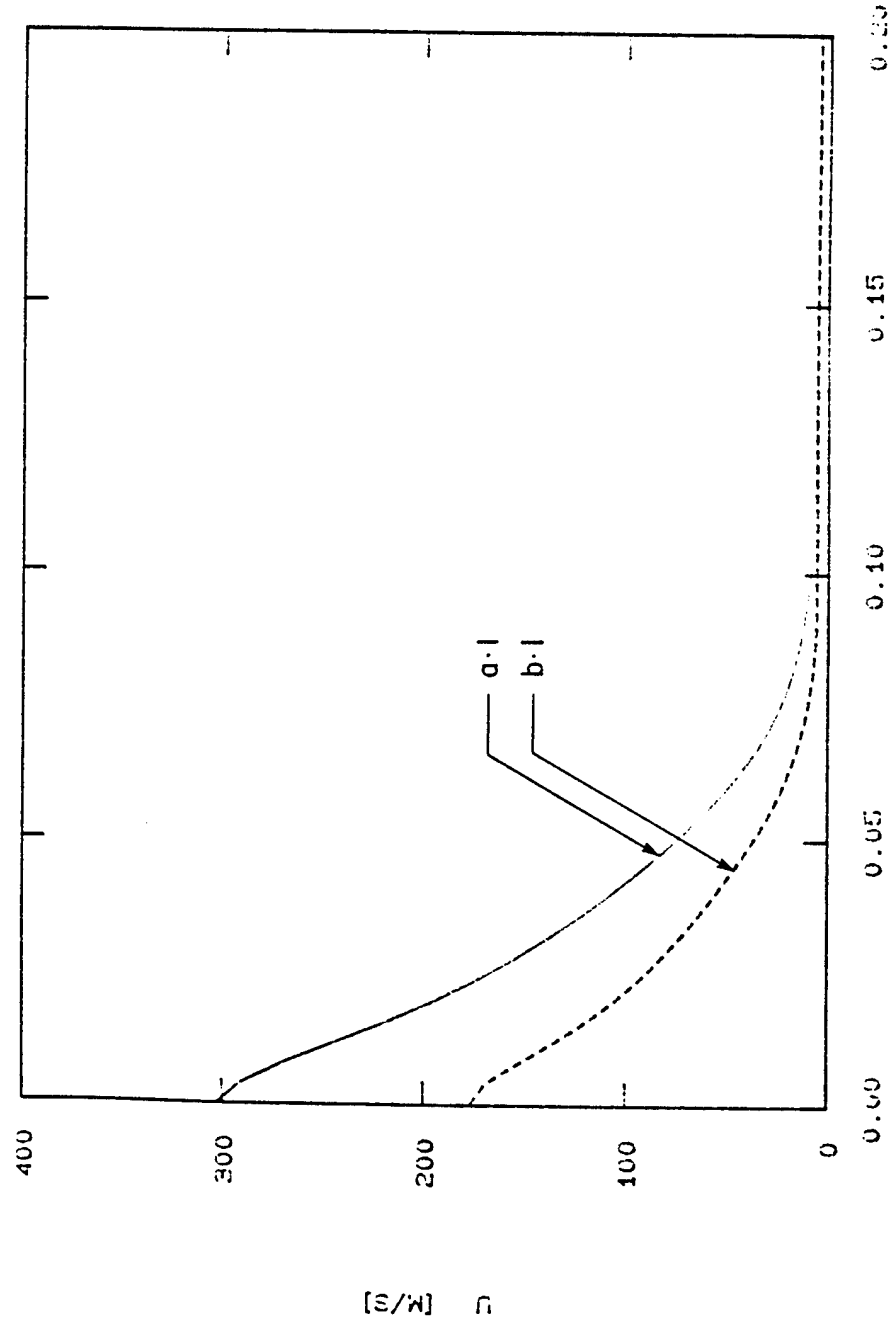

2.37-a Axial velocity profiles over the entrance region of the reactor for cases a.1 and b.1.

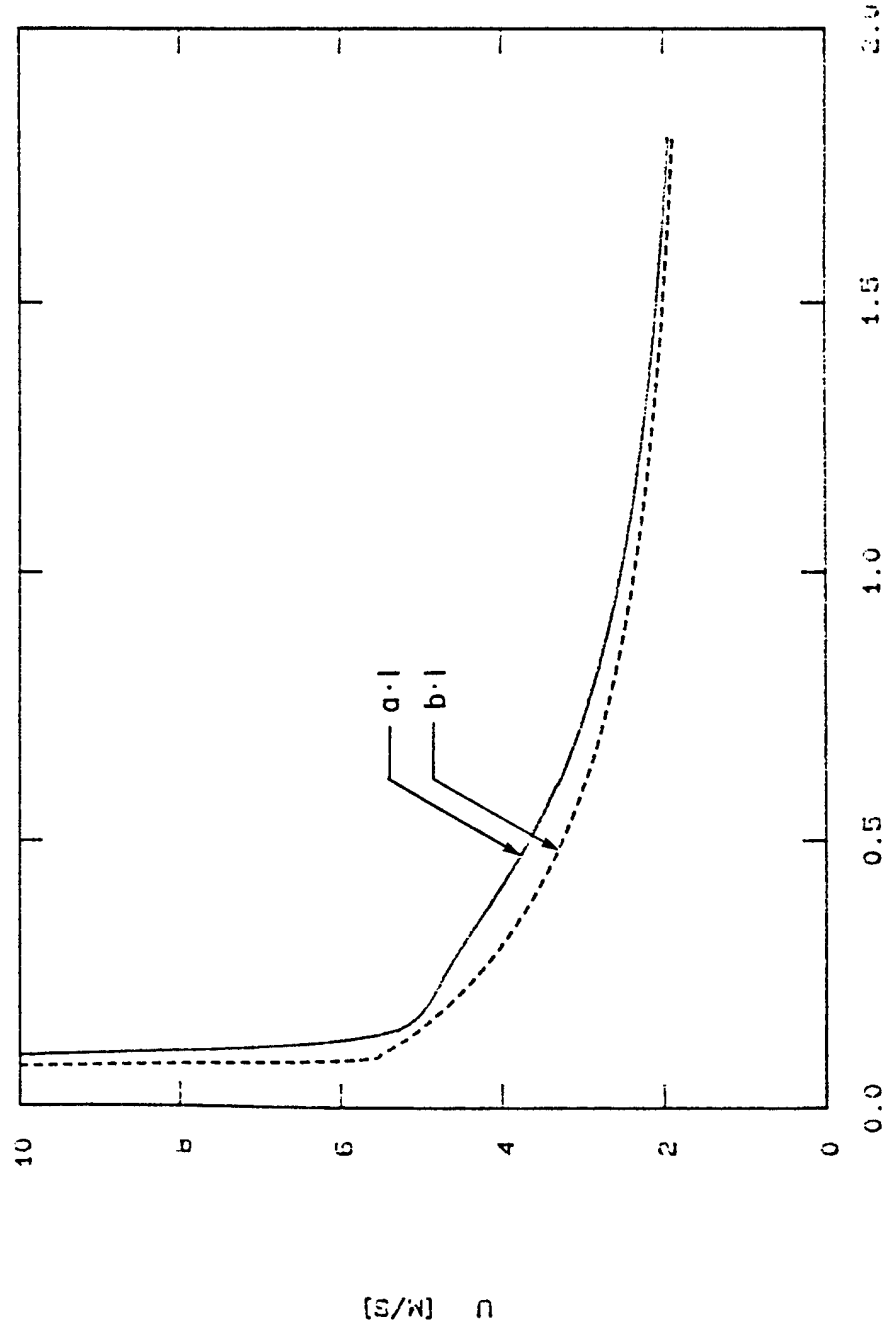

2.37-b Axial velocity profiles along the centerline of the reactor for cases a.1 and b.1.

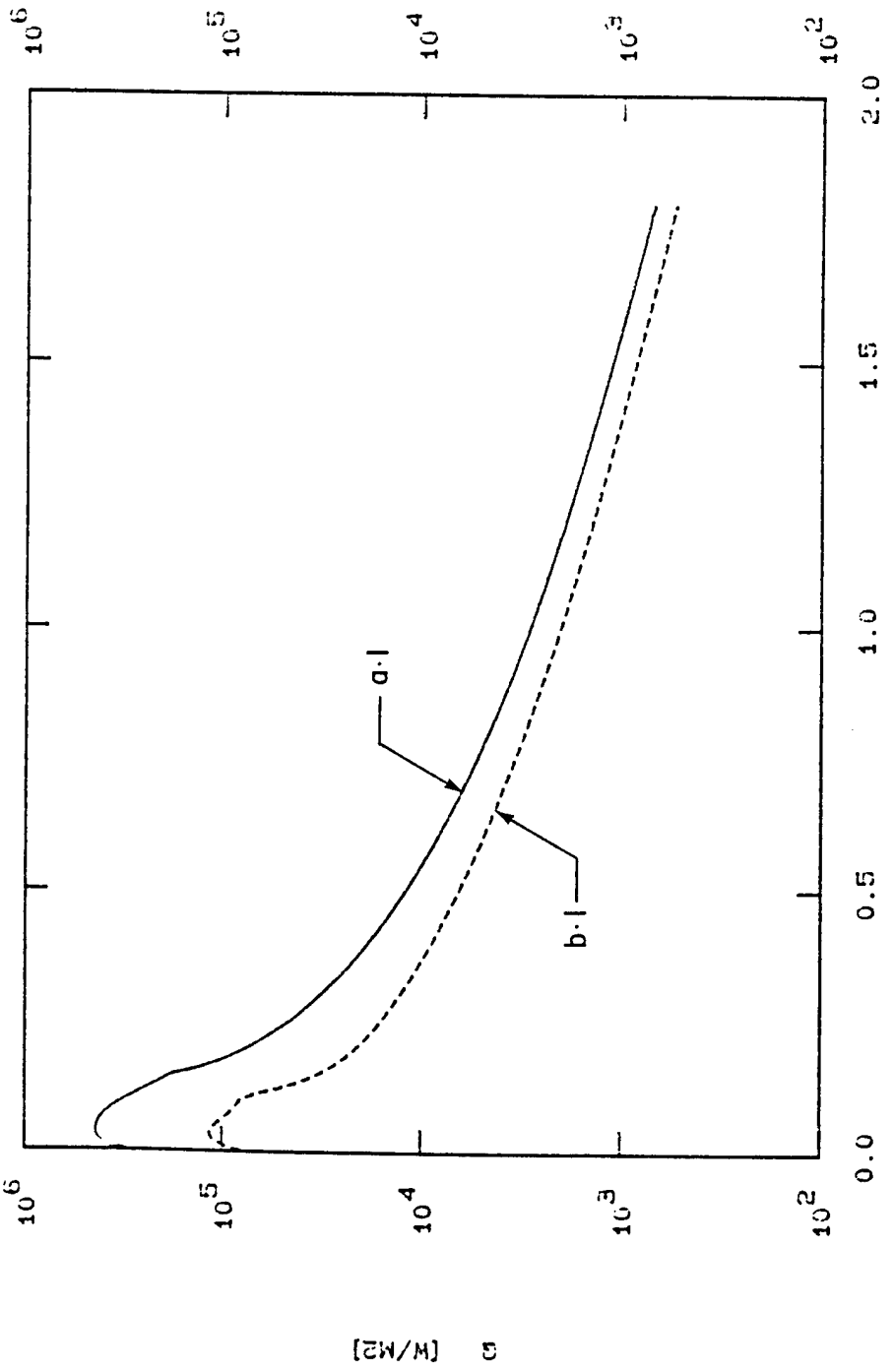

2.38 Heat flux to the reactor wall for cases a.l and b.l.

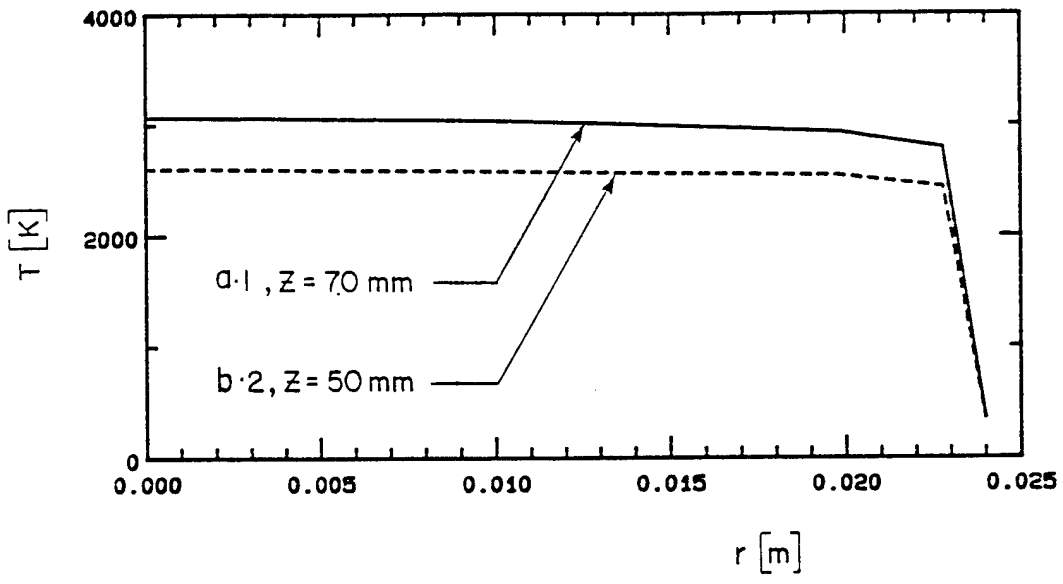

a

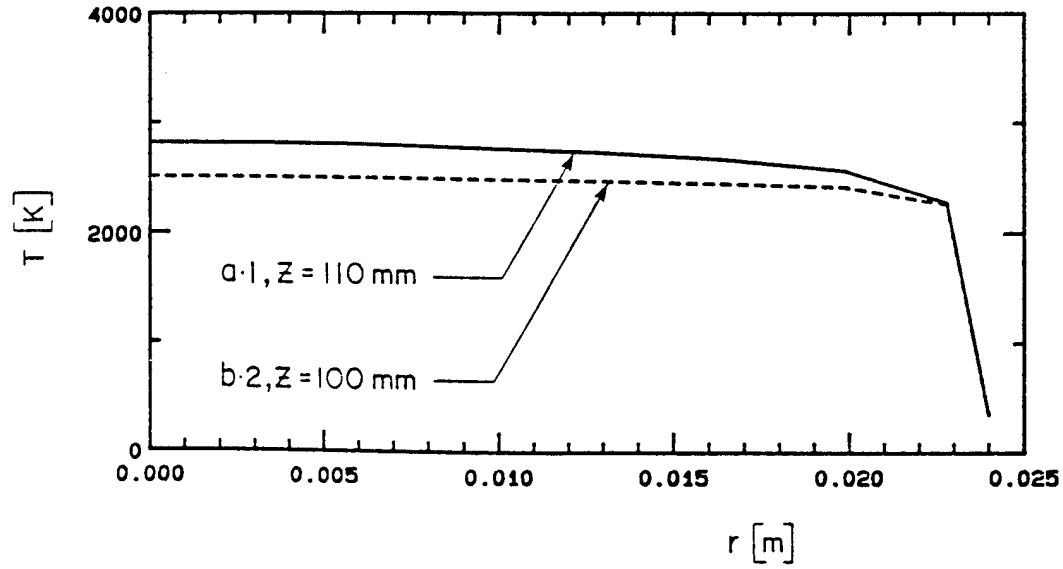

2.39 Radial temperature profiles at different levels in the reactor for cases a.1 and b.2.

a) z = 50 mm
b) z = 100 mm
c) z = 300 mm
d) d = 600 mm
e) z = 900 mm
f) z = 1200 mm
g) z = 1500 mm
h) z = 1800 mm

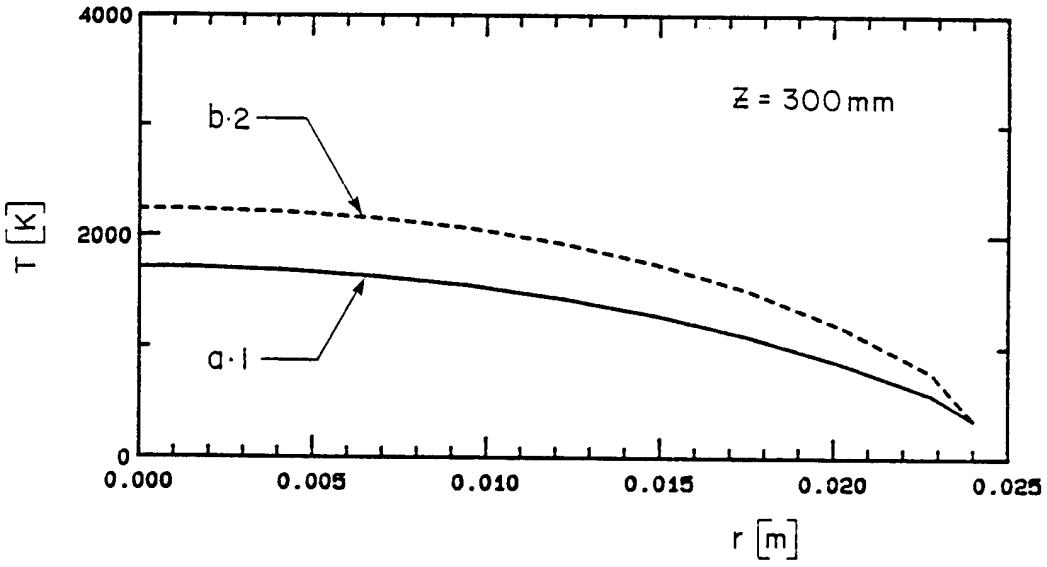

c

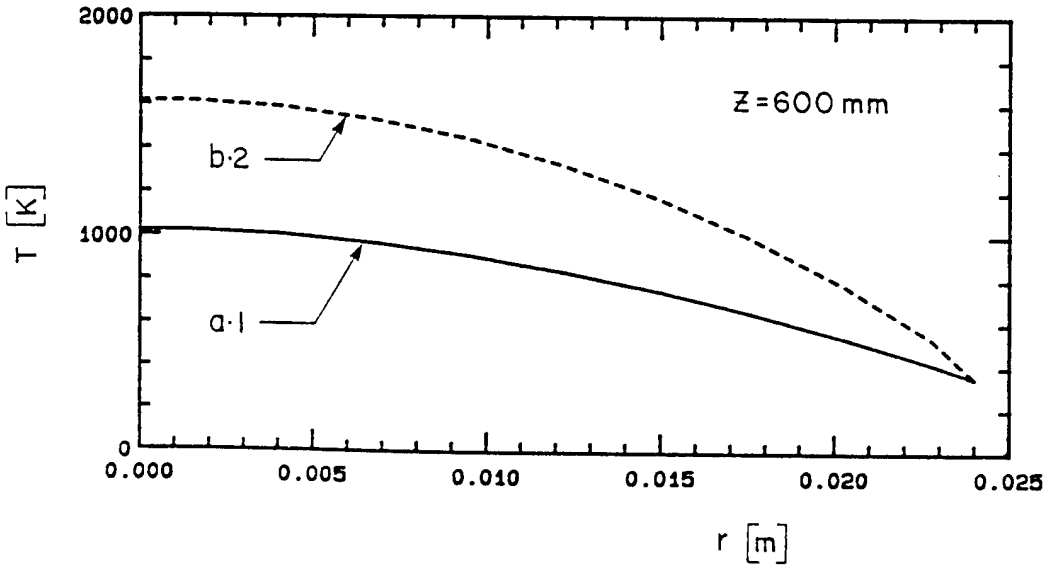

d

Fig. 2.39 (cont.)

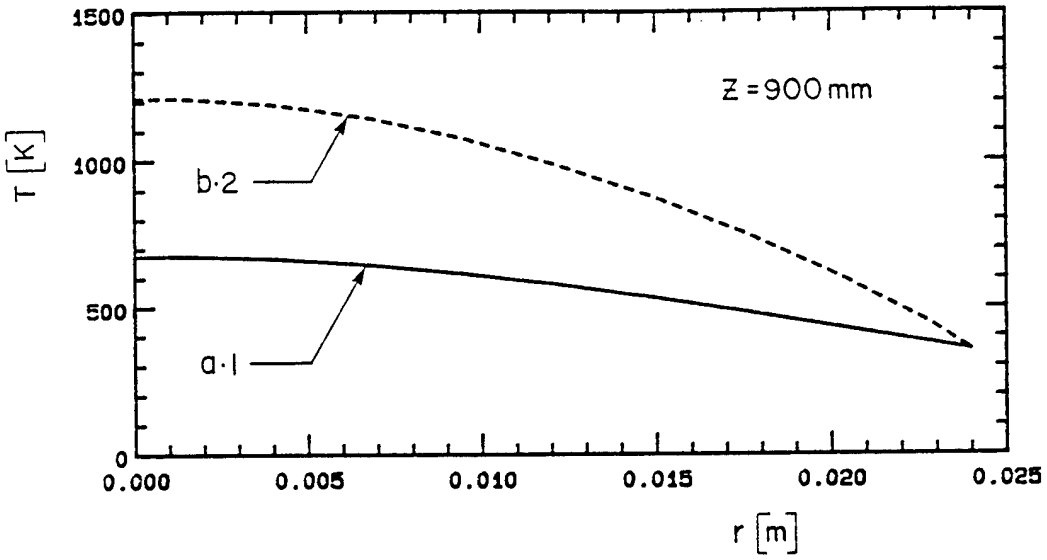

e

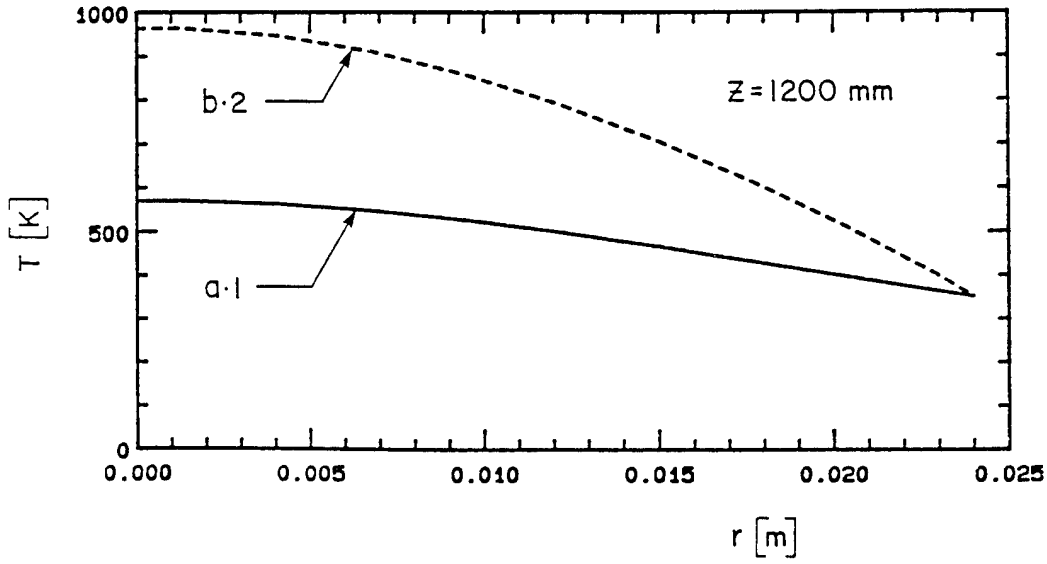

f

Fig. 2.39 (cont.)

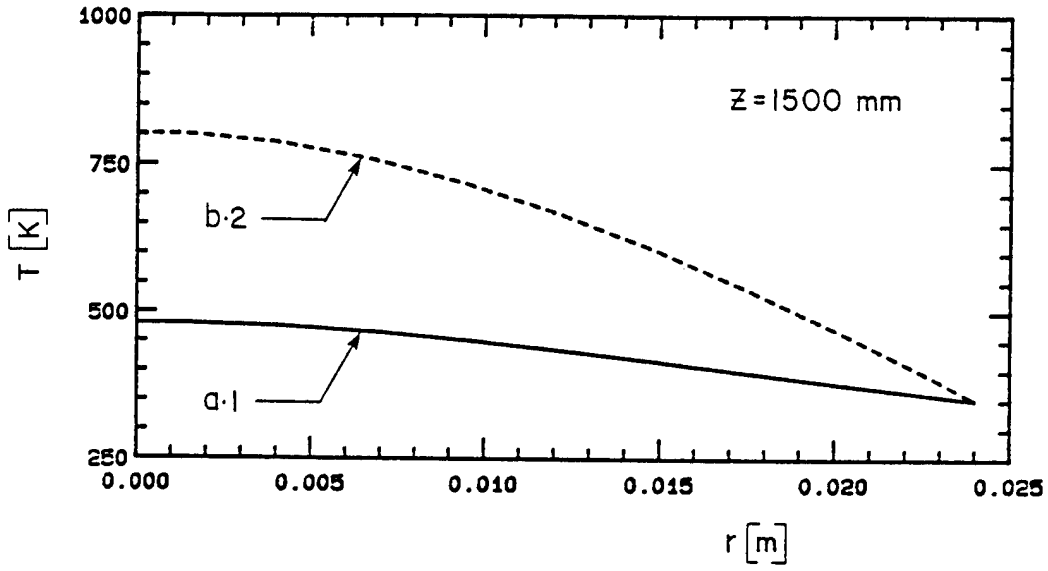

g

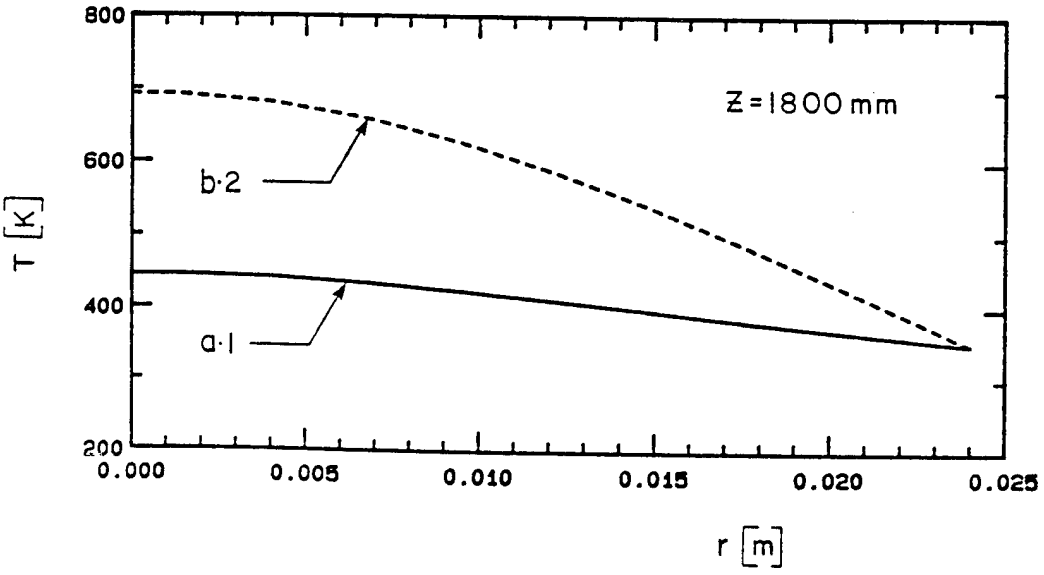

h

Fig. 2.39 (cont.)

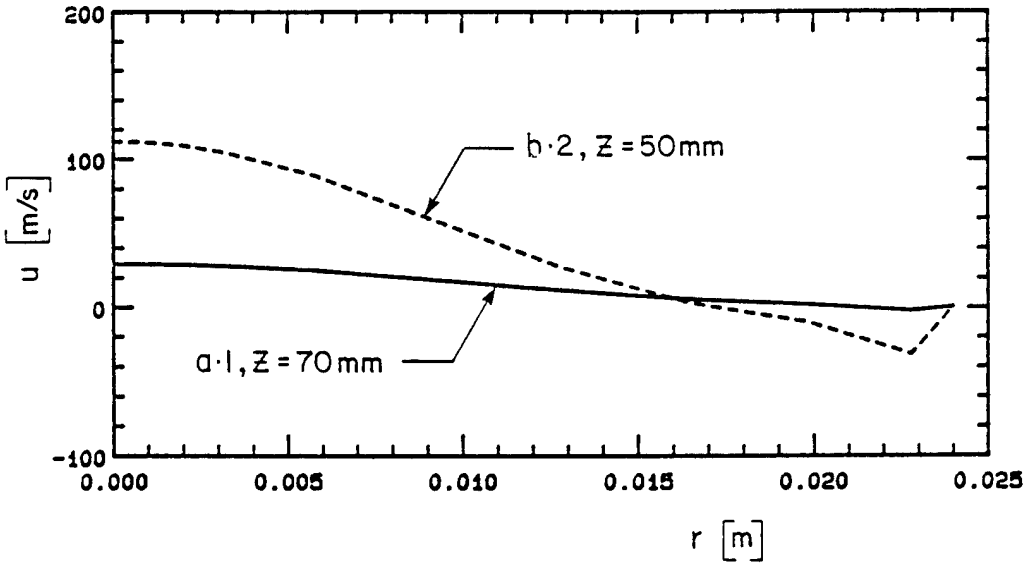

a

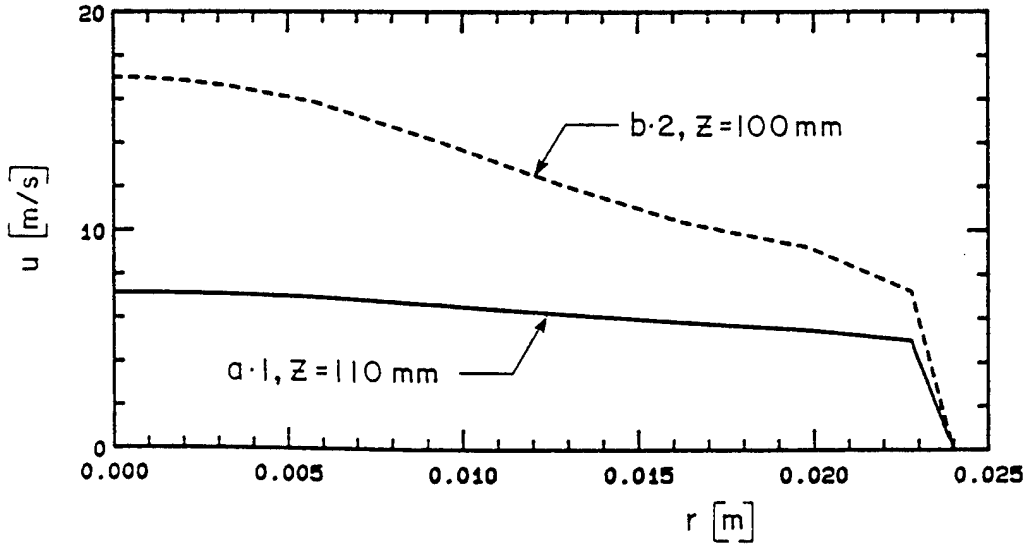

b

2.40 Radial velocity profiles at different levels in the reactor for cases a.1 and b.2.

a) z = 50 mm
b) z = 100 mm
c) z = 300 mm
d) d = 600 mm
e) z = 900 mm
f) z = 1200 mm
g) z = 1500 mm
h) z = 1800 mm

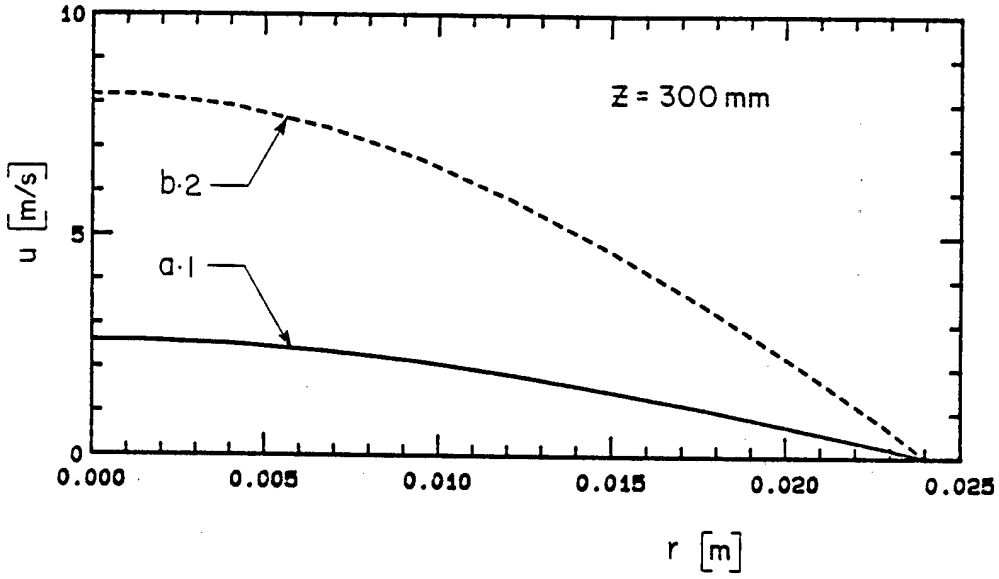

c

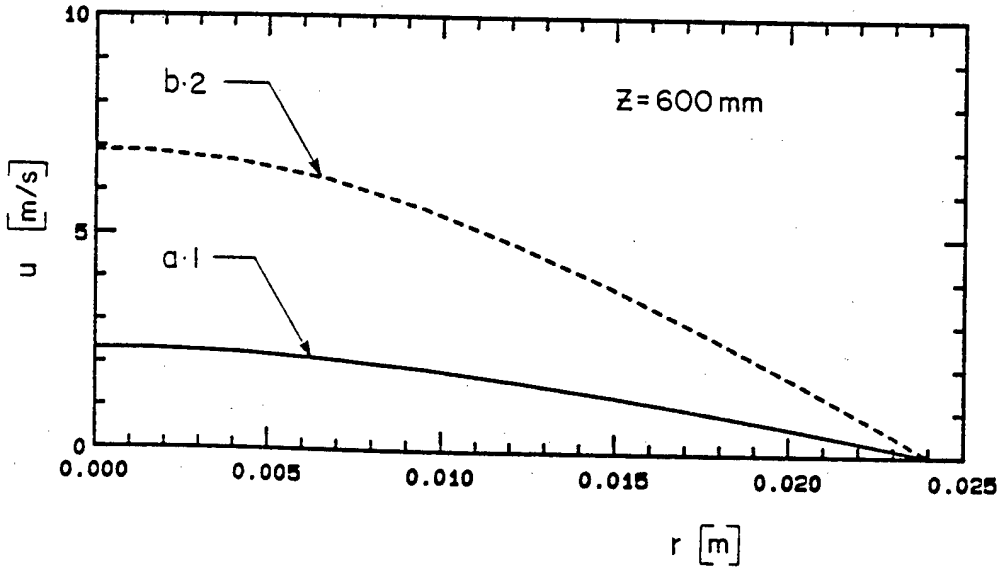

d

Fig. 2.40 (cont.)

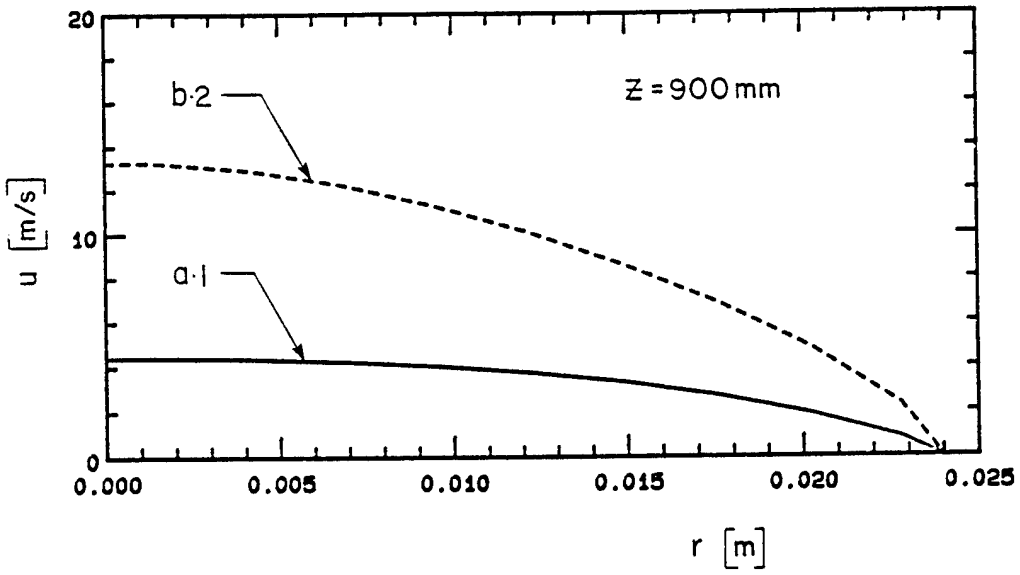

e

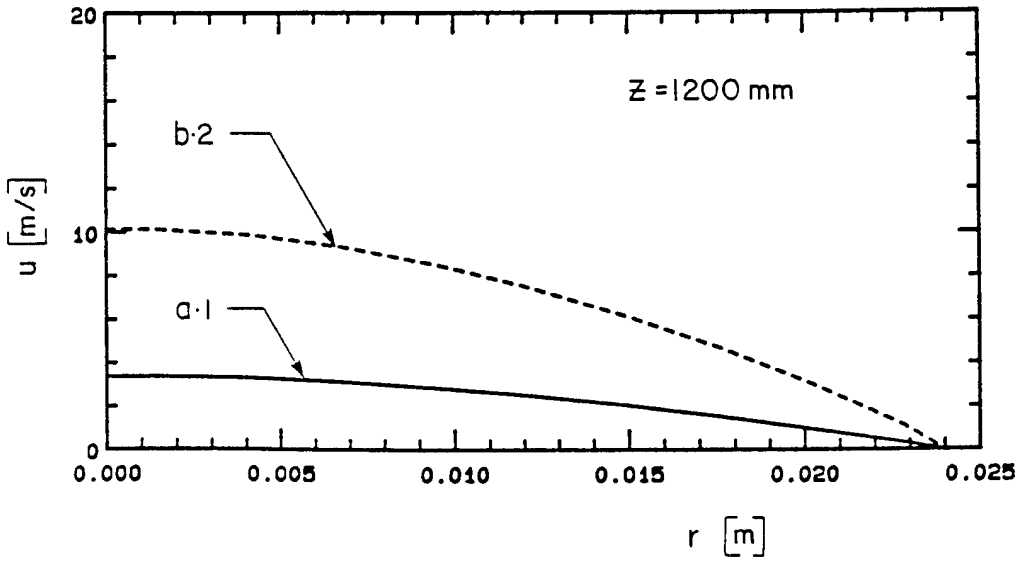

f

Fig. 2.40 (cont.)

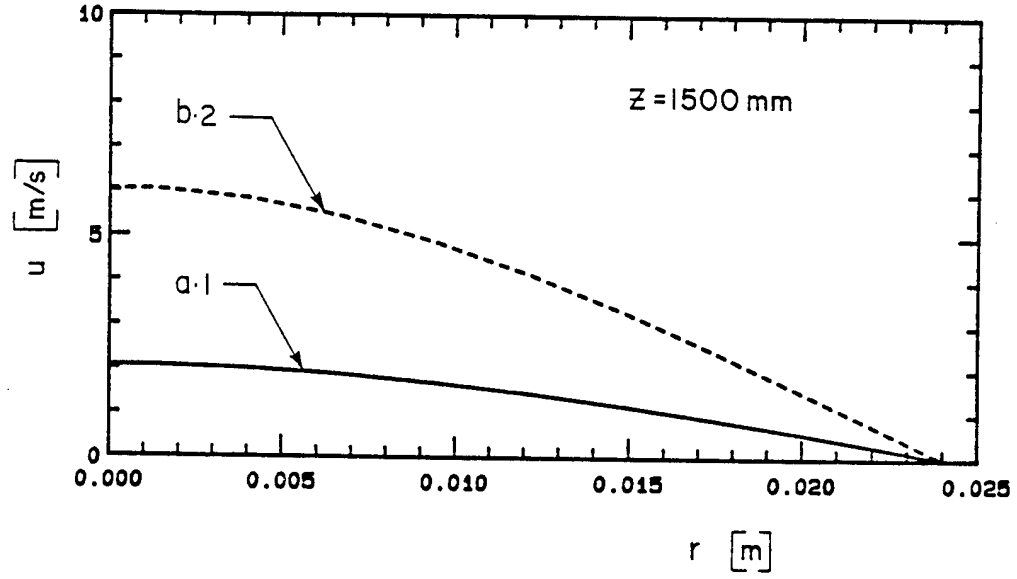

g

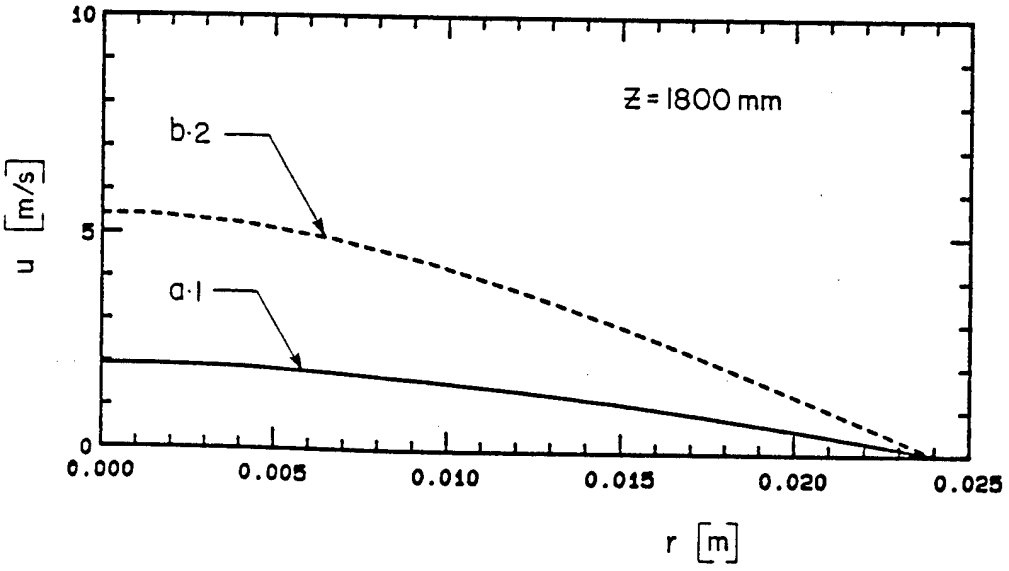

h

Fig. 2.40 (cont.)

Since for case b.2, Re is higher than for case a.1, therefore the bulk temperature stays at a higher value compared to a.1. This case demonstrates that flow rate could have an important influence on the gas temperature field in the reactor. Figures 2.41 and 2.42 compare the temperature and axial velocity decay on the axis of symmetry between these two cases. The rate of decay for case a.1 is much higher than for case b.2. Figure 2.43 shows the wall heat flux distribution for the two cases. Although, the inlet power for the two cases are the same, the losses for a.1 at the entrance region are much higher.

2.6 SUMMARY AND CONCLUSIONS

From the present study it may be concluded that,

a) While the Reynolds number based on the reactor diameter is laminar, the entrance region is turbulent ($z < 100$ mm). The turbulence is caused by the step height of the reactor which for the present torch geometry is 20 mm.

b) The inlet turbulence is not beneficial. This is bacause, under the assumption of constant wall temperature, between 45% to 65% of the inlet power could be lost to the walls in a short distance (less than 10% of the reactor length). This situation could be improved by
   - Reducing the step height.
   - Expansion of the jet in a diverging nozzle.

c) For a fixed inlet power, the gas flow rate has an important influence on the temperature field in the reactor. Higher flow rates sustain higher temperatures away from the inlet.

d) It is recommended that the wall temperature and heat flux distribution be determined experimentally. The reattachment point at the entrance region should also be measured by measuring the pressure distribution on the wall. These measurements will help to validate the boundary conditions and the assumption used in this study.

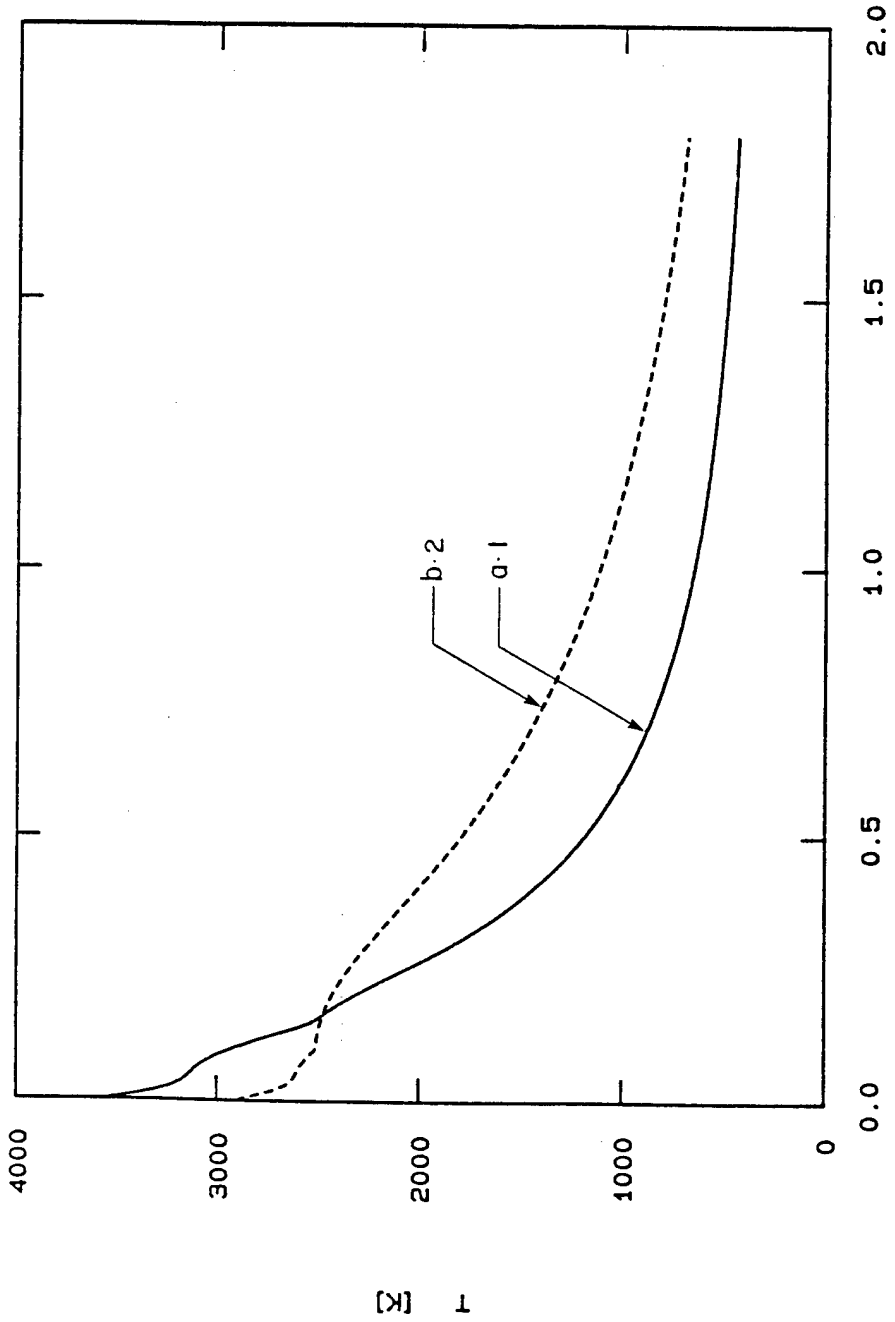

2.41 Axial temperature profile along the centerline of the reactor for cases a.1 and b.2.

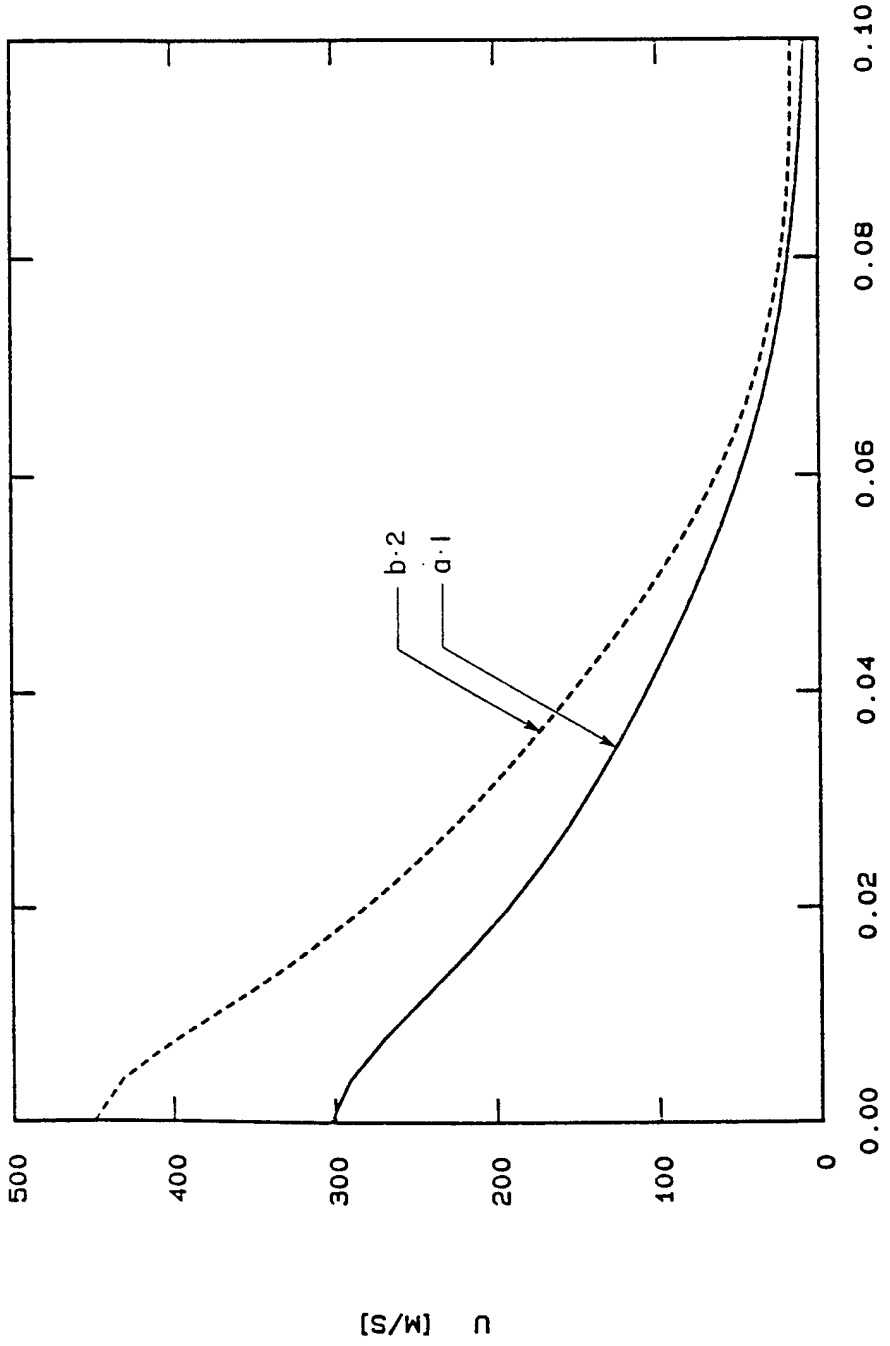

2.42-a Axial velocity profiles over the entrance region of the reactor for cases a.1 and b.2.

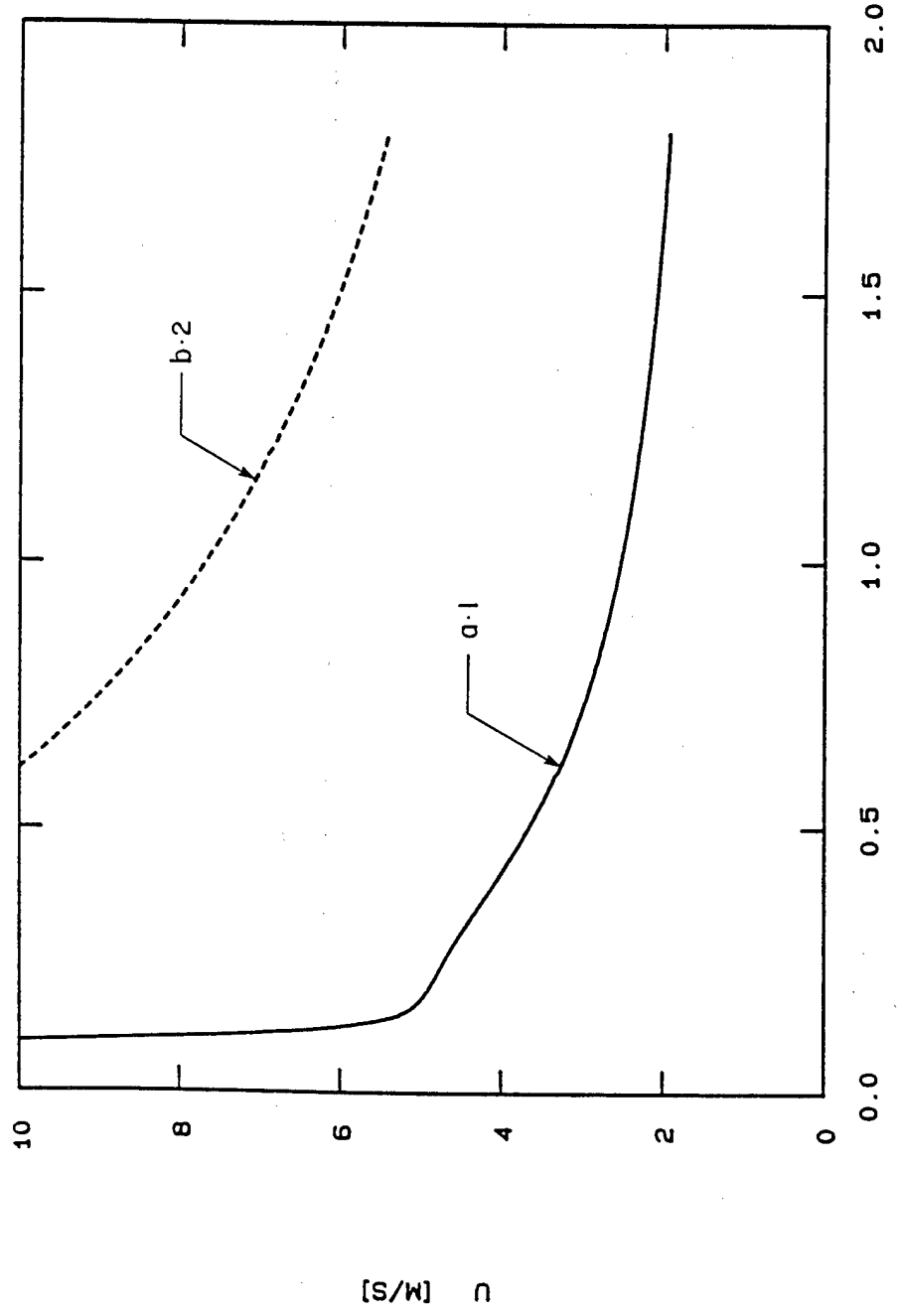

2.42-b Axial velocity profiles along the centerline of the reactor for cases a.1 and b.2.

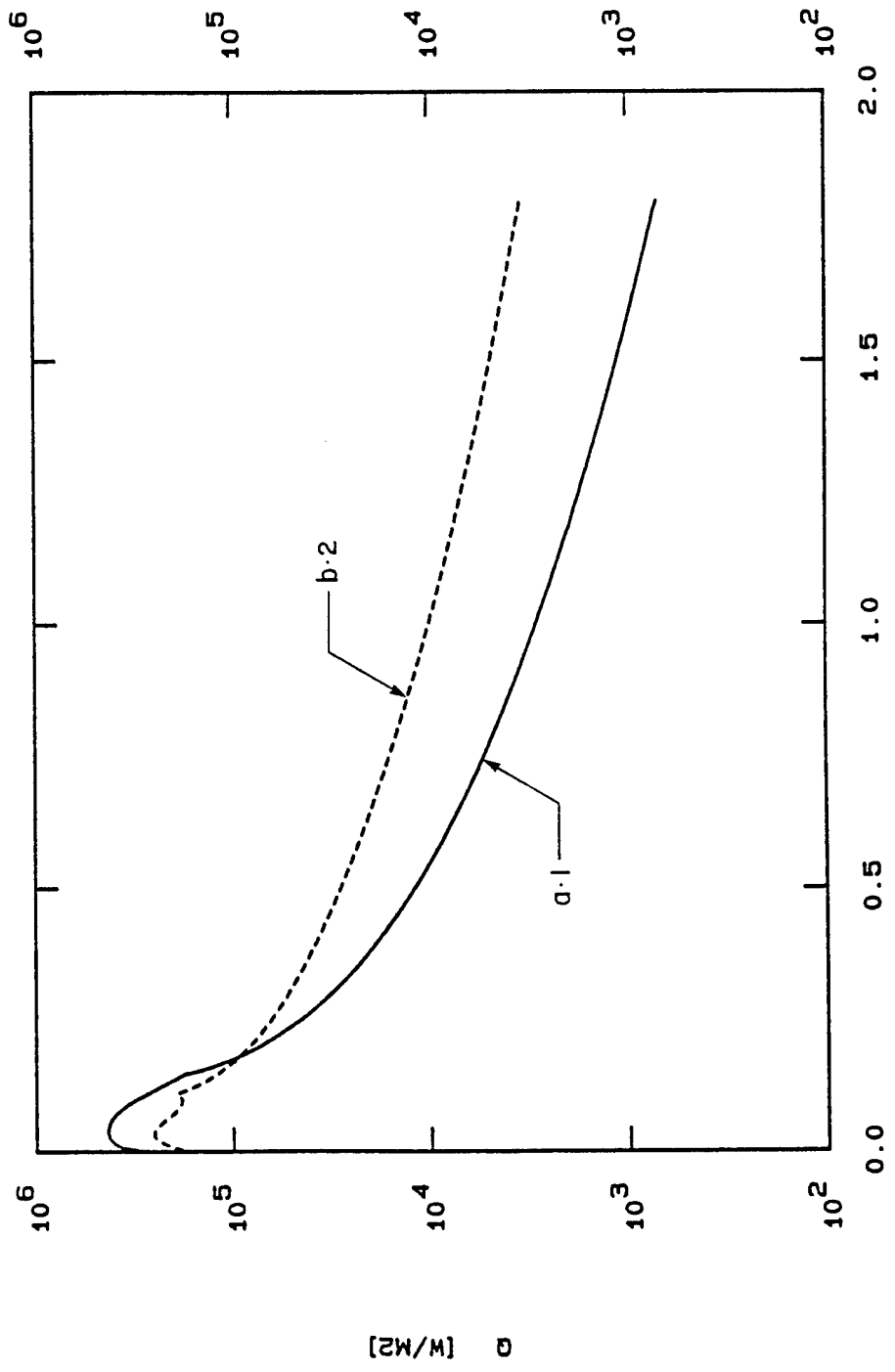

2.43 Heat flux to the wall of the reactor for cases a.1 and b.2.

BIBLIOGRAPHY

2.1 Eckert, E.R.G. and Drake, R.M., "Analysis of Heat and Mass Transfer", McGraw Hill (1972).

2.2 Schichting, "Boundary Layer Theory", McGraw Hill, (1979).

2.3 Patankar, S.V., "Numerical Heat Transfer and Fluid Flow", McGraw Hill (1980).

2.5 Hirschfelder J.O., Curtiss C.F., Bird R.B.; "Molecular Theory of Gases and Liquids", John Wiley & Sons, (1964).

2.6 Goldstein R.J., Eriksen V.L., Olson R.M., Eckert E.R.G.; "Laminar Separation, Reattachment, and Transition of the Flow Over a Downstream-Facing Step", J. Basic Eng., 92, p. 732 (1970).

3. THERMODYNAMIC EQUILIBRIUM CALCULATIONS FOR THE SYSTEM: H_2-Ar-CH_4-$SiC\ell_4$

3.1 INTRODUCTION

In this section we consider a closed chemical system consisting of N chemical species with a fixed number of moles of different element (H, Ar, C, Cℓ, Si).

Calculation of the equilibrium composition can be performed using either of the following two different methods [3.1]:

The first is based on the law of mass action written for each of the independent chemical reactions involved and the mass balance constraints (conservation of the elementary species) together with the electrical charge conservation. This leads to a set of non-linear equations that are solved using Newton's method.

The second consists in finding the number density of each of the species, Ni, that satisfies the constraints of minimum Gibbs free energy while satisfying the mass and the electrical charge conservation laws. The main advantage of this method which has been used in the present study is that it works equally well for gaseous mixtures and for mixtures containing liquid and solid phases. Moreover the reaction routes need not to be known.

3.2 EQUATIONS FOR THE COMPOSITION

3.2.1 Ideal gas

Neglecting the interactions between charged particles as well as the interactions between neutral atoms or molecules, the Gibbs free energy can be written as;

$$G = \sum_{i=1}^{N} \mu_i N_i \qquad (3\text{-}1)$$

Where,

N is the total number of species

N_i the number of particles of chemical specie i, ($N_i = n_i . V$), V being the total volume of the plasma

μ_i the chemical potential written:

$$\mu_i = \mu_i^{\circ}(T) + kT \text{ Log } (p_i/p) \qquad (3\text{-}2)$$

In Eq. 3-2, μ_i° stands for the chemical potential which is function of the temperature T, and p_i is the partial pressure of specie i, in the mixture, while p the total pressure and k the Boltzmann's constant ($k = 1.380308\ 10^{-23}$ J/K/part)

The chemical potentials, μ_i°, are found either in tables such as those of NASA [3.2], Barin and Knacke [3.3] JANAF [3.4] and of the University of Grenoble in France [3.5]. It should be pointed out that the Gibbs free energy of the species, i, which is a function of temperatures, T, is given in tables or can be calculated with the help of the partition functions:

$$g_i^{\circ} \equiv \mu_i^{\circ} = - kT \text{ Log } \left(\frac{kT}{p} \left(\frac{2\pi m_i kT}{h^2}\right)\right)^{3/2} - kT \text{ Log } Q_{int}^{i} + e_i^{\circ} \qquad (3\text{-}3)$$

where h is the Planck's constant, m_i the mass of the particle of chemical specie i, e_i° and Q_{int}^{i} the internal partition function.

Other thermodynamic functions can also be calculated with the help of the partition functions such as;

The enthalpy:

$$h_i^\circ = kT \frac{\partial \text{ Log } Q_{int}^i}{\partial T} + \frac{5}{2} kT + e_i^\circ \qquad (3\text{-}4)$$

the specific heat;

$$c_{pi} = k \left[2T \frac{\partial \text{ Log } Q_{int}^i}{\partial T} + T^2 \frac{\partial^2 \text{ Log } Q_{int}^i}{\partial T^2} + \frac{5}{2} \right] \qquad (3\text{-}5)$$

and the entropy

$$s_i^\circ = k \text{ Log } \left[\frac{kT}{p} \left(\frac{2\pi m_i kT}{h^2} \right)^{3/2} \right] + k \text{ Log } Q_{int}^i + kT \frac{\partial \text{ Log } Q_{int}^i}{\partial T} + \frac{5}{2} k \qquad (3\text{-}6)$$

Multiplying the above Eqs.(3-3)-(3-6) by the Avagadro's number one obtains the corresponding properties per mole of the mixture.

3.2.2 Corrections for real gases

a) Interactions between charged particles

When temperature increases i.e. when electron molar fraction becomes higher than 5%, interactions between charged particles can

no more be neglected and Coulomb's type potential (at large intermolecular distances: proportional to 1/r) results in an interaction energy. This energy is determined with the help of the Debye-Hückel approximation. The correction to the Gibbs free energy is given by:

$$\delta G_{DH} = - \frac{kTV}{8\pi d^3} \qquad (3\text{-}7)$$

where d is the Debye's length defined by:

$$d = \left[\frac{\varepsilon_o kT}{e^2 \sum_{i=1}^{N} z_i^2 n_i^2} \right]^{1/2} \qquad (3\text{-}8)$$

z_i being the charge number of specie i and ε_o the vacuum permittivity.

The Coulombic field results also in a pressure correction according to the following equation.

$$\delta p_{DH} = - \frac{kT}{24.\pi.d^3} \qquad (3\text{-}9)$$

b) Virtual correction

The state equation $pV/(N_t kT)=1$, where N_t stands for the total number of particles, is only valid for a dilute gas and has to be modified to account for intermolecular potential functions (depending on the distance r between particles in $1/r^n$ with $n > 6$) at high pressures. In fact this virial correction should be taken into account as soon as the distance r_i, below which the interaction potential, is smaller than the mean free path ℓ of the corresponding species. This correction is then written

$$\frac{pV}{N_t kT} = 1 + B(T).\frac{N_t}{V} \qquad (3\text{-}10)$$

Where B(T) is the second virial coefficient which can be calculated as function of the interaction potential [3.6].

For a system containing different species i, B(T) can be written as;

$$B(T) = \sum_{i=1}^{N} \frac{n_i\, n_j}{n^2} B_{ij}(T) \qquad (3\text{-}11)$$

With $n = \sum_{i=1}^{N} n_i$ $(n=N_t/V)$

i and j varying from 1 to N.

3.2.3 Multiphase system

According to the preceding corrections, the volume V, assumed to be the one of the gas phase, is calculated by

$$V = \frac{N_t kT\left(1 + \sum_{i=1}^{N} B(T) \left(\frac{N_i}{N_t}\right)^2 p\right)}{p + \frac{kT}{24.\pi.d^3}} \qquad (3\text{-}12)$$

The Gibbs free energy is written

$$G = \sum_{i=1}^{N} \mu_i N_i - \frac{k\ TV}{8\pi d^3} \qquad (3\text{-}13)$$

and one has for a solid specie

$$\mu_i = \mu_i^{\circ}(T) \qquad (3\text{-}14)$$

for a liquid specie (supposed to be an ideal solution)

$$\mu_i = \mu_i^{\circ}(T) + kT\ \mathrm{Log}\ \left(\frac{Ni}{N\ell}\right) \qquad (3\text{-}15)$$

with;

$N\ell = \sum_{i=1}^{L} Ni$, L being the total number of liquid species

for a gaseous specie

$$\mu_i = \mu_i^{\circ}(T) + kT\ \mathrm{Log}\ \frac{p_i}{p} + kT.p.B(T)\ \left(1 + \frac{p.B(T)}{2}\right) Ni \qquad (3\text{-}16)$$

3.3 PARTITION FUNCTION

3.3.1 Monoatomic species

In this case the internal partition function Q_{int} is equal to the electronic partition function given for each specie i, by

$$Q_e^i = \sum_j g_j \exp\left(-E_j/kT\right) \tag{3-17}$$

Where g_j is the statistical weight and E_j the energy of the electrically excited state j.

The main problem that arise when calculating, Q_e, is the limitation of the summation and the choice of a reliable theory. Neglecting the fluctuating microfields we have assumed that the bound electron is free when it can not be identified with a given field. Then the corresponding ionization potential lowering δE_i is given [3.7] by:

$$\delta E_i = \frac{(z+1)e^2}{4\pi\varepsilon_o d} \tag{3-18}$$

Where; d is the Debye's length given by Eq. (3-8) and z the electric charge of the particle of chemical specie i.

As the levels close to ionization limit are hydrogenoids [3.7,3.10] we calculate the last quantum number n* for the summation by

$$n^* = \left[\frac{(z+1)^2\ \Delta E_H}{\delta\ E_i^{\,z}}\right]^{1/2} \tag{3-19}$$

where ΔE_H is the ionization potential of hydrogen

In fact, as demonstrated by Fauchais [3.11] and Capitelli [3.10], provided the same limitation theory is used for all the species involved, the results obtained for the plasma composition are within 3% for the main species whatever the limitation theory may be (bigger differences are obtained for minor species with molar fractions below 10^{-3}).

3.3.2 Diatomic species

In this case, two types of calculations are possible: The first does not take into account the limitation of the rotational-vibrational quantum states [3.12]. Q_{int} is then written as:

$$Q_{int} = \frac{1}{\sigma} \sum_{e} g_e \exp\left(\frac{-E_e}{kT}\right) . Q_v(e) . Q_r(v,e) . Q_{cor}(e) \qquad (3\text{-}20)$$

Where, $Q_v(e)$, $Q_r(e)$ and $Q_{cor}(e)$ are respectively the vibrational, rotational and correction (for anharmonicity and centrifugal force partition functions, σ=1 for heteronuclear species (SiCℓ for example) and σ=2 for homonuclear species (H_2 for example).

This simple formula, however, does not give satisfactory results when the fundamental state of the molecule is a multiplet (NO, O_2^+ for example) and a more complex formula has to be used [3.13]:

$$Q_{int} = \frac{1}{\sigma} \sum_{e} g_e \exp\left(-\frac{E_e}{kT}\right) \sum_{v=0}^{v_{max}} \sum_{J=0}^{V_{max}} (2J+1) \exp\left(-\frac{E_{v,J}(e)}{kT}\right) \qquad (3\text{-}21)$$

$$E_{v,J}(e) = (\omega_e - \omega_e x_e)\, v - \omega_e x_e v^2 + B_v\, J(J+1) - D_v J^2(J+1) + H_v\, J^3(J+1)^3 \qquad (3\text{-}22)$$

Where v and J are the vibrational and rotational quantum numbers respectively, ω_e, $\omega_e x_e$ are constants for a given electronic state e and B_v, D_v and H_v are constants for a vibrational state.

3.4 COMPUTATION METHOD

We have minimized the Gibbs free energy given by Eq.(3-13) together with the constraints: conservation of the mass of the atoms and constant pressure

$$p = \sum_{i=1}^{N} NikT - \frac{kT}{24\pi d} \qquad (3\text{-}23)$$

For that, we have used the Lagrange's function obtained from the Taylor's development to the second order of G/RT and from the constraints. We have chosen the steepest descent method for this minimization.

As it is an iterative method we start from an arbitrary composition N_i^0 with which we calculate new values N_i^1 used again as initial values. We assume that the convergence is obtained when

$$\text{Max}\left[\varepsilon_i = \frac{\left[N_i^{(k)} - N_i^{(k-1)}\right]}{N_i^{(k)}}, \; i = 1 \ldots N\right] < \varepsilon \qquad (3\text{-}24)$$

where ε is the precision of the calculation fixed at a value comprised between 10^{-4} and 10^{-6}.

The stability and convergence criteria are the classical ones [3.14]. In order to simplify our equations when derivating G, we have considered the virial and Debye correction terms as constants in spite of the fact that they depend on the N_i. This can be justified by the following facts:

- These terms are corrections and they have a second order effect on the slope of the function

- The corrective terms at the iterative step k + 1 are calculated with the values of N_i obtained at step k. In gas phase, these terms vary continuously with N_i and are thus calculated exactly when the solution is reached.

3.5 DATA

3.5.1 Thermodynamic data

We have chosen as reference the species existing at room temperature (T=298.15 K, p= 1 atm), i.e. H_2, $SiC\ell_4$, CH_4... and not H, Si, Cℓ...

We assume then that their formation enthalpy is zero. When Eqs. (3-3) and (3-4), are multiplied by Avogadro's number to obtain the data related to one mole, we need to calculate E_i^{298}, the formation enthalpy of specie i, related to one reference energy state. This is done as shown in the following example for H,

$$\begin{array}{lll} 298\ K & \tfrac{1}{2}\ H_2 \xleftarrow{E_H^{298}} & H \\ 0\ K & \tfrac{1}{2}\ H_2 \xrightarrow{D_H/2} & H \end{array}$$

Where D_H is the dissociation energy of H_2 (103.262 kcal/mole)

$$E_H^{298} = E_{H_2}^{298} - \frac{1}{2} c_p^* (H_2) + \frac{D_H}{2} + c_p^* (H) \qquad (3\text{-}25)$$

$$\text{with } c_p^*(i) = \int_0^{298} c_p(i)\, dT \qquad (3\text{-}26)$$

$$E_{H_2}^{298} = 0 \qquad \text{by definition}$$

3.5.2 Thermodynamic data from the tables

We have used mainly the tables of Gordon and McBride [3.2] and of Barin and Knacke [3.3]. However these tables are not normalized and, in order to reduce the computation time, instead of storing the data in files we have interpolated them using polynominals.

a) NASA

In these tables, the data are already interpolated by polynominals. Usually two sets of coefficients are given for the temperature range 300 K - 5 000 K, the first between 300 and T intermediate and the second between T intermediate and 5 000 K. The following equations are used:

$$c_p = R\,(a_1 + a_2\,T + a_3\,T^2 + a_4\,T^3 + a_5\,T^4) \qquad (3\text{-}27)$$

$$H_T = R\,(a_1\,T + \frac{a_2}{2}\,T^2 + \frac{a_3}{3}\,T^3 + \frac{a_4}{4}\,T^4 + \frac{a_5}{5}\,T^5 + a_6) \qquad (3\text{-}28)$$

$$S = K\,(a_1\,\mathrm{Log}\,T + a_2\,T + \frac{a_3}{2}\,T^2 + \frac{a_4}{3}\,T^3 + \frac{a_5}{4}\,T^4 + a_7) \qquad (3\text{-}29)$$

The following species have been taken from NASA tables:

Gaseous species

e, CH, CH_3, C_2, C_2H, C_2H_4, $C\ell$, $C\ell^-$, $HC\ell$, Si^+, SiO_2, $SiC\ell_2$, $SiC\ell_4$, SiH_4, SiC_2, $CC\ell_4$, C^-, CH_2, CH_4, C_2^-, C_2H_2, C_3, $C\ell^+$, $C\ell_2$, Si, SiC, $SiC\ell$, $SiC\ell_3$, SiH, Si_2, Si_3

Solid species C, Si

Liquid species Si

a) Barin and Knacke

We have interpolated the data by the following polynominals:

$$c_p = a_1 + a_2\, 10^{-3}\, T + \frac{a_3}{T^2}\, 10^5 + a_4\, 10^{-6}\, T^2 \qquad (3\text{-}30)$$

$$H = a_1\, T + \frac{a_2}{2}\, 10^{-3}\, T^2 - \frac{a_3}{T}\, 10^5 + \frac{2_4}{3}\, 10^{-6}\, T^3 + a_5 \qquad (3\text{-}31)$$

$$S = a_1\, \mathrm{Log}\, T + a_2\, 10^{-3}\, T - \frac{a_3}{2T^2}\, 10^5 + \frac{a_4}{2}\, 10^{-6}\, T^2 + a_6 \qquad (3\text{-}32)$$

To determine the coefficients a_5 and a_6 we choose a different temperature for which we know the values of enthalpy and entropy. Thus these coefficients are given by:

$$a_5 = H_{ref} - \left(a_1 T_{ref} + \frac{a_2}{2} 10^{-3} T_{ref}^2 - a_3 \frac{10^5}{T_{ref}} + \frac{a_4 10^{-6} T_{ref}^3}{3}\right) \quad (3\text{-}33)$$

$$a_6 = S_{ref} - \left(a_1 \text{ Log } T_{ref} + a_2 10^{-3} T_{ref} - \frac{a_3 10}{2T_{ref}^2} + \frac{a_4 10 T_{ref}}{2}\right) \quad (3\text{-}34)$$

The following species have been taken from these tables:

Solid species: Si_2H_6 and SiC

3.5.3 Partition functions

Starting from the tables of C.E. Moore [3.15] and using Eqs. (3-17) and (3-19), we have calculated Q_{int} for the following species: H, H^+, C^+, Ar, H^-, C, Ar^+.

We have calculated the partition function of H_2 with the help of Eq. (3-27) and using the data of Spindler [3.16].

3.6 RESULTS OF THE COMPUTATIONS FOR THE H_2-Ar-CH_4-$SiCl_4$ SYSTEM

Typical results of the equilibrium composition as function of temperature are given in Figs. 3-1 and 3-2 for the temperature ranges 300-2800 K and 2800-6300 K respectively. Full tabulated data at 100 K intervals are given in Appendex A.

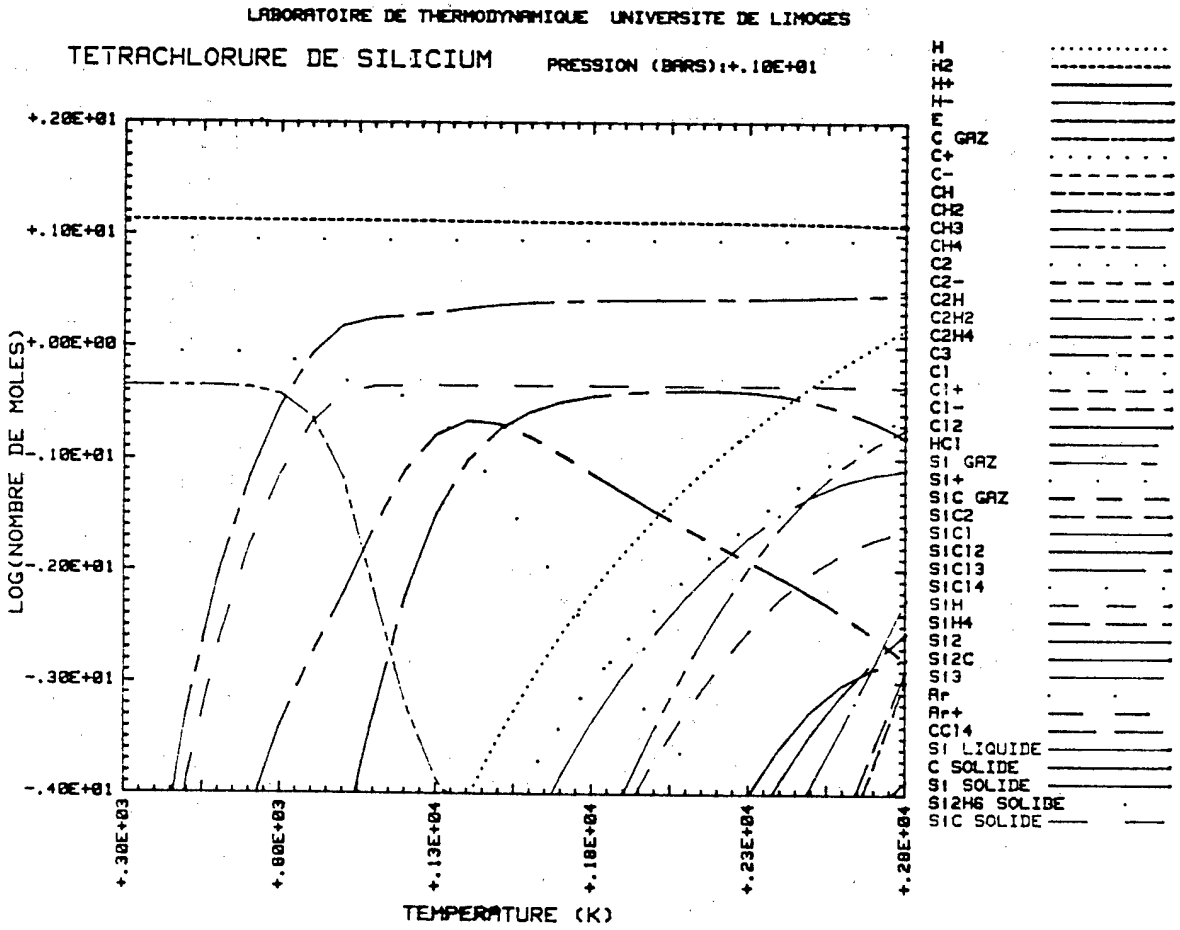

3.1 Equilibrium composition as function of temperature (330-2800 K) for the system H_2-Ar-CH_4-$SiCl_4$.

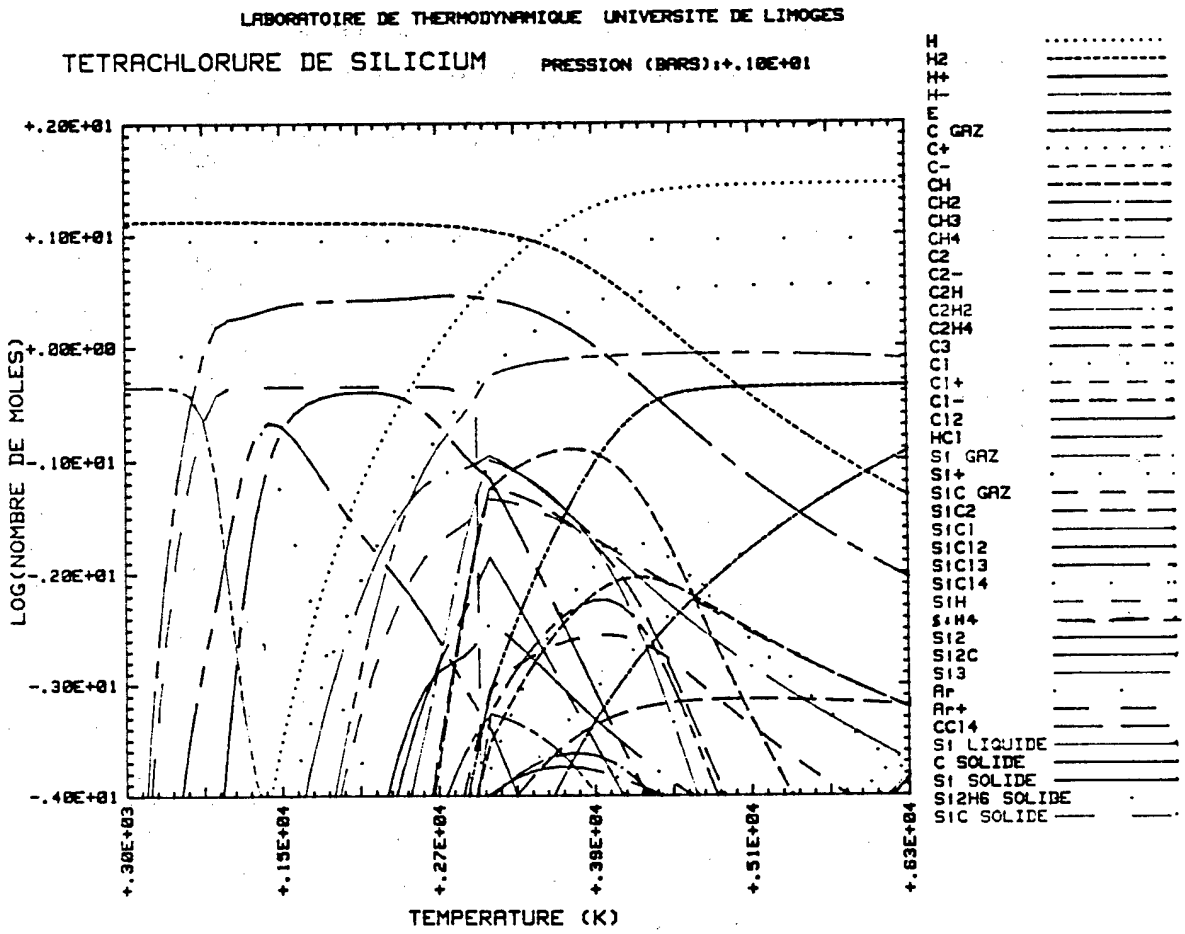

3.2 Equilibrium composition as function of temperature (2800-64000 K) for the system H_2-Ar-CH_4-$SiCl_4$.

BIBLIOGRAPHY

3.1 Van Zeggeren F., Storey S.H., "The computation of chemical equilibria, University Press (1970).

3.2 Gordon, S., McBride B.J., Thermodata -NASA, SP273 (1971).

3.3 Barin I., Knacke O., "Thermochemical properties of inorganic substances", Springer Verlag, Berlin, Heidelberg, N.Y. (1973).

3.4 JANAF Thermochemical Tables - Dow Thermochemical Corp. (1960-1972).

3.5 Banque de données thermodynamiques, Thermodata, Bibliothèque universitaire de Saint-Martin d'Hyères, Grenoble (1977).

3.6 Hirschfelder J.O., Curtiss Ch.F., Bird R.B., "Molecular theory of gases and liquid", John Wiley and Sons, N.Y. (1967).

3.7 Griem H.R., "Plasma Spectroscopy", McGraw Hill Book Co. (1964).

3.10 Capitelli M., Ficocelli E., Molinari E. "Equilibrium composition and thermodynamic properties of mixed plasmas" University of Bari, Italy (1972).

3.11 Fauchais, P. "Etude des propriétés thermodynamiques des plasmas d'arc" Thèse d'Etat, Université de Poitiers, France (1968).

3.12 Bayard S., "Contribution au calcul des fonctions de partition des plasmas azote-silicium-aluminium et détermination des températures à partir du fond continu de l'azote", Thèse de 3e cycle, Université de Limoges, France (1974).

3.13 Stupochenko E.U., Stakhanov I.P., Samuilov E.U., Pleshanov A.S. and Rozhoedtvenskii I.B., "Thermodynamic properties of air between 1 000 and 12 000 K and 0.001 and 1 000 atm", Physical Gas Dynamics, Predvoditelev A.S.(ed.), Pergamon Press (1967).

3.14 Sutre P., Malenge J.P. "Détermination autoriatique de l'équilibre thermodynamique des systèmes chimiques soumis à des températures isothermes et isobare".

3.15 Moore C.E., Atomic Energy Levels, NBS circular 467, 1, (1949), NBS circular 467, 2, (1952), NBS circular 467, 3, (1958).

3.16 Spindler R.J. "Final report: optical functions for molecular hydrogen" NASA, sept-30th (1966).

4. CHEMICAL KINETICS OF THE HOMOGENEOUS REACTIONS OCCURING IN PLASMA PROCESSES

4.1 INTRODUCTION

When the plasma is in thermodynamical equilibrium, its chemical composition is determined, for a given temperature and pressure, by the thermodynamical properties of the different species in the mixture. In this case, various calculation methods based on the mass action laws written for all the reactions involved or, what is equivalent, on the minimization of the Gibbs free energy of the system, allow the computation of the mole numbers of the different chemical components of the system [4.1].

If a departure from the equilibrium state is occuring under the influence of an external perturbation, as, for example, a sudden temperature change, the system must react in order to restore the equilibrium state and this, with a rate which is a characteristic of the efficiency of the involved processes. The "near equilibrium" approximation allows to introduce the concept of "chemical time", known as the characteristic time of the system to recover its equilibrium state.

a) Chemical time

Let us consider the reaction written below in which the forward reaction from left to right proceeds with the specific rate constant k_d, while the reverse reaction is characterized by the specific rate constant k_r.

$$\sum_{i=1}^{I} \nu_i' A_i \underset{k_r}{\overset{k_d}{\rightleftharpoons}} \sum_{i=1}^{I} \nu_i'' A_i \qquad (4\text{-}1)$$

Where

A_i is the i^{th} chemical component, and

ν'_i and ν''_i are the stoechiometric coefficients

k_d and k_r can strongly dependent on the temperature and may be expressed by the well known modified Arrhenius relationship,

$$k = A\ T^n \exp\ (-\ E/RT) \qquad (4\text{-}2)$$

where A is a constant, E the activation energy and T^n a preexponential factor taking into acount the entropy change during the reaction.

Let y_i be the concentration of the i^{th} component A_i in the mixture. In the case of chemical equilibrium where the concentrations are written $y_i(e)$, the mass action law states for the above reaction (4-1):

$$\prod_{i=1}^{I} y_{i(e)}^{a_i} = (RT)\ (-\sum_{i=1}^{I} a_i)\ K_p(T) \qquad (4\text{-}3)$$

where $a_i = \nu'_i - \nu''_i$ and where $K_p(T)$ is the equilibrium constant related to the standard Gibbs free energy variation, ΔG^o, by:

$$\text{Log}\ K_p(T) = -\ \frac{\Delta G^o}{RT} \qquad (4\text{-}4)$$

Starting from time zero with concentration $y_i(0)$ for the i^{th}-specie, at time t, the concentration y_i is determined by the progression degree of the reaction, η:

$$y_i - y_{i(0)} = (\nu_i'' - \nu_i') \eta \qquad (4\text{-}5)$$

Denoting η_0 and η_e the values of η respectively at time t=0 and when equilibrium state is reached, the "near equilibrium" approximation maybe written as

$$\eta - \eta_e = (\eta_0 - \eta_e) \exp\left(-\frac{t}{\tau_{chem}}\right) \qquad (4\text{-}6)$$

where τ_{chem} appearing in the exponential term is the chemical time, which may be evaluated from the equilibrium concentrations by [4.2]:

$$\tau_{chem} = \left[k_d \prod_{i=1}^{I} y_{i(e)}^{\nu_i'} \cdot \sum_{i=1}^{I} \frac{a_i^2}{y_{i(e)}} \right]^{-1} \qquad (4\text{-}7)$$

Typically, the values of τ_{chem} lies in the range 10^{-5}, 10^{-4}s when the temperature is under 5 000 K, such is the case in the mixing region of the reactants with the plasma flow.

b) Time scale - Criterium for equilibrium

In a flowing medium, the time scale is defined as the ratio of a characteristic length to the velocity of the flow. The former is usually related to the spatial evolution of a given parameter in the reactor. For example, if the temperature is chosen as this parameter, one has:

$$L_T = \frac{\vec{T(r)}}{\vec{\nabla_r T}} \qquad (4\text{-}8)$$

Thus the time such, τ_m, is given by the relation:

$$\tau_m = L_T/v \qquad (4\text{-}9)$$

where v is the flow velocity.

Typically, the characteristic length, L_T, is about 1 to 3 cm in a plasma jet produced by a conventional plasma torch and the velocity is a few hundreds of m/s. In that case:

$$\tau_m \sim 10^{-5} - 10^{-4}\ s$$

with a r.f. plasma torch the flow velocities are about one order of magnitude lower and accordingly the time scale.

$$\tau_m \sim 10^{-4} - 10^{-3}\ s$$

The comparison between the time scale and the chemical time allows to define three types of reactive systems.

If $\tau_{chem} >> \tau_m$, the chemical reactions proceed sufficiently slowly compared to the change of the flow parameters to leave the composition unchanged.

While, when $\tau_{chem} >> \tau_m$, the reactions are fast enough to be equilibrated, whatever the flow velocity may be. This is the case of chemical equilibrium, where the composition is completly determined by T and r.

The problem arises when $\tau_{chem} \sim \tau_m$, called "relaxed flow". In this case the composition is only predictable through the chemical kinetics calculations.

4.2 KINETIC MODELING

Considering a system composed of I chemical species which are connected through J reactions, each of which with a specific rate constant k_j. The system is submitted, under constant pressure p, to a given temperature history, T(t), which represents the time evolution of the temperature seen by a gas particle entrained by the plasma flow. In this case, it can be shown that the time variation of the concentration of the i^{th} component is described by:

$$\frac{d\, y_i}{dt} = \omega_i - y_i \left[\frac{p}{RT} \sum_{k=1}^{I} \omega_k + \frac{1}{1} \frac{dT}{dt}\right] \qquad (4\text{-}10)$$

where ω_i is the production-destruction rate of the i^{th} species given by:

$$\omega_i = \sum_{j=1}^{J} k_j \, (\nu'_{ji} - \nu''_{ji}) \prod_{\ell=1}^{I} y_\ell^{\nu'_{j\ell}} \qquad (4\text{-}11)$$

If the initial concentrations $y_i(0)$ is known, the problem is to solve the set of non-linear differential equations to obtain the evolution of the different concentrations as function of time.

The main difficulty for the integration stability arises from the fact that the chemical times associated to each specie are spread over orders of magnitude giving rise to a numerical phenomena called "stifness" [4.3]. The differential equation governing the time evolution of the i^{th} specie may be re-written in the form:

$$\frac{d\, y_i}{dt} = P_i - \frac{y_i}{\tau_i} \qquad (4\text{-}12)$$

where P_i stands for the production rate of the i^{th} component and τ_i is the chemical time. In choosing the numerical method for the integration, the following criterium has to be satisfied:

$$\Delta t << \min (t_i) \qquad (4\text{-}13)$$

with $i = 1,2..I$

where Δt is the time step required for a stable solution. Generally this condition leads to a prohibitive calculation time. So a very specific numerical method has to be carefully choosen to reach stable solutions in a reasonnable computing time, such as the method proposed by Gear [4.4] and Hindmarch and Byrnes [4.5] or the method developped at the University of Limoges and which is based on Newton polynamials predictions of the solutions [4.6].

4.3 AN EXAMPLE ($SiCl_4$,H_2) CHEMICAL SYSTEM - THE PROBLEM OF THE KINETIC DATA

The kinetic model has been used to calculate the reduction of $SiCl_4$ injected into a hydrogen plasma. Unfortunately, the kinetic data concerning the chemical species involved in such a system are scarce and often not constant. Vurzel et al [4.7] are the sole source of rate constants for the following transformations.

$$SiCl_4 \rightarrow SiCl_2 + 2Cl \qquad (4\text{-}14)$$

$$SiCl_2 \rightarrow Si(g) + 2Cl \qquad (4\text{-}15)$$

These rate constants have been determined experimentally for temperatures between 4 000 and 6 000 K for the pyrolysis of $SiC\ell_4$ in an argon plasma. The data for the reverse processes have been calculated using those of the forward reactions and the equilibrium constant:

$$\frac{k_d}{k_r} = (RT)\ (-\sum_{i=1}^{I} a_i)\quad K_p(T) \tag{4-16}$$

$C\ell_2$, H_2 and $HC\ell$ have also been taken into account using the tables by Prud'homme [4.8] and from Baulch [4.9]. Table 4.1 Summarizes the 14 reactions taken into account. Unfortunately, all the reactions of the type;

$$SiC\ell_n + H \rightarrow SiC\ell_{n-1} + HC\ell \tag{4-17}$$

$$SiC\ell_n + H_2 \rightarrow SiC\ell_{n-1} + HC\ell + H \tag{4-18}$$

are missing and intermediate chlorides such as $SiC\ell_3$ and $SiC\ell$ have not been considered. Thus the modelling is incomplete and probably does not correctly represents the situation at temperatures between 2 000 and 5 000 K.

Nevertheless, in spite of the lack of data, the performed calculations can be useful as an indication of the different parameters involved.

Fig. 4-1 shows the kinetic of $SiC\ell_4$ pyrolysis with a heating rate of 10^8 K/s. The reaction for the formation of $SiC\ell_2$ starts at about 10^{-5} s. At 10^{-4} s the reaction: $SiC\ell_4 \rightarrow SiC\ell_2 + C\ell_2$ would have to progressed to about 50% and completed in 10^{-3} s. On the other hand for a heating rate of 10^6 K/s the reaction starts only after 10^{-3} s, and after 0.1 s if the heating rate is 10^{-4} K/s.

Table 4.1 Reaction rates constants

REACTION		B	α	E
$SiCl_4 = SiCl_2 + Cl$	(d)	5E8	0	+ 88
	(r)	4.54E.50	2	-83.240
$SiCl_2 = Si(g) + 2Cl$	(d)	5E7	0	126
	(r)	3.23E.49	2	-84.330
Cl2 + M = 2Cl + M	(d)	7.58E.19	-3.1	57.1
	(r)	3.57E.9	-2.1	- 4.535
H + HCl = Cl + H2	(d)	1.36E.12	0.68	4.7
	(r)	2.236E.12	0.68	5.668
HCl + M = H + Cl + M	(d)	8.18E.19	- 3	102.170
	(r)	8.027E.9	- 2	6.081
Cl + HCl = Cl_2 + H	(d)	2.99E.10	0	49
	(r)	5.344E.10	0	1.874
H_2 + M = 2 H + M	(d)	1.22E19	-2.5	103.2
	(r)	0.776E.7	- 2	0

Where: $k = BT^{\alpha} \exp(-E/R.T.)$

d: direct. r: reverse. E (kcal/mole)

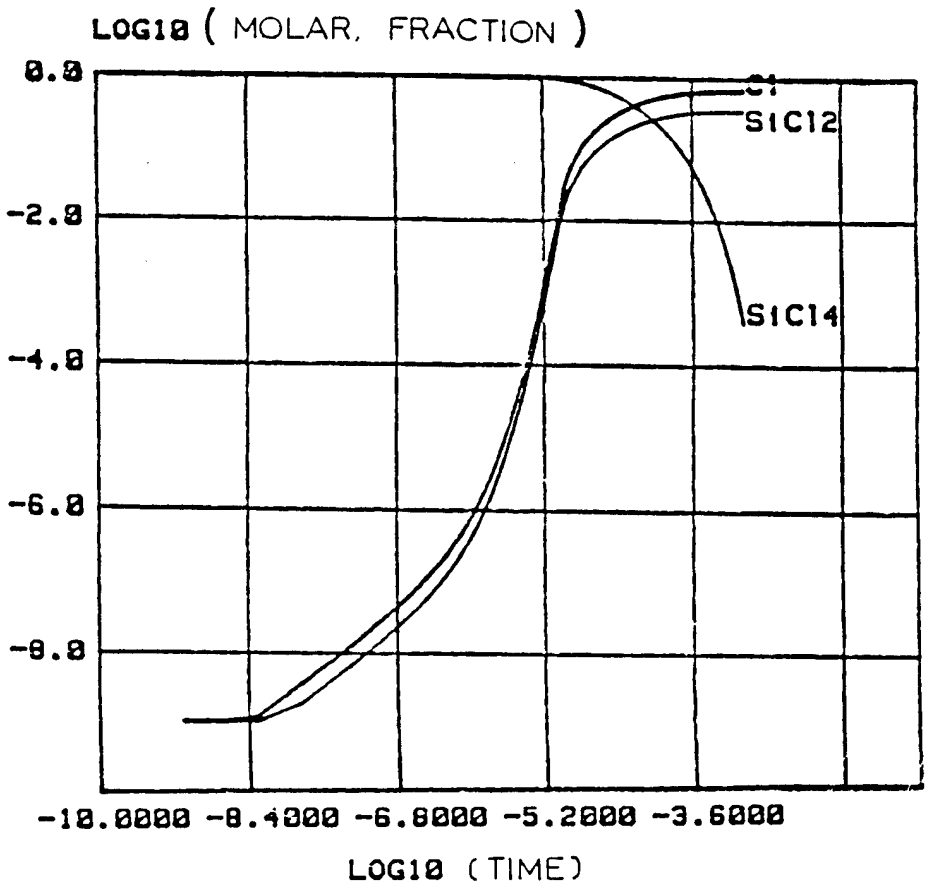

4.1 $SiC\ell_4$ Pyrolysis.

Taking into account the three reactions:

$$SiCl_4 \rightarrow SiCl_2 + 2Cl \qquad (4\text{-}19)$$

$$Si + 2Cl \rightarrow SiCl_2 \qquad (4\text{-}20)$$

$$SiCl_2 + 2Cl \rightarrow SiCl_4 \qquad (4\text{-}21)$$

and heating the reaction mixture from 2 000 K to 4 000 K in 2ms (10^6 K/s), then quenching at the same cooling rate, one obtains the results shown in Fig. 4-2 indicating that the Si molar fraction reaches a maximum a few milliseconds after the temperature starts to decrease. This is due to the fast recombination of Cl with Si, first resulting in $SiCl_2$ and then in $SiCl_4$. Even with a quenching rate of 10^8 K/s, the results are quite similar indicating that it is necessary to trap the free chlorine to prevent its recombination with Si. So, it is necessary to introduce the effect of hydrogen on the chemical behaviour of the system in order to see its influence on chlorine trapping. The reactions considered are listed in Table 4.1 and the results obtained for the mixture ($SiCl_4/H_2$) are shown in Fig. 4-3.

The temperature history is the same as the one represented in Fig. 4-2. The maximum of Si concentration appears in this case to take place at about the same moment as in the $SiCl_4$ pyrolysis. However in the cooling stage, due to the trapping of the free chlorine atoms by the hydrogen, the Si molar fraction remains constant up to the end of the process (0.05%). If the maximum temperature is 6 000 K instead of 4 000 K, the recovered Si correspond to about 4% (molar fraction). For a mixture containing 5 moles of H_2, 1 mole of $SiCl_4$, heated up to 6 000 K, 60% of the $SiCl_4$ can be recovered as free Si.

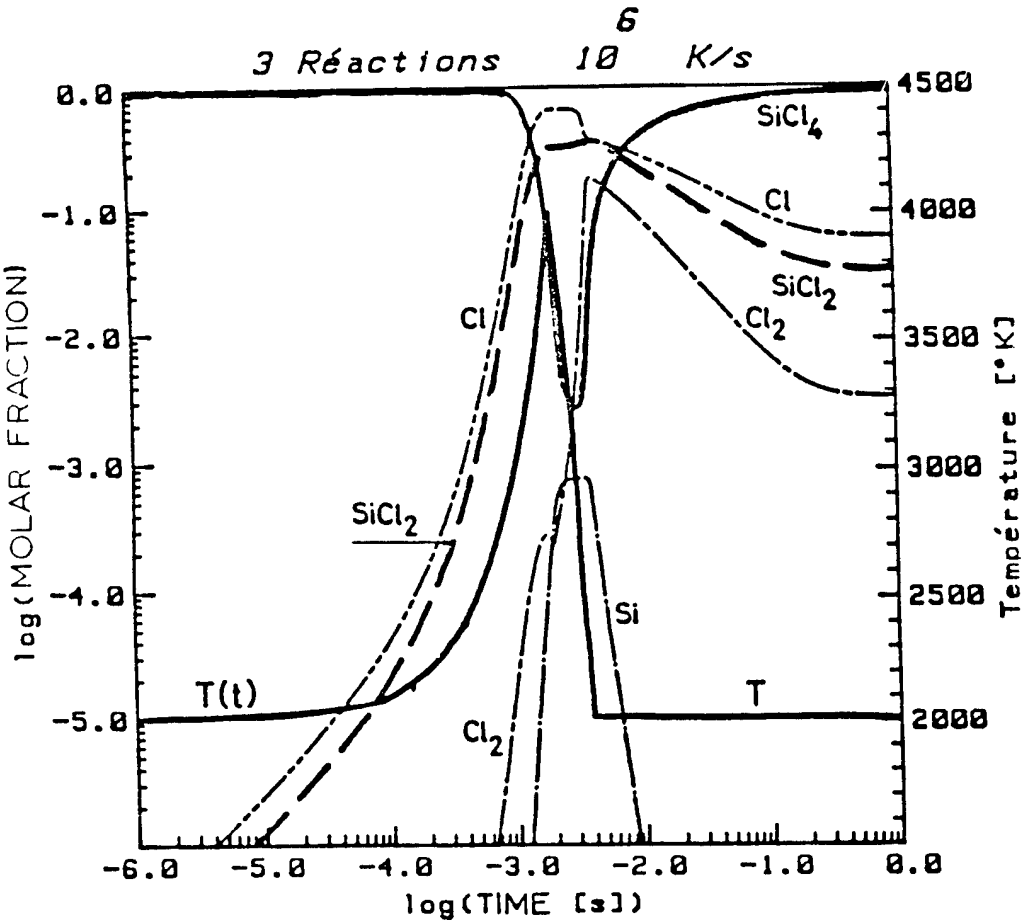

4.2 Complete $SiCl_4$ Pyrolysis.

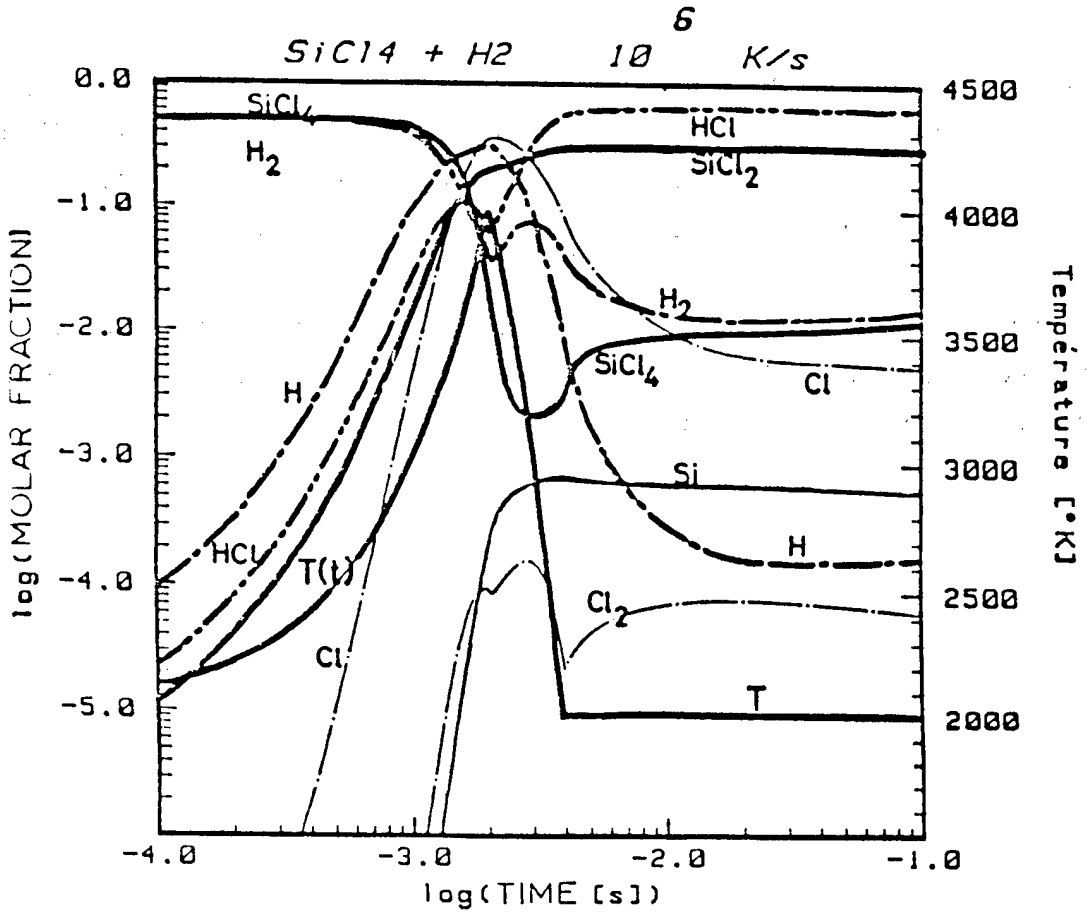

4.3 Kinetics of the reactions between $SiCl_4$ and H_2 for a heating rate of 10^6 K/s.

4.4 CONCLUSION

The used kinetic model appears to be a very powerfull tool for the prediction, even qualitative, of the chemical behaviour of a real system provided a reasonnable knowledge of the temperature history of the mixture, generally available from temperature and velocity measurements.

The principal problem, however, is the knowledge of the rate constants for the reactions involved and which can be numerous in complex mixture such as the one involving ($SiC\ell_4$, CH_4, H_2).

BIBLIOGRAPHY

4.1 W.D. Seider, R. Gautam, C.W. White, American Chem. Soc., 124, (1980).

4.2 M. Barrére, R. Prud'homme, "Equations fondamentales de l'aerothermodrimie", Ed. Masson (1973).

4.3 Warner, D.P., J. Phys. Chem. 81, 25 (1977).

4.4 Gear, C.W., Commun A.C.M., 19, 176 (1971).

4.5 Hindmarsh, A.C., Byrnes, G.P., TOMS, 1, 71 (1975).

4.6 J.F. Coudert, E. Bourdin, P. Fauchais, Plasma Chemistry and Plasma Processing, 2, (1982).

4.7 F.B. Vurzel, L.S. Polak and V.S. Shchipachev, High Energy Chem. 1, 230 (1969).

4.8 R. Prud'homme et al. Rapport ONERA, Paris (1969).

4.9 D.L. Baulch. High Temperature Reaction Rate Data, No 4, Leeds (1969).

5. REVIEW OF NUCLEATION AND GROWTH THEORY OF FINE PARTICLE FORMATION BY GAS PHASE REACTIONS

5.1 INTRODUCTION

Nucleation and growth phenomena are of fundamental importance for the particle formation process through gas phase reactions. In the case of homogeneous nucleation, the particle formation process occurs by the following sequence of events [5.1].

a) The gas phase reaction proceeds sufficiently so that the supersaturation ratio exceeds a certain critical value.

b) The nucleation occurs suddently over a relatively short time period (1 μs).

c) The nucleation terminates due to the loss of nucleating species from the gas phase by diffusion to the freshly formed particles.

d) The particles continue to grow with no new particles formed and particles grow through physical condensation and particle coagulation.

Nucleation may also occur, however, when other particles are present (either solids or liquids) and this is known as the heterogeneous nucleation process. In the heterogeneous nucleation process, the nucleation rate is greatly influenced by the geometry and chemical and physical surface properties of the pre-existing particles.

In general, the sequence of particle formation by homogeneous nucleation through gas phases reactions can be summarized as shown in Fig. 5.1. In the following, the various particle formation processes will be discussed.

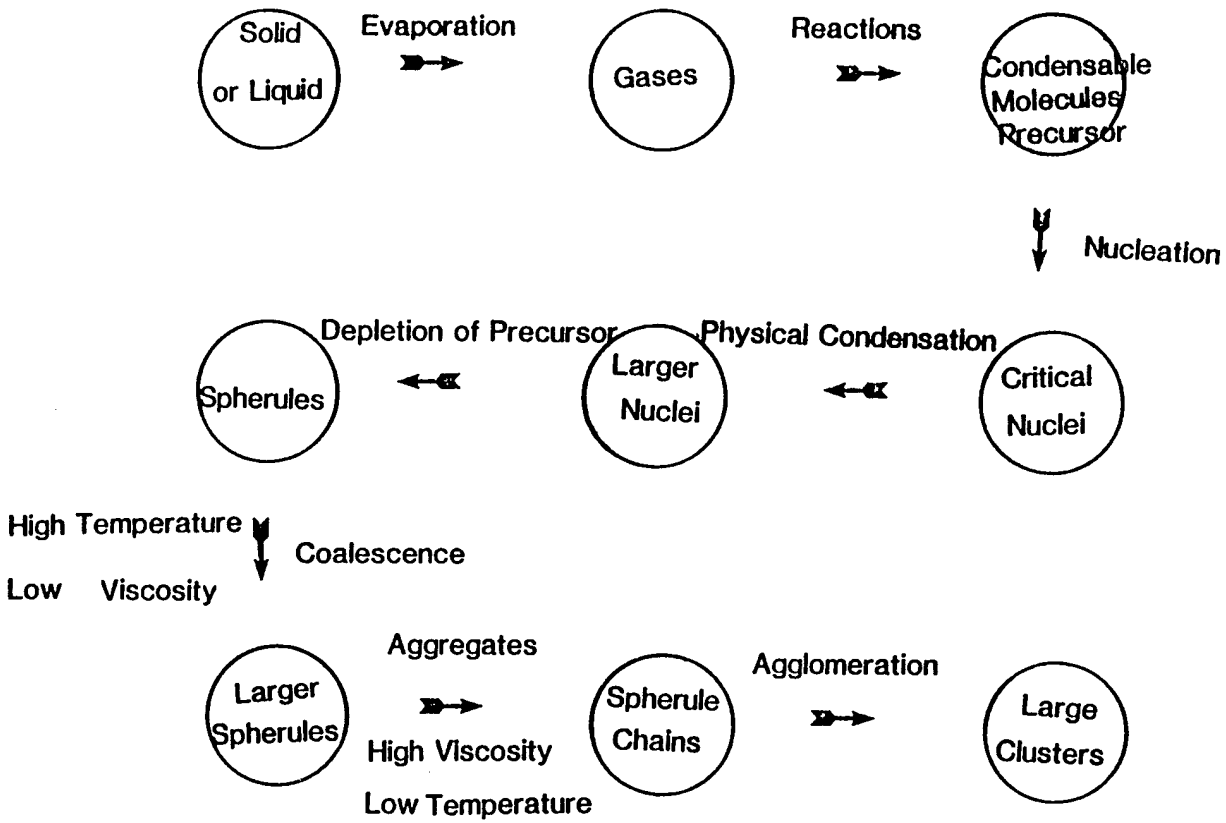

5.1 Conceptual diagram for particle nucleation and growth.

5.2 HOMOGENEOUS NUCLEATION

Although heterogeneous nuclei (in small concentrations) are usually present, homogeneous nucleation is the prevailing mechanism for particle formation from vapor phase reactions. In this nucleation process, stable condensation nuclei are formed in a supersaturated vapor via random growth of small condensed aggregates or clusters of vapor molecules. The minimum work required to form a stationary spherical cluster includes the change of bulk energy and the creation of surface energy, i.e.

$$\Delta G = (U_l - U_v)i + 4\pi r^2\sigma \qquad (5\text{-}1)$$

where i is the number of molecules in the cluster, U_l and U_v are the chemical potentials per molecule in the equilibrium bulk liquid phase and the supersaturated vapor prevailing outside the liquid particle, respectively; σ is the surface tension, and $4\pi r^2$ is the surface area of a particle.

The first term represents the bulk energy (<0), and the second term the surface energy term (<0). Eq. (5-1) describes the activation barrier which must be overcome before condensation can proceed. From this equation a critical radius can be derived for the cluster (which is the nucleus)

$$r_c = \frac{2v\sigma}{U_v - U_l} \qquad (5\text{-}2)$$

where v is the molecular volume of the liquid phase

$$v = \frac{4\pi r^3}{3}/i$$

Clusters smaller than this size tend to evaporate, while the larger clusters tend to grow.

For an ideal vapor phase, the difference in chemical potentials may be expressed as

$$U_v - U_l = kT \ln \frac{P_l}{P_\infty} \tag{5-3}$$

where P_l/P_∞ is the ratio of pressure of the condensable vapor pressure P_l to the vapor pressure of the condensed phase P_∞ (saturation pressure).

Therefore, the critical radius becomes

$$r_c = \frac{2v\sigma}{kT \ln \frac{P_l}{P_\infty}} \tag{5-4}$$

The work required for forming a nucleus is

$$\Delta G^* = \frac{16\pi}{3} \left\{ \frac{v}{kT \ln \frac{P_i}{P_\infty}} \right\}^2 \cdot \sigma^3 \tag{5-5}$$

Therefore, as the supersaturation ratio (P_l/P_∞) is increased, the number of molecules necessary to form a cluster of critical size becomes smaller, and the nucleation energy decreases.

If the nuclei are in thermodynamic equilibrium with the vapor molecules and if every collision of a vapor molecule with a nucleus results in a stable particle, then the kinetic theory of molecular collisions combined with thermodynamics provides an expression for the equilibrium nucleation rate [5.2], i.e.

$$I = \left(\frac{\sigma v^2}{4\pi k T r_c^2}\right) 4\pi r_c^2 \frac{P_v \alpha_c}{\sqrt{2\pi m k T}} n_1 \exp\left(\frac{-4}{3}\frac{\sigma \pi r_c^2}{kT}\right) \qquad (5\text{-}6)$$

where α_c is the condensation coefficient, $P_v/\sqrt{2\pi m k T}.n_1$ is the number of vapor molecules impinging per unit surface area and per unit time, m is the mass of a vapor molecule, n_1 is the number density of vapor molecules, k is the Boltzmann constant, r_c is the critical radius of the nucleus, and σ is the surface tension. From this equation follows that the frequency of formation of critical nuclei by spontaneous nucleation is proportional to $\exp(\frac{-\Delta G}{kT})$, i.e. the free energy of formation of a nucleus plays a role similar to that of the activation energy in conventional chemical kinetics, but while the latter activation energy is a constant in magnitude, ΔG, in contrast, changes markedly with the supersaturation ratio [5.3].

This classical nucleation theory shows two significant aspects: The first is the correct prediction of the strong dependence of the rate or nucleation on the extent of the supersaturation ratio. Below the critical supersaturation ratio, no significant homogeneous nucleation occurs, while slightly above the critical value for nucleation, the nucleation rate is appreciable. The critical supersaturation ratio for species i is defined as the value of (P_1/P_∞) required to yield 1 nucleus/cm^3. Thus I=1 nuclei/cm^3 is taken to be the point at which the supersaturation ratio of the gas phase is sufficient to produce copious homogeneous nucleation of the condensed phase [5.4].

The second is that the equation also predicts the general dependence of the nucleation rate on temperature and on the surface energy (σ^3). Usually a 5% change in surface tension leads to changes in the nucleation by an order of magnitude [5.2]. For organic solutions, such as ethanol, toluence, detectable production of droplets requires a value of supersaturation in the neighbourhood of 5, and values rank typically from about 4.5 to about 7 [5.5]. But for inorganic solids, such as iron, potassium, etc. with surface energies of the order of 10^3 erg/cm^2, supersaturation ratios as high as 10^5 are usually required [5.6].

The theory of homogeneous nucleation can be divided into two major groups, the classical Volmer-Becker-Doring theory [5.7,5.8] and the Lothe-Pound theory [5.9]. In the classical theory the following two major assumptions are made.

a) The flat film surface tension is used to describe the surface energy of the vapor clusters.
b) The clusters are assumed to be a rest, undergoing neither translational nor rotational motion [5.10].

This classical theory was modified by Lothe-Pound using statistical mechanics to eliminate the above mentioned assumptions. The results of these two group of theories are listed in Table 5.1 [5.10]. The modified theory predicts nucleation rates as much as 10^{12}-10^{18} times higher than the classical theory. Experimental data indicate that the classical theory is more accurate than the results of the Lothe-Pound theory for some liquids (water, methanol, octane) and for certain other liquids (ammonia, iron) the opposite is true [5.3].

In many cases, nucleation processes are not simply physical vapor deposition; they involve chemical reactions as well for particle formation via gas phase chemical reactions. The reacting gases A+B, reacting to form intermediate vapor molecules AB(g), which then nucleate to form particles, AB(s), follow the general scheme

Table 5.1-a Nucleation rates in classical theory

FRANKEL $$J_F = [\xi_c \frac{4\pi a^{*2} P_A}{(2\pi m k T)^{1/2}}] [\frac{a^{1/2} v_m}{2\pi a^{*2} (kT)^{1/2}}] [\frac{P_A}{kT} \exp(-\frac{4a^{*2}\sigma}{3kT})]$$

ZELDOVLCH $$J_z = J_F$$

VOLMER (1929) $$J_v = J_F \frac{8\pi v_m (\sigma/kT)^{3/2}}{(\ell n S)^2}$$

BECKER-DOERING $$J_{BD} = J_F (g^*)^{-2/3}$$

SUNDQULST-ORLANI $$J_{SO} = J_F (2)^{-g^*}$$

Where:
- g^* : critical nucleus size
- V_m : mulecular volume of condensed phase
- P_A : pressure of vapor in system
- S : supersaturation ratio
- a^* : critical radius for nucleation $a^* = \frac{2\sigma v_m}{kT \ln S}$

Table 5.1-b Nucleation rates in modified (non-classical) formulations

LOTHE-POUND $$J_{LP} = [\xi_c \frac{4\pi a^{*2}_{LP} P_A}{(2\pi mkT)^{1/2}}][\frac{\sigma^{1/2} v_m}{2\pi a^{*2}_{LP}(kT)^{1/2}}][4.4\times10^{-2}(\frac{mkT}{v_m})^3 \frac{a^{*1/2}}{h^5} \exp(-\frac{4a^{*2}_{LP}\sigma}{3kT})]$$

ABRAHAM $$J_A = [\xi_c \frac{4\pi a^{*2} P_A}{(2\pi mkT)^{1/2}}][\frac{\sigma^{1/2} v_m}{2\pi a^{*2}(kT)^{1/2}}][\frac{4.4\times10^{-2}(\frac{mkT}{v_m})^{3/2} a^{*3/2} v}{h^2(\frac{64}{15})^{3/2}\pi^5} \exp(-\frac{4\pi a^{*2} e}{3kT})]$$

Where:

$$\text{Critical radius } a^*_{LP} = \frac{2\sigma v_m}{kT \ell n S}(1 - \frac{3kT}{2\pi\sigma a^{*2}_{LP}})$$

$$\text{Critical radius } a^* = \frac{2\sigma v_m}{kT \ell n S}$$

$$\underset{\text{reaction}}{A(g) + B(g) = AB(g)} = \underset{\text{nucleation}}{AB(s)}$$

The supersasturation for the intermediate vapor AB(g) is [5.1].

$$S = \frac{P_{AB}}{P_{AB}^{e}} \tag{5-7}$$

where P_{AB}^{e} is the equilibrium pressure of AB(g) with the solid phase AB(s). In general, for the raction

$$aA(g) + bB(g) = cC(s) + dD(g) \tag{5-8}$$

the supersaturation ratio is

$$S = K \frac{P_A^a P_B^b}{P_D^d} \tag{5-9}$$

where K is the equilibrium constant of Eq. (5-8).

If the supersaturation ratio exceeds a critical value, nucleation processes will occur just as in physical vapor deposition [5.11].

More details about homogeneous nucleation can be found in references [5.3,5.5,5.12].

5.3 QUENCH OF HOMOGENEOUS NUCLEATION IN THE PRESENCE OF PARTICLES

The rate of new particle formation by homogeneous nucleation is, in the classical theory, assumed to be unaffected by the particles present in the gas. However, a growing particle (foreign particle or particle formed by prior nucleation) depletes the surrounding vapor due to the mass flux to the particle surface. This leads to a

variation of the radial distribution of the molecular partial pressure and the temperature (due to release of latent heat). The consequence of the mass flux to the pre-existing particles is a reduction of the rate of homogeneous nucleation for the remaining gas pecies.

Sometimes, condensation of the condensable vapor species on the surface of preexisting inorganic particles (heterogeneous condensation) may take place during cooling of the gas phase, and the gas phase may become sufficiently supersaturated with respect to some of the inorganic compounds so that homogeneous nucleation of many fine particles may also take place in the gas phase. And this leads to the formation of a large number density of very fine particles among the pre-existing bigger particles.

A theoretical analysis has been done to determine whether homogeneous nucleation of inorganic particles may occur during cooling of combustion gases in the presence of preexisting inorganic particles. This analysis involves:

a) Calculation of equilibrium concentrations of condensable vapor species at each temperature.

b) A calculation of the rate of the condensable vapor species depletion from the combustion gases during cooling by heterogeneous condensation on pre-existing inorganic particles.

c) Application of the classical theory of homogeneous nucleation to determine whether homogeneous nucleation will occur after condensation. If $P > P_{cr}$ (critical vapor pressure), homogeneous nucleation will occur [5.4].

A detailed theoretical analysis of the influence of preexisting aerosol on the size distribution evolution and on the rate of nucleation and criteria for inhibition of nucleation by initial aerosols can be found in references [5.10,5.13,5.14].

5.4 PARTICLE GROWTH

After particles have nucleated, they start to grow. In a rapidly quenched flame, for example, particle nucleation occurs rapidly and ceases before particle growth itself ceases. In such flames, chemical reactions and physical vapor condensation are extremely rapid and complete, i.e. stable fine droplets are formed almost instantaneously. These particles will undoubtedly collide with each other because of Brownian motion, resulting in coagulation, which is the primary reason for particle growth.

At higher temperatures, particles will frequently collide and coalesce to form bigger particles due to lower viscosity of these particles. As these particles cool and begin to freeze but continue to collide, they may stick togeter but do not coalesce, forming aggregates. Collision among aggregates continue even after they become solids. These aggregates are held together by physical rather than fusion bonds, forming clusters known as agglomerates. Agglometates can be decomposed by high energy agitation provided the products are suspended in a liquid. Aggregates are bound by fusion bonds and are much more stable, i.e. they cannot be fragmented by agitation [5.16].

Thus, after particle nucleation, particle growth occurs through the following mechanisms:

- Physical condensation (surface growth).
- Coagulation which includes coalescence, aggregation and agglomeration.

5.4.1 Condensational Growth

After nucleation, gas molecules diffuse to the surface of the particles reducing the vapor concentration around the particles and thus reducing further homogeneous nucleation around the particles. Condensational growth is, therefore, a process in which vapor deposits on the existing particles and particles grow by surface adsorption and diffusion. Molecular diffusion is therefore, and important factor for condensational growth.

The rate of condensational growth of a spherical particle of diameter d_p depends on the flux of the molecular gas which is a function of the Knudsen number, $Kn = l/d_p$, where l is the mean free path of the condensing vapor, d_p is the particle diameter. For Kn<<1, the transport processes are well described by the continum theory and the rate of condensation is given by [5.15].

$$v = 2\pi d_p D\ (p_i - p_i^e)kT \qquad (5\text{-}10)$$

where D is the diffusion coefficient, p_i is the partial pressure of the vapor, p_i^e is the equilibrium pressure of the condensed phase.

In the case when kn>>1 i.e. in the free molecular region, the kinetic theory of gases maybe readily applied, and the rate of condensation is given by [5.15].

$$v = \frac{\pi d_p^2 \alpha_i (p_i - p_i^e)}{(2\pi m k T)^{1/2}} \qquad (5\text{-}11)$$

where α_i is the condensation coefficient.

For intermediate values of Kn, only approximate descriptions of the transport processes are possible, and the rate of condensation is [5.15].

$$v = \frac{\pi d_p^2 D(P_i - p_i^e)}{kT} \cdot \frac{1 + Kn}{1+1.71Kn+1.33Kn^2} . \qquad (5\text{-}12)$$

Based on this assumption, the mass flux and temperature profile around growing particles has been modeled by three different authors [5.10,5.17].

The particle size due to condensational growth may be estimated, if coalescence and chain forming are neglected. A model by Smith [5.18] assumes that gas vapors deposit on the initially homogeneously nucleated nuclei. After the vapor phase becomes depleted, the maximum radius of the spherical particle is

$$R = [\frac{3M}{4\pi A\rho} \exp (\frac{4xr_c^2\sigma}{3kT})]^{1/3} \qquad (5\text{-}13)$$

Where M is the molecular weight of the precursor, A is the Avagadro number, ρ is the particle density, σ is the surface tension, r_c is the critical radius of the nucleus.

This is also the particle size of primary spherules in aggregates.

5.4.2 Particle coagulation

After condensation growth is completed and separate particles have been formed, particles will collide with each other if the

particle concentrations are high and if they stay in the high temperature zone for longer time periods. At high temperature (low viscosity) the particles tend to coalesce to form bigger particles. While at low temperature (high viscosity), they tend to form chain-like aggregates. However, initial coagulation is always due to coalescence. If the molecular mobility of the initial particles is sufficiently high, particles will collide and fuse to form large quasi-spherical particles. For soot formation in a flame, for example, the number of nuclei per spherule is of the order of a few up to ten and subsequent to the early stages of particle formation, colliding particles stick together but do not fuse giving rise to aggregates in which the individual particles can be seen.

a) Coalescence

After condensational growth, the particle grow by coalescence (sometimes growth by coalescence and condensational growth occur at the same time).

Soot formation studies show that collisions that occur in the first 1-2 ms following nucleation lead always to coalescence, and coalescence reduces the number of identifiable particles by a factor of approximately ten. Its effects is an increase of the spherule radius by approximately $10^{1/3}$ [5.19]. For particles which are governed by the frequency of Brownian motion (free molecular coagulation), and assuming that collision coalescence is the dominating process, particle number densities are determined by the collision frequency and by the sticking coefficient [5-19], i.e.

$$n = \frac{n_o}{\left[1+1.35\times10^{-13}\alpha_i n_o^{5/6} T^{1/2} f_v^{1/6} t\right]^{6/5}} \qquad (5\text{-}14)$$

and the particle size is

$$R = \left(\frac{3C_o M}{4\pi\rho An}\right)^{4/3} \qquad (5\text{-}15)$$

Where R is particle radius, f_v is the particle volume fraction, n_0 is the initial particle concentration, t is the time, n is the particle concentration, A is the Avagadro number, ρ is the density of the particles, C_0 is the gas concentration, M is the molecular weight of the condensable gas, T is absolute temperature, and α_i is the sticking coefficient.

In general, for growth through Brownian collision and coalescence, the nucleation and surface reactions are irrelevant for the final particle size. The growth rate is a strong function of the concentration, the sticking coefficient, and the ultimate particle is strongly affected by the flame temperature through its relationship to residence time.

For coalescence with particle collisions in the continuum regime, the final particle number density becomes [5-20].

$$n = \frac{n_0}{(1+4kTn_0 t/3\mu)} \qquad (5\text{-}16)$$

Where μ is the gas viscosity

A more detailed analysis about particle coalescence for both the continuum regime and the free molecular Brownian growth regime can be found in references [5.19,5.21].

b) Aggregates

Rapid coalescence is a reasonable mechanism for growing droplets of low viscosity and in dilute systems. It represents an oversimplification for particles with large viscosity and/or high concentration. For oxides with high viscosities due to tempering or cooling and for high concentrations, particle collide faster than they can fuse. In this situation, growth is a process of simultaneous inter-aggregate collision and intra- aggregate fusion, and the particles grow as flocs or aggregates comprised of numerous small primary or proto- particles. Two factors are important and have to be calculated. One is the size of the primary or proto-particles, the smallest discrete unit in the aggregates. The second is the overall size or mass of the clusters.

Most of the primary particles in the aggregates are surrounded by many atoms and the fusion rate becomes independent of the collision frequency, the aggregate size and the concentration. Based on the classical approach of Frenkel [5-23], the rate of growth of primary particles can be expressed by

$$\frac{dR_p}{dt} = [(1+\alpha)^{1/3}-1]\sigma/\mu \qquad (5\text{-}17)$$

where R_p is the primary particle radius, σ is the surface tension, μ represents the viscosity, and α is the number of neighbours fusing with the center particle of a cell. The final particle size R_p is the same as given by Eq. (5-13).

Let N_p be the number of primary or individual identifiable units comprising the unit floc, then $\dot{N}_p$

is a function of both the collision rate and the fusion rate. Assuming uniform flocs and free molecular Brownian behavior, then $\dot{N}_p$ can be derived as [5.22].

$$\dot{N}_p = [(3cBC_0M/\pi\rho A)(3kT/\rho)^{1/2}R_p^{-5/2} \times N_p^{0.3}] - 2N_p\sigma a/(a+2)\mu R_p \quad (5\text{-}19)$$

where $\dot{N}_p$ is the rate of change of the primary particles per aggregate through flocculation and coalescence, M is the molecular weight, R_p is the radius of the primary particles, ρ is the density of the particle, A is Avagadro number, C_0 is the molecular gas concentration, μ is the viscosity, σ is the surface tension, a is the number of surrounding particles, B is the bulkness factor to account for loose packing in aggregates.

A more detailed manipulation of the aggregate growth prediction for both continuum regime and the free molecular Brownian growth regime can be found in references [5.23,5.24].

c) Agglomeration

Not much work has been done about particle growth during the agglomeration stage, this is because agglomerates are just held by physical rather than fusion bonds and they can easily be fragmented by agitation. Thus, there is not much physical significance to the treatment of agglomerates.

BIBLIOGRAPHY

5.1 R.S. Dahlin, Ja-An Su, L.K. Peters, AIChE Journal, 27, 404 (1981).

5.2 S. Kotake, I.I. Glass, Prog. Aerospace Science, 19, 129-146 (1981).

5.3 A.C. Zettemyer (Ed.) Nucleation, Morral Dekker, New York.

5.4 M.J. McNallian, Combustion and Flames, 42, (1981).

5.5 F.F. Abraham, Homogeneous Nucleation Theory, Academic Press, N.Y. (1974).

5.6 J. Hecht, W.P. West, M.A. Norton, Surface Science, 106, 131 (1980).

5.7 M. Vol.mer, Z. Elektrochem, 35, 555 (1929).

5.8 R. Becker, W. Doring, Ann. Phys. (Leipzig), 24, 719 (1935).

5.9 J. Lothe, G.M. Pound, J. Chem. Phys., 36, 2080 (1962).

5.10 M.K. Alam, Ph.D. thesis, Cal. Tech., (1984).

5.11 A. Kato, J. HoJo, Y. Okabe, Memoir of the Faculty of Engineering, Kyushu University, 41, 319 (1981).

5.12 J.P. Hirth, G.H. Pound, Condensation and Evaporation, Nucleation and Growth Kinetics, Progress in Materials Science, McMillan, N.Y. (1963).

5.13 M.K. Alam, R.C. Flagan, J. of Colloid and Interface Science, 97, 232 (1984).

5.14 A.J. Peshy, R.C. Flange, J.H. Stenfeld, J. of Colloid and Surface Science, 82, 465 (1981).

5.15 S.K. Fridlander, Smoke, Dust, and Haze, Fundamentals of Aerosol Behavior, John-Wiley and Sons, N.Y. (1977).

5.16 G.D. Ulrich, C & En, 62, 23 (1984).

5.17 N.A. Fuchs, A.G. Sutugin, Ann Arbor Sci. Publication, London (1980).

5.18 G.W. Smith, Combustion and Flames, 48, 265 (1982).

5.19 G.D. Ulrich, Comb. Sci. and Tech., 4, 47 (1971).

5.20 S.C. Graham, J.B. Hombeer, J.L. Rosenfeld, Proc. Roy. Soc. Lon. A.-344, 259 (1975).

5.21 D.C. Solga, C.W. Smith, Eds, Particulate Carbon Formation During Combustion, Plenum Press, N.Y. (1981).

5.22 G.D. Ulrich, J.W. Riehl, J. Colloid & Interface, 17, 257 (1982).

5.23 G.D. Ulrich, N.S. Subramanian, Combust. Sci. Technol., 17, 119 (1977).

5.24 F. Gelbard, J.H. Seinfeld, J. of Colloid and Interface Science, 48, 363 (1979).

6. SUMMARY AND CONCLUSIONS

While each of the sections dealing with the different specific studies presented in this report had its separate discussion and conclusions, a number of important points of general nature have to be underlined in relation to this investigation. These are presented in this section in the following.

- In any mathematical modelling effort, it is imperative that computations should go hand-in-hand with the experimental program in order to validate the numerous assumptions involved. In the present study, this point is particularly important because of the complexity of the model that had to be developed involving both turbulent and laminar flow regimes. It is therefore recommended that a specific attention be given to the comparison of the results given in this report with appropriate experimental data. This could obviously be useful in a later stage of the investigation for the refinement of the mathematical model to approach as closely as possible the experimental conditions.

  The following parameters could be used for such a comparison

  - Temperature and velocity profiles along the axis of the reactor.
  - Heat flux to the reactor wall.
  - Back-pressure at the inlet section of the reactor.

- The next step in this investigation should also involve the incorporation of the reaction kinetic in the mathematical model in order to compute the concentration field in the reactor. The principal obstacle here is the lack of information on

the kinetic rate constants as function of temperature. A specific effort should therefore be devoted to a literature search of appropriate kinetic data, at least for the principal reactions involved. The selections of the chemical species to be considered could be done in the light of the results of the equilibrium composition calculations given in the present report.

- While incorporation of any of the nucleation and growth models in the final model of the reactor system is still a long term objective, the literature review presented in this report represents a first step in the right direction on the basis of which modifications of the reactor wall temperature profile could be envisaged in an attempt to achieve a better control on the particle size distribution of the silicon carbide powder obtained.

APPENDIX A

EQUILIBRIUM COMPOSITION AS FUNCTION OF THEMPERATURE FOR THE SYSTEM H_2-Ar-CH_4-$SiC\ell_4$

Nomemclature

- T Absolute temperature (K)
- CS Specific heat at constant pressure (J/kgK)
- H Enthalpy (J/kg)
- S Entropy (J/kgK)
- G Gibbs free energy (J/kg)
- MV Density (kg/m^3)

The tables give the molar quantities for each of the listed 44 species

The original composition of the mixture at 300 K has been based on the following feed rates:

GAS	FEED RATES Sℓ/min	FEED RATES moles/min	COMPOSITION molar fraction
Ar	200	8.923	0.337
H_2	300	13.384	0.566
CH_4	10	0.446	0.019
$SiC\ell_4$	20	0.892	0.038
TOTAL		23.646	1.000

TETRACHLORURE DE SILICIUM PRESSION: 1.000E+00 ATMS

T: 300 CS:+.242E+04 H:-.145E+07 S:+.582E+04 G:-.330E+07 MV:+.279E+03

H	: +.1000E-14	H2	: +.1339E+02
H+	: +.1000E-14	H-	: +.1000E-14
E	: +.1000E-14	C GAZ	: +.1000E-14
C+	: +.1000E-14	C-	: +.1000E-14
CH	: +.1000E-14	CH2	: +.1000E-14
CH3	: +.1000E-14	CH4	: +.4464E+00
C2	: +.1000E-14	C2-	: +.1000E-14
C2H	: +.1000E-14	C2H2	: +.1000E-14
C2H4	: +.1000E-14	C3	: +.1000E-14
Cl	: +.1000E-14	Cl+	: +.1000E-14
Cl-	: +.1000E-14	Cl2	: +.1000E-14
HCl	: +.2110E-07	Si GAZ	: +.1000E-14
Si+	: +.1000E-14	SiC GAZ	: +.1000E-14
SiC2	: +.1000E-14	SiCl	: +.1000E-14
SiCl2	: +.1000E-14	SiCl3	: +.5313E-14
SiCl4	: +.8829E+00	SiH	: +.1000E-14
SiH4	: +.1000E-14	Si2	: +.1000E-14
Si2C	: +.1000E-14	Si3	: +.1000E-14
Ar	: +.8929E+01	Ar+	: +.1000E-14
CCl4	: +.1000E-14	Si LIQUIDE	: +.1000E-14
C SOLIDE	: +.1000E-14	Si SOLIDE	: +.1000E-14
Si2H6 SOLIDE	: +.1000E-14	SiC SOLIDE	: +.5277E-08

T: 400 CS:+.225E+04 H:-.123E+07 S:+.646E+04 G:-.394E+07 MV:+.279E+03

H	: +.1000E-14	H2	: +.1339E+02
H+	: +.1000E-14	H-	: +.1000E-14
E	: +.1000E-14	C GAZ	: +.1000E-14
C+	: +.1000E-14	C-	: +.1000E-14
CH	: +.1000E-14	CH2	: +.1000E-14
CH3	: +.1000E-14	CH4	: +.4464E+00
C2	: +.1000E-14	C2-	: +.1000E-14
C2H	: +.1000E-14	C2H2	: +.1000E-14
C2H4	: +.1000E-14	C3	: +.1000E-14
Cl	: +.1000E-14	Cl+	: +.1000E-14
Cl-	: +.1000E-14	Cl2	: +.1000E-14
HCl	: +.9768E-05	Si GAZ	: +.1000E-14
Si+	: +.1000E-14	SiC GAZ	: +.1000E-14
SiC2	: +.1000E-14	SiCl	: +.1000E-14
SiCl2	: +.1000E-14	SiCl3	: +.2503E-09
SiCl4	: +.8829E+00	SiH	: +.1000E-14
SiH4	: +.1619E-13	Si2	: +.1000E-14
Si2C	: +.1000E-14	Si3	: +.1000E-14
Ar	: +.8929E+01	Ar+	: +.1000E-14
CCl4	: +.1000E-14	Si LIQUIDE	: +.1000E-14
C SOLIDE	: +.1000E-14	Si SOLIDE	: +.1000E-14
Si2H6 SOLIDE	: +.1000E-14	SiC SOLIDE	: +.2442E-05

TETRACHLORURE DE SILICIUM PRESSION: 1.000E+00 ATMS

T: 500 CS:+.197E+04 H:-.103E+07 S:+.691E+04 G:-.465E+07 MV:+.279E+03

H	: +.1000E-14	H2	: +.1339E+02
H+	: +.1000E-14	H-	: +.1000E-14
E	: +.1000E-14	C GAZ	: +.1000E-14
C+	: +.1000E-14	C-	: +.1000E-14
CH	: +.1000E-14	CH2	: +.1000E-14
CH3	: +.1000E-14	CH4	: +.4463E+00
C2	: +.1000E-14	C2-	: +.1000E-14
C2H	: +.1000E-14	C2H2.	: +.1000E-14
C2H4	: +.1000E-14	C3	: +.1000E-14
Cl	: +.1000E-14	Cl+	: +.1000E-14
Cl-	: +.1000E-14	Cl2	: +.1000E-14
HCl	: +.5426E-03	Si GAZ	: +.1000E-14
Si+	: +.1000E-14	SiC GAZ	: +.1000E-14
SiC2	: +.1000E-14	SiCl	: +.1000E-14
SiCl2	: +.4720E-13	SiCl3	: +.9860E-07
SiCl4	: +.8827E+00	SiH	: +.1000E-14
SiH4	: +.1650E-11	Si2	: +.1000E-14
Si2C	: +.1000E-14	Si3	: +.1000E-14
Ar	: +.8929E+01	Ar+	: +.1000E-14
CCl4	: +.1000E-14	Si LIQUIDE	: +.1000E-14
C SOLIDE	: +.1000E-14	Si SOLIDE	: +.1000E-14
Si2H6 SOLIDE	: +.1000E-14	SiC SOLIDE	: +.1356E-03

T: 600 CS:+.178E+04 H:-.854E+06 S:+.723E+04 G:-.539E+07 MV:+.279E+03

H	: +.7523E-15	H2	: +.1339E+02
H+	: +.1000E-14	H-	: +.1000E-14
E	: +.1000E-14	C GAZ	: +.1000E-14
C+	: +.1000E-14	C-	: +.1000E-14
CH	: +.1000E-14	CH2	: +.1000E-14
CH3	: +.3945E-15	CH4	: +.4442E+00
C2	: +.1000E-14	C2-	: +.1000E-14
C2H	: +.1000E-14	C2H2	: +.1000E-14
C2H4	: +.8129E-13	C3	: +.1000E-14
Cl	: +.1000E-14	Cl+	: +.1000E-14
Cl-	: +.1000E-14	Cl2	: +.1000E-14
HCl	: +.8784E-02	Si GAZ	: +.1000E-14
Si+	: +.1000E-14	SiC GAZ	: +.1000E-14
SiC2	: +.1000E-14	SiCl	: +.1000E-14
SiCl2	: +.4472E-10	SiCl3	: +.4388E-05
SiCl4	: +.8807E+00	SiH	: +.1000E-14
SiH4	: +.1343E-10	Si2	: +.1000E-14
Si2C	: +.1000E-14	Si3	: +.1000E-14
Ar	: +.8929E+01	Ar+	: +.1000E-14
CCl4	: +.1000E-14	Si LIQUIDE	: +.1000E-14
C SOLIDE	: +.1000E-14	Si SOLIDE	: +.1000E-14
Si2H6 SOLIDE	: +.1000E-14	SiC SOLIDE	: +.2195E-02

TETRACHLORURE DE SILICIUM PRESSION: 1.000E+00 ATMS

T: 700 CS:+.171E+04 H:-.682E+06 S:+.749E+04 G:-.615E+07 MV:+.278E+03

H	: +.4320E-12	H2	: +.1339E+02
H+	: +.1000E-14	H-	: +.1000E-14
E	: +.1000E-14	C GAZ	: +.1000E-14
C+	: +.1000E-14	C-	: +.1000E-14
CH	: +.1000E-14	CH2	: +.1000E-14
CH3	: +.2318E-12	CH4	: +.4299E+00
C2	: +.1000E-14	C2-	: +.1000E-14
C2H	: +.1000E-14	C2H2	: +.1000E-14
C2H4	: +.2725E-10	C3	: +.1000E-14
Cl	: +.2705E-14	Cl+	: +.1000E-14
Cl-	: +.1000E-14	Cl2	: +.1000E-14
HCl	: +.6622E-01	Si GAZ	: +.1000E-14
Si+	: +.1000E-14	SiC GAZ	: +.1000E-14
SiC2	: +.1000E-14	SiCl	: +.1000E-14
SiCl2	: +.5030E-08	SiCl3	: +.6011E-04
SiCl4	: +.8663E+00	SiH	: +.1000E-14
SiH4	: +.3868E-10	Si2	: +.1000E-14
Si2C	: +.1000E-14	Si3	: +.1000E-14
Ar	: +.8929E+01	Ar+	: +.1000E-14
CCl4	: +.1000E-14	Si LIQUIDE	: +.1000E-14
C SOLIDE	: +.1000E-14	Si SOLIDE	: +.1000E-14
Si2H6 SOLIDE	: +.1000E-14	SiC SOLIDE	: +.1654E-01

T: 800 CS:+.185E+04 H:-.497E+06 S:+.773E+04 G:-.695E+07 MV:+.275E+03

H	: +.5077E-10	H2	: +.1339E+02
H+	: +.1000E-14	H-	: +.1000E-14
E	: +.1000E-14	C GAZ	: +.1000E-14
C+	: +.1000E-14	C-	: +.1000E-14
CH	: +.1000E-14	CH2	: +.1000E-14
CH3	: +.2542E-10	CH4	: +.3729E+00
C2	: +.1000E-14	C2-	: +.1000E-14
C2H	: +.1000E-14	C2H2	: +.3007E-13
C2H4	: +.1869E-08	C3	: +.1000E-14
Cl	: +.1239E-11	Cl+	: +.1000E-14
Cl-	: +.1000E-14	Cl2	: +.6818E-15
HCl	: +.2942E+00	Si GAZ	: +.1000E-14
Si+	: +.1000E-14	SiC GAZ	: +.1000E-14
SiC2	: +.1000E-14	SiCl	: +.1000E-14
SiCl2	: +.1625E-06	SiCl3	: +.4025E-03
SiCl4	: +.8090E+00	SiH	: +.1000E-14
SiH4	: +.7502E-10	Si2	: +.1000E-14
Si2C	: +.1000E-14	Si3	: +.1000E-14
Ar	: +.8929E+01	Ar+	: +.1000E-14
CCl4	: +.1000E-14	Si LIQUIDE	: +.1000E-14
C SOLIDE	: +.1000E-14	Si SOLIDE	: +.1000E-14
Si2H6 SOLIDE	: +.1000E-14	SiC SOLIDE	: +.7345E-01

TETRACHLORURE DE SILICIUM PRESSION: 1.000E+00 ATMS

T: 900 CS:+.222E+04 H:-.275E+06 S:+.797E+04 G:-.777E+07 MV:+.270E+03

H	: +.2083E-08	H2	: +.1339E+02
H+	: +.1000E-14	H-	: +.1000E-14
E	: +.1000E-14	C GAZ	: +.1000E-14
C+	: +.1000E-14	C-	: +.1000E-14
CH	: +.1000E-14	CH2	: +.1000E-14
CH3	: +.7088E-09	CH4	: +.2362E+00
C2	: +.1000E-14	C2-	: +.1000E-14
C2H	: +.1000E-14	C2H2	: +.9295E-11
C2H4	: +.2674E-07	C3	: +.1000E-14
Cl	: +.1335E-09	Cl+	: +.1000E-14
Cl-	: +.1000E-14	Cl2	: +.1265E-12
HCl	: +.8423E+00	Si GAZ	: +.1000E-14
Si+	: +.1000E-14	SiC GAZ	: +.1000E-14
SiC2	: +.1000E-14	SiCl	: +.2650E-15
SiCl2	: +.2544E-05	SiCl3	: +.1693E-02
SiCl4	: +.6710E+00	SiH	: +.1000E-14
SiH4	: +.1535E-09	Si2	: +.1000E-14
Si2C	: +.1000E-14	Si3	: +.1000E-14
Ar	: +.8929E+01	Ar+	: +.1000E-14
CCl4	: +.1000E-14	Si LIQUIDE	: +.1000E-14
C SOLIDE	: +.1000E-14	Si SOLIDE	: +.1000E-14
Si2H6 SOLIDE	: +.1000E-14	SiC SOLIDE	: +.2102E+00

T: 1000 CS:+.236E+04 H:-.387E+05 S:+.821E+04 G:-.861E+07 MV:+.262E+03

H	: +.4091E-07	H2	: +.1339E+02
H+	: +.1000E-14	H-	: +.1000E-14
E	: +.1000E-14	C GAZ	: +.1000E-14
C+	: +.1000E-14	C-	: +.1000E-14
CH	: +.1000E-14	CH2	: +.1000E-14
CH3	: +.4257E-08	CH4	: +.6792E-01
C2	: +.1000E-14	C2-	: +.1000E-14
C2H	: +.1000E-14	C2H2	: +.1665E-09
C2H4	: +.4010E-07	C3	: +.1000E-14
Cl	: +.4454E-08	Cl+	: +.1000E-14
Cl-	: +.1000E-14	Cl2	: +.5067E-11
HCl	: +.1520E+01	Si GAZ	: +.1000E-14
Si+	: +.1000E-14	SiC GAZ	: +.1000E-14
SiC2	: +.1000E-14	SiCl	: +.6114E-13
SiCl2	: +.3199E-04	SiCl3	: +.5853E-02
SiCl4	: +.4985E+00	SiH	: +.1000E-14
SiH4	: +.6056E-09	Si2	: +.1000E-14
Si2C	: +.1000E-14	Si3	: +.1000E-14
Ar	: +.8929E+01	Ar+	: +.1000E-14
CCl4	: +.1000E-14	Si LIQUIDE	: +.1000E-14
C SOLIDE	: +.1000E-14	Si SOLIDE	: +.1000E-14
Si2H6 SOLIDE	: +.1000E-14	SiC SOLIDE	: +.3785E+00

TETRACHLORURE DE SILICIUM PRESSION: 1.000E+00 ATMS

T: 1100 CS:+.179E+04 H:+.141E+06 S:+.839E+04 G:-.948E+07 MV:+.260E+03

H	: +.4681E-06	H2	: +.1338E+02
H+	: +.1000E-14	H-	: +.1000E-14
E	: +.1000E-14	C GAZ	: +.1000E-14
C+	: +.1000E-14	C-	: +.1000E-14
CH	: +.1000E-14	CH2	: +.1000E-14
CH3	: +.4790E-08	CH4	: +.6345E-02
C2	: +.1000E-14	C2-	: +.1000E-14
C2H	: +.1000E-14	C2H2	: +.1207E-09
C2H4	: +.3807E-08	C3	: +.1000E-14
Cl	: +.5721E-07	Cl+	: +.1000E-14
Cl-	: +.1000E-14	Cl2	: +.5501E-10
HCl	: +.1785E+01	Si GAZ	: +.8216E-15
Si+	: +.1000E-14	SiC GAZ	: +.1000E-14
SiC2	: +.1000E-14	SiCl	: +.1424E-10
SiCl2	: +.5038E-03	SiCl3	: +.2355E-01
SiCl4	: +.4188E+00	SiH	: +.2001E-13
SiH4	: +.6974E-08	Si2	: +.1000E-14
Si2C	: +.1000E-14	Si3	: +.1000E-14
Ar	: +.8929E+01	Ar+	: +.1000E-14
CCl4	: +.1000E-14	Si LIQUIDE	: +.1000E-14
C SOLIDE	: +.1000E-14	Si SOLIDE	: +.1000E-14
Si2H6 SOLIDE	: +.1000E-14	SiC SOLIDE	: +.4401E+00

T: 1200 CS:+.161E+04 H:+.302E+06 S:+.852E+04 G:-.104E+08 MV:+.259E+03

H	: +.3573E-05	H2	: +.1335E+02
H+	: +.1000E-14	H-	: +.1000E-14
E	: +.1000E-14	C GAZ	: +.1000E-14
C+	: +.1000E-14	C-	: +.1000E-14
CH	: +.1000E-14	CH2	: +.1000E-14
CH3	: +.3879E-08	CH4	: +.6448E-03
C2	: +.1000E-14	C2-	: +.1000E-14
C2H	: +.1000E-14	C2H2	: +.5046E-10
C2H4	: +.2911E-09	C3	: +.1000E-14
Cl	: +.4433E-06	Cl+	: +.1000E-14
Cl-	: +.1000E-14	Cl2	: +.3408E-09
HCl	: +.1873E+01	Si GAZ	: +.4115E-12
Si+	: +.1000E-14	SiC GAZ	: +.1000E-14
SiC2	: +.1000E-14	SiCl	: +.1638E-08
SiCl2	: +.5672E-02	SiCl3	: +.7888E-01
SiCl4	: +.3526E+00	SiH	: +.4944E-11
SiH4	: +.7122E-07	Si2	: +.1000E-14
Si2C	: +.1000E-14	Si3	: +.1000E-14
Ar	: +.8929E+01	Ar+	: +.1000E-14
CCl4	: +.1000E-14	Si LIQUIDE	: +.1000E-14
C SOLIDE	: +.1000E-14	Si SOLIDE	: +.1000E-14
Si2H6 SOLIDE	: +.1000E-14	SiC SOLIDE	: +.4458E+00

TETRACHLORURE DE SILICIUM PRESSION: 1.000E+00 ATMS

T: 1300 CS:+.178E+04 H:+.479E+06 S:+.865E+04 G:-.113E+08 MV:+.258E+03

H	: +.2000E-04	H2	: +.1328E+02
H+	: +.1000E-14	H-	: +.1000E-14
E	: +.1000E-14	C GAZ	: +.1000E-14
C+	: +.1000E-14	C-	: +.1000E-14
CH	: +.1000E-14	CH2	: +.1342E-14
CH3	: +.4703E-08	CH4	: +.1346E-03
C2	: +.1000E-14	C2-	: +.1000E-14
C2H	: +.1000E-14	C2H2	: +.5150E-10
C2H4	: +.7009E-10	C3	: +.1000E-14
Cl	: +.2604E-05	Cl+	: +.1000E-14
Cl-	: +.1000E-14	Cl2	: +.1711E-08
HCl	: +.2014E+01	Si GAZ	: +.5370E-10
Si+	: +.1000E-14	SiC GAZ	: +.1000E-14
SiC2	: +.1000E-14	SiCl	: +.6364E-07
SiCl2	: +.3194E-01	SiCl3	: +.1655E+00
SiCl4	: +.2391E+00	SiH	: +.3535E-09
SiH4	: +.3428E-06	Si2	: +.7499E-15
Si2C	: +.6016E-15	Si3	: +.1000E-14
Ar	: +.8929E+01	Ar+	: +.1000E-14
CCl4	: +.1000E-14	Si LIQUIDE	: +.1000E-14
C SOLIDE	: +.1000E-14	Si SOLIDE	: +.1000E-14
Si2H6 SOLIDE	: +.1000E-14	SiC SOLIDE	: +.4463E+00

T: 1400 CS:+.187E+04 H:+.666E+06 S:+.878E+04 G:-.122E+08 MV:+.258E+03

H	: +.8776E-04	H2	: +.1319E+02
H+	: +.1000E-14	H-	: +.1000E-14
E	: +.1000E-14	C GAZ	: +.1000E-14
C+	: +.1000E-14	C-	: +.1000E-14
CH	: +.1000E-14	CH2	: +.1224E-13
CH3	: +.8486E-08	CH4	: +.5368E-04
C2	: +.1000E-14	C2-	: +.1000E-14
C2H	: +.5431E-15	C2H2	: +.1240E-09
C2H4	: +.4871E-10	C3	: +.1000E-14
Cl	: +.1222E-04	Cl+	: +.1000E-14
Cl-	: +.1000E-14	Cl2	: +.7179E-08
HCl	: +.2194E+01	Si GAZ	: +.2257E-08
Si+	: +.7948E-14	SiC GAZ	: +.1000E-14
SiC2	: +.1000E-14	SiCl	: +.9691E-06
SiCl2	: +.9529E-01	SiCl3	: +.2181E+00
SiCl4	: +.1231E+00	SiH	: +.8843E-08
SiH4	: +.8489E-06	Si2	: +.1674E-12
Si2C	: +.6828E-13	Si3	: +.2879E-14
Ar	: +.8929E+01	Ar+	: +.1000E-14
CCl4	: +.1000E-14	Si LIQUIDE	: +.1000E-14
C SOLIDE	: +.1000E-14	Si SOLIDE	: +.1000E-14
Si2H6 SOLIDE	: +.1000E-14	SiC SOLIDE	: +.4463E+00

TETRACHLORURE DE SILICIUM PRESSION: 1.000E+00 ATMS

T: 1500 CS:+.180E+04 H:+.846E+06 S:+.890E+04 G:-.131E+08 MV:+.257E+03

H	: +.3170E-03	H2	: +.1311E+02
H+	: +.1000E-14	H-	: +.1000E-14
E	: +.1000E-14	C GAZ	: +.1000E-14
C+	: +.1000E-14	C-	: +.1000E-14
CH	: +.1000E-14	CH2	: +.1112E-12
CH3	: +.1891E-07	CH4	: +.3235E-04
C2	: +.1000E-14	C2-	: +.1000E-14
C2H	: +.8743E-14	C2H2	: +.4759E-09
C2H4	: +.6365E-10	C3	: +.1000E-14
Cl	: +.4656E-04	Cl+	: +.1000E-14
Cl-	: +.7398E-14	Cl2	: +.2470E-07
HCl	: +.2352E+01	Si GAZ	: +.4284E-07
Si+	: +.3559E-13	SiC GAZ	: +.1000E-14
SiC2	: +.1000E-14	SiCl	: +.7593E-05
SiCl2	: +.1812E+00	SiCl3	: +.2042E+00
SiCl4	: +.5104E-01	SiH	: +.1069E-06
SiH4	: +.1391E-05	Si2	: +.1005E-10
Si2C	: +.3043E-11	Si3	: +.3177E-12
Ar	: +.8929E+01	Ar+	: +.1000E-14
CCl4	: +.1000E-14	Si LIQUIDE	: +.1000E-14
C SOLIDE	: +.1000E-14	Si SOLIDE	: +.1000E-14
Si2H6 SOLIDE	: +.1000E-14	SiC SOLIDE	: +.4464E+00

T: 1600 CS:+.168E+04 H:+.101E+07 S:+.901E+04 G:-.140E+08 MV:+.256E+03

H	: +.9778E-03	H2	: +.1305E+02
H+	: +.1000E-14	H-	: +.1000E-14
E	: +.1000E-14	C GAZ	: +.1000E-14
C+	: +.1000E-14	C-	: +.1000E-14
CH	: +.1150E-14	CH2	: +.9052E-12
CH3	: +.4494E-07	CH4	: +.2454E-04
C2	: +.1000E-14	C2-	: +.1000E-14
C2H	: +.1379E-12	C2H2	: +.2148E-08
C2H4	: +.1121E-09	C3	: +.1000E-14
Cl	: +.1481E-03	Cl+	: +.1000E-14
Cl-	: +.2650E-12	Cl2	: +.7076E-07
HCl	: +.2464E+01	Si GAZ	: +.4754E-06
Si+	: +.3013E-12	SiC GAZ	: +.3682E-15
SiC2	: +.9945E-14	SiCl	: +.3826E-04
SiCl2	: +.2611E+00	SiCl3	: +.1564E+00
SiCl4	: +.1896E-01	SiH	: +.7999E-06
SiH4	: +.1823E-05	Si2	: +.2581E-09
Si2C	: +.7087E-10	Si3	: +.1174E-10
Ar	: +.8929E+01	Ar+	: +.1000E-14
CCl4	: +.1000E-14	Si LIQUIDE	: +.1000E-14
C SOLIDE	: +.1000E-14	Si SOLIDE	: +.1000E-14
Si2H6 SOLIDE	: +.1000E-14	SiC SOLIDE	: +.4464E+00

TETRACHLORURE DE SILICIUM PRESSION: 1.000E+00 ATMS

T: 1700 CS:+.158E+04 H:+.117E+07 S:+.910E+04 G:-.150E+08 MV:+.256E+03

H	: +.2648E-02	H2	: +.1302E+02
H+	: +.1000E-14	H-	: +.1000E-14
E	: +.1534E-14	C GAZ	: +.7767E-15
C+	: +.1000E-14	C-	: +.1000E-14
CH	: +.2044E-13	CH2	: +.6293E-11
CH3	: +.1055E-06	CH4	: +.2106E-04
C2	: +.1000E-14	C2-	: +.1000E-14
C2H	: +.1872E-11	C2H2	: +.9694E-08
C2H4	: +.2211E-09	C3	: +.1000E-14
Cl	: +.4065E-03	Cl+	: +.1000E-14
Cl-	: +.3318E-11	Cl2	: +.1747E-06
HCl	: +.2536E+01	Si GAZ	: +.3626E-05
Si+	: +.3357E-11	SiC GAZ	: +.1207E-13
SiC2	: +.2600E-12	SiCl	: +.1435E-03
SiCl2	: +.3205E+00	SiCl3	: +.1090E+00
SiCl4	: +.6901E-02	SiH	: +.4309E-05
SiH4	: +.2127E-05	Si2	: +.3770E-08
Si2C	: +.1034E-08	Si3	: +.2156E-09
Ar	: +.8929E+01	Ar+	: +.1000E-14
CCl4	: +.1000E-14	Si LIQUIDE	: +.1000E-14
C SOLIDE	: +.1000E-14	Si SOLIDE	: +.1000E-14
Si2H6 SOLIDE	: +.1000E-14	SiC SOLIDE	: +.4464E+00

T: 1800 CS:+.153E+04 H:+.133E+07 S:+.919E+04 G:-.159E+08 MV:+.255E+03

H	: +.6430E-02	H2	: +.1299E+02
H+	: +.1000E-14	H-	: +.1000E-14
E	: +.2531E-13	C GAZ	: +.1767E-13
C+	: +.1000E-14	C-	: +.1000E-14
CH	: +.2765E-12	CH2	: +.3697E-10
CH3	: +.2361E-06	CH4	: +.1931E-04
C2	: +.1000E-14	C2-	: +.1000E-14
C2H	: +.2084E-10	C2H2	: +.4066E-07
C2H4	: +.4451E-09	C3	: +.1000E-14
Cl	: +.9896E-03	Cl+	: +.1000E-14
Cl-	: +.2908E-10	Cl2	: +.3836E-06
HCl	: +.2579E+01	Si GAZ	: +.2101E-04
Si+	: +.2915E-10	SiC GAZ	: +.2673E-12
SiC2	: +.4929E-11	SiCl	: +.4383E-03
SiCl2	: +.3599E+00	SiCl3	: +.7349E-01
SiCl4	: +.2600E-02	SiH	: +.1833E-04
SiH4	: +.2338E-05	Si2	: +.3705E-07
Si2C	: +.1063E-07	Si3	: +.2469E-08
Ar	: +.8929E+01	Ar+	: +.1000E-14
CCl4	: +.1000E-14	Si LIQUIDE	: +.1000E-14
C SOLIDE	: +.1000E-14	Si SOLIDE	: +.1000E-14
Si2H6 SOLIDE	: +.1000E-14	SiC SOLIDE	: +.4464E+00

TETRACHLORURE DE SILICIUM PRESSION: 1.000E+00 ATMS

T: 1900 CS:+.152E+04 H:+.148E+07 S:+.927E+04 G:-.169E+08 MV:+.255E+03

H	: +.1424E-01	H2	: +.1298E+02
H+	: +.1000E-14	H-	: +.1000E-14
E	: +.3082E-12	C GAZ	: +.2965E-12
C+	: +.1000E-14	C-	: +.1000E-14
CH	: +.2914E-11	CH2	: +.1849E-09
CH3	: +.4977E-06	CH4	: +.1835E-04
C2	: +.1000E-14	C2-	: +.1000E-14
C2H	: +.1891E-09	C2H2	: +.1543E-06
C2H4	: +.8771E-09	C3	: +.1000E-14
Cl	: +.2185E-02	Cl+	: +.1000E-14
Cl-	: +.1988E-09	Cl2	: +.7677E-06
HCl	: +.2606E+01	Si GAZ	: +.9845E-04
Si+	: +.1992E-09	SiC GAZ	: +.4255E-11
SiC2	: +.7000E-10	SiCl	: +.1151E-02
SiCl2	: +.3845E+00	SiCl3	: +.4962E-01
SiCl4	: +.1039E-02	SiH	: +.6510E-04
SiH4	: +.2486E-05	Si2	: +.2711E-06
Si2C	: +.8280E-07	Si3	: +.2015E-07
Ar	: +.8929E+01	Ar+	: +.1000E-14
CCl4	: +.1000E-14	Si LIQUIDE	: +.1000E-14
C SOLIDE	: +.1000E-14	Si SOLIDE	: +.1000E-14
Si2H6 SOLIDE	: +.1000E-14	SiC SOLIDE	: +.4464E+00

T: 2000 CS:+.155E+04 H:+.163E+07 S:+.935E+04 G:-.179E+08 MV:+.255E+03

H	: +.2918E-01	H2	: +.1296E+02
H+	: +.1000E-14	H-	: +.1151E-14
E	: +.2918E-11	C GAZ	: +.3809E-11
C+	: +.1000E-14	C-	: +.1000E-14
CH	: +.2464E-10	CH2	: +.8000E-09
CH3	: +.9889E-06	CH4	: +.1781E-04
C2	: +.1849E-14	C2-	: +.1000E-14
C2H	: +.1417E-08	C2H2	: +.5291E-06
C2H4	: +.1668E-08	C3	: +.1000E-14
Cl	: +.4448E-02	Cl+	: +.1000E-14
Cl-	: +.1110E-08	Cl2	: +.1426E-05
HCl	: +.2623E+01	Si GAZ	: +.3885E-03
Si+	: +.1113E-08	SiC GAZ	: +.5119E-10
SiC2	: +.7714E-09	SiCl	: +.2690E-02
SiCl2	: +.3988E+00	SiCl3	: +.3401E-01
SiCl4	: +.4442E-03	SiH	: +.2001E-03
SiH4	: +.2592E-05	Si2	: +.1570E-05
Si2C	: +.5147E-06	Si3	: +.1264E-06
Ar	: +.8929E+01	Ar+	: +.1000E-14
CCl4	: +.1000E-14	Si LIQUIDE	: +.1545E-26
C SOLIDE	: +.1000E-14	Si SOLIDE	: +.1000E-14
Si2H6 SOLIDE	: +.1000E-14	SiC SOLIDE	: +.4464E+00

TETRACHLORURE DE SILICIUM PRESSION: 1.000E+00 ATMS

T: 2100 CS:+.162E+04 H:+.179E+07 S:+.942E+04 G:-.188E+08 MV:+.255E+03

H	: +.5588E-01	H2	: +.1294E+02
H+	: +.1000E-14	H-	: +.1207E-13
E	: +.2226E-10	C GAZ	: +.3889E-10
C+	: +.1000E-14	C-	: +.1000E-14
CH	: +.1724E-09	CH2	: +.3051E-08
CH3	: +.1864E-05	CH4	: +.1758E-04
C2	: +.3329E-13	C2-	: +.1000E-14
C2H	: +.9002E-08	C2H2	: +.1658E-05
C2H4	: +.3067E-08	C3	: +.6656E-14
Cl	: +.8463E-02	Cl+	: +.1000E-14
Cl-	: +.5217E-08	Cl2	: +.2494E-05
HCl	: +.2635E+01	Si GAZ	: +.1325E-02
Si+	: +.5239E-08	SiC GAZ	: +.4847E-09
SiC2	: +.6837E-08	SiCl	: +.5700E-02
SiCl2	: +.4049E+00	SiCl3	: +.2377E-01
SiCl4	: +.2025E-03	SiH	: +.5440E-03
SiH4	: +.2655E-05	Si2	: +.7461E-05
Si2C	: +.2641E-05	Si3	: +.6359E-06
Ar	: +.8929E+01	Ar+	: +.1000E-14
CCl4	: +.1000E-14	Si LIQUIDE	: +.3589E-32
C SOLIDE	: +.1000E-14	Si SOLIDE	: +.1000E-14
Si2H6 SOLIDE	: +.1000E-14	SiC SOLIDE	: +.4464E+00

T: 2200 CS:+.174E+04 H:+.197E+07 S:+.950E+04 G:-.198E+08 MV:+.255E+03

H	: +.1010E+00	H2	: +.1291E+02
H+	: +.1000E-14	H-	: +.1012E-12
E	: +.1405E-09	C GAZ	: +.3276E-09
C+	: +.1000E-14	C-	: +.1000E-14
CH	: +.1029E-08	CH2	: +.1049E-07
CH3	: +.3375E-05	CH4	: +.1768E-04
C2	: +.4778E-12	C2-	: +.1000E-14
C2H	: +.5014E-07	C2H2	: +.4862E-05
C2H4	: +.5534E-08	C3	: +.1105E-12
Cl	: +.1522E-01	Cl+	: +.1000E-14
Cl-	: +.2110E-07	Cl2	: +.4154E-05
HCl	: +.2648E+01	Si GAZ	: +.3964E-02
Si+	: +.2124E-07	SiC GAZ	: +.3733E-08
SiC2	: +.5052E-07	SiCl	: +.1106E-01
SiCl2	: +.4031E+00	SiCl3	: +.1688E-01
SiCl4	: +.9783E-04	SiH	: +.1323E-02
SiH4	: +.2661E-05	Si2	: +.2956E-04
Si2C	: +.1143E-04	Si3	: +.2598E-05
Ar	: +.8929E+01	Ar+	: +.1000E-14
CCl4	: +.1000E-14	Si LIQUIDE	: +.1768E-36
C SOLIDE	: +.1000E-14	Si SOLIDE	: +.1000E-14
Si2H6 SOLIDE	: +.1000E-14	SiC SOLIDE	: +.4464E+00

TETRACHLORURE DE SILICIUM PRESSION: 1.000E+00 ATMS

T: 2300 CS:+.193E+04 H:+.216E+07 S:+.958E+04 G:-.208E+08 MV:+.254E+03

H	: +.1734E+00	H2	: +.1286E+02
H+	: +.1000E-14	H-	: +.6926E-12
E	: +.7453E-09	C GAZ	: +.2368E-08
C+	: +.1000E-14	C-	: +.1000E-14
CH	: +.5425E-08	CH2	: +.3339E-07
CH3	: +.5971E-05	CH4	: +.1828E-04
C2	: +.5792E-11	C2-	: +.1000E-14
C2H	: +.2560E-06	C2H2	: +.1382E-04
C2H4	: +.1008E-07	C3	: +.1574E-11
Cl	: +.2612E-01	Cl+	: +.1000E-14
Cl-	: +.7452E-07	Cl2	: +.6668E-05
HCl	: +.2667E+01	Si GAZ	: +.1044E-01
Si+	: +.7527E-07	SiC GAZ	: +.2404E-07
SiC2	: +.3233E-06	SiCl	: +.1968E-01
SiCl2	: +.3911E+00	SiCl3	: +.1209E-01
SiCl4	: +.4950E-04	SiH	: +.2878E-02
SiH4	: +.2575E-05	Si2	: +.9734E-04
Si2C	: +.4205E-04	Si3	: +.8515E-05
Ar	: +.8929E+01	Ar+	: +.1000E-14
CCl4	: +.1000E-14	Si LIQUIDE	: +.2641E-40
C SOLIDE	: +.1000E-14	Si SOLIDE	: +.1000E-14
Si2H6 SOLIDE	: +.1000E-14	SiC SOLIDE	: +.4463E+00

T: 2400 CS:+.221E+04 H:+.238E+07 S:+.966E+04 G:-.218E+08 MV:+.253E+03

H	: +.2846E+00	H2	: +.1279E+02
H+	: +.1000E-14	H-	: +.3917E-11
E	: +.3358E-08	C GAZ	: +.1530E-07
C+	: +.1000E-14	C-	: +.1000E-14
CH	: +.2621E-07	CH2	: +.1014E-06
CH3	: +.1056E-04	CH4	: +.1974E-04
C2	: +.6322E-10	C2-	: +.4037E-14
C2H	: +.1264E-05	C2H2	: +.3984E-04
C2H4	: +.1926E-07	C3	: +.2093E-10
Cl	: +.4321E-01	Cl+	: +.1000E-14
Cl-	: +.2316E-06	Cl2	: +.1043E-04
HCl	: +.2699E+01	Si GAZ	: +.2411E-01
Si+	: +.2350E-06	SiC GAZ	: +.1325E-06
SiC2	: +.1864E-05	SiCl	: +.3188E-01
SiCl2	: +.3657E+00	SiCl3	: +.8621E-02
SiCl4	: +.2585E-04	SiH	: +.5564E-02
SiH4	: +.2362E-05	Si2	: +.2615E-03
Si2C	: +.1317E-03	Si3	: +.2160E-04
Ar	: +.8929E+01	Ar+	: +.1000E-14
CCl4	: +.1000E-14	Si LIQUIDE	: +.2608E-44
C SOLIDE	: +.1000E-14	Si SOLIDE	: +.1000E-14
Si2H6 SOLIDE	: +.1000E-14	SiC SOLIDE	: +.4462E+00

TETRACHLORURE DE SILICIUM PRESSION: 1.000E+00 ATMS

T: 2500 CS:+.259E+04 H:+.264E+07 S:+.975E+04 G:-.228E+08 MV:+.252E+03

H	: +.4490E+00	H2	: +.1268E+02
H+	: +.1000E-14	H-	: +.1849E-10
E	: +.1294E-07	C GAZ	: +.9171E-07
C+	: +.1000E-14	C-	: +.1000E-14
CH	: +.1200E-06	CH2	: +.3020E-06
CH3	: +.1907E-04	CH4	: +.2261E-04
C2	: +.6601E-09	C2-	: +.6635E-13
C2H	: +.6344E-05	C2H2	: +.1218E-03
C2H4	: +.4012E-07	C3	: +.2813E-09
Cl	: +.6935E-01	Cl+	: +.1000E-14
Cl-	: +.6368E-06	Cl2	: +.1602E-04
HCl	: +.2748E+01	Si GAZ	: +.4844E-01
Si+	: +.6497E-06	SiC GAZ	: +.6368E-06
SiC2	: +.1005E-04	SiCl	: +.4656E-01
SiCl2	: +.3247E+00	SiCl3	: +.6019E-02
SiCl4	: +.1367E-04	SiH	: +.9464E-02
SiH4	: +.2011E-05	Si2	: +.5608E-03
Si2C	: +.3495E-03	Si3	: +.4079E-04
Ar	: +.8929E+01	Ar+	: +.1000E-14
CCl4	: +.1000E-14	Si LIQUIDE	: +.1118E-49
C SOLIDE	: +.1000E-14	Si SOLIDE	: +.1000E-14
Si2H6 SOLIDE	: +.1000E-14	SiC SOLIDE	: +.4457E+00

T: 2600 CS:+.306E+04 H:+.295E+07 S:+.985E+04 G:-.239E+08 MV:+.250E+03

H	: +.6837E+00	H2	: +.1253E+02
H+	: +.1000E-14	H-	: +.7383E-10
E	: +.4314E-07	C GAZ	: +.5232E-06
C+	: +.1000E-14	C-	: +.6314E-15
CH	: +.5319E-06	CH2	: +.8980E-06
CH3	: +.3562E-04	CH4	: +.2766E-04
C2	: +.6844E-08	C2-	: +.9970E-12
C2H	: +.3338E-04	C2H2	: +.4043E-03
C2H4	: +.9292E-07	C3	: +.4005E-08
Cl	: +.1083E+00	Cl+	: +.1247E-14
Cl-	: +.1558E-05	Cl2	: +.2417E-04
HCl	: +.2809E+01	Si GAZ	: +.8478E-01
Si+	: +.1601E-05	SiC GAZ	: +.2714E-05
SiC2	: +.5192E-04	SiCl	: +.6105E-01
SiCl2	: +.2706E+00	SiCl3	: +.4047E-02
SiCl4	: +.7168E-05	SiH	: +.1415E-01
SiH4	: +.1575E-05	Si2	: +.9551E-03
Si2C	: +.7898E-03	Si3	: +.5662E-04
Ar	: +.8929E+01	Ar+	: +.1000E-14
CCl4	: +.1000E-14	Si LIQUIDE	: +.1000E-14
C SOLIDE	: +.1000E-14	Si SOLIDE	: +.1000E-14
Si2H6 SOLIDE	: +.1000E-14	SiC SOLIDE	: +.4446E+00

TETRACHLORURE DE SILICIUM PRESSION: 1.000E+00 ATMS

T: 2700 CS:+.360E+04 H:+.331E+07 S:+.996E+04 G:-.249E+08 MV:+.248E+03

H	: +.1009E+01	H2	: +.1234E+02
H+	: +.1069E-14	H-	: +.2545E-09
E	: +.1267E-06	C GAZ	: +.2861E-05
C+	: +.1000E-14	C-	: +.7339E-14
CH	: +.2295E-05	CH2	: +.2666E-05
CH3	: +.6846E-04	CH4	: +.3583E-04
C2	: +.7069E-07	C2-	: +.1389E-10
C2H	: +.1834E-03	C2H2	: +.1446E-02
C2H4	: +.2364E-06	C3	: +.6024E-07
Cl	: +.1643E+00	Cl+	: +.6160E-14
Cl-	: +.3427E-05	Cl2	: +.3552E-04
HCl	: +.2865E+01	Si GAZ	: +.1312E+00
Si+	: +.3554E-05	SiC GAZ	: +.1041E-04
SiC2	: +.2585E-03	SiCl	: +.7230E-01
SiCl2	: +.2108E+00	SiCl3	: +.2589E-02
SiCl4	: +.3648E-05	SiH	: +.1884E-01
SiH4	: +.1142E-05	Si2	: +.1323E-02
Si2C	: +.1546E-02	Si3	: +.5967E-04
Ar	: +.8929E+01	Ar+	: +.1000E-14
CCl4	: +.1000E-14	Si LIQUIDE	: +.1000E-14
C SOLIDE	: +.1000E-14	Si SOLIDE	: +.1000E-14
Si2H6 SOLIDE	: +.1000E-14	SiC SOLIDE	: +.4410E+00

T: 2800 CS:+.425E+04 H:+.373E+07 S:+.101E+05 G:-.259E+08 MV:+.245E+03

H	: +.1447E+01	H2	: +.1210E+02
H+	: +.5157E-14	H-	: +.7792E-09
E	: +.3366E-06	C GAZ	: +.1479E-04
C+	: +.1900E-14	C-	: +.7418E-13
CH	: +.9479E-05	CH2	: +.7750E-05
CH3	: +.1323E-03	CH4	: +.4783E-04
C2	: +.7013E-06	C2-	: +.1767E-09
C2H	: +.1009E-02	C2H2	: +.5321E-02
C2H4	: +.6287E-06	C3	: +.9000E-06
Cl	: +.2411E+00	Cl+	: +.2787E-13
Cl-	: +.6896E-05	Cl2	: +.5027E-04
HCl	: +.2896E+01	Si GAZ	: +.1854E+00
Si+	: +.7233E-05	SiC GAZ	: +.3631E-04
SiC2	: +.1224E-02	SiCl	: +.7914E-01
SiCl2	: +.1553E+00	SiCl3	: +.1579E-02
SiCl4	: +.1788E-05	SiH	: +.2306E-01
SiH4	: +.7859E-06	Si2	: +.1585E-02
Si2C	: +.2716E-02	Si3	: +.5205E-04
Ar	: +.8929E+01	Ar+	: +.1000E-14
CCl4	: +.1000E-14	Si LIQUIDE	: +.1000E-14
C SOLIDE	: +.1000E-14	Si SOLIDE	: +.1000E-14
Si2H6 SOLIDE	: +.1000E-14	SiC SOLIDE	: +.4283E+00

TETRACHLORURE DE SILICIUM PRESSION: 1.000E+00 ATMS

T: 2900 CS:+.520E+04 H:+.425E+07 S:+.102E+05 G:-.270E+08 MV:+.242E+03

H	: +.2023E+01	H2	: +.1180E+02
H+	: +.2231E-13	H-	: +.2208E-08
E	: +.8428E-06	C GAZ	: +.6917E-04
C+	: +.1933E-13	C-	: +.6480E-12
CH	: +.3579E-04	CH2	: +.2099E-04
CH3	: +.2437E-03	CH4	: +.6210E-04
C2	: +.6071E-05	C2-	: +.1929E-08
C2H	: +.5018E-02	C2H2	: +.1812E-01
C2H4	: +.1565E-05	C3	: +.1149E-04
Cl	: +.3411E+00	Cl+	: +.1124E-12
Cl-	: +.1309E-04	Cl2	: +.6770E-04
HCl	: +.2878E+01	Si GAZ	: +.2545E+00
Si+	: +.1394E-04	SiC GAZ	: +.1166E-03
SiC2	: +.5268E-02	SiCl	: +.8431E-01
SiCl2	: +.1128E+00	SiCl3	: +.9478E-03
SiCl4	: +.8633E-06	SiH	: +.2752E-01
SiH4	: +.5405E-06	Si2	: +.1846E-02
Si2C	: +.4560E-02	Si3	: +.4468E-04
Ar	: +.8929E+01	Ar+	: +.1000E-14
CCl4	: +.1000E-14	Si LIQUIDE	: +.1000E-14
C SOLIDE	: +.1000E-14	Si SOLIDE	: +.1000E-14
Si2H6 SOLIDE	: +.1000E-14	SiC SOLIDE	: +.3844E+00

T: 3000 CS:+.679E+04 H:+.493E+07 S:+.104E+05 G:-.281E+08 MV:+.239E+03

H	: +.2763E+01	H2	: +.1143E+02
H+	: +.8412E-13	H-	: +.6063E-08
E	: +.2084E-05	C GAZ	: +.2753E-03
C+	: +.1528E-12	C-	: +.4806E-11
CH	: +.1158E-03	CH2	: +.4940E-04
CH3	: +.3969E-03	CH4	: +.7246E-04
C2	: +.4021E-04	C2-	: +.1650E-07
C2H	: +.1967E-01	C2H2	: +.4951E-01
C2H4	: +.3143E-05	C3	: +.1024E-03
Cl	: +.4651E+00	Cl+	: +.3921E-12
Cl-	: +.2442E-04	Cl2	: +.8633E-04
HCl	: +.2798E+01	Si GAZ	: +.3673E+00
Si+	: +.2653E-04	SiC GAZ	: +.3482E-03
SiC2	: +.1939E-01	SiCl	: +.9401E-01
SiCl2	: +.8611E-01	SiCl3	: +.5940E-03
SiCl4	: +.4328E-06	SiH	: +.3456E-01
SiH4	: +.3968E-06	Si2	: +.2436E-02
Si2C	: +.7932E-02	Si3	: +.4728E-04
Ar	: +.8929E+01	Ar+	: +.6301E-15
CCl4	: +.5065E-15	Si LIQUIDE	: +.1000E-14
C SOLIDE	: +.1000E-14	Si SOLIDE	: +.1000E-14
Si2H6 SOLIDE	: +.1000E-14	SiC SOLIDE	: +.2597E+00

TETRACHLORURE DE SILICIUM PRESSION: 1.000E+00 ATMS

T: 3100 CS:+.917E+04 H:+.585E+07 S:+.107E+05 G:-.292E+08 MV:+.236E+03

H	: +.3694E+01	H2	: +.1095E+02
H+	: +.2786E-12	H-	: +.1627E-07
E	: +.5138E-05	C GAZ	: +.9053E-03
C+	: +.9145E-12	C-	: +.2952E-10
CH	: +.3102E-03	CH2	: +.9721E-04
CH3	: +.5474E-03	CH4	: +.7240E-04
C2	: +.1904E-03	C2-	: +.1035E-06
C2H	: +.5643E-01	C2H2.	: +.1003E+00
C2H4	: +.4670E-05	C3	: +.5715E-03
Cl	: +.6147E+00	Cl+	: +.1195E-11
Cl-	: +.4517E-04	Cl2	: +.1049E-03
HCl	: +.2665E+01	Si GAZ	: +.5626E+00
Si+	: +.5043E-04	SiC GAZ	: +.9417E-03
SiC2	: +.5705E-01	SiCl	: +.1107E+00
SiCl2	: +.6972E-01	SiCl3	: +.3917E-03
SiCl4	: +.2270E-06	SiH	: +.4595E-01
SiH4	: +.3095E-06	Si2	: +.3692E-02
Si2C	: +.1394E-01	Si3	: +.6280E-04
Ar	: +.8929E+01	Ar+	: +.2054E-14
CCl4	: +.8293E-15	Si LIQUIDE	: +.1000E-14
C SOLIDE	: +.1000E-14	Si SOLIDE	: +.1000E-14
Si2H6 SOLIDE	: +.1000E-14	SiC SOLIDE	: +.1022E-19

T: 3200 CS:+.754E+04 H:+.660E+07 S:+.109E+05 G:-.304E+08 MV:+.231E+03

H	: +.4827E+01	H2	: +.1045E+02
H+	: +.9954E-12	H-	: +.3494E-07
E	: +.1024E-04	C GAZ	: +.1884E-02
C+	: +.3898E-11	C-	: +.9442E-10
CH	: +.5314E-03	CH2	: +.1244E-03
CH3	: +.5009E-03	CH4	: +.4888E-04
C2	: +.3809E-03	C2-	: +.2310E-06
C2H	: +.7047E-01	C2H2	: +.9019E-01
C2H4	: +.3127E-05	C3	: +.9114E-03
Cl	: +.8010E+00	Cl+	: +.3985E-11
Cl-	: +.6904E-04	Cl2	: +.1272E-03
HCl	: +.2548E+01	Si GAZ	: +.6204E+00
Si+	: +.7955E-04	SiC GAZ	: +.1209E-02
SiC2	: +.5421E-01	SiCl	: +.9598E-01
SiCl2	: +.4276E-01	SiCl3	: +.1996E-03
SiCl4	: +.9394E-07	SiH	: +.4426E-01
SiH4	: +.1796E-06	Si2	: +.2988E-02
Si2C	: +.8857E-02	Si3	: +.3328E-04
Ar	: +.8929E+01	Ar+	: +.7264E-14
CCl4	: +.9198E-15	Si LIQUIDE	: +.1000E-14
C SOLIDE	: +.1000E-14	Si SOLIDE	: +.1000E-14
Si2H6 SOLIDE	: +.1000E-14	SiC SOLIDE	: +.1162E-22

TETRACHLORURE DE SILICIUM PRESSION: 1.000E+00 ATMS

T: 3300 CS:+.852E+04 H:+.745E+07 S:+.111E+05 G:-.315E+08 MV:+.224E+03

H	: +.6179E+01	H2	: +.9859E+01
H+	: +.3304E-11	H-	: +.7079E-07
E	: +.1956E-04	C GAZ	: +.3737E-02
C+	: +.1528E-10	C-	: +.2783E-09
CH	: +.8701E-03	CH2	: +.1535E-03
CH3	: +.4466E-03	CH4	: +.3246E-04
C2	: +.7225E-03	C2-	: +.4816E-06
C2H	: +.8508E-01	C2H2	: +.7929E-01
C2H4	: +.2045E-05	C3	: +.1384E-02
Cl	: +.1013E+01	Cl+	: +.1228E-10
Cl-	: +.1006E-03	Cl2	: +.1474E-03
HCl	: +.2386E+01	Si GAZ	: +.6676E+00
Si+	: +.1207E-03	SiC GAZ	: +.1488E-02
SiC2	: +.4992E-01	SiCl	: +.8081E-01
SiCl2	: +.2554E-01	SiCl3	: +.9829E-04
SiCl4	: +.3736E-07	SiH	: +.4153E-01
SiH4	: +.1020E-06	Si2	: +.2348E-02
Si2C	: +.5505E-02	Si3	: +.1717E-04
Ar	: +.8929E+01	Ar+	: +.2399E-13
CCl4	: +.9381E-15	Si LIQUIDE	: +.1000E-14
C SOLIDE	: +.1000E-14	Si SOLIDE	: +.1000E-14
Si2H6 SOLIDE	: +.1000E-14	SiC SOLIDE	: +.1000E-14

T: 3400 CS:+.951E+04 H:+.841E+07 S:+.114E+05 G:-.327E+08 MV:+.217E+03

H	: +.7750E+01	H2	: +.9179E+01
H+	: +.1023E-10	H-	: +.1359E-06
E	: +.3599E-04	C GAZ	: +.7089E-02
C+	: +.5542E-10	C-	: +.7614E-09
CH	: +.1363E-02	CH2	: +.1823E-03
CH3	: +.3864E-03	CH4	: +.2107E-04
C2	: +.1302E-02	C2-	: +.9421E-06
C2H	: +.9916E-01	C2H2	: +.6786E-01
C2H4	: +.1297E-05	C3	: +.2002E-02
Cl	: +.1246E+01	Cl+	: +.3516E-10
Cl-	: +.1406E-03	Cl2	: +.1640E-03
HCl	: +.2188E+01	Si GAZ	: +.7060E+00
Si+	: +.1776E-03	SiC GAZ	: +.1769E-02
SiC2	: +.4477E-01	SiCl	: +.6657E-01
SiCl2	: +.1494E-01	SiCl3	: +.4713E-04
SiCl4	: +.1439E-07	SiH	: +.3819E-01
SiH4	: +.5662E-07	Si2	: +.1814E-02
Si2C	: +.3382E-02	Si3	: +.8773E-05
Ar	: +.8929E+01	Ar+	: +.7436E-13
CCl4	: +.8845E-15	Si LIQUIDE	: +.1000E-14
C SOLIDE	: +.1000E-14	Si SOLIDE	: +.1000E-14
Si2H6 SOLIDE	: +.1000E-14	SiC SOLIDE	: +.1000E-14

TETRACHLORURE DE SILICIUM PRESSION: 1.000E+00 ATMS

T: 3500 CS:+.104E+05 H:+.945E+07 S:+.117E+05 G:-.339E+08 MV:+.210E+03

H	+.9520E+01	H2	+.8412E+01
H+	+.2963E-10	H-	+.2478E-06
E	+.6394E-04	C GAZ	+.1289E-01
C+	+.1867E-09	C-	+.1943E-08
CH	+.2045E-02	CH2	+.2081E-03
CH3	+.3232E-03	CH4	+.1329E-04
C2	+.2231E-02	C2-	+.1735E-05
C2H	+.1114E+00	C2H2	+.5635E-01
C2H4	+.7920E-06	C3	+.2761E-02
Cl	+.1495E+01	Cl+	+.9411E-10
Cl-	+.1888E-03	Cl2	+.1757E-03
HCl	+.1965E+01	Si GAZ	+.7373E+00
Si+	+.2548E-03	SiC GAZ	+.2042E-02
SiC2	+.3924E-01	SiCl	+.5393E-01
SiCl2	+.8615E-02	SiCl3	+.2213E-04
SiCl4	+.5402E-08	SiH	+.3452E-01
SiH4	+.3071E-07	Si2	+.1389E-02
Si2C	+.2067E-02	Si3	+.4490E-05
Ar	+.8929E+01	Ar+	+.2174E-12
CCl4	+.7747E-15	Si LIQUIDE	+.1000E-14
C SOLIDE	+.1000E-14	Si SOLIDE	+.1000E-14
Si2H6 SOLIDE	+.1000E-14	SiC SOLIDE	+.1000E-14

T: 3600 CS:+.112E+05 H:+.106E+08 S:+.119E+05 G:-.352E+08 MV:+.203E+03

H	+.1145E+02	H2	+.7573E+01
H+	+.8066E-10	H-	+.4301E-06
E	+.1099E-03	C GAZ	+.2249E-01
C+	+.5870E-09	C-	+.4639E-08
CH	+.2938E-02	CH2	+.2279E-03
CH3	+.2605E-03	CH4	+.8096E-05
C2	+.3641E-02	C2-	+.3010E-05
C2H	+.1205E+00	C2H2	+.4521E-01
C2H4	+.4632E-06	C3	+.3624E-02
Cl	+.1751E+01	Cl+	+.2367E-09
Cl-	+.2446E-03	Cl2	+.1817E-03
HCl	+.1727E+01	Si GAZ	+.7631E+00
Si+	+.3580E-03	SiC GAZ	+.2295E-02
SiC2	+.3365E-01	SiCl	+.4314E-01
SiCl2	+.4912E-02	SiCl3	+.1022E-04
SiCl4	+.1986E-08	SiH	+.3076E-01
SiH4	+.1626E-07	Si2	+.1062E-02
Si2C	+.1263E-02	Si3	+.2322E-05
Ar	+.8929E+01	Ar+	+.6026E-12
CCl4	+.6332E-15	Si LIQUIDE	+.1000E-14
C SOLIDE	+.1000E-14	Si SOLIDE	+.1000E-14
Si2H6 SOLIDE	+.1000E-14	SiC SOLIDE	+.1000E-14

TETRACHLORURE DE SILICIUM PRESSION: 1.000E+00 ATMS

T: 3700 CS:+.116E+05 H:+.117E+08 S:+.123E+05 G:-.365E+08 MV:+.196E+03

H	: +.1348E+02	H2	: +.6686E+01
H+	: +.2070E-09	H-	: +.7116E-06
E	: +.1830E-03	C GAZ	: +.3766E-01
C+	: +.1727E-08	C-	: +.1038E-07
CH	: +.4037E-02	CH2	: +.2390E-03
CH3	: +.2016E-03	CH4	: +.4746E-05
C2	: +.5647E-02	C2-	: +.4915E-05
C2H	: +.1250E+00	C2H2	: +.3488E-01
C2H4	: +.2579E-06	C3	: +.4509E-02
Cl	: +.2004E+01	Cl+	: +.5624E-09
Cl-	: +.3060E-03	Cl2	: +.1820E-03
HCl	: +.1487E+01	Si GAZ	: +.7844E+00
Si+	: +.4946E-03	SiC GAZ	: +.2517E-02
SiC2	: +.2820E-01	SiCl	: +.3419E-01
SiCl2	: +.2779E-02	SiCl3	: +.4663E-05
SiCl4	: +.7184E-09	SiH	: +.2707E-01
SiH4	: +.8395E-08	Si2	: +.8136E-03
Si2C	: +.7732E-03	Si3	: +.1221E-05
Ar	: +.8929E+01	Ar+	: +.1592E-11
CCl4	: +.4849E-15	Si LIQUIDE	: +.1000E-14
C SOLIDE	: +.1000E-14	Si SOLIDE	: +.1000E-14
Si2H6 SOLIDE	: +.1000E-14	SiC SOLIDE	: +.1000E-14

T: 3800 CS:+.117E+05 H:+.129E+08 S:+.126E+05 G:-.378E+08 MV:+.189E+03

H	: +.1554E+02	H2	: +.5786E+01
H+	: +.5030E-09	H-	: +.1124E-05
E	: +.2953E-03	C GAZ	: +.6044E-01
C+	: +.4763E-08	C-	: +.2177E-07
CH	: +.5297E-02	CH2	: +.2395E-03
CH3	: +.1494E-03	CH4	: +.2666E-05
C2	: +.8288E-02	C2-	: +.7519E-05
C2H	: +.1236E+00	C2H2	: +.2571E-01
C2H4	: +.1357E-06	C3	: +.5281E-02
Cl	: +.2246E+01	Cl+	: +.1268E-08
Cl-	: +.3703E-03	Cl2	: +.1770E-03
HCl	: +.1254E+01	Si GAZ	: +.8023E+00
Si+	: +.6743E-03	SiC GAZ	: +.2692E-02
SiC2	: +.2301E-01	SiCl	: +.2690E-01
SiCl2	: +.1566E-02	SiCl3	: +.2111E-05
SiCl4	: +.2573E-09	SiH	: +.2355E-01
SiH4	: +.4232E-08	Si2	: +.6266E-03
Si2C	: +.4739E-03	Si3	: +.6551E-06
Ar	: +.8929E+01	Ar+	: +.4024E-11
CCl4	: +.3494E-15	Si LIQUIDE	: +.1000E-14
C SOLIDE	: +.1000E-14	Si SOLIDE	: +.1000E-14
Si2H6 SOLIDE	: +.1000E-14	SiC SOLIDE	: +.1000E-14

TRICHLORURE DE SILICIUM PRESSION: 1.000E+00 ATMS

T: 3900 CS:+.115E+05 H:+.140E+08 S:+.129E+05 G:-.392E+08 MV:+.183E+03

H	: +.1754E+02	H2	: +.4908E+01
H+	: +.1160E-08	H-	: +.1697E-05
E	: +.4620E-03	C GAZ	: +.9267E-01
C+	: +.1229E-07	C-	: +.4267E-07
CH	: +.6620E-02	CH2	: +.2286E-03
CH3	: +.1056E-03	CH4	: +.1431E-05
C2	: +.1143E-01	C2-	: +.1070E-04
C2H	: +.1157E+00	C2H2	: +.1797E-01
C2H4	: +.6705E-07	C3	: +.5751E-02
Cl	: +.2469E+01	Cl+	: +.2727E-08
Cl-	: +.4344E-03	Cl2	: +.1677E-03
HCl	: +.1039E+01	Si GAZ	: +.8172E+00
Si+	: +.9089E-03	SiC GAZ	: +.2799E-02
SiC2	: +.1814E-01	SiCl	: +.2108E-01
SiCl2	: +.8817E-03	SiCl3	: +.9537E-06
SiCl4	: +.9188E-10	SiH	: +.2030E-01
SiH4	: +.2088E-08	Si2	: +.4863E-03
Si2C	: +.2902E-03	Si3	: +.3601E-06
Ar	: +.8928E+01	Ar+	: +.9777E-11
CCl4	: +.2376E-15	Si LIQUIDE	: +.1000E-14
C SOLIDE	: +.1000E-14	Si SOLIDE	: +.1000E-14
Si2H6 SOLIDE	: +.1000E-14	SiC SOLIDE	: +.1000E-14

T: 4000 CS:+.109E+05 H:+.151E+08 S:+.132E+05 G:-.405E+08 MV:+.178E+03

H	: +.1940E+02	H2	: +.4087E+01
H+	: +.2552E-08	H-	: +.2457E-05
E	: +.7016E-03	C GAZ	: +.1351E+00
C+	: +.2963E-07	C-	: +.7798E-07
CH	: +.7848E-02	CH2	: +.2072E-03
CH3	: +.7107E-04	CH4	: +.7319E-06
C2	: +.1465E-01	C2-	: +.1404E-04
C2H	: +.1014E+00	C2H2	: +.1179E-01
C2H4	: +.3084E-07	C3	: +.5730E-02
Cl	: +.2667E+01	Cl+	: +.5618E-08
Cl-	: +.4953E-03	Cl2	: +.1556E-03
HCl	: +.8462E+00	Si GAZ	: +.8297E+00
Si+	: +.1213E-02	SiC GAZ	: +.2819E-02
SiC2	: +.1367E-01	SiCl	: +.1649E-01
SiCl2	: +.4980E-03	SiCl3	: +.4321E-06
SiCl4	: +.3292E-10	SiH	: +.1736E-01
SiH4	: +.1012E-08	Si2	: +.3809E-03
Si2C	: +.1766E-03	Si3	: +.2031E-06
Ar	: +.8928E+01	Ar+	: +.2290E-10
CCl4	: +.1529E-15	Si LIQUIDE	: +.1000E-14
C SOLIDE	: +.1000E-14	Si SOLIDE	: +.1000E-14
Si2H6 SOLIDE	: +.1000E-14	SiC SOLIDE	: +.1000E-14

TETRACHLORURE DE SILICIUM PRESSION: 1.000E+00 ATMS

T: 4100 CS:+.100E+05 H:+.161E+08 S:+.134E+05 G:-.419E+08 MV:+.173E+03

H	: +.2107E+02	H2	: +.3350E+01
H+	: +.5370E-08	H-	: +.3420E-05
E	: +.1035E-02	C GAZ	: +.1863E+00
C+	: +.6641E-07	C-	: +.1323E-06
CH	: +.8789E-02	CH2	: +.1777E-03
CH3	: +.4540E-04	CH4	: +.3562E-06
C2	: +.1727E-01	C2-	: +.1678E-04
C2H	: +.8225E-01	C2H2	: +.7183E-02
C2H4	: +.1311E-07	C3	: +.5123E-02
Cl	: +.2837E+01	Cl+	: +.1113E-07
Cl-	: +.5505E-03	Cl2	: +.1418E-03
HCl	: +.6804E+00	Si GAZ	: +.8401E+00
Si+	: +.1606E-02	SiC GAZ	: +.2734E-02
SiC2	: +.9716E-02	SiCl	: +.1290E-01
SiCl2	: +.2831E-03	SiCl3	: +.1974E-06
SiCl4	: +.1192E-10	SiH	: +.1476E-01
SiH4	: +.4853E-09	Si2	: +.3013E-03
Si2C	: +.1062E-03	Si3	: +.1175E-06
Ar	: +.8928E+01	Ar+	: +.5186E-10
CCl4	: +.9331E-16	Si LIQUIDE	: +.1000E-14
C SOLIDE	: +.1000E-14	Si SOLIDE	: +.1000E-14
Si2H6 SOLIDE	: +.1000E-14	SiC SOLIDE	: +.1000E-14

T: 4200 CS:+.895E+04 H:+.170E+08 S:+.136E+05 G:-.434E+08 MV:+.169E+03

H	: +.2251E+02	H2	: +.2712E+01
H+	: +.1085E-07	H-	: +.4596E-05
E	: +.1487E-02	C GAZ	: +.2419E+00
C+	: +.1379E-06	C-	: +.2078E-06
CH	: +.9269E-02	CH2	: +.1440E-03
CH3	: +.2750E-04	CH4	: +.1650E-06
C2	: +.1850E-01	C2-	: +.1809E-04
C2H	: +.6119E-01	C2H2	: +.4029E-02
C2H4	: +.5115E-08	C3	: +.4042E-02
Cl	: +.2978E+01	Cl+	: +.2127E-07
Cl-	: +.5983E-03	Cl2	: +.1276E-03
HCl	: +.5419E+00	Si GAZ	: +.8484E+00
Si+	: +.2108E-02	SiC GAZ	: +.2540E-02
SiC2	: +.6441E-02	SiCl	: +.1011E-01
SiCl2	: +.1625E-03	SiCl3	: +.9131E-07
SiCl4	: +.4389E-11	SiH	: +.1250E-01
SiH4	: +.2313E-09	Si2	: +.2406E-03
Si2C	: +.6264E-04	Si3	: +.6980E-07
Ar	: +.8928E+01	Ar+	: +.1138E-09
CCl4	: +.5410E-16	Si LIQUIDE	: +.1000E-14
C SOLIDE	: +.1000E-14	Si SOLIDE	: +.1000E-14
Si2H6 SOLIDE	: +.1000E-14	SiC SOLIDE	: +.1000E-14

TETRACHLORURE DE SILICIUM PRESSION: 1.000E+00 ATMS

T: 4300 CS:+.780E+04 H:+.178E+08 S:+.138E+05 G:-.448E+08 MV:+.166E+03

H	: +.2373E+02	H2	: +.2175E+01
H+	: +.2113E-07	H-	: +.5988E-05
E	: +.2084E-02	C GAZ	: +.2953E+00
C+	: +.2652E-06	C-	: +.3020E-06
CH	: +.9205E-02	CH2	: +.1103E-03
CH3	: +.1584E-04	CH4	: +.7303E-07
C2	: +.1793E-01	C2-	: +.1753E-04
C2H	: +.4158E-01	C2H2.	: +.2076E-02
C2H4	: +.1835E-08	C3	: +.2793E-02
Cl	: +.3094E+01	Cl+	: +.3940E-07
Cl-	: +.6381E-03	Cl2	: +.1137E-03
HCl	: +.4289E+00	Si GAZ	: +.8549E+00
Si+	: +.2746E-02	SiC GAZ	: +.2254E-02
SiC2	: +.3957E-02	SiCl	: +.7950E-02
SiCl2	: +.9445E-04	SiCl3	: +.4297E-07
SiCl4	: +.1652E-11	SiH	: +.1055E-01
SiH4	: +.1103E-09	Si2	: +.1940E-03
Si2C	: +.3612E-04	Si3	: +.4246E-07
Ar	: +.8928E+01	Ar+	: +.2423E-09
CCl4	: +.2994E-16	Si LIQUIDE	: +.1000E-14
C SOLIDE	: +.1000E-14	Si SOLIDE	: +.1000E-14
Si2H6 SOLIDE	: +.1000E-14	SiC SOLIDE	: +.1000E-14

T: 4400 CS:+.667E+04 H:+.185E+08 S:+.140E+05 G:-.463E+08 MV:+.164E+03

H	: +.2472E+02	H2	: +.1735E+01
H+	: +.3980E-07	H-	: +.7592E-05
E	: +.2855E-02	C GAZ	: +.3403E+00
C+	: +.4745E-06	C-	: +.4088E-06
CH	: +.8656E-02	CH2	: +.8046E-04
CH3	: +.8744E-05	CH4	: +.3114E-07
C2	: +.1585E-01	C2-	: +.1540E-04
C2H	: +.2602E-01	C2H2	: +.9909E-03
C2H4	: +.6119E-09	C3	: +.1706E-02
Cl	: +.3186E+01	Cl+	: +.7089E-07
Cl-	: +.6699E-03	Cl2	: +.1008E-03
HCl	: +.3386E+00	Si GAZ	: +.8595E+00
Si+	: +.3548E-02	SiC GAZ	: +.1918E-02
SiC2	: +.2266E-02	SiCl	: +.6282E-02
SiCl2	: +.5568E-04	SiCl3	: +.2063E-07
SiCl4	: +.6385E-12	SiH	: +.8907E-02
SiH4	: +.5295E-10	Si2	: +.1577E-03
Si2C	: +.2040E-04	Si3	: +.2643E-07
Ar	: +.8928E+01	Ar+	: +.5015E-09
CCl4	: +.1595E-16	Si LIQUIDE	: +.1000E-14
C SOLIDE	: +.1000E-14	Si SOLIDE	: +.1000E-14
Si2H6 SOLIDE	: +.1000E-14	SiC SOLIDE	: +.1000E-14

TETRACHLORURE DE SILICIUM PRESSION: 1.000E+00 ATMS

T: 4500 CS:+.564E+04 H:+.190E+08 S:+.141E+05 G:-.478E+08 MV:+.162E+03

H	: +.2551E+02	H2	: +.1381E+01
H+	: +.7272E-07	H-	: +.9406E-05
E	: +.3832E-02	C GAZ	: +.3741E+00
C+	: +.7981E-06	C-	: +.5215E-06
CH	: +.7796E-02	CH2	: +.5656E-04
CH3	: +.4685E-05	CH4	: +.1298E-07
C2	: +.1301E-01	C2-	: +.1250E-04
C2H	: +.1528E-01	C2H2	: +.4472E-03
C2H4	: +.1940E-09	C3	: +.9458E-03
Cl	: +.3258E+01	Cl+	: +.1243E-06
Cl-	: +.6944E-03	Cl2	: +.8900E-04
HCl	: +.2672E+00	Si GAZ	: +.8627E+00
Si+	: +.4548E-02	SiC GAZ	: +.1579E-02
SiC2	: +.1230E-02	SiCl	: +.4992E-02
SiCl2	: +.3333E-04	SiCl3	: +.1012E-07
SiCl4	: +.2539E-12	SiH	: +.7523E-02
SiH4	: +.2570E-10	Si2	: +.1294E-03
Si2C	: +.1137E-04	Si3	: +.1680E-07
Ar	: +.8928E+01	Ar+	: +.1010E-08
CCl4	: +.8290E-17	Si LIQUIDE	: +.1000E-14
C SOLIDE	: +.1000E-14	Si SOLIDE	: +.1000E-14
Si2H6 SOLIDE	: +.1000E-14	SiC SOLIDE	: +.1000E-14

T: 4600 CS:+.477E+04 H:+.195E+08 S:+.143E+05 G:-.492E+08 MV:+.161E+03

H	: +.2614E+02	H2	: +.1099E+01
H+	: +.1292E-06	H-	: +.1143E-04
E	: +.5052E-02	C GAZ	: +.3975E+00
C+	: +.1279E-05	C-	: +.6359E-06
CH	: +.6817E-02	CH2	: +.3886E-04
CH3	: +.2473E-05	CH4	: +.5368E-08
C2	: +.1016E-01	C2-	: +.9623E-05
C2H	: +.8630E-02	C2H2	: +.1956E-03
C2H4	: +.6008E-10	C3	: +.4932E-03
Cl	: +.3315E+01	Cl+	: +.2126E-06
Cl-	: +.7125E-03	Cl2	: +.7852E-04
HCl	: +.2113E+00	Si GAZ	: +.8646E+00
Si+	: +.5785E-02	SiC GAZ	: +.1273E-02
SiC2	: +.6476E-03	SiCl	: +.3992E-02
SiCl2	: +.2028E-04	SiCl3	: +.5079E-08
SiCl4	: +.1040E-12	SiH	: +.6367E-02
SiH4	: +.1266E-10	Si2	: +.1069E-03
Si2C	: +.6316E-05	Si3	: +.1089E-07
Ar	: +.8928E+01	Ar+	: +.1983E-08
CCl4	: +.4263E-17	Si LIQUIDE	: +.1000E-14
C SOLIDE	: +.1000E-14	Si SOLIDE	: +.1000E-14
Si2H6 SOLIDE	: +.1000E-14	SiC SOLIDE	: +.1000E-14

TETRACHLORURE DE SILICIUM PRESSION: 1.000E+00 ATMS

T: 4700 CS:+.408E+04 H:+.199E+08 S:+.144E+05 G:-.507E+08 MV:+.160E+03

H	: +.2663E+02	H2	: +.8762E+00
H+	: +.2240E-06	H-	: +.1366E-04
E	: +.6556E-02	C GAZ	: +.4129E+00
C+	: +.1976E-05	C-	: +.7509E-06
CH	: +.5858E-02	CH2	: +.2644E-04
CH3	: +.1303E-05	CH4	: +.2233E-08
C2	: +.7719E-02	C2-	: +.7181E-05
C2H	: +.4793E-02	C2H2	: +.8482E-04
C2H4	: +.1860E-10	C3	: +.2497E-03
Cl	: +.3360E+01	Cl+	: +.3558E-06
Cl-	: +.7253E-03	Cl2	: +.6929E-04
HCl	: +.1677E+00	Si GAZ	: +.8654E+00
Si+	: +.7301E-02	SiC GAZ	: +.1015E-02
SiC2	: +.3375E-03	SiCl	: +.3212E-02
SiCl2	: +.1254E-04	SiCl3	: +.2609E-08
SiCl4	: +.4393E-13	SiH	: +.5403E-02
SiH4	: +.6341E-11	Si2	: +.8900E-04
Si2C	: +.3532E-05	Si3	: +.7195E-08
Ar	: +.8928E+01	Ar+	: +.3797E-08
CCl4	: +.2196E-17	Si LIQUIDE	: +.1000E-14
C SOLIDE	: +.1000E-14	Si SOLIDE	: +.1000E-14
Si2H6 SOLIDE	: +.1000E-14	SiC SOLIDE	: +.1000E-14

T: 4800 CS:+.354E+04 H:+.203E+08 S:+.144E+05 G:-.522E+08 MV:+.159E+03

H	: +.2702E+02	H2	: +.7013E+00
H+	: +.3791E-06	H-	: +.1610E-04
E	: +.8391E-02	C GAZ	: +.4229E+00
C+	: +.2970E-05	C-	: +.8672E-06
CH	: +.4992E-02	CH2	: +.1797E-04
CH3	: +.6915E-06	CH4	: +.9429E-09
C2	: +.5791E-02	C2-	: +.5282E-05
C2H	: +.2658E-02	C2H2	: +.3704E-04
C2H4	: +.5853E-11	C3	: +.1255E-03
Cl	: +.3394E+01	Cl+	: +.5830E-06
Cl-	: +.7337E-03	Cl2	: +.6124E-04
HCl	: +.1337E+00	Si GAZ	: +.8654E+00
Si+	: +.9143E-02	SiC GAZ	: +.8068E-03
SiC2	: +.1766E-03	SiCl	: +.2602E-02
SiCl2	: +.7886E-05	SiCl3	: +.1371E-08
SiCl4	: +.1912E-13	SiH	: +.4602E-02
SiH4	: +.3238E-11	Si2	: +.7461E-04
Si2C	: +.2000E-05	Si3	: +.4833E-08
Ar	: +.8928E+01	Ar+	: +.7097E-08
CCl4	: +.1143E-17	Si LIQUIDE	: +.1000E-14
C SOLIDE	: +.1000E-14	Si SOLIDE	: +.1000E-14
Si2H6 SOLIDE	: +.1000E-14	SiC SOLIDE	: +.1000E-14

TETRACHLORURE DE SILICIUM PRESSION: 1.000E+00 ATMS

T: 4900 CS:+.313E+04 H:+.206E+08 S:+.145E+05 G:-.538E+08 MV:+.158E+03

H	: +.2733E+02	H2	: +.5639E+00
H+	: +.6280E-06	H-	: +.1875E-04
E	: +.1061E-01	C GAZ	: +.4294E+00
C+	: +.4369E-05	C-	: +.9857E-06
CH	: +.4242E-02	CH2	: +.1227E-04
CH3	: +.3718E-06	CH4	: +.4065E-09
C2	: +.4334E-02	C2-	: +.3870E-05
C2H	: +.1487E-02	C2H2	: +.1644E-04
C2H4	: +.1891E-11	C3	: +.6350E-04
Cl	: +.3421E+01	Cl+	: +.9369E-06
Cl-	: +.7387E-03	Cl2	: +.5423E-04
HCl	: +.1072E+00	Si GAZ	: +.8646E+00
Si+	: +.1136E-01	SiC GAZ	: +.6426E-03
SiC2	: +.9361E-04	SiCl	: +.2122E-02
SiCl2	: +.5037E-05	SiCl3	: +.7367E-09
SiCl4	: +.8569E-14	SiH	: +.3934E-02
SiH4	: +.1686E-11	Si2	: +.6293E-04
Si2C	: +.1152E-05	Si3	: +.3297E-08
Ar	: +.8928E+01	Ar+	: +.1296E-07
CCl4	: +.6042E-18	Si LIQUIDE	: +.1000E-14
C SOLIDE	: +.1000E-14	Si SOLIDE	: +.1000E-14
Si2H6 SOLIDE	: +.1000E-14	SiC SOLIDE	: +.1000E-14

T: 5000 CS:+.282E+04 H:+.209E+08 S:+.146E+05 G:-.553E+08 MV:+.158E+03

H	: +.2757E+02	H2	: +.4558E+00
H+	: +.1020E-05	H-	: +.2162E-04
E	: +.1326E-01	C GAZ	: +.4338E+00
C+	: +.6311E-05	C-	: +.1107E-05
CH	: +.3607E-02	CH2	: +.8446E-05
CH3	: +.2031E-06	CH4	: +.1795E-09
C2	: +.3254E-02	C2-	: +.2841E-05
C2H	: +.8428E-03	C2H2	: +.7459E-05
C2H4	: +.6304E-12	C3	: +.3260E-04
Cl	: +.3443E+01	Cl+	: +.1479E-05
Cl-	: +.7409E-03	Cl2	: +.4816E-04
HCl	: +.8642E-01	Si GAZ	: +.8631E+00
Si+	: +.1402E-01	SiC GAZ	: +.5139E-03
SiC2	: +.5047E-04	SiCl	: +.1741E-02
SiCl2	: +.3267E-05	SiCl3	: +.4046E-09
SiCl4	: +.3951E-14	SiH	: +.3376E-02
SiH4	: +.8957E-12	Si2	: +.5337E-04
Si2C	: +.6746E-06	Si3	: +.2282E-08
Ar	: +.8928E+01	Ar+	: +.2317E-07
CCl4	: +.3252E-18	Si LIQUIDE	: +.1000E-14
C SOLIDE	: +.1000E-14	Si SOLIDE	: +.1000E-14
Si2H6 SOLIDE	: +.1000E-14	SiC SOLIDE	: +.1000E-14

TETRACHLORURE DE SILICIUM PRESSION: 1.000E+00 ATMS

T: 5100 CS:+.258E+04 H:+.211E+08 S:+.146E+05 G:-.568E+08 MV:+.157E+03

H	: +.2775E+02	H2	: +.3706E+00
H+	: +.1625E-05	H-	: +.2471E-04
E	: +.1641E-01	C GAZ	: +.4369E+00
C+	: +.8976E-05	C-	: +.1233E-05
CH	: +.3074E-02	CH2	: +.5870E-05
CH3	: +.1130E-06	CH4	: +.8127E-10
C2	: +.2458E-02	C2-	: +.2096E-05
C2H	: +.4856E-03	C2H2.	: +.3467E-05
C2H4	: +.2174E-12	C3	: +.1705E-04
Cl	: +.3459E+01	Cl+	: +.2294E-05
Cl-	: +.7408E-03	Cl2	: +.4289E-04
HCl	: +.7013E-01	Si GAZ	: +.8608E+00
Si+	: +.1716E-01	SiC GAZ	: +.4131E-03
SiC2	: +.2774E-04	SiCl	: +.1438E-02
SiCl2	: +.2150E-05	SiCl3	: +.2269E-09
SiCl4	: +.1872E-14	SiH	: +.2909E-02
SiH4	: +.4854E-12	Si2	: +.4550E-04
Si2C	: +.4023E-06	Si3	: +.1599E-08
Ar	: 1.8928E+01	Ar+	: +.4054E-07
CCl4	: +.1785E-18	Si LIQUIDE	: +.1000E-14
C SOLIDE	: +.1000E-14	Si SOLIDE	: +.1000E-14
Si2H6 SOLIDE	: +.1000E-14	SiC SOLIDE	: +.1000E-14

T: 5200 CS:+.240E+04 H:+.214E+08 S:+.147E+05 G:-.583E+08 MV:+.157E+03

H	: +.2790E+02	H2	: +.3031E+00
H+	: +.2544E-05	H-	: +.2801E-04
E	: +.2011E-01	C GAZ	: +.4390E+00
C+	: +.1259E-04	C-	: +.1362E-05
CH	: +.2630E-02	CH2	: +.4123E-05
CH3	: +.6398E-07	CH4	: +.3775E-10
C2	: +.1871E-02	C2-	: +.1557E-05
C2H	: +.2846E-03	C2H2	: +.1652E-05
C2H4	: +.7765E-13	C3	: +.9090E-05
Cl	: +.3472E+01	Cl+	: +.3503E-05
Cl-	: +.7389E-03	Cl2	: +.3832E-04
HCl	: +.5726E-01	Si GAZ	: +.8579E+00
Si+	: +.2086E-01	SiC GAZ	: +.3341E-03
SiC2	: +.1555E-04	SiCl	: +.1194E-02
SiCl2	: +.1436E-05	SiCl3	: +.1298E-09
SiCl4	: +.9106E-15	SiH	: +.2516E-02
SiH4	: +.2682E-12	Si2	: +.3896E-04
Si2C	: +.2441E-06	Si3	: +.1134E-08
Ar	: +.8928E+01	Ar+	: +.6956E-07
CCl4	: +.9987E-19	Si LIQUIDE	: +.1000E-14
C SOLIDE	: +.1000E-14	Si SOLIDE	: +.1000E-14
Si2H6 SOLIDE	: +.1000E-14	SiC SOLIDE	: +.1000E-14

TETRACHLORURE DE SILICIUM PRESSION: 1.000E+00 ATMS

T: 5300 CS:+.227E+04 H:+.216E+08 S:+.147E+05 G:-.599E+08 MV:+.157E+03

H	+.2802E+02	H2	+.2494E+00
H+	+.3920E-05	H-	+.3153E-04
E	+.2444E-01	C GAZ	+.4406E+00
C+	+.1745E-04	C-	+.1495E-05
CH	+.2258E-02	CH2	+.2928E-05
CH3	+.3690E-07	CH4	+.1798E-10
C2	+.1435E-02	C2-	+.1166E-05
C2H	+.1698E-03	C2H2	+.8071E-06
C2H4	+.2870E-13	C3	+.4947E-05
Cl	+.3483E+01	Cl+	+.5270E-05
Cl-	+.7355E-03	Cl2	+.3435E-04
HCl	+.4706E-01	Si GAZ	+.8542E+00
Si+	+.2519E-01	SiC GAZ	+.2718E-03
SiC2	+.8884E-05	SiCl	+.9967E-03
SiCl2	+.9712E-06	SiCl3	+.7566E-10
SiCl4	+.4541E-15	SiH	+.2185E-02
SiH4	+.1511E-12	Si2	+.3350E-04
Si2C	+.1506E-06	Si3	+.8126E-09
Ar	+.8928E+01	Ar+	+.1171E-06
CCl4	+.5698E-19	Si LIQUIDE	+.1000E-14
C SOLIDE	+.1000E-14	Si SOLIDE	+.1000E-14
Si2H6 SOLIDE	+.1000E-14	SiC SOLIDE	+.1000E-14

T: 5400 CS:+.217E+04 H:+.218E+08 S:+.148E+05 G:-.614E+08 MV:+.156E+03

H	+.2812E+02	H2	+.2064E+00
H+	+.5949E-05	H-	+.3526E-04
E	+.2947E-01	C GAZ	+.4418E+00
C+	+.2390E-04	C-	+.1632E-05
CH	+.1948E-02	CH2	+.2102E-05
CH3	+.2167E-07	CH4	+.8781E-11
C2	+.1111E-02	C2-	+.8795E-06
C2H	+.1031E-03	C2H2	+.4041E-06
C2H4	+.1097E-13	C3	+.2747E-05
Cl	+.3491E+01	Cl+	+.7817E-05
Cl-	+.7309E-03	Cl2	+.3088E-04
HCl	+.3891E-01	Si GAZ	+.8496E+00
Si+	+.3021E-01	SiC GAZ	+.2224E-03
SiC2	+.5172E-05	SiCl	+.8364E-03
SiCl2	+.6654E-06	SiCl3	+.4490E-10
SiCl4	+.2318E-15	SiH	+.1904E-02
SiH4	+.8664E-13	Si2	+.2890E-04
Si2C	+.9435E-07	Si3	+.5878E-09
Ar	+.8928E+01	Ar+	+.1937E-06
CCl4	+.3314E-19	Si LIQUIDE	+.1000E-14
C SOLIDE	+.1000E-14	Si SOLIDE	+.1000E-14
Si2H6 SOLIDE	+.1000E-14	SiC SOLIDE	+.1000E-14

TETRACHLORURE DE SILICIUM PRESSION: 1.000E+00 ATMS

T: 5500 CS:+.209E+04 H:+.220E+08 S:+.148E+05 G:-.630E+08 MV:+.156E+03

H	: +.2819E+02	H2	: +.1719E+00
H+	: +.8899E-05	H-	: +.3919E-04
E	: +.3527E-01	C GAZ	: +.4426E+00
C+	: +.3239E-04	C-	: +.1773E-05
CH	: +.1688E-02	CH2	: +.1525E-05
CH3	: +.1295E-07	CH4	: +.4392E-11
C2	: +.8668E-03	C2-	: +.6689E-06
C2H	: +.6363E-04	C2H2	: +.2072E-06
C2H4	: +.4334E-14	C3	: +.1555E-05
Cl	: +.3498E+01	Cl+	: +.1144E-04
Cl-	: +.7251E-03	Cl2	: +.2786E-04
HCl	: +.3236E-01	Si GAZ	: +.8443E+00
Si+	: +.3599E-01	SiC GAZ	: +.1830E-03
SiC2	: +.3066E-05	SiCl	: +.7053E-03
SiCl2	: +.4614E-06	SiCl3	: +.2711E-10
SiCl4	: +.1211E-15	SiH	: +.1664E-02
SiH4	: +.5057E-13	Si2	: +.2500E-04
Si2C	: +.5999E-07	Si3	: +.4288E-09
Ar	: +.8928E+01	Ar+	: +.3151E-06
CCl4	: +.1963E-19	Si LIQUIDE	: +.1000E-14
C SOLIDE	: +.1000E-14	Si SOLIDE	: +.1000E-14
Si2H6 SOLIDE	: +.1000E-14	SiC SOLIDE	: +.1000E-14

T: 5600 CS:+.204E+04 H:+.222E+08 S:+.149E+05 G:-.645E+08 MV:+.156E+03

H	: +.2825E+02	H2	: +.1439E+00
H+	: +.1314E-04	H-	: +.4333E-04
E	: +.4192E-01	C GAZ	: +.4433E+00
C+	: +.4345E-04	C-	: +.1917E-05
CH	: +.1469E-02	CH2	: +.1118E-05
CH3	: +.7875E-08	CH4	: +.2248E-11
C2	: +.6819E-03	C2-	: +.5127E-06
C2H	: +.3993E-04	C2H2	: +.1087E-06
C2H4	: +.1766E-14	C3	: +.8975E-06
Cl	: +.3503E+01	Cl+	: +.1654E-04
Cl-	: +.7185E-03	Cl2	: +.2521E-04
HCl	: +.2708E-01	Si GAZ	: +.8380E+00
Si+	: +.4261E-01	SiC GAZ	: +.1513E-03
SiC2	: +.1848E-05	SiCl	: +.5973E-03
SiCl2	: +.3235E-06	SiCl3	: +.1663E-10
SiCl4	: +.6456E-16	SiH	: +.1460E-02
SiH4	: +.3001E-13	Si2	: +.2168E-04
Si2C	: +.3866E-07	Si3	: +.3152E-09
Ar	: +.8929E+01	Ar+	: +.5043E-06
CCl4	: +.1183E-19	Si LIQUIDE	: +.1000E-14
C SOLIDE	: +.1000E-14	Si SOLIDE	: +.1000E-14
Si2H6 SOLIDE	: +.1000E-14	SiC SOLIDE	: +.1000E-14

TETRACHLORURE DE SILICIUM PRESSION: 1.000E+00 ATMS

T: 5700 CS:+.200E+04 H:+.224E+08 S:+.149E+05 G:-.661E+08 MV:+.156E+03

H	: +.2830E+02	H2	: +.1212E+00
H+	: +.1914E-04	H-	: +.4765E-04
E	: +.4948E-01	C GAZ	: +.4438E+00
C+	: +.5777E-04	C-	: +.2063E-05
CH	: +.1284E-02	CH2	: +.8278E-06
CH3	: +.4865E-08	CH4	: +.1177E-11
C2	: +.5408E-03	C2-	: +.3958E-06
C2H	: +.2545E-04	C2H2	: +.5827E-07
C2H4	: +.7415E-15	C3	: +.5274E-06
Cl	: +.3507E+01	Cl+	: +.2364E-04
Cl-	: +.7110E-03	Cl2	: +.2289E-04
HCl	: +.2279E-01	Si GAZ	: +.8308E+00
Si+	: +.5014E-01	SiC GAZ	: +.1258E-03
SiC2	: +.1132E-05	SiCl	: +.5079E-03
SiCl2	: +.2292E-06	SiCl3	: +.1036E-10
SiCl4	: +.3513E-16	SiH	: +.1283E-02
SiH4	: +.1809E-13	Si2	: +.1884E-04
Si2C	: +.2522E-07	Si3	: +.2332E-09
Ar	: +.8928E+01	Ar+	: +.7951E-06
CCl4	: +.7255E-20	Si LIQUIDE	: +.1000E-14
C SOLIDE	: +.1000E-14	Si SOLIDE	: +.1000E-14
Si2H6 SOLIDE	: +.1000E-14	SiC SOLIDE	: +.1000E-14

T: 5800 CS:+.197E+04 H:+.226E+08 S:+.149E+05 G:-.676E+08 MV:+.156E+03

H	: +.2834E+02	H2	: +.1026E+00
H+	: +.2757E-04	H-	: +.5215E-04
E	: +.5803E-01	C GAZ	: +.4442E+00
C+	: +.7612E-04	C-	: +.2212E-05
CH	: +.1127E-02	CH2	: +.6189E-06
CH3	: +.3053E-08	CH4	: +.6289E-12
C2	: +.4322E-03	C2-	: +.3078E-06
C2H	: +.1646E-04	C2H2	: +.3190E-07
C2H4	: +.3204E-15	C3	: +.3153E-06
Cl	: +.3511E+01	Cl+	: +.3340E-04
Cl-	: +.7027E-03	Cl2	: +.2084E-04
HCl	: +.1928E-01	Si GAZ	: +.8225E+00
Si+	: +.5865E-01	SiC GAZ	: +.1050E-03
SiC2	: +.7043E-06	SiCl	: +.4335E-03
SiCl2	: +.1640E-06	SiCl3	: +.6541E-11
SiCl4	: +.1948E-16	SiH	: +.1132E-02
SiH4	: +.1107E-13	Si2	: +.1640E-04
Si2C	: +.1665E-07	Si3	: +.1734E-09
Ar	: +.8928E+01	Ar+	: +.1236E-05
CCl4	: +.4520E-20	Si LIQUIDE	: +.1000E-14
C SOLIDE	: +.1000E-14	Si SOLIDE	: +.1000E-14
Si2H6 SOLIDE	: +.1000E-14	SiC SOLIDE	: +.1000E-14

TETRACHLORURE DE SILICIUM PRESSION: 1.000E+00 ATMS

T: 5900 CS:[illegible] H:+.228E+08 S:+.150E+05 G:-.692E+08 MV:+.156E+03

H	: +.[illegible]E+02	H2	: +.8735E-01
H+	: +.[illegible]E-04	H-	: +.5681E-04
E	: +.[illegible]E-01	C GAZ	: +.4445E+00
C+	: +.[illegible]E-04	C-	: +.2362E-05
CH	: +.[illegible]E-03	CH2	: +.4670E-06
CH3	: +.1945E-08	CH4	: +.3430E-12
C2	: +.3479E-03	C2-	: +.2410E-06
C2H	: +.1080E-04	C2H2	: +.1782E-07
C2H4	: +.1423E-15	C3	: +.1917E-06
Cl	: +.3514E+01	Cl+	: +.4672E-04
Cl-	: +.6937E-03	Cl2	: +.1902E-04
HCl	: +.1640E-01	Si GAZ	: +.8132E+00
Si+	: +.6821E-01	SiC GAZ	: +.8800E-04
SiC2	: +.4443E-06	SiCl	: +.3712E-03
SiCl2	: +.1185E-06	SiCl3	: +.4187E-11
SiCl4	: +.1099E-16	SiH	: +.9998E-03
SiH4	: +.6870E-14	Si2	: +.1428E-04
Si2C	: +.1110E-07	Si3	: +.1296E-09
Ar	: +.8928E+01	Ar+	: +.1895E-05
CCl4	: +.2861E-20	Si LIQUIDE	: +.1000E-14
C SOLIDE	: +.1000E-14	Si SOLIDE	: +.1000E-14
Si2H6 SOLIDE	: +.1000E-14	SiC SOLIDE	: +.1000E-14

T: 6000 CS:+.195E+04 H:+.230E+08 S:+.150E+05 G:-.707E+08 MV:+.156E+03

H	: +.2841E+02	H2	: +.7471E-01
H+	: +.5536E-04	H-	: +.6160E-04
E	: +.7839E-01	C GAZ	: +.4447E+00
C+	: +.1291E-03	C-	: +.2514E-05
CH	: +.8786E-03	CH2	: +.3555E-06
CH3	: +.1257E-08	CH4	: +.1908E-12
C2	: +.2820E-03	C2-	: +.1899E-06
C2H	: +.7186E-05	C2H2	: +.1014E-07
C2H4	: +.6487E-16	C3	: +.1184E-06
Cl	: +.3516E+01	Cl+	: +.6470E-04
Cl-	: +.6840E-03	Cl2	: +.1742E-04
HCl	: +.1402E-01	Si GAZ	: +.8027E+00
Si+	: +.7889E-01	SiC GAZ	: +.7404E-04
SiC2	: +.2840E-06	SiCl	: +.3188E-03
SiCl2	: +.8629E-07	SiCl3	: +.2714E-11
SiCl4	: +.6309E-17	SiH	: +.8852E-03
SiH4	: +.4320E-14	Si2	: +.1245E-04
Si2C	: +.7474E-08	Si3	: +.9725E-10
Ar	: +.8928E+01	Ar+	: +.2869E-05
CCl4	: +.1837E-20	Si LIQUIDE	: +.1000E-14
C SOLIDE	: +.1000E-14	Si SOLIDE	: +.1000E-14
Si2H6 SOLIDE	: +.1000E-14	SiC SOLIDE	: +.1000E-14

APPENDIX B

INSTRUMENTATION SPECIFICATIONS

PJR INSTRUMENT LIST

Tag #	Manufacturer	Model
FT-110	Sierra	830-21-3-600SLM, H2-V4
FT-120	Sierra	730-16-2-700SLM, Ar-V4
FT-210	Sierra	830-22-0-2800SLM, H2-V4
FT-310	Sierra	730-16-2-700SLM, Ar-V4
FT-310	Sierra	830-22-0-2800SLM-V4
FT-570	Foxboro	E83L-01S70SI
FT-571	Foxboro	E83L-01S70SI
PT-560	Foxboro	841GM-AI
PT-660	Foxboro	841GM-AI
DPT-680	Foxboro	843DP-H2I-M
LT-740	Foxboro	843DP-H2I-M
LSH-740	Anderson	Flotech Model L6EPB-SS3S
LSL-440	Anderson	Flotech Model L6EPB-SS3S
PSL-160	United Electric	H100-191-M201
PSL-260	Untied Electric	H100-191-M201
DPSH	United Electric	J21K-S150
DPSH	United Electric	J21K-S150
FSL-750	Gems	FS-200 ADJ
FSL-571	Gems	FS-200 ADJ
PCV-011	Fisher	Type 630
PCV-021	Fisher	Type 630
FCV-110	Badger	1/2" ATO "G" Trim
FCV-120	Badger	1/2" ATC "D" Trim
FCV-210	Badger	1/2" ATO "D" Trim
FCV-220	Badger	1/2" ATC "D" Trim
FCV-310	Badge	1/2" ATO "E" Trim
LCV-740	Fisher	1" 513-R-B (3/4" Microfor)
FY-110	Fisher	Type 546
FY-120	Fisher	Type 546
FY-210	Fisher	Type 546
FY-220	Fisher	Type 546
FY-310	Fisher	Type 546
LY-740	Fisher	Type 546
PCV-Inst Air	Fisher	64R
TY-360	Halmar	LFZ1

Tag #	Manufacturer	Model
FZ-010	Whitey	SS-45S8-133NC
FSV-010	Asco	8320A5
FZ-680	Asco	8262B202
FZ-681	Asco	8262B202
FZ-682	Asco	8262B202
FZ-683	Asco	8262B202
FZ-740	Asco	8210B54
FSV-120	Asco	8320A5
FSV-220	Asco	8320A5
FSV	Asco	8320A5
FSV	Asco	8320A5
FSV	Asco	8320A5
FSV	Asco	8320A5
PSE-740	Continental	2" CDCV
FI-130	Pilot Plant Stock	
FI-450	Brooks	1110-06
FI-740	Brooks	1303
Relay Panel	Shop Stock	
Relays (16)	Potter & Brumfield	KRPA11DGN
T/C Cable	Dekoron	1820-10630

I/O LIST FOR PJR SCALEUP

ANALOG INPUTS (4-20 MA)

FT-110	Primary H2
FT-120	Primary Ar
FT-210	Secondary H2
FT-220	Secondary Ar
FT-310	Tertiary H2
FT-570	Cooling Water to Starter Unit
FT-571	Cooling Water to Reactor Coils
IT	Torch Current
VT	Torch Voltage
LT-740	Scrubber Level
PT-560	Reactor Pressure
PE-660	Baghouse Outlet Pressure
DPT-???	Baghouse Differential Pressure

ANALOG INPUTS (THERMOCOUPLE OR MILLIVOLT)

TE-160	Primary Gas Feed
TE-260	Secondary Gas Feed
TE-360	Tertiary H2 Feed
TE-361	Tertiary H2 Feed
TE-363	Tertiary H2/CH3SiCl3 Feed
TE-380	Tertiary H2 Feed Heat Tape Shutdown
TE-570	Cooling Water to Starter Unit
TE-571	Cooling Water from Starter Unit
TE-572→576	Reactor Cooling Water Tubes (5)
TE-577	Reactor Cooling Water Outlet
TE-580→596	Reactor Wall Temperatures (17)
TE-660	Reactor Product Outlet
TE-740	Scrubber Liquid Outlet
TE-780	Scrubber Overhead Outlet

ANALOG OUTPUTS (4-20 MA)

FCV-110	Primary H2
FCV-120	Primary Ar
FCV-210	Secondary H2
FCV-220	Secondary Ar
FCV-310	Tertiary H2
LCV-740	Scrubber Level
JY-550	Torch Power Level

DIGITAL INPUTS

PSL-160	Primary Gas Feed
PSL-270	Secondary Gas Feed
HS-???	Local Shutdown
LSH-741	Scrubber High Level
LSL-741	Scrubber Low Level
	DP Switch on Ar/CH3SiCl3 Clean Outs

DIGITAL OUTPUTS (24 VDC)

FZ-010	H2 Feed
XY-???	Metering Pump On/Off
TSH-???	Heat Tape On/Off
XY-???	Starter Circuit Permissive
FZ-680	Baghouse Ar Blowback #1
FZ-681	Baghouse Ar Blowback #2
FZ-682	Baghouse Ar Blowback #3
FZ-683	Baghouse Ar Blowback #4
FZ-740	Scrubber Liquid Feed On/Off
	Power Supply Permissive
	Add 4 Valves to Ch3SiCl3 Clean Outs
	4 Cables Minimum

THE STANDARD OIL COMPANY
CONTROL VALVES

	ITEM NO.	1	2	3
	MANUFACTURER			
	MODEL NO			
	TAG NO.	FCV - 110	FCV - 120	FCV - 210
	SERVICE DESCRIPTION	PRIMARY H2	PRIMARY ARGON	SECONDARY H2
DESIGN & CONSTRUCTION	BODY TYPE (GLOBE, ETC.)			
	FUNCTION (THROTTLING, ETC.)			
	NOMINAL SIZE			
	BODY CONNECTIONS & RATING			
	REDUCED AREA PORTS			
	MATERIALS : BODY			
	PLUG			
	SEAT			
	VALVE CHARACTERISTIC			
	CALCULATED Cv	~~0.056~~ 0.025	~~0.31~~ 0.138	~~0.28~~ 0.125
	VALVE Cv			
	INPUT SIGNAL	3-15 PSIG		
	VALVE TO: ~~OPEN w/INCREASE OF~~			
	CLOSE w/INCREASE OF	FLOW	FLOW	FLOW
	FAIL POSITION	FC	FO	FC
	TIGHT SHUTOFF			
	ISA LEAKAGE CLASS			
OPTIONS	VALVE POSITIONER	NO	NO	NO
	FILTER REGULATOR			
PROCESS DATA	FLUID THRU VALVE	HYDROGEN	ARGON	HYDROGEN
	CORROSION DUE TO			
	INLET TEMPERATURE - NOR./MAX.	77°F	77°F	77°F
	INLET PRESSURE - NOR./MAX.	205 PSIG / 250 PSIG	205 PSIG / 250 PSIG	205 PSIG / 250 PSIG
	PRESSURE DROP	110 PSI	110 PSI	110 PSI
	NORMAL FLOW (SCFM)	14.4	5.3 - 17.65	72 SCFM
	MAX. FLOW	20	20	100 SCFM
	M.W. / S.G.	2.02 / 0.07	39.95 / 1.38	2.02 / 0.07
	VISCOSITY			
	LINE SIZE			

THE STANDARD OIL COMPANY

CONTROL VALVES

	ITEM NO.	4	5	6
	MANUFACTURER			
	MODEL NO			
	TAG NO.	FCV- 220	FCV-210	LCV-740
	SERVICE DESCRIPTION	SECONDARY ARGON	TERTIARY H2	SCRUBBER WATER
DESIGN & CONSTRUCTION	BODY TYPE (GLOBE, ETC.)			
	FUNCTION (THROTTLING, ETC.)			
	NOMINAL SIZE			
	BODY CONNECTIONS & RATING			
	REDUCED AREA PORTS			
	MATERIALS : BODY			
	PLUG			
	SEAT			
	VALVE CHARACTERISTIC			
	CALCULATED Cv	~~0.31~~ 0.138	~~0.16~~ 0.071	2.83
	VALVE Cv			
	INPUT SIGNAL			
	VALVE TO: OPEN w/INCREACE OF			LEVEL
	CLOSE w/INCREASE OF	FLOW	FLOW	
	FAIL POSITION	FO	FC	FC
	TIGHT SHUTOFF	STANDARD		
	ISA LEAKAGE CLASS			
OPTIONS	VALVE POSITIONER	NO	NO	
	FILTER REGULATOR			
PROCESS DATA	FLUID THRU VALVE	ARGON	HYDROGEN	WATER
	CORROSION DUE TO	—	—	1.3 wt % HCl
	INLET TEMPERATURE - NOR./MAX.	77°F	77°F	77°F
	INLET PRESSURE - NOR./MAX.	205 PSIG / 250 PSIG	205 PSIG / 250 PSIG	2PSIG / 5 PSIG
	PRESSURE DROP	110 PSI	110 PSI	2 PSIG
	NORMAL FLOW	5.3 - 17.65 SCFM	40.5 SCFM	4 GPM
	MAX. FLOW	20 SCFM	50 SCFM	
	M.W. / S.G.	39.95 / 1.38	2.02 / 0.07	
	VISCOSITY			
	LINE SIZE			

MASS FLOW SENSOR
SPECIFICATION SHEET

TAG NO	FT-110	FT-210	FT-310
SERVICE	PRIMARY H2	SECONDARY H2	TERTIARY H_2
PROCESS DATA			
FLUID	HYDROGEN	HYDROGEN	HYDROGEN
FLOW RATE			
MINIMUM			
NORMAL	408 SLM	2040 SLM	1150 SLM
MAXIMUM	600 SLM	2800 SLM	1700 SLM
TEMPERATURE	77°F	77°F	77°F
PRESSURE	205 PSIG	205 PSIG	205 PSIG
CALIBRATED RANGE	0-600 SLM	0-2800 SLM	0-1700 SLM
MANUFACTURER	SIERRA	SIERRA	SIERRA
MODEL NO	830-21-3-(600 SLM, H2)-V4	830-22-0-(2200 SLM, H2) - V4	830-22-0-(1700 SLM, H_2)-V
INSTRUMENT RANGE	0-1400 SLM H_2	0-2800 SLM H2	0-2800 SLM H_2
SIGNAL OUTPUT	4-20 ma	4-20 ma	4-20 ma
PROCESS CONNECTION	1" NPT	1½" NPT	1½" NPT
WETTED PARTS	316 SS	316 SS	316 SS
GASKETS	VITON	VITON	VITON
ACCURACY	±1% CALIBRATED RANGE	±1% FULL SCALE	±1% CALIBRATED RANGE
REPEATABILITY	±0.2% CALIBRATED RANGE	±0.2% FULL SCALE	±0.2% CALIBRATED RANGE
POWER SUPPLY	± 15 VDC	±15VDC	±15 VDC
OPTIONS	1-5 UNIT BULK POWER SUPPLY		
PRICE	$2885 w/Power Supply	$3,080	$3,080

MASS FLOW SENSOR SPECIFICATION SHEET

TAG NO	FT-120	FT-220
SERVICE	PRIMARY ARGON	SECONDARY ARGON
PROCESS DATA		
FLUID	ARGON	ARGON
FLOW RATE		
MINIMUM	150 SLM	150 SLM
NORMAL	500 SLM	500 SLM
MAXIMUM	700 SLM	700 SLM
TEMPERATURE	77 °F	77 °F
PRESSURE	205 PSIG	205 PSIG
CALIBRATED RANGE	0 - 700 SLM	0 - 700 SLM
MANUFACTURER	SIERRA	SIERRA
MODEL NO	730-16-2(700SLM, Ar) -V4	730-16-2-(700SLM, Ar)-V4
INSTRUMENT RANGE	0-800 SLM Ar (0-550 SLM N_2)	0-800 SLM Ar (0-550 SLM N_2)
SIGNAL OUTPUT	4-20 ma	4-20 ma
PROCESS CONNECTION	1 1/4"	1 1/4"
WETTED PARTS	316 SS	316 SS
GASKETS	VITON	VITON
ACCURACY	±2% OF READING + ½% FULL SCALE	±2% OF READING + ½% OF FULL SCALE
REPEATABILITY	±0.2% FULL SCALE	±0.2% FULL SCALE
POWER SUPPLY	+24 VDC (300 ma)	+24 VDC (300 ma)
OPTIONS	Cast Enclosure	Cast Enclosure
PRICE	$1255=	$1255=

THE STANDARD OIL COMPANY

PURCHASE ORDER

FOXBORO CO.
7123 PEARL ROAD
MIDDLEBURG HTS., OH 44130
ATTN: DOROTHY

IMPORTANT

04	13	87

PURCHASE ORDER DATE

72 0154 03810

PURCHASE ORDER NUMBER

CONTRACT/S.A. NUMBER

1. ABOVE PURCHASE ORDER AND/OR CONTRACT/S.A. NUMBERS MUST APPEAR ON ALL DOCUMENTS AND PACKAGES PERTAINING TO THIS ORDER.
2. MAIL SHIPPING NOTICE TO DESTINATION.
3. MAIL INVOICE IN QUADRUPLICATE WITH ORIGINAL BILL OF LADING, PAID FREIGHT OR EXPRESS BILLS TO:

THE STANDARD OIL COMPANY
4440 WARRENSVILLE CENTER ROAD
CLEVELAND, OHIO 44128
ATTN: ACCTS. PAYABLE

A.F.E. OR ACCOUNT(S) CHARGEABLE

19-0391-0786

SHIP TO:

THE STANDARD OIL COMPANY
19501 EMERY ROAD
CLEVELAND, OHIO 44128
ATTN: DAVE BEACH

Y DATE	SHIP VIA	VENDOR'S NO.
	BEST WAY	
	F.O.B. SHIPPING POINT	TAX STATUS CHARGE

DITY E	DESCRIPTION	QUANTITY (NUMBER OF UNITS OF MEASURE)	UNIT OF MEASURE	PRICE PER UNIT OF MEASURE	TRADE DISCOUNT %
	FOXBORO MODEL E83L-01S70SI VORTEX FLOWMETERS PER BELOW: LINE SIZE: 1" CONNECTION: 1" NPT FLOW RANGE: 3-45 GPM WATER @ 60° F & 60 PSIG OUTPUT: 4-20 MU TAGS: FT-570, FT-571	2	EA.	$1,161.00	
	FOXBORO MODEL 841GM-AI GAUGE PRESSURE TRANSMITTERS; RANGE LIMITS OF 7.5 AND 30 PSIG WITH 4-20 MU OUTPUT, CALIBRATE 0-30 PSIG	2	EA.	410.00	
	FOXBORO MODEL 843DP-H2I-M; INCLUDES STANDARD HOUSING; 75-300 IN H_2O RANGE LIMITS; 1/2" NPT CONNECTIONS & MOUNTING SET, CALIBRATE 0-75 IN H_2O	2	EA.	565.00	
	THIS IS CONFIRMATION OF AN ORAL PURCHASE CONTRACT MADE BY TELEPHON BETWEEN YOUR DOROTHY (216) 842-9300, AND OUR STEVE GRANT 581-5864 O 4/9/87. THIS IS NOT AN ADDITIONAL OFFER: DO NOT DUPLICATE.				

L. GRANT (216) 581-5864
STANDARD OIL COMPANY
0 WARRENSVILLE CENTER ROAD
VELAND, OHIO 44128

RECEIVED BY:

DATE RECEIVED:

ORNL/Sub/84-00214/1

INTERNAL DISTRIBUTION

1-2. Central Research Library
3. Document Reference Section
4-5. Laboratory Records Department
6. Laboratory Records, ORNL RC
7. ORNL Patent Section
8-10. M&C Records Office
11. L. F. Allard, Jr.
12. B. R. Appleton
13. R. L. Beatty
14. P. F. Becher
15. T. M. Besmann
16. P. J. Blau
17. A. Bleier
18. E. E. Bloom
19. K. W. Boling
20. R. A. Bradley
21. C. R. Brinkman
22. V. R. Bullington
23. R. S. Carlsmith
24. P. T. Carlson
25. J. V. Cathcart
26. G. M. Caton
27. R. H. Cooper, Jr.
28. S. A. David
29. J. H. DeVan
30. J. I. Federer
31. M. K. Ferber
32. W. Fulkerson
33. R. L. Graves
34. D. L. Greene
35. M. A. Janney
36-40. D. R. Johnson
41. R. R. Judkins
42. M. A. Karnitz
43. H. D. Kimrey, Jr.
44. T. G. Kollie
45. T. B. Lindemer
46. K. C. Liu
47. E. L. Long, Jr.
48. W. D. Manly
49. R. W. McClung
50. D. L. McElroy
51. J. R. Merriman
52. A. J. Moorhead
53. T. A. Nolan
54. J. L. Rich
55. C. R. Richmond
56. J. M. Robbins
57. M. W. Rosenthal
58. M. L. Santella
59. A. C. Schaffhauser
60. G. M. Slaughter
61. W. B. Snyder, Jr.
62. E. J. Soderstrom
63. D. P. Stinton
64. R. W. Swindeman
65. V. J. Tennery
66. T. N. Tiegs
67. J. R. Weir, Jr.
68. F. W. Wiffen
69. R. K. Williams
70. S. G. Winslow
71. C. S. Yust

EXTERNAL DISTRIBUTION

72. Donald F. Adams
University of Wyoming
Mechanical Engineering
Department
Laramie, WY 82071

73. Jane W. Adams
Corning Glass Works
SP-DV-21
Corning, NY 14831

74. J. Ahmad
Battelle Columbus Laboratories
Engineering Mechanics
Department
505 King Avenue
Columbus OH 43201-2693

75. Richard L. Allor
Ford Motor Company
Material Systems Reliability
Division
20000 Rotunda Drive
Post Office Box 2053
Dearborn, MI 48121-2053

76. Richard T. Alpaugh
U.S. Department of Energy
Office of Transportation
Systems
1000 Independence Avenue, S.W.
Forrestal Building CE-151
Washington DC 20585

77. Norman C. Anderson
Product Manager
Ceradyne, Inc.
Ceramic-to-Metal Division
3169 Redhill Avenue
Costa Mesa, CA 92626

78. H. Arbabi
Brunel University
Department of Materials
Technology
Uxbridge Middlesex UB8 3PH
UNITED KINGDOM

79. V. S. Avva
NC A&T State University
Department of Mechanical
Engineering
Greensboro, NC 27411

80. Kirit J. Bahnsali
U.S. Army Materials Technology
SLCMT-EMM
405 Arsenal Street
Watertown, MA 02172

81. John M. Bailey
Research Consultant
Caterpillar Inc.
Research Department
Technical Center, Building L
Post Office Box 1875
Peoria, IL 61656-1875

82. Murray Bailey
NASA Lewis Research Center
21000 Brookpark Road
MS:77-6
Cleveland, OH 44135

83. R. R. Baker
Vice President
Ceradyne, Inc.
3169 Red Hill Avenue
Costa Mesa, CA 92626

84. J. Gary Baldoni
GTE Laboratories Inc.
40 Sylvan Road
Waltham, MA 02254

85. P. M. Barnard
Principal Design Engineer
(Materials)
Ruston Gas Turbines Limited
New Products Division
Firth Road
Lincoln LN6 7AA
ENGLAND

86. A. L. Bement, Jr.
Vice President, Technical
Resources
TRW, Inc.
23555 Euclid Avenue
Cleveland, OH 44117

87. M. Bentele
Xamag, Inc.
259 Melville Avenue
Fairfield, CT 06430

88. Clifton G. Bergeron
Head
University of Illinois
Department of Ceramic Engineering
105 South Goodwin Avenue
204 Ceramic Building
Urbana, IL 61801

89. Deane I. Biehler
Supervising Engineer
Caterpillar Inc.
Engineering and Research Materials
Technical Center, Building E
Post Office Box 1875
Peoria, IL 61656-1875

90. William D. Bjorndahl
TRW, Inc.
Materials Characterization and Chemical Analysis Department
One Space Park
Building 01, Room 2060
Redondo Beach, CA 90278

91. Dan Blake
Manager, Material Science
Solar Energy Research Institute
1617 Cole Boulevard
Golden, CO 80401

92. Keith Blandford
Vice President, General Manager
Boride Products, Inc.
2879 Aero Park Drive
Traverse City, MI 49684

93. Paul N. Blumberg
President
Ricardo-ITI
645 Blackhawk Drive
Westmont, IL 60559

94-98. Wolfgang D. G. Boecker
Carborundum Company
Niagara Falls R&D Center
Post Office Box 832
Niagara Falls, NY 14302

99. Larry P. Boesch
Engineering and Economics Research, Inc.
1801 Alexander Bell Drive, Suite 400
Reston, VA 22091-4344

100. Tibor Bornemisza
Chief Engineer
Sundstrand Turbomach
Division of Sundstrand Corporation
4400 Ruffin Road
Post Office Box 85757
San Diego, CA 92138-5757

101. Han Juergen Bossmeyer
Vice President
BMW Technologies, Inc.
Watermill Center
800 South Street
Waltham, MA 02154

102. J. A. M. Boulet
University of Tennessee
310 Perkins Hall
Knoxville, TN 37996

103. Steve Bradley
Signal UOP Research Center
50 UOP Plaza
Des Plaines, IL 60016-6187

104. Raymond. J. Bratton
Manager, Ceramic Science
Westinghouse Electric Corporation
R&D Center
1310 Beulah Road
Pittsburgh, PA 15235

105. Catherine E. Brown
E. I. DuPont de Nemours & Company, Inc.
Experimental Station
Information Center E302/301
Wilmington, DE 19898

106. J. J. Brown
Virginia Polytechnic Institute and State University
Department of Materials Engineering
Blacksburg, VA 24061

107. S. L. Bruner
Ceramatec, Inc.
2425 South 900 West
Salt Lake City, UT 84119

108. W. Bryzik
U.S. Army Tank Automotive Command
R&D Center, Propulsion Systems Division
Warren, MI 48090

109. S. T. Buljan
GTE Laboratories Inc.
40 Sylvan Road
Waltham, MA 02254

110. John M. Byrne, Jr.
Manager, Business Development
PPG Industries, Inc.
Corporate Development Department
One PPG Place
Pittsburgh PA 15272

111. Donald J. Campbell
Air Force Wright Aeronautical Laboratory AFWAL/POX
Wright-Patterson AFB, OH 45433

112. Larry E. Campbell
President/CEO
American Matrix, Inc.
118 Sherlake Drive
Knoxville, TN 37922

113. Roger Cannon
Rutgers University
Department of Ceramics
Bowser Road
Post Office Box 909
Piscataway, NJ 08855-0909

114. Harry W. Carpenter
Consultant
19945 Acre Street
Northridge, CA 91324

115. David Carruthers
Allied-Signal Aerospace Company
Garrett Auxiliary Power Division
2739 East Washington Street
Post Office Box 5227
Phoenix, AZ 85010

116. Jere G. Castor
Allied-Signal Aerospace Company
Garrett Auxiliary Power Division
2739 East Washington Street
Post Office Box 5227
Phoenix, AZ 85010

117. En-sheng Chen
B&C Engineering Research
13906 Dentwood Drive
Houston, TX 77014

118. Albert A. Chesnes
Director, Heat Engine Propulsion Division
U.S. Department of Energy
Office of Transportation Systems
1000 Independence Avenue, S.W.
Forrestal Building CE-151, 5G-048
Washington, DC 20585

119. Frank Childs
EG&G, Inc.
Idaho National Engineering Laboratory
Post Office Box 1625
Idaho Falls, ID 83415

120. Gilbert Y. Chin
Bell Telephone Laboratories
R&D
Murray Hill, NJ 07974

121. Melvin H. Chiogioji
Director
U.S. Department of Energy
Office of Transportation Systems
1000 Independence Avenue, S.W.
Forrestal Building CE-15
Washington DC 20585

122. William J. Chmura
Torrington Company
Corporate Research
59 Field Street
Torrington, CT 06790

123. Eugene V. Clark
Vice President, Technology Engineering
Turbine Metal Technology, Inc.
7327 Elmo Street
Tujunga, CA 91042-2204

124. William L. Cleary
Associate Division Director
ORI, Inc.
1375 Piccard Drive
Rockville, MD 20850

125. Jack L. Clem
General Manager
J. M. Huber Corporation
Carbon Black Division
Post Office Box 2831
Borger, TX 79008-2831

126. Harry E. Cook
Director
Chrysler Motors Corporation
Automotive Research and Technical Planning
1200 Chrysler Drive
Highland Park, MI 48288-1118

127. Stephen Copley
Professor and Chairman
University of Southern California
Materials Science Department
Los Angeles, CA 90089-0241

128. John A. Coppola
Vice President, Technology
Carborundum Company
Post Office Box 156
Niagara Falls, NY 14302

129. Normand D. Corbin
Norton Company
Advanced Ceramics
Goddard Road
Northboro, MA 01532-1545

130. Charles H. Craig
Defense Technology Security
400 Army-Navy Drive, Suite 300
Arlington, VA 22202

131. William J. Croft
U.S. Army Materials Technology Laboratory
405 Arsenal Street
Watertown, MA 02172

132. Gary M. Crosbie
Research Scientist
Ford Motor Company
Material Systems Reliability Department
20000 Rotunda Drive
Building SRL, Room S-2079
Post Office Box 2053
Dearborn, MI 48121-2053

133. Floyd W. Crouse, Jr.
U.S. Department of Energy
Morgantown Energy Technology Center
Collins Ferry Road
Post Office Box 880
Morgantown, WV 26505

134. Raymond Cutler
Ceramatec, Inc.
2425 South 900 West
Salt Lake City, UT 84119

135. David A. Dalman
Research Manager
Dow Chemical Company
Central Research, Organic Specialties
1776 Building
Midland, MI 48674

136. James I. Dalton
Research Scientist
Reynolds Metals Company
Metallurgy Laboratory
Fourth and Canal Streets
Post Office Box 27003
Richmond, VA 23219

137. Stephen C. Danforth
Rutgers University
Bowser Road
Post Office Box 909
Piscataway, NJ 08854

138. Robert F. Davis
North Carolina State University
Materials Engineering Department
232 Riddick Laboratory
Box 7907
Raleigh, NC 27695

139. Evelyn M. DeLiso
Corning Glass Works
Corning, NY 14831

140. J. Franklyn DeRidder
Material Scientist
Omni Electro Motive, Inc.
12 Seely Hill Road
Newfield, NY 14867

141. Alan L. Dragoo
Materials Scientist
National Institute of Standards and Technology
Inorganic Materials Division
Gaithersburg, MD 20899

142. Keith F. Dufrane
Battelle Columbus Laboratories
505 King Avenue
Columbus, OH 43201

143. Edmund M. Dunn
GTE Laboratories Inc.
40 Sylvan Road
Waltham, MA 02254

144. Jeremy D. Dunning
Director
Indiana University
Industrial Research Liaison Program
Bloomington, IN 47405

145. Sunil Dutta
NASA Lewis Research Center
21000 Brookpark Road
MS:49-3
Cleveland, OH 44135

146. Paul N. Dyer
Air Products and Chemicals, Inc.
Post Office Box 538
Allentown, PA 18105

147. Robert J. Eagan
Manager, Chemistry and Ceramics
Sandia National Laboratories
Department 1840
Post Office Box 5800
Albuquerque, NM 87185

148. Christopher A. Ebel
Business Development Manager
Carborundum Company
Technology Division
Post Office Box 337
Niagara Falls, NY 14302

149. J. J. Eberhardt
Director
U.S. Department of Energy
Energy Conversion and Utilization Technologies Program
1000 Independence Avenue, S.W.
Forrestal Building CE-12
Washington, DC 20585

150. William A. Ellingson
Argonne National Laboratory
9700 South Cass Avenue
Argonne, IL 60439

151. Charles D. Estes
Professional Staff Member
U.S. Senate
Committee on Appropriations
SD-152 Dirksen Senate Office Bldg.
Washington, DC 20510

152. John N. Eustis
Chief, Waste Heat Recovery Branch
U.S. Department of Energy
Office of Industrial Programs
1000 Independence Avenue, S.W.
Forrestal Building CE-141
Washington, DC 20585

153. Peggy Evanich
National Aeronautics and Space Administration
Energy Systems Office
Washington DC 20546

154. Anthony G. Evans
University of California
College of Engineering
Santa Barbara, CA 93106

155. Robert C. Evans
Manager
NASA Lewis Research Center
Vehicular Gas Turbine and Diesel Project Office
21000 Brookpark Road
MS:77-6
Cleveland, OH 44135

156. Katherine T. Faber
Assistant Professor
Ohio State University
Department of Ceramic Engineering
2041 College Road
Columbus, OH 43210

157. John W. Fairbanks
U.S. Department of Energy
Office of Transportation Systems
1000 Independence Avenue, S.W.
Forrestal Building CE-151, 5G-042
Washington DC 20585

158. Larry Farrell
Babcock and Wilcox
Old Forrest Road
Lynchburg, VA 24505

159. Rolf Fasth
Chem Systems, Inc.
303 South Broadway
Tarrytown, NY 10591

160. H. W. Foglesong
Dow Corning.Corporation
3901 South Saginaw Road
Midland, MI 48686

161. Thomas F. Foltz
Manager, Product Applications
Avco Corporation
Special Materials Division
Two Industrial Avenue
Lowell, MA 01851

162. Robert G. Frank
Technology Assessment Group
10793 Bentley Pass Lane
Cincinnati, OH 45140

163. Douglas W. Freitag
LTV Aerospace and Defense Company
High Temperature Materials Research
Post Office Box 225907, MS:TH-85
Dallas, TX 75265

164. P. A. Gaydos
Battelle Columbus Laboratories
505 King Avenue
Columbus, OH 43201

165. George E. Gazza
U.S. Army Materials Technology Laboratory
Ceramics Research Division
405 Arsenal Street
Watertown, MA 02172

166. Charles M. Gilmore
George Washington University
Department of Civil, Mechanical, and Environmental Engineering
Washington DC 20052

167. Paul Glance
Director
Concept Analysis
R&D
950 Stephenson Highway
Dupont Automotive Development Bldg.
Troy, MI 48007-7013

168. Fred M. Glaser
U.S. Department of Energy
Office of Fossil Energy
FE-14 GTN
Germantown, MD 20545

169. Joseph W. Glatz
Naval Air Propulsion Test Center
Systems Technology Division
Box 7176, PE 34
Trenton, NJ 08628

170. W. M. Goldberger
Director
Superior Graphite Company
R&D
2175 East Broad Street
Columbus, OH 43209

171. Stephen T. Gonczy
Signal UOP Research Center
Materials Science Department
50 UOP Plaza
Des Plaines, IL 60016-6187

172. Robert J. Gottschall
U.S. Department of Energy
Office of Material Sciences
ER-131 GTN, MS:G-256
Germantown, MD 20545

173. Earl Graham
Cleveland State University
Department of Chemical Engineering
Euclid Avenue at East 24th Street
Cleveland, OH 44115

174. Kenneth Green
Senior Development Engineer
Coors Ceramics Company
17750 West 32nd Street
Golden, CO 80401

175. Robert E. Green, Jr.
Director
Johns Hopkins University
Center for Nondestructive Evaluation
Maryland Hall 107
Baltimore, MD 21218

176. Lance E. Groseclose
General Motors Corporation
Allison Gas Turbine Division
Post Office Box 420
Indianapolis, IN 46206-0420

177. P. Ulf Gummeson
Vice President
Hoeganaes
R&D
River Road and Taylors Lane
Riverton, NJ 08077

178. Bimleshwar P. Gupta
Program Manager, Solar Thermal Program
Solar Energy Research Institute
Solar Heat Research Division
1617 Cole Boulevard
Golden, CO 80401

179. M. D. Gurney
NIPER
Post Office Box 2128
Bartlesville, OK 74005

180. John P. Gyekenyesi
NASA Lewis Research Center
21000 Brookpark Road
MS:49-7
Cleveland, OH 44135

181. J. J. Habeeb
Senior Chemist
Esso Petroleum Canada
Research Division
Post Office Box 3022
Sarina Ontario N7T 7MI
CANADA

182. H. T. Hahn
Pennsylvania State University
ESM Department
227 Hammond Building
University Park, PA 16802

183. Nabil S. Hakim
Mechanical Analysis
Detroit Diesel Corporation
13400 West Outer Drive
Detroit, MI 48239

184. John W. Halloran
Vice President, Technology
CPS Superconductor Corporation
840 Memorial Drive
Cambridge, MA 02139

185. Friedrich Harbach
Head
Asea Brown Boveri AG
Department of Functional Ceramics
Eppelheimer Strasse 82
D-6900 Heidelberg 1
WEST GERMANY

186. Kay Hardman-Rhyne
DARPA
1400 Wilson Boulevard
Arlington, VA 22209

187. R. A. Harmon
Consultant
25 Schalren Drive
Latham, NY 12110

188. Stephen D. Hartline
Norton Company
Advanced Ceramics
Goddard Road
Northboro, MA 01532-1545

189. Michael H. Haselkorn
Senior Project Engineer-Ceramics
Caterpillar Inc.
Engineering Research Materials Technical Center, Building E
Post Office Box 1875
Peoria, IL 61656-1875

190. Willard E. Hauth
Section Manager
Dow Corning Corporation
Composite Development Ceramics Program
3901 South Saginaw Road
Midland, MI 48640

191. Kevin L. Haynes
Senior Engineer, Design
McDonnell Douglas Astronautics Company
Post Office Box 516, MS:107/1
St. Louis, MO 63166

192. Norman L. Hecht
University of Dayton Research Institute
300 College Park
Dayton, OH 45469-0001

193. S. S. Hecker
Deputy Division Leader
Los Alamos National Laboratory
Material Science and Technology Division, G-756
Post Office Box 1663
Los Alamos, NM 87545

194. Peter W. Heitman
General Motors Corporation
Allison Gas Turbine Division
Post Office Box 420, W-5
Indianapolis, IN 46206-0420

195. Richard L. Helferich
Duriron Company, Inc.
Post Office Box 1145
Dayton, OH 45401

196. H. E. Helms
General Motors Corporation
Allison Gas Turbine Division
Post Office Box 420
Indianapolis, IN 46206-0420

197. Thomas L. Henson
Director, Research and Engineering
GTE Products Corporation
Chemical & Metallurgical Division
Hawes Street
Towanda, PA 18848-0504

198. Thomas P. Herbell
NASA Lewis Research Center
21000 Brookpark Road
MS:49-3
Cleveland, OH 44135

199. Hendrik Heystek
Bureau of Mines
Tuscaloosa Research Center
Post Office Box L
University, AL 35486

200. Robert V. Hillery
Manager, Coating Materials and Processes
General Electric Company
One Neumann Way
Post Office Box 156301
Cincinnati, OH 45215

201. Jonathan W. Hinton
Vice President, Business Operations
Lanxide Corporation
Tralee Industrial Park
Newark, DE 19714-6077

202. Joe Homeny
Professor
University of Illinois
Department of Materials Science and Engineering
105 South Goodwin Avenue
Ceramics Building
Urbana, IL 61801

203. A. T. Hopper
Battelle Columbus Laboratories
Engineering Mechanics Department
505 King Avenue
Columbus, OH 43201-2693

204. George Hsu
Jet Propulsion Laboratory
4800 Oak Grove Drive
MS:512-103
Pasadena, CA 91109

205. Shih Hsu
Digital Equipment Corporation
77 Reed Road
MS:HL02-1/L8
Hudson, MA 01749-2895

206. Stephen M. Hsu
Chief
National Institute of Standards and Technology
Ceramics Division
Gaithersburg, MD 20899

207. Harold A. Huckins
President
Princeton Advanced Technology, Inc.
56 Finley Road
Princeton, NJ 08540

208. Fred Huettic
Vice President
Advanced Ceramic Technology, Inc.
17 Deerfield Road
East Brunswick, NJ 08816

209. 0. Richard Hughes
Coordinator, University Research
Celanese Research Company
86 Morris Avenue
Summit, NJ 07901

210. Joseph E. Hunter, Jr.
General Motors Corporation
Research Labs, Metallurgy Department
30200 Mound Road
Warren, MI 48090-9055

211. Louis C. Ianniello
Director
U.S. Department of Energy
Office of Material Sciences
ER-13 GTN
Germantown, MD 20545

212. Robert Ingel
Naval Research Laboratory
4555 Overlook Avenue, S.W.
Code:63-70
Washington DC 20375

213. M. S. Inoue
Vice President
Kyocera International, Inc.
Corporate Technology and Planning
8611 Balboa Avenue
San Diego, CA 92123-1580

214. Robert H. Insley
Champion Spark Plug Company
Ceramic Division
20000 Conner Avenue
Detroit, MI 48234

215. Curtis A. Johnson
General Electric Company
Research Laboratory
Post Office Box 8
Schenectady, NY 12301

216. Larry Johnson
Director
Argonne National Laboratory
Center for Transportation Research
9700 South Cass Avenue
Building 362
Argonne, IL 60439

217. L. A. Joo
Associate Director, Research
Great Lakes Research Corporation
Post Office Box 1031
Elizabethton, TN 37643

218. A. David Joseph
Vice President
Sealed Power Corporation
R&D
100 Terrace Plaza
Muskegon, MI 49443

219. Debra Joslin
University of Tennessee
Metallurgical Engineering Department
Knoxville, TN 37996

220. Adam Jostsons
Director, Advanced Materials
Australian Nuclear Science & Technology Organisation
Lucas Heights Research Laboratories
New Illawarra Road
Lucas Heights New South Wales
AUSTRALIA

221. Roy Kamo
President
Adiabatics, Inc.
630 South Mapleton
Columbus, IN 47201

222. Allan Katz
Air Force Wright Aeronautical Laboratory
Metals and Ceramics Division
Materials Laboratory, AFWAL/MLLM
Wright-Patterson AFB OH 45433

223. R. N. Katz
Chief Materials Technologist
U.S. Army Materials Technology Laboratory
405 Arsenal Street
Watertown, MA 02172

224. Ted Kawaguchi
Tokai Carbon
375 Park Avenue, Suite 3802
New York, NY 10152

225. Frederick L. Kennard, III
Supervisor, Ceramic Research
General Motors Corporation
AC Spark Plug Division,
Department 32-24
1300 North Dort Highway
Flint, MI 48556

226. J. R. Kidwell
AGT 101 Assistant Project Engineer
Allied-Signal Aerospace Company
Garrett Auxiliary Power Division
2739 East Washington Street
Post Office Box 5227
Phoenix, AZ 85010

227. Max Klein
Senior Scientist, Thermodynamics
Gas Research Institute
8600 West Bryn Mawr Avenue
Chicago, IL 60631

228. C. E. Knapp
Norton Company
8001 Daly Street
Niagara Falls Ontario L2G 6S2
CANADA

229. A. S. Kobayashi
University of Washington
Department of Mechanical Engineering
MS:FUIO
Seattle, WA 98195

230. Wolfgang Kollenberg
Projektleitung Material-Rohstofforschung - PLR
Kernforschungsanlage Juelich GmbH
Postfach 1913
D-5170 Juelich
WEST GERMANY

231. David M. Kotchick
Allied-Signal Aerospace Company
AiResearch Los Angeles Division
2525 West 190th Street
Torrance, CA 90509

232. Bruce Kramer
George Washington University
Aerodynamic Center
Room T715
Washington, DC 20052

233. Saunders B. Kramer
Manager, AGT Program
U.S. Department of Energy
Office of Transportation Systems
1000 Independence Avenue, S.W.
Forrestal Building CE-151
Washington DC 20585

234. Dan M. Kreiner
T800 Program. Manager
Allied-Signal Aerospace Company
AiResearch Tucson Division
Post Office Box 38001
Tucson, AZ 85740-8001

235. A. S. Krieger
President
Radiation Science, Inc.
Post Office Box 293
Belmont, MA 02178

236. Pieter Krijgsman
Ceramic Design Int. Hold., Ltd.
Post Office Box 68
8050 AB Hattem
THE NETHERLANDS

237. Jack H. L'Amoreaux
Manager, Special Projects
Applied Ceramics
Post Office Box 29664
Atlanta, GA 30359

238. W. J. Lackey
Georgia Tech Research Institute
Energy and Materials Sciences
Georgia Institute of Technology
Atlanta, GA 30332

239. Everett A. Lake
Air Force Wright Aeronautical Laboratory
AFWAL/POSL
Wright-Patterson AFB OH 45433-6563

240. Hari S. Lamba
Senior Experimental Metallurgist
General Motors Corporation
Electro-Motive Division
LaGrange, IL 60525

241. Manfred Langer
Volkswagen AG
Forschung-Neue Technologien
Werkstofftechnologie
D-3180 Wolfsburg 1
WEST GERMANY

242. James Lankford
Southwest Research Institute
Department of Materials Sciences
6220 Culebra Road
Post Office Drawer 28510
San Antonio, TX 78284

243. David C. Larsen
Corning Glass Works
Materials Research Department
Sullivan Park, FR-51
Corning, NY 14831

244. S. K. Lau
Carborundum Company
Technology Division
Post Office Box 832
Niagara Falls, NY 14302

245. Harry A. Lawler
Senior Product Specialist
Carborundum Company
Niagara Falls R&D Center
Post Office Box 832
Niagara Falls, NY 14302

246. Alan Lawley
Drexel University
Materials Engineering
Philadelphia, PA 19104

247. Jean Lecostaouec
Textron Speciality Materials
2 Industrial Avenue
Lowell MA 01851

248. Daniel Lee
Temescon
2850 7th Street
Berkeley, CA 94710

249. June-Gunn Lee
Korea Advanced Institute of Science and Technology
Post Office Box 131
Dong Dac Mun Seoul
KOREA

250. E. M. Lenoe
Air Force Office of Scientific Research
Office of Naval Research
Liaison Office, Far East
APO San Francisco, CA 96503-0110

251. Stanley R. Levine
NASA Lewis Research Center
21000 Brookpark Road
Cleveland, OH 44135

252. David Lewis
Naval Research Laboratory
Materials Science and Technology
4555 Overlook Avenue, S.W.
Code 63-70
Washington, DC 20375

253. Bill Long
Babcock and Wilcox
Post Office Box 1260
Lynchburg, VA 24505

254. L. A. Lott
EG&G, Inc.
Idaho National Engineering Laboratory
Post Office Box 1625
Idaho Falls, ID 83415

255. Raouf 0. Loutfy
President
Materials and Electrochemical Research Corporation
7960 South Kolb Road
Tucson, AZ 85706

256. Bryan K. Luftglass
Staff Consultant
Chem Systems, Inc.
303 South Broadway
Tarrytown, NY 10591

257. Robert Lundberg
Research Engineer
Swedish Institute for Silicate Research
Box 5403
S-402 29 Gothenburg
SWEDEN

258. Michael J. Lynch
General Electric Company
Medical Systems Group
Post Office Box 414, 7B-36
Milwaukee, WI 53201

259. James W. MacBeth
Manager, Market Development
Carborundum Company
Structural Ceramics Division
Box 1054
Niagara Falls, NY 14302

260. Vincent L. Magnotta
Senior Principal Development Engineer
Air Products and Chemicals, Inc.
Technical Diversification R&D
Post Office Box 538
Allentown, PA 18105

261. Tai-il Mah
Technical Manager
Universal Energy Systems
Ceramics and Composites Research
4401 Dayton-Xenia Road
Dayton, OH 45432

262. L. Manes
Material Scientist
Commission of the European Communities
Joint Research Centre
Ispra Establishment
1-21020 Ispra (Varese)
ITALY

263. Giel Marijnissen
Director
Interturbine R&D
R&D
Post Office Box 4339
5944 ZG Arcen
THE NETHERLANDS

264. Gerald R. Martin
Manager, Technology
Fleetguard, Inc.
Cookeville, TN 38501

265. J. W. McCauley
U.S. Army Materials Technology Laboratory
SLCMT-OMM
405 Arsenal Street
Watertown, MA 02172-0001

266. Bryan J. McEntire
Manager, Gas Turbine Operations
Norton Company
TRW Ceramics
Goddard Road
Northboro, MA 01532-1545

267. Thomas D. McGee
Iowa State University
Department of Materials Science and Engineering
Ames, IA 50011

268. H. Christopher McGowan
President
Advanced Ceramic Technology, Inc.
72 Veronica Avenue, Unit 10
Somerset, NJ 08873

269. Malcolm G. McLaren
Head
Rutgers University
Department of Ceramics
Bowser Road
Busch Campus
Post Office Box 909
Piscataway, NJ 08854

270. Arthur F. McLean
Consultant
6225 North Camino Almonte
Tucson, AZ 85718

271-275. B. L. Mehosky
Development Engineer, R&D
British Petroleum
4440 Warrensville Center Rd.
Cleveland, OH 44128

276. Joseph J. Meindl
Reynolds International, Inc.
6603 West Broad Street
Post Office Box 27002
Richmond, VA 23230

277. D. Messier
U.S. Army Materials Technology Laboratory
DRXMR-MC
405 Arsenal Street
Watertown, MA 02172

278. Brad Miller
Norton Company
Advanced Ceramics
Goddard Road
Northboro, MA 01532-1545

279. Amar Mishra
Group Leader
Engelhard Corporation
R&D
Menlo Park, CN-28
Edison, NJ 08818

280. Bill Moehle
Ethyl Corporation
R&D Laboratories
Post Office Box 341
Baton Rouge, LA 70821

281. Helen Moeller
Babcock and Wilcox
Post Office Box 11165
Lynchburg, VA 24506-1165

282. Frederick E. Moreno
President
Turbo Energy Systems, Inc.
2858 South Roosevelt
Tempe, AZ 85282

283. Peter E. D. Morgan
Technical Staff
Rockwell International
Structural Ceramics Science Center
1049 Camino Dos Rios
Post Office Box 1085
Thousand Oaks, CA 91360

284. Lawrence M. Murphy
Manager
Solar Energy Research Institute
Thermal Systems Research Branch
1617 Cole Boulevard
Golden, CO 80401

285. Solomon Musikant
General Electric Company
Space Systems Division
Post Office Box 8555, MS:U-1219
Philadelphia, PA 19101

286. Pero Nannelli
Pennwalt Corporation
900 First Avenue
Post Office Box C
King of Prussia, PA 19406-0018

287. William D. Nix
Stanford University
Department of Materials Science and Engineering
Stanford, CA 94305

288. Richard D. Nixdorf
Vice President
American Matrix, Inc.
118 Sherlake Drive
Knoxville, TN 37922

289. S. D. Nunn
University of Michigan
Materials Science and Engineering
Ann Arbor, MI 48109

290. Brian M. O'Connor
Manager
Lubrizol Corporation
Tribology Section
29400 Lakeland Boulevard
Wickliffe, OH 44092

291. W. Richard Ott
Alfred University
Center for Advanced Ceramic Technology
Alfred, NY 14802

292. William C. Owen
Sundstrand Turbomach
Division of Sundstrand Corporation
4400 Ruffin Road
Post Office Box 85757
San Diego, CA 92138-5757

293. Muktesh Paliwal
GTE Products Corporation
Hawes Street
Towanda, PA 18848-0504

294. Joseph E. Palko
Senior Engineer
General Electric Company
Research Laboratory
TTD Building, 55-113
Schenectady, NY 12345

295. Hayne Palmour, III
North Carolina State University
Engineering Research Services Division
2158 Burlington Engineering Labs
Post Office Box 5995
Raleigh, NC 27607

296. Joseph N. Panzarino
Norton Company
Advanced Ceramics
Goddard Road
Northboro, MA 01532-1545

297. Pellegrino Papa
Manager, Technical and Business Development
Corning Glass Works
Corning Technical Products Division
Corning, NY 14831

298. Arvid E. Pasto
Technical Staff
GTE Laboratories Inc.
40 Sylvan Road
Waltham, MA 02254

299. James W. Patten
Director, Materials Engineering
Cummins Engine Company, Inc.
Box 3005, Mail Code 50183
Columbus, IN 47202-3005

300. Timothy M. Pattison
Textron Lycoming
550 Main Street
MS:LSMI
Stratford, CT 06497

301. Robert A. Penty.
Development Engineer
Eastman Kodak Company
Manufacturing Technology Department, Apparatus Division
901 Elmgrove Road
Rochester, NY 14650

302. Gary R. Peterson
U.S. Department of Energy
Idaho Operations Office
785 D.O.E. Place
Idaho Falls, ID 83402

303. R. Byron Pipes
University of Delaware
Center for Composite Materials
2001 Spencer Laboratory
Newark DE 19716

304. Bruce J. Pletka
Michigan Technological University
Department of Metallurgical Engineering
Houghton, MI 49931

305. Robert C. Pohanka
Office of Naval Research
800 North Quincy Street
Code 431
Arlington, VA 22217

306. J. P. Pollinger
Allied-Signal Aerospace Company
Garrett Ceramic Components Division
19800 South Van Ness Avenue
Torrance, CA 90509

307. Stephen C. Pred
Product Manager
ICD Group, Inc.
1100 Valley Brook Avenue
Lyndhurst, NJ 07071

308. Karl M. Prewo
United Technologies Corporation
Research Center
Silver Lane
MS:24
East Hartford, CT 06108

309. Hubert B. Probst
Chief Scientist
NASA Lewis Research Center
Materials Division
21000 Brookpark Road
MS:49-1
Cleveland, OH 44135

310. Joseph M. Proud
Director
GTE Laboratories Inc.
Materials Science Laboratory
40 Sylvan Road
Waltham, MA 02254

311. D. W. Prouse
Ceramatec, Inc.
2425 South 900 West
Salt Lake City, UT 84119

312. Carr Lane Quackenbush
Norton Company
Advanced Ceramics
Goddard Road
Northboro, MA 01532-1545

313. Brian Quigy
National Aeronautics and Space Administration
Energy Systems Office
Washington, DC 20546

314. George Quinn
U.S. Army Materials Technology Laboratory
405 Arsenal Street
Watertown, MA 02172

315. Dennis T. Quinto
Kennametal, Inc.
Phillip M. McKenna Laboratory
Post Office Box 639
Greensburg, PA 15601

316. Dennis W. Readey
Colorado School of Mines
Department of Metallurgy and Materials Engineering
Golden, CO 80401

317. Michael J. Readey
Principal Engineer
Coors Ceramics Company
R&D
17750 West 32nd Street
Golden, CO 80401

318. Robert R. Reeber
U.S. Army Research Office
Post Office Box 12211
Research Triangle Park, NC 27709

319. K. L. Reifsnider
Virginia Polytechnic Institute and State University
Department of Engineering Science and Mechanics
Blacksburg, VA 24061

320. Paul Rempes
Engineering Specialist
Williams International
2280 West Maple Road
Post Office Box 200
Walled Lake, MI 48088

321. Theresa M. Resetar
U.S. Army Materials Technology Laboratory
Materials Characterization Center
405 Arsenal Street
SLCMT-OMM
Watertown, MA 02172

322. K. T. Rhee
Rutgers University
College of Engineering
Bowser Road
Post Office Box 909
Piscataway, NJ 08854

323. Roy W. Rice
W. R. Grace and Company
7379 Route 32
Columbus, MD 21044

324. David W. Richerson
Ceramatec, Inc.
2425 South 900 West
Salt Lake City, UT 84119

325. Scott L. Richlen
U.S. Department of Energy
Office of Industrial Programs
1000 Independence Avenue, S.W.
Forrestal Building CE-141
Washington, DC 20585

326. Paul Rieth
Ferro Corporation
661 Willet Road
Buffalo, NY 14218-9990

327. Michael A. Rigdon
Institute for Defense Analyses
1801 Beauregard Street
Alexandria, VA 22311

328. John E. Ritter, Jr.
University of Massachusetts
Mechanical Engineering Department
Amherst, MA 01003

329-333. R. S. C. Rogers
Carborundum Company
Niagara Falls R&D Center
Post Office Box 832
Niagara Falls, NY 14302

334. Martha J. Rohr
U.S. Department of Energy
Oak Ridge Operations
Federal Office Building
Post Office Box 2001, MS:AMERD
Oak Ridge, TN 37831

335. Giulio A. Rossi
Norton Company
Advanced Ceramics
Goddard Road
Northboro, MA 01532-1545

336. Barry R. Rossing
Lanxide Corporation
Tralee Industrial Park
Newark, DE 19711

337. Donald W. Roy
Manager, Carbide and Optical Material
Coors Ceramics Company
R&D
17750 West 32nd Street
Golden, CO 80401

338. Bruce Rubinger
Gobal
50 Milk Street, 15th Floor
Boston, MA 02109

339. Robert Ruh
Air Force Wright Aeronautical Laboratory
Metals and Ceramics Division
Materials Laboratory, AFWAL/MLLM
Wright-Patterson AFB OH 45433

340. Robert J. Russell, Sr.
Divisional Vice President, Technology and Planning
Norton Company
Advanced Ceramics
Goddard Road
Northboro, MA 01532-1545

341. George P. Safol
Westinghouse Electric Corporation
R&D Center
1310 Beulah Road
Pittsburgh, PA 15235

342. J. A. Salem
NASA Lewis Research Center
21000 Brookpark Road
Cleveland, OH 44135

343. J. Sankar
North Carolina A&T State University
Department of Mechanical Engineering
Greensboro, NC 27411

344. Vin K. Sarin
Boston University
Department of Manufacturing Engineering
44 Cummington Street
Boston, MA 02215

345. Maxine L. Savitz
Director
Allied-Signal Aerospace Company
Garrett Ceramic Components Division
19800 South Van Ness Avenue
Torrance, CA 90509

346. Richard Schapery
Texas A&M University
Civil Engineering Department
College Station, TX 77843

347. Jim Schienle
Allied-Signal Aerospace Company
Garrett Auxiliary Power Division
2739 East Washington Street
Post Office Box 5227, MS:1302-2P
Phoenix, AZ 85010

348. Liselotte J. Schioler
Air Force Office of Scientific Research
Bolling AFB
Washington DC 20332-6448

349. Richard A. Schmidt
Associate Section Manager
Battelle Columbus Laboratories
Mechanics Section
505 King Avenue
Columbus, OH 43201-2693

350. Arnie Schneck
Deere & Company Technical Center
Post Office Box 128
Wood-Ridge, NJ 07075

351. Matthew Schreiner
Applications Engineer
ALANX Products L.P.
101 Lake Drive
Newark, DE 19702

352. John Schuldies
Industrial Ceramic Technology, Inc.
37 Enterprise Drive
Ann Arbor, MI 48103

353. R. B. Schulz
Manager
U.S. Department of Energy
Office of Transportation Systems
1000 Independence Avenue, S.W.
Forrestal Building CE-151, 5G-046
Washington, DC 20585

354. Wesley J. C. Schuster President
Thermo Electron Corporation Metals Division
115 Eames Street
Post Office Box 340
Wilmington, MA 01887

355. Murray A. Schwartz
Bureau of Mines
2401 Eye Street, N.W.
Washington, DC 20241

356. Douglas B. Schwarz
Dow Chemical Company
52 Building
Midland, MI 48674

357. Thomas M. Sebestyen
U.S. Army Tank Automotive Command
AMSTA-RGRT
Warren, MI 48397-5000

358. Brian Seegmiller
Senior Development Engineer
Coors Ceramics Company
17750 West 32nd Street
Golden, CO 80401

359. S. G. Seshadri
Research Associate
Carborundum Company
Niagara Falls R&D Center
Post Office Box 832
Niagara Falls, NY 14302

360. Peter T. B. Shaffer
Executive Vice President
Advanced Refractory
Technologies, Inc.
699 Hertel Avenue
Buffalo, NY 14207

361. Laurel M. Sheppard
Associate Editor
Advanced Materials and
Processes
Route 87
Metals Park, OH 44073

362. Dinesh K. Shetty
University of Utah
Department of Materials Science
and Engineering
Salt Lake City, UT 84112

363. Jack D. Sibold
Coors Ceramics Company
17750 West 32nd Street
Golden, CO 80401

364. Neal Sigmon
U.S. House of Representatives
Appropriations Committee
Rayburn Building, Room B308
Washington, DC 20515

365. Richard Silberglitt
Quest Research Corporation
7600 Leesburg Pike #A
Falls Church, VA 22043

366. A. Sinha
North Carolina A&T State
University
Department of Mechanical
Engineering
Greensboro, NC 27411

367. Maurice J. Sinnott
University of Michigan
Chemical and Metallurgical
Engineering
438 West Engineering Building
Ann Arbor, MI 48109-2136

368. S. R. Skaggs
Los Alamos National Laboratory
Program Office
Post Office Box 1663, MS:F-682
Los Alamos, NM 87545

369. J. Thomas Smith
Vice President
GTE Valenite
Materials Manufacturing
1100 West 13th Mile Road
Madison Heights, MI 48071

370. Jay R. Smyth
Senior Development Specialist
Allied-Signal Aerospace Company
Garrett Auxiliary Power Division
2739 East Washington Street
Post Office Box 5227
MS:93-172/1302-2K
Phoenix, AZ 85010

371. Rafal Sobotowski
British Petroleum
R&D
3092 Broadway Avenue
Cleveland, OH 44115

372. E. Solidum
Allied-Signal Aerospace
Company
Garrett Ceramic Components
Division
19800 South Van Ness Avenue
Torrance, CA 90509

373. Thomas M. Sopko
Investment Analyst
Lubrizol Enterprises, Inc.
29400 Lakeland Boulevard
Wickliffe, OH 44092

374. Richard M. Spriggs
Director
Alfred University
Center for Advanced Ceramic Technology
Alfred, NY 14802

375. M. Srinivasan
Carborundum Company
Niagara Falls R&D Center
Post Office Box 832
Niagara Falls, NY 14302

376. Gordon L. Starr
Manager
Cummins Engine Company, Inc.
Metallic/Ceramic Materials Department
Box 3005, Mail Code 50183
Columbus IN 47202-3005

377. Harold L. Stocker
Manager, Low Heat Rejection Program
General Motors Corporation
Allison Gas Turbine Division
2001 South Tibbs Avenue
Post Office Box 420, T-23
Indianapolis, IN 46206-0420

378. Paul D. Stone
Dow Chemical Company
1801 Building
Midland, MI 48674

379-383. Roger Storm
Director
Carborundum Company
Niagara Falls R&D Center
Post Office Box 832
Niagara Falls NY 14302

384. E. E. Strain
Program Manager, AGT 101
Allied-Signal Aerospace Company
Garrett Auxiliary Power Division, Department 76-50
2739 East Washington Street
Building 1302-1N
Post Office Box 5227, MS:301-2N
Phoenix, AZ 85010

385. Thomas N. Strom
NASA Lewis Research Center
21000 Brookpark Road, 77-6
Cleveland, OH 44135

386. Jerry Strong
Albright & Wilson
Post Office Box 26229
Richmond, VA 23260

387. Richard Suddeth
Boeing Motor Airplane Company
Post Office Box 7730, MS:K-76-67
Wichita, KS 67277

388. Paul Sutor
Midwest Research Institute
425 Volker Boulevard
Kansas City, MO 64116

389. P. L. Sutton
U.S. Department of Energy
Office of Transportation Systems
1000 Independence Avenue, S.W.
Forrestal Building CE-151
Washington DC 20585

390. J. J. Swab
U.S. Army Materials Technology Laboratory
Ceramics Research Division, SLCMT-EMC
405 Arsenal Street
Watertown, MA 02172

391. John W. Swain, Jr.
Kollmorgen Corporation
PCK Technology Division
15424 Garrison Lane
Southgate, MI 48195

392. Lewis Swank
Ford Motor Company
Material Systems Reliability Department
20000 Rotunda Drive
Building SRL, Room S-2023
Post Office Box 2053
Dearborn, MI 48121-2053

393. Truett Sweeting
Technical Branch Manager
Carborundum Company
Niagara Falls R&D Center
Post Office Box 832
Niagara Falls, NY 14302

394. Stephen R. Tan
ICI Advanced Materials
Post Office Box 11
The Heath, Runcorn Cheshire
WA7 4QE
ENGLAND

395. Chris Tarry
GTE Products Corporation
Hawes Street
Towanda, PA 18848

396. Anthony C. Taylor
Staff Director
U.S. House of Representatives
Committee on Science and Technology
Rayburn Building, Room 2321
Washington DC 20515

397. Monika 0. Ten Eyck
Carborundum Technical Ceramics GmbH
Nobelstrasse 6
D4050 Monchengladbach-Wickrath
WEST GERMANY

398. John K. Tien
Director
Columbia University
Center for Strategic Materials
1137 S.W. Mudd Building
New York, NY 10027

399. T. Y. Tien
University of Michigan
Materials and Metallurgical Engineering
Dow Building
Ann Arbor, MI 48109-2136

400. Julian M. Tishkoff
Directorate, Aerospace Sciences
Air Force Office of Scientific Research
(AFOSR/WC) Bolling AFB
Washington DC 20332

401. Louis E. Toth
National Science Foundation
Division of Materials Research
1800 "G" Street, N.W.
Washington DC 20550

402. Richard E. Tressler
Chairman
Pennsylvania State University
Ceramic Science and Engineering
201 Steidle Building
University Park, PA 16802

403. W. T. Tucker
General Electric Company
Research Laboratory
Post Office Box 8
Schenectady, NY 12301

404. Donald L. Vaccari
Chief, Structural Mechanics
General Motors Corporation
Allison Gas Turbine Division
2001 South Tibbs Avenue
Post Office Box 420, Speed Code TIOB
Indianapolis, IN 46241

405. 0. Van Der Biest
Katholieke Universiteit Leuven
Departement Metaalkunde en Toegepaste
de Croylaan 2
B-3030 Leuven
BELGIUM

406. Edward C. Van Reuth
President
Technology Strategies, Inc.
10722 Shingle Oak Court
Burke, VA 22015

407. Mark Van Roode
Solar Turbines, Inc.
2200 Pacific Highway
Mail Zone R-I
San Diego, CA 92138

408-412. V. Venkateswaran
Carborundum Company
Niagara Falls R&D Center
Post Office Box 832
Niagara Falls, NY 14302

413. Ted Vojnovich
Assistant Program Manager
U.S. Department of Energy
Office of Transportation Systems
1000 Independence Avenue, S.W.
Forrestal Building CE-151
Washington DC 20585

414. K. E. Voss
Engelhard Corporation
Research Department
Menlo Park, CN-28
Edison, NJ 08818

415. John B. Wachtman, Jr.
Director, Center for Ceramics Research
Rutgers University
College of Engineering
Bowser Road
Post Office Box 909
Piscataway, NJ 08855-0909

416. Harlan L. Watson
U.S. House of Representatives
Committee on Science and Technology
Rayburn Building, Suite 2321
Washington DC 20515

417. John D. Watson
Manager Materials R&D
Broken Hill Proprietary Co., Ltd.
Melbourne Research Laboratories
245 Wellington Road
Mulgrave 3170 Victoria
AUSTRALIA

418. C. David Weiss
Staff Engineer, Engineering Research Materials
Caterpillar Inc.
Technical Center
Building E
Post Office Box 1875
Peoria, IL 61656-1875

419. James J. Wert
Vanderbilt University
Box 1621, Station B
Nashville, TN 37235

420. Albert R. C. Westwood
Corporate Director
Martin Marietta Laboratories R&D
1450 South Rolling Road
Baltimore, MD 21227

421. Thomas J. Whalen
Ford Motor Company
Material Systems Reliability
Department 20000 Rotunda Drive
Building SRL, Room S-2023
Post Office Box 2053
Dearborn, MI 48121-2053

422. Sheldon M. Wiederhorn
National Institute of Standards and Technology
Inorganic Materials Division
Gaithersburg, MD 20899

423. James C. Williams
General Manager, Aircraft Engines Division
General Electric Company
Engineering Materials Technology Labs
One Neumann Way
Cincinnati, OH 45215-6301

424. Janette R. Williams
Product Manager
Kollmorgen Corporation
PCK Technology Division
322 L.I.E. South Service Road
Melville, NY 11747

425. Craig A. Willkens
Norton Company
Advanced Ceramics
Goddard Road
Northboro, MA 01532-1545

426. Roger R. Wills
Manager, Advanced Ceramic Components
TRW, Inc.
Valve Division
1455 East 185th Street
Cleveland, OH 44110

427. J. M. Wimmer
Supervisor, Nonmetallic Materials Group
Allied-Signal Aerospace Company
Garrett Auxiliary Power Division
2739 East Washington Street
Post Office Box 5227, MS:1302-2P
Phoenix, AZ 85010

428. David Wirth
Vice President
Coors Ceramics Company
Technical Operations & Engineering
17750 West 32nd Street
Golden, CO 80401

429. Thomas J. Wissing
Manager, Government Contract Administration
Eaton Corporation
Engineering & Research Center
26201 Northwestern Highway
Post Office Box 766
Southfield, MI 48037

430. Dale Wittmer
Southern Illinois University at Carbondale
Department of Mechanical Engineering
Carbondale, IL 62901

431. Stanley M. Wolf
Materials Program Manager
U.S. Department of Energy
Energy Conversion and Utilization Technologies Program
1000 Independence Avenue, S.W.
Forrestal Building CE-12
Washington DC 20585

432. George W. Wolter
Howmet Turbine Components Corporation
Technical Center
699 Benston Road
Whitehall, MI 49461

433. James C. Wood
NASA Lewis Research Center
21000 Brookpark Road
MS:500-210
Cleveland, OH 44135

434. Roger P. Worthen
Principal Engineer
Eaton Corporation
Engineering and Research Center
26201 Northwestern Highway
Post Office Box 766
Southfield, MI 48076

435. J. G. Wurm
Division Head
Commission of the European Communities
Advanced Materials Research Programme
Rue de la Loi 200
B-1049 Brussels
BELGIUM

436. Harry C. Yeh
Ceramic Supervisor
Allied-Signal Aerospace Company
Garrett Ceramic Components Division
19800 South Van Ness Avenue
Torrance, CA 90509

437. Thomas M. Yonushonis
Cummins Engine Company, Inc.
Box 3005, Mail Code 50183
Columbus, IN 47202-3005

438. Don Zabierek
Air Force Wright Aeronautical Laboratory
AFWAL/POTC
Wright-Patterson AFB OH 45433

439. Charles Zeh
U.S. Department of Energy
Morgantown Energy Technology Center
Post Office Box 880
Morgantown, WV 26505

440. Anne Marie Zerega
U.S. Department of Energy
Office of Transportation Systems
1000 Independence Avenue, S.W.
Forrestal Building CE-15
Washington DC 20585

441. Martin Zlotnick
Nichols Research Corporation
8618 Westwood Center Drive, Suite 200
Vienna, VA 22180-2222

442. Klaus M. Zwilsky
Executive Director
National Research Council
National Materials Advisory Board
2101 Constitution Avenue
Washington, DC 20418

443. Office of Assistant Manager for Energy Research and Development
U.S. Department of Energy
Oak Ridge Operations Office
P.O. Box 2001
Oak Ridge, TN 37831-8600

444-453. U.S. Department of Energy
Office of Scientific and Technical Information
Office of Information Services
P.O. Box 62
Oak Ridge, TN 37831

For distribution by microfiche as shown in DOE/OSTI-4500, Distribution Category UC-332